Adsorption and Diffusion in Nanoporous Materials

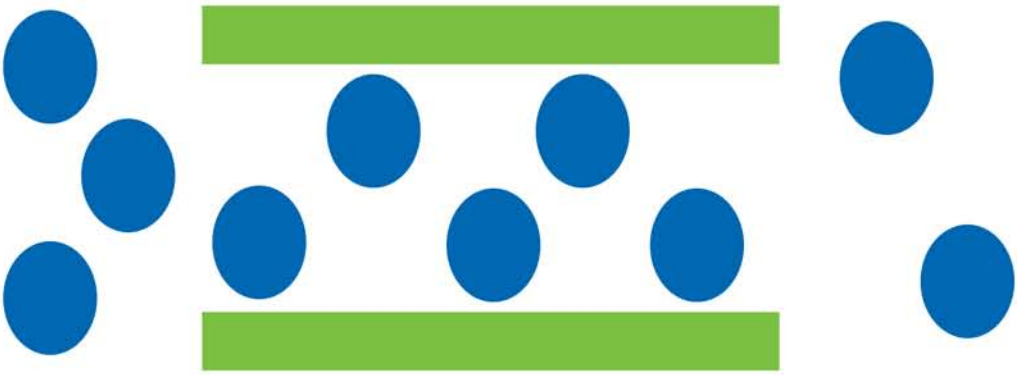

Rolando M.A. Roque-Malherbe

CRC Press
Taylor & Francis Group

Adsorption and Diffusion in Nanoporous Materials

Adsorption and Diffusion in Nanoporous Materials

Rolando M.A. Roque-Malherbe

CRC Press
Taylor & Francis Group
Boca Raton London New York

CRC Press is an imprint of the
Taylor & Francis Group, an informa business

CRC Press
Taylor & Francis Group
6000 Broken Sound Parkway NW, Suite 300
Boca Raton, FL 33487-2742

Printed in the United States of America on acid-free paper
10 9 8 7 6 5 4 3 2 1

International Standard Book Number-10: 1-4200-4675-6 (Hardcover)
International Standard Book Number-13: 978-1-4200-4675-5 (Hardcover)

Library of Congress Cataloging-in-Publication Data

Roque-Malherbe, Rolando M.A.
Adsorption and diffusion in nanoporous materials / author/editor (s) Rolando M.A. Roque-Malherbe.
p. cm.
Includes bibliographical references and index.
ISBN-13: 978-1-4200-4675-5 (alk. paper)
ISBN-10: 1-4200-4675-6 (alk. paper)
1. Porous materials. 2. Nanostructured materials. 3. Diffusion. 4. Adsorption. I. Title.

TA418.9.P6R67 2007
620.1'16--dc22 2006030712

Visit the Taylor & Francis Web site at
http://www.taylorandfrancis.com

and the CRC Press Web site at
http://www.crcpress.com

Dedication

This book is dedicated to my mother, Silvia;
my father, Rolando; my wife, Teresa; our sons, Edelin,
Rolando, Ruben, and Daniel; our grandchildren,
Sarah, Rolando, Natalie, and Nicolas; and
all our pets, very especially to Zeolita and Trosia.

Preface

The increase in the concentration of molecules from a gaseous phase in the neighboring solid surface was recognized in 1777 by Fontana and Scheele, and the term ***ADSORPTION*** to describe the effect was coined by Kayser in 1881. On the other hand, ***DIFFUSION*** is a general property of matter related to the tendency of a system to occupy all its accessible states. The quantitative study of this phenomenon started in 1850–1855 with the works of Adolf Fick and Thomas Graham.

The development of new materials is a basic objective of materials science research. This interest is fueled by the progress in all fields of industry and technology. For example, the evolution of the electronic industry initiated the development of smaller and smaller elements. The size of these components is approaching nanometer dimensions, and as this dominion is entered, scientists have found that properties of materials with nanometer dimensions, i.e., on the length scale of about 1–100 nm, can differ from those of the bulk material. In these dimensions, adsorption and diffusion are important methods of characterization. They are processes that determine the governing laws of important fields of application of nanoporous materials.

According to the definition of the International Union of Pure and Applied Chemistry (IUPAC), ***POROUS MATERIALS*** are classified as microporous materials, which are those with pore diameters between 0.3 and 2 nm; mesoporous materials; which are those that have pore diameters between 2 and 50 nm, and macroporous materials; which are those with pores bigger than 50 nm. Within the class of porous materials, nanoporous materials, such as zeolites and related materials, mesoporous molecular sieves, the majority of silica, and active carbons are the most widely studied and applied. In the cases of crystalline and ordered nanoporous material such as zeolites and related materials and mesoporous molecular sieves, classification as nanoporous materials is not discussed. However, amorphous porous materials may possess, together with pores with sizes less than 100 nm, larger pores. Even in this case, in the majority of instances, the nanoporous component is the most important part of the porosity.

Adsorption and diffusion have a manifold value, since they are not only powerful means for the characterization of nanopoorus materials but are also important industrial operations. The adsorption of a gas can bring information of the microporous volume, the mesopore area, the volume and size of the pores, and the heat of adsorption. On the other hand, diffusion controls the molecular transport of gases in porous media and also brings morphological information, in the case of amorphous materials, and structural information, in the case of crystalline and ordered materials.

Crystalline, ordered, and amorphous microporous and mesoporous materials, such as microporous and mesoporous molecular sieves, amorphous silica and alumina, active carbons, and other materials obtained by different techniques, are the source

of a collection of advanced materials with exceptional properties and applications in many fields such as optics, electronics, ionic conduction, ionic exchange, gas separation, membranes, coatings, catalysts, catalysts supports, sensors, pollution abatement, detergency, and biology.

This book is derived from some of the author's previous books, chapters of books, and papers. The author has tried to present a state-of-the-art description of some of the most important aspects of the **THEORY** and **PRACTICE** of adsorption and diffusion, fundamentally of gases in microporous crystalline, mesoporous ordered, and micro/mesoporous amorphous materials.

The adsorption process in multicomponent systems will not be discussed in this book with the exception of the final chapter, which analyzes adsorption from the liquid phase. Fundamentally, we are studying adsorption and diffusion from the point of view of materials science. That is, we are interested in the methods for the use of single-component adsorption and diffusion in the characterization of the adsorbent surface, pore volume, pore size distribution, and the study of the parameters characterizing single-component transport processes in porous systems. Also studied in the text are: adsorption energetic, adsorption thermodynamics, and dynamic adsorption in plug-flow bed reactors. The structure or morphology and the methods of synthesis and modification of silica, active carbons, zeolites and related materials, and mesoporous molecular sieves are discussed in the text as well. Other adsorbents normally used in different applications, such as alumina, titanium dioxide, magnesium oxide, clays, and pillared clays are not discussed.

From the point of view of the application of dynamic adsorption systems, the author will analyze the use of adsorbents to clean gas or liquid flows by the removal of a low-concentration impurity, applying a plug-flow adsorption reactor (PFAR) where the output of the operation of the PFAR is a breakthrough curve.

Finally, the book is dedicated to my family. It is also devoted to the advisors of my postgraduate studies and the mentors in my postdoctoral fellowships. In particular, I would like to recognize Dr. Professor Jürgen Büttner, advisor of my M.Sc. studies, who was the first to explain to me the importance of the physics and chemistry of surfaces in materials science. I would like also to acknowledge my senior Ph.D. tutor, the late Professor Alekzander A. Zhujovistskii, who, in 1934, was the first to recognize the complementary role of the adsorption field and capillary condensation in adsorption in porous materials and was later one of the creators of gas chromatography. He taught me how to "see" inside scientific data using general principles. Also, I wish to recognize my junior Ph.D. tutor, Professor Boris S. Bokstein, a well-know authority in the study of transport phenomena, who motivated me to study diffusion. I want, as well, to acknowledge the mentors of my postdoctoral fellowships, Professor Fritz Storbeck, who gave me the opportunity to be in contact with the most advanced methods of surface studies; Professor Evgenii D. Shchukin, one of the creators of a new science, physicochemical mechanics, who taught me the importance of surface phenomena in materials science; and the late academic Mijail M. Dubinin and Professor A.V. Kiseliov, two of the most important scientists in the field of adsorption science and technology during the last century. Both of

them gave me the opportunity to more deeply understand their philosophy of adsorption systems.

Professor Rolando M.A. Roque-Malherbe, Ph.D.
Las Piedras, Puerto Rico, USA

Author

Professor Rolando M.A. Roque-Malherbe was born in 1948 in Güines, Havana, Cuba. He finished his B.S. in physics at Havana University (1970), his specialization (M.S. equivalent degree) in surface physics in the National Center for Scientific Research–Technical University of Dresden, Germany (1972), and his Ph.D. in physics at the Moscow Institute of Steel and Alloys, Russia (1978). He completed postdoctoral stays at the Technical University of Dresden, Moscow State University, Technical University of Budapest, and the Institute of Physical Chemistry and Central Research Institute for Chemistry of the Russian and Hungarian Academies of Science (1978–1984). Professor Roque-Malherbe headed a research group in the National Center for Scientific Research–Higher Pedagogical Institute in Varona, Havana, Cuba (1980–1992), which is a world leader in the study and application of natural zeolites. In 1993, after a confrontation with the Cuban regime, he left Cuba with his family as a political refugee. From 1993 to 1999, he worked at the Institute of Chemical Technology, Valencia, Spain; Clark Atlanta University, Atlanta, Georgia; and Barry University, Miami, Florida. From 1999 to 2004 he was dean and full professor of the School of Science at Turabo University (TU), Gurabo, Puerto Rico, and currently is the Director of the Institute of Physico-Chemical Applied Research at TU. He has published 112 papers, 3 books, 5 chapters, 15 patents, 29 abstracts, and has given more than 200 presentations at scientific conferences. He is currently an American citizen.

Table of Contents

1 Statistical Mechanics

1.1 INTRODUCTION

Statistical mechanics, or statistical physics, also named statistical thermodynamics in equilibrium systems, was originated in the work of Maxwell and Boltzmann on the kinetics theory of gases (1860–1900) [1–11]. Later, in his book *Elementary Principles of Statistical Physics,* Gibbs (1902) made a major advance in the theory and methods of calculation. In the twentieth century, Einstein, Fermi, Bose, Tolman, Langmuir, Landau, Fowler, Guggenheim, Kubo, Hill, Bogoliubov, and others contributed to the subsequent development and fruitful application of statistical mechanics [1–11].

Statistical mechanics deals with macroscopic systems, which consist of a collection of particles, for example, photons, electrons, atoms, or molecules, with composition, structure, and function. In statistical mechanics the term state has two meanings: the microstate, or quantum state, and the macrostate, or thermodynamic state.

1.1.1 Thermodynamic Functions and Relationships

Statistical physics, as will be shown in the present chapter, is a very comprehensive methodology for the calculation, for example, of the thermodynamic functions characterizing a macroscopic system. The fundamental equation of thermodynamics for a bulk mixture (i.e., a number of components included in the same homogeneous phase is [1,2]:

$$dU = TdS - PdV + \sum_i \mu_i dn_i$$

where $U(S,V,n_i)$ is the internal energy of the system; S, its entropy; V, its volume; T, its temperature; μ_i, the chemical potentials; and n_i, the number of moles, of one of the N components which form the system.

Similarly, using the Legendre transformations (see Appendix 1.1), by which the product of the substituted variables, in the present case, TS will be subtracted:

$$F = U - TS$$

one gets a new thermodynamic function, in the present case, $F(T,V,n_i)$, the Helmholtz free energy.

At this point, an additional thermodynamic function, the enthalpy, could also be defined [1,2]:

$$H = U + PV.$$

After that, the Gibbs function, or free enthalpy, is also obtained, with the help of the Legendre transformation [1,2]:

$$G = H - TS$$

It is also possible to define the grand potential, or Massieu function [10]:

$$\Omega = F - \sum \mu_i n_i$$

Subsequently, the corresponding set of differential equations for a bulk mixture are [1,2,10]:

$$dF = -SdT - PdV + \sum_i \mu_i dn_i$$

$$d\Omega = -SdT - PdV - \sum_i n_i d\mu_i$$

$$dH = TdS - VdP + \sum_i \mu_i dn_i$$

$$dG = -SdT + VdP + \sum_i \mu_i dn_i$$

The grand potential, which is generally absent from textbooks on thermodynamics, has a particular meaning in statistical thermodynamics. It is the thermodynamic potential for a system with fixed volume, V, chemical potentials, μ_i, and temperature, T, and as will be later shown, is related to the grand canonical partition, which is one of the magnitudes calculated with the help of the methods of statistical thermodynamics.

Table 1.1 reports some thermodynamic relations [10].

1.2 DEFINITION OF MICROSTATE AND MACROSTATE

A **microstate** is defined as a state of the system where all the parameters of the component particles are specified [7]. In quantum mechanics, in a system in a stationary state the energy levels and the state of the particles in terms of quantum numbers are used to specify the parameters of a microstate. At any given time the

TABLE 1.1
Thermodynamic Relations

$T = \left(\frac{\partial U}{\partial S}\right)_{V,n_i}$	$-P = \left(\frac{\partial U}{\partial V}\right)_{S,n_i}$	$\mu_i = \left(\frac{\partial U}{\partial n_i}\right)_{S,V,n_j(j\neq i)}$
$-S = \left(\frac{\partial F}{\partial T}\right)_{V,n_i}$	$-P = \left(\frac{\partial F}{\partial V}\right)_{T,n_i}$	$\mu_i = \left(\frac{\partial F}{\partial n_i}\right)_{T,V,n_j(j\neq i)}$
$T = \left(\frac{\partial H}{\partial T}\right)_{P,n_i}$	$V = \left(\frac{\partial H}{\partial P}\right)_{S,n_i}$	$\mu_i = \left(\frac{\partial H}{\partial n_i}\right)_{S,P,n_j(j\neq i)}$
$-S = \left(\frac{\partial G}{\partial T}\right)_{P,n_i}$	$V = \left(\frac{\partial G}{\partial P}\right)_{T,n_i}$	$\mu_i = \left(\frac{\partial G}{\partial n_i}\right)_{T,P,n_j(j\neq i)}$
$-S = \left(\frac{\partial \Omega}{\partial T}\right)_{V,\mu_i}$	$-P = \left(\frac{\partial \Omega}{\partial P}\right)_{T,\mu_i}$	$-n_i = \left(\frac{\partial \Omega}{\partial \mu_i}\right)_{T,V,n_i(i\neq j)}$

system will be in a definite quantum state, *j,* characterized by a certain wave function, φ_j, which is a function of a huge number of spatial and spin coordinates, an energy, E_j, and a set of quantum numbers [7].

A **macrostate** is defined as a state of the system where the distribution of particles over the energy levels is specified [7]. The macrostate includes different energy levels and particles having particular energies. That is, it contains many microstates. However, following the principles of thermodynamics [1,2], it is known that, for a single component system, we only need to designate three macroscopic parameters, i.e., (*P,V,T*), (*P,V,N*), or (*E,V,N*), where *P is* pressure, *V is* volume, *T is* temperature, and *N* is the number of particles, in order to specify the thermodynamic state of an equilibrium single-component system. In this case, the equation of state for the system relates the three variables to a fourth. For example, for an ideal gas we have:

$$PV = nRT = NkT.$$

in which $R = 8.31451$ [$JK^{-1}mol^{-1}$] is the ideal gas constant, where $R = N_A k$, in which $N_A = 6.02214 \times 10^{23}$ [mol^{-1}] is the Avogadro number, and $k = 1.38066$ [JK^{-1}], is the Boltzmann constant.

In an ideal gas, we assume that the molecules are noninteracting, i.e., they do not affect each other's energy levels. Each particle possesses a certain energy, and at $T > 0$, the system possesses a total energy, E. From quantum mechanics, we know that the possible energies, if we consider the particles confined in a cubic box of volume, $V = abc$ (see Figure 1.1), are [8]:

$$E(n_1, n_2, n_3) = \frac{h^2}{8m}\left(\frac{n_1^2}{a^2} + \frac{n_2^2}{b^2} + \frac{n_3^2}{c^2}\right)$$

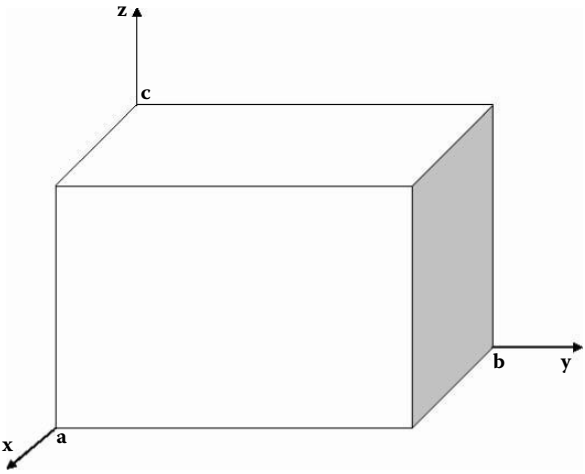

FIGURE 1.1 Box of volume $V = abc$, where the molecules of the ideal gas are confined.

For a square box where $a = b = c = L$,

$$E(n_1,n_2,n_3) = \frac{h^2}{8L^2m}(n_1^2 + n_2^2 + n_3^2) = \frac{h^2N^2}{8m}$$

where $N^2 = (n_1^2 + n_2^2 + n_3^2)$, and n_1, n_2, and n_3, are the quantum numbers, each of which could be any integer number except zero. Then, a macrostate of the ideal gas, with an energy:

$$\mathrm{E} = \sum_{n_1}\sum_{n_2}\sum_{n_3} E(n_1,n_2,n_3)$$

and N molecules, is compatible with a huge number of different (n_1, n_2, n_3) quantum numbers corresponding with different microstates. Therefore, a macrostate or thermodynamic state of a system is composed of, or is compatible with a huge number, Ω, of microstates or quantum states [7,8].

Finally it is necessary to state that the macrostate is experimentally observable, while the microstate is usually not observable.

1.3 DEFINITION OF ENSEMBLE

An ensemble is a hypothetical collection of an extremely high number of systems, each of which is in the same macrostate as the system of interest. These systems show a wide variety of microstates, each compatible with the given macrostate. That is, an ensemble is an imaginary collection of replications of the system of interest, where **N** is the number of systems in the ensemble, which is a very large number (that is, $\mathrm{N} \to \infty$) [7,8]. The number of systems in the ensemble, in a state with a

given energy, E_i, is denoted by n_i. Then the total number of systems in the ensemble can be calculated as:

$$\mathbf{N} = \sum_{i=1}^{\Omega} n_i,$$

and the summation is taken over all the Ω accessible E_i energy states allowable for the concrete system in study.

Now it is necessary to make some postulates in order to mathematically deal with the ensemble concept.

First Postulate: The measured time average of a macroscopic property in the system of interest is equal to the average value of that property in the ensemble [2,7]:

$$\overline{E} = \sum_{i=1}^{\Omega} p_i E_i \tag{1.1}$$

where p_i is the probability of finding the system in one of the Ω possible states or allowed states in the chosen thermodynamic macroscopic state, and the summation is taken over all the energy states allowable for the concrete system in study.

Second Postulate: The entropy is defined as [9]:

$$S = -k \sum_{i=1}^{\Omega} p_i \ln p_i \tag{1.2}$$

where p_i is the probability of finding the system in one of the Ω possible states or allowed states in the chosen thermodynamic macroscopic state, and k is the Boltzmann constant [2].

Third Postulate: For a thermodynamic system of fixed volume, composition, and temperature, all quantum states that have equal energy have equal probability of occurring.

Finally, it is necessary to state that, in statistical mechanics, for a closed system, the equilibrium state is the state with the maximum entropy, which is one of the statements of the Second Law of Thermodynamics [6].

1.4 THE CANONICAL ENSEMBLE

The canonical ensemble represents a system which is in a heat bath, at constant temperature and volume, and with a fixed number of particles, N [7,8]. That is, a system which is in thermal equilibrium with a large bath. Since energy can flow to and from the bath, the system is, as was previously stated, described by the bath temperature, T, rather than by a fixed energy, E [7,8]. Such a system, and the statistical method based on it, are referred to as a canonical ensemble.

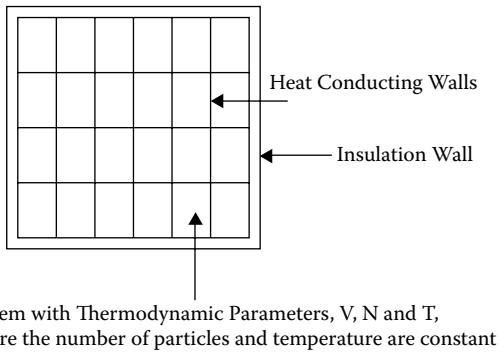

FIGURE 1.2 Representation of the canonical ensemble.

We represent the canonical ensemble as a collection of **N** systems, all in contact with each other and isolated from the rest of the universe [8] (see Figure 1.2). Consequently each system in the canonical ensemble is immersed in a bath consisting of the rest of the system replica and isolated [7,8].

The possible energy states of the systems in the ensemble are: $E_j = E_j(V, N)$. Since all the systems in the ensemble have the same volume, V, and number of particles, N, then all the systems in the ensemble have the same set of energy states [8]. The number of systems in the energy state, E_i, is n_i. Therefore, following the third postulate, the probability of select a system in the ensemble with energy E_i is [7]:

$$p_i = \frac{n_i}{\mathrm{N}} \tag{1.3}$$

where **N** is the whole number of systems in the canonical ensemble,

$$\sum_{i=1}^{\Omega} p_i = 1,$$

and the average energy of the systems in the ensemble is:

$$\overline{E} = \sum_{i=1}^{\Omega} p_i E_i$$

To calculate the probability distribution for the canonical ensemble, we only need to find the conditions for maximum entropy of the whole canonical ensemble system as expressed in Figure 1.2. In this scheme, the canonical ensemble is represented as a thermodynamic closed system composed of a collection of replicated systems enclosed by a wall, which do not allow the exchange of energy and matter

with the rest of the universe [7,8]. Therefore, based on the second postulate and the additive property of entropy, we need to calculate the maximum of [9]:

$$S = -k\mathrm{N}\sum_{i=1}^{\Omega} p_i \ln p_i$$

where the summation is taken over all the states allowable for the system under study. Then, the calculation of the maximum is under the following two conditions [8]:

$$\sum_{i=1}^{\Omega} n_i = \mathrm{N} \quad \text{and} \quad \sum_{i=1}^{\Omega} n_i E_i = \mathrm{E}$$

where **N** is the total number of systems in the ensemble, and E is the total energy of the ensemble. Now dividing by **N**:

$$S = -k\sum_{i=1}^{\Omega} p_i \ln p_i$$

under the following conditions:

$$\sum_{i=1}^{\Omega} p_i = 1 \quad \text{and} \quad \sum_{i=1}^{\Omega} p_i E_i = \overline{E}$$

where $\overline{E}$, is the average energy in a system of the ensemble. Now to apply the method of the Lagrange multipliers [12,13] (see Appendix 1.2) we must define the following auxiliary function [9]:

$$f = -k\sum_{i=1}^{\Omega} p_i \ln p_i + \alpha\sum_{i=1}^{\Omega} p_i + \beta\sum_{i=1}^{\Omega} p_i E_i \tag{1.4}$$

as a result, the maximum condition is:

$$\frac{\partial f}{\partial p_i} = -k \ln p_i + 1 - \alpha + \beta E_i p_i = 0$$

Thus:

$$p_i = \frac{\exp[-\beta E_i]}{Z} \tag{1.5}$$

and:

$$Z = \sum_{i=1}^{\Omega} \exp[-\beta E_i] \tag{1.6}$$

is the canonical partition function. Finally, to be definite it is necessary to state that the summations are carried out over all the allowable energy states of the system under study.

1.5 EVALUATION OF α AND β FOR THE CANONICAL ENSEMBLE

The Helmholtz energy, *F*, of a concrete system is defined by [8]:

$$F = U - TS \tag{1.7}$$

Then in the frame of statistical thermodynamics[1] [6–8],

$$\sum_{i=1}^{\Omega} p_i E_i = \overline{E} = U \tag{1.8}$$

is the internal energy of the system;

$$S = -k \sum_{i=1}^{\Omega} p_i \ln p_i \tag{1.9}$$

is its entropy; and T is its temperature. Consequently in the frame of the canonical ensemble, substituting Equation 1.5 in Equations 1.8 and 1.9, and then substituting in Equation 1.7 and using Equation 1.6, it is easy to show that:

$$S = k\beta U + k \ln Z \tag{1.10}$$

$$k\beta U - S = k \ln Z \tag{1.10a}$$

Consequently, if we take

$$\beta = \frac{1}{kT} \tag{1.11}$$

and

$$F = -kT \ln Z \tag{1.12}$$

[1] This statement could be considered as a postulate as well.

TABLE 1.2
Thermodynamic Parameters Calculated with the Help of the Canonical Partition Function

$$U = kT^2\left(\frac{\partial \ln Z}{\partial T}\right) \qquad P = kT\left(\frac{\partial \ln Z}{\partial V}\right) \qquad S = k\left[\ln Z + T\left(\frac{\partial \ln Z}{\partial T}\right)\right]$$

$$G = kT\left[-\ln Z + T\frac{\partial \ln Z}{\partial V}\right] \qquad H = kT\left[T\left(\frac{\partial \ln Z}{\partial T}\right) + V\frac{\partial \ln Z}{\partial V}\right] \qquad \mu_i = -kT\left(\frac{\partial \ln Z}{\partial n_i}\right)$$

it follows that Equation 1.10 will be equivalent to Equation 1.7. Subsequently, one can calculate all thermodynamics functions by the use of the partition function, since the Helmholtz free energy, F, could operate as a starting point (see Table 1.2) [8–10].

1.6 THE GRAND CANONICAL ENSEMBLE

The grand canonical ensemble represents a system that is in a heat bath, at constant temperature and volume, and with a variable number of particles *N*. That is, a system which is in thermal equilibrium with a large bath, with which it is possible to exchange particles. Since energy and particles can flow to and from the bath, the system is described by the bath temperature, T, and the chemical potential, μ [8]. Such a system, and the statistical method based on it, are referred to as a grand canonical ensemble (GCE).

To calculate the probability distribution for the grand canonical ensemble, as was previously stated in the case of the canonical ensemble, we need to find the state of maximum entropy of the whole grand canonical ensemble system. In Figure 1.3, the GCE is represented as a thermodynamically closed system composed of a collection of replicated systems enclosed by a wall, which do not allow the

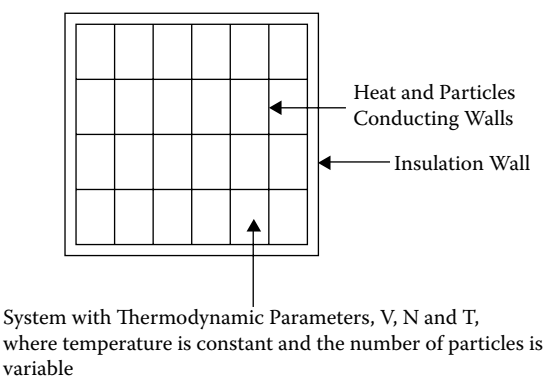

FIGURE 1.3 Representation of the grand canonical ensemble.

exchange of energy and matter with the rest of the universe. Therefore, based in the second postulate, we need to calculate the maximum of [9]:

$$S = -k\sum_{i=1}^{\Omega}\sum_{n=1}^{N} p_{i,n}\ln p_{i,n} \tag{1.13}$$

To be specific, it is essential to state that the summation is carried out over all the allowable energy states (i.e., from 1 to Ω) and for all the possible particle numbers (from 1 to N).

In the present case, the maximum is calculated under the following three conditions[1] [8]:

$$\sum_{i=1}^{\Omega}\sum_{j=1}^{N} p_{i,j} = 1 \tag{1.14a}$$

$$\sum_{i=1}^{\Omega}\sum_{j=1}^{N} E_i(V,j)p_{i,j} = \overline{E} \tag{1.14b}$$

and

$$\sum_{i=1}^{\Omega}\sum_{j=1}^{N} jp_{i,j} = \overline{N} \tag{1.14c}$$

where $\overline{E}$ and $\overline{N}$ are, respectively, the average energy and number of particles in a system of the ensemble.

At this point, in order to use the method of the Lagrange multipliers [12,13] (see Appendix 1.2) to calculate the maximum of the entropy, we must define the following auxiliary function [9]:

$$F = -k\sum_{i=1}^{\Omega}\sum_{j=1}^{N} p_{i,j}\ln p_{i,j} + \alpha\sum_{i=1}^{\Omega}\sum_{j=1}^{N} p_{i,j} + \beta\sum_{i=1}^{\Omega}\sum_{j=1}^{N} E_i(V,j)p_{i,j} + \gamma\sum_{i=1}^{\Omega}\sum_{j=1}^{N} np_{i,j} \tag{1.15}$$

therefore, the maximum condition is:

$$\frac{\partial f}{\partial p_{i,j}} = -k\ln p_{i,j} + 1 - \alpha + \beta E(V,j) + \gamma j = 0 \tag{1.16}$$

Consequently:

$$p_{i,j} = \frac{\exp[-\beta E_i(V,j)]\exp[-\gamma j]}{\Theta} \tag{1.17}$$

[1] The present case was divided by N, the number of systems in the ensemble with all the expressions in 1.14.

where:

$$\Theta = \sum_{i=1}^{\Omega}\sum_{j=1}^{N} \exp[-\beta E_i]\exp[-\gamma j] = \sum_{j=1}^{N} Z(j)\exp[-\gamma j] \tag{1.18}$$

is the grand canonical partition function, and $Z(n)$ is the canonical partition function of a system with j particles.

1.7 EVALUATION OF α, β, AND γ FOR THE GRAND CANONICAL ENSEMBLE

In the frame of thermodynamics, entropy could also be expressed for a concrete single component system by [9]:

$$S = \frac{U - \mu n + PV}{T} \tag{1.19}$$

From this equation it is possible to show that [1,2]:

$$TdS = dU + PdV - \mu dn \tag{1.20}$$

where $U = \bar{E}$ is the internal energy of the system or average energy; T, its temperature; S, its entropy; P, the pressure; V, the volume; μ, the chemical potential; and

$$n = \frac{\overline{N}}{N_A},$$

the average number of moles.

In the framework of the grand canonical ensemble, differentiating Equation 1.14b [8]:

$$d\bar{E} = dU = \sum_{i=1}^{\Omega}\sum_{j=1}^{N} E_i(V,j)dp_{i,j} + \sum_{i=1}^{\Omega}\sum_{j=1}^{N} p_{i.j}dE(V,j) \tag{1.21}$$

If we now substitute Equation 1.17 in Equation 1.21, we obtain:

$$d\bar{E} = -\frac{1}{\beta}\left\{\sum_{jN}[\gamma N + \ln p_{jN} + \ln\Theta]dp_{jn}\right\} + \sum_{jN} p_{jN}\frac{\partial E(V,N)_j}{\partial V}dV \tag{1.22}$$

Using Equation 1.14c, it is easy to show that [8]:

$$d\overline{N} = \sum_{i,j} j dp_{jn} \tag{1.23}$$

since Equation 1.22 could be simplified to [8]:

$$d\overline{E} + pdV + \frac{\gamma}{\beta} d\overline{N} = -\frac{1}{\beta} d\left\{ \sum_{jN} [p_{,j} \ln p_{i,j}] \right\} \tag{1.24}$$

If we now compare Equation 1.20 and Equation 1.24, it is possible to show that:

$$\mu = -\frac{\gamma}{\beta} \tag{1.25}$$

and

$$TdS = -\frac{1}{\beta} d\left\{ \sum_{i,j} [p_{i,j} \ln p_{i,j}] \right\} \tag{1.26}$$

Consequently if:

$$\beta = \frac{1}{kT} \tag{1.27a}$$

and

$$\gamma = -\frac{\mu}{kT} \tag{1.27b}$$

substituting Equations 1.27a and 1.27b in Equation 1.13 and applying Equation 1.19, we will get [8,9]:

$$S = \frac{\overline{E}}{T} - \frac{N\mu}{T} + k \ln \Theta = \frac{U}{T} - \frac{N\mu}{T} + \frac{PV}{T} \tag{1.28}$$

Hence:

$$P = kT \left(\frac{\partial \ln \Theta(V,T,\mu)}{\partial V} \right)_{\mu,T} \tag{1.29a}$$

and

$$\overline{N} = kT\left(\frac{\partial \ln \Theta(V,T,\mu)}{\partial \mu}\right)_{V,T} \tag{1.29b}$$

1.8 CANONICAL PARTITION FUNCTION FOR A SYSTEM OF NONINTERACTING PARTICLES

Once the system's canonical partition function, *Z,* has been calculated, by the summation of

$$\exp\left[-\frac{E_i}{kT}\right],$$

over all the possible Ω accessible quantum states of the system, then all the thermodynamic properties of the system are readily established. However, the existence of forces between the molecules composing the system in study make *Z* extremely difficult to evaluate. Nevertheless, for a system with no intermolecular forces we can relatively easily evaluate *Z.*

Let the Hamiltonian operator, $\overline{H}$, for such a system without interactions between the constituent molecules be the sum of separate terms for individual molecules with no interaction terms between molecules [1,2]:

$$\overline{H} = \sum_{j=1}^{N} \overline{H}_j \tag{1.30}$$

where $j = 1$ to $N,$ in which N is the number of molecules. Then the energy of the whole system is:

$$E_j = \varepsilon_{1,r} + \varepsilon_{2,s} + \ldots + \varepsilon_{N,w} \tag{1.31}$$

and

$$Z = \sum_j \exp \frac{-[\varepsilon_{1,r} + \varepsilon_{2,s} + \ldots + \varepsilon_{N,w}]}{kT} \tag{1.32}$$

The allowed energies for the single molecule are [1,2]:

$$\overline{H}_j \varphi_{j,r} = \varepsilon_{j,r} \varphi_{j,r} \tag{1.33}$$

If the molecules are distinguishable from one another, by being confined to different locations in space as, for example, occur in a crystal, or in a system of localized adsorption, then the sum over all possible quantum states of the system is [1,2]:

$$Z = \sum_r \sum_s \sum_l \cdots \sum_w \exp\frac{-[\varepsilon_{1,r}]}{kT} \exp\frac{-[\varepsilon_{2,s}]}{kT} \exp\frac{-[\varepsilon_{3,l}]}{kT} \cdots \exp\frac{-[\varepsilon_{N,w}]}{kT}$$

then:

$$Z = \sum_r \exp\frac{-[\varepsilon_{1,r}]}{kT} . \sum_s \exp\frac{-[\varepsilon_{2,s}]}{kT} . \sum_l \exp\frac{-[\varepsilon_{3,l}]}{kT} \cdots \sum_w \exp\frac{-[\varepsilon_{N,w}]}{kT}$$

We can now define the molecular partition function as [1,2,8]:

$$Z_i = \sum_r \exp\frac{-[\varepsilon_{i,r}]}{kT}. \tag{1.34}$$

Consequently, for a system of distinguishable molecules [1,2,8]:

$$Z = \prod_i Z_i. \tag{1.35}$$

Now if all the molecules happen to be of the same kind, then $Z_1 = Z_2 = \ldots = Z_N = q$ [1,2,8]; then:

$$Z = q^N. \tag{1.36}$$

If the molecules are identical and are restricted to be in a specific zone of space as, for example, an ideal gas, or an adsorption mobile system, then the molecules are nonlocalized, and there is no way to distinguish one molecule from the other. Therefore, a situation where molecule **1** is in state **r** and molecule **2** is in state **s** is the same as molecule **1** is in state **s** and molecule **2** in state **r**. The situation previously described could be expressed in terms of quantum mechanics as [1,2,8]:

$$\varphi_r(1)\varphi_s(2)\varphi_l(3)\ldots\varphi_w(N) = \varphi_s(1)\varphi_r(2)\varphi_r(3)\ldots\varphi_r(N). \tag{1.37}$$

Consequently, if we permute the molecules, 1,2,3, …, *N,* among all the possible molecular states *r,s,l, …, w,* we will obtain identical wave functions. As is shown in Appendix 1.3, the number of permutations of *N* objects is *N!* [12]. Consequently, the correct value for Z for a system of N noninteracting indistinguishable molecules is [1,2,8]:

$$Z = \frac{q^N}{N!} \tag{1.38}$$

1.9 FACTORIZATION OF THE MOLECULAR PARTITION FUNCTION

The energy of a molecule is the sum of different contributions from the motion of its different degrees of freedom, such as translation, *T*, rotation, *R*, vibration, *V*, and the electronic contribution, *E*; therefore [1,2]:

$$\varepsilon_i = \varepsilon_i^T + \varepsilon_i^R + \varepsilon_i^V + \varepsilon_i^E \tag{1.39}$$

Given that the molecular energy is a sum of independent contributions, then the molecular, or particle partition function could be factorized into a product of different contributions [1,2,8]:

$$q = \sum_i \exp\frac{-[\varepsilon_i]}{kT} = \sum_i \frac{-[\varepsilon_i^T + \varepsilon_i^R + \varepsilon_i^V + \varepsilon_i^E]}{kT}$$

As a result [1,2,8]:

$$q = \sum_i \exp\frac{-[\varepsilon_i^T]}{kT}.\sum_i \exp\frac{-[\varepsilon_i^R]}{kT}.\sum_i \exp\frac{-[\varepsilon_i^V]}{kT}.\sum_i \exp\frac{-[\varepsilon_i^E]}{kT} = q^T q^R q^V q^E$$

where [1,2,7,8]:

$$q^T = \sum_i \exp\frac{-[\varepsilon_i^T]}{kT}. = \frac{V(2\pi mkT)^{3/2}}{h^3} \tag{1.40}$$

is the translational partition function, where h is the Planck constant, m is the mass of the molecule, k is the Boltzmann constant, and T is the absolute temperature. Besides [1,2,7,8]:

$$q^R = \sum_i \exp\frac{-[\varepsilon_i^R]}{kT} = \frac{IkT}{h^2} \tag{1.41a}$$

is the rotational partition function for a two-atom homonuclear rotor molecule, where I is the rotor moment of inertia. A two-particle rotor consists of particles of mass m constrained to remain a fixed distance from each of them [1,2]. For an N-atomic molecule with three axes of rotation, the rotational partition function is [10]:

$$q^R = \frac{\pi^{1/2}}{\sigma_\sigma}\prod_i^{3N-6}\left(\frac{8\pi^2 I_i kT}{h^2}\right)^{1/2} \tag{1.41b}$$

which is valid for $T >> \theta_i$, and where r is the symmetry number, I_i are the moments of inertia, and:

$$\theta_i = \frac{8\pi^2 I_i k}{h^2}$$

Furthermore, [1,2,8,10]:

$$q^V = \sum_i \exp\frac{-[\varepsilon_i^V]}{kT} = \frac{1}{1-\exp[-\theta_V/kT]} \tag{1.42}$$

is the vibrational partition function for a molecular vibration mode. In a polyatomic molecule, each vibrational mode will have its own partition function, and the overall partition function is [1,2,8]:

$$q^V = q^V(1)q^V(2)q^V(3)\ldots q^V(r)$$

where $q^V(r)$ is the partition function for the r normal vibration mode. Finally, it is necessary to state that:

$$\theta_V = \frac{hf}{k}$$

is the characteristic vibration temperature, where h is the Planck constant, k is the Boltzmann constant, and f is the characteristic frequency of vibration of the concrete mode of vibration.

Finally:

$$q^E = \sum_i \exp\frac{-[\varepsilon_i^E]}{kT} = 1 \tag{1.43}$$

is the electronic partition function which is normally equal to one.

Components of the molecular partition function are summarized in Table 1.3.

1.10 DENSITY FUNCTIONAL THEORY (DFT)

The present methodology is based fundamentally on the work of Hohemberg, Kohn, and Sham [14,15], who developed a methodology for the calculation of the ground-state electron probability density, $\rho(\bar{r})$, in quantum systems such as atoms and molecules. Hohemberg and Kohn [14] proved a theorem that states that the ground energy and all other properties of a ground state molecule are uniquely determined

TABLE 1.3
Components of the Molecular Partition Function

$q^T = \frac{V(2\pi mkT)^{3/2}}{h^3}$	$q^R = \frac{IkT}{h^2}$
$q^V = \frac{1}{1-\exp[-\theta_V/kT]}$	$q^E = \sum_i \exp\frac{-[\varepsilon_i^E]}{kT} = 1$

by the ground state electron probability density of the system. Therefore, E_{gs} is a functional of ρ, that is [2]:

$$E_{gs} = E_{gs}[\rho(\bar{r})]$$

where the brackets indicates a functional relation [12,13] (see Appendix 1.4).

The basic variable in density functional theory (DFT), applied to an N-particle classical system, is the single-particle density, $\rho(\bar{r})$, which is defined for an N-particle system by integrating the N-particle distribution function, $P(\bar{r}_1,\bar{r}_2,\ldots\bar{r}_N)$, over N–1 variables [16]:

$$\rho(\bar{r}_1) = N\int\ldots\int d\bar{r}_2.d\bar{r}_3\ldots d\bar{r}_N P(\bar{r}_1,\bar{r}_2,\ldots\bar{r}_N)$$

and represents locally the number of particles per unit volume. Thus integrating, the total number N is [16]:

$$\int_V \rho(\bar{r})d\bar{r} = N$$

This concept of single-particle density is valid for both quantum systems, such as atoms and molecules, and classical many-particle systems [14,16] like a fluid immersed in an external potential, which is the case of interest here. For a classical system of N atoms, the Hamiltonian is:

$$H_N = \sum_{i=1}^{N}\frac{p_i^2}{2m} + \Phi(\bar{r}_1,\bar{r}_2\ldots\bar{r}_N) + \sum_{i=1}^{N} U_{ext}^i(\bar{r}_i)$$

$$H_N = K.E. + \Phi + U_{ext}$$

where p_i is the momentum of particle i, $\Phi(\bar{r}_1,\bar{r}_2\ldots\bar{r}_N)$, is the total interatomic potential energy, and U_{ext}^i, is the one-body external potential. In the second equality, K.E. is

the kinetic energy, Φ is again the total interatomic potential energy of the system of N particles, and [17]:

$$U_{ext} = \sum_{i=1}^{N} U_{ext}^{i}(\bar{r}_i).$$

Now, $P_N(H_N)$, the probability of finding the system in one of the possible states allowed to the classical system, included in the grand canonical ensemble (GCE), is expressed as follows [17]:

$$P_N(H_N) = \frac{\exp[-\beta H_N]\exp[-\gamma N]}{\Theta}$$

where $\beta = 1/kT$, $\gamma = -\mu/kT$, and Θ is the grand canonical partition function.

In the frame of the density functional theory, $P_N(H_N)$, must be considered as a unique functional of $\bar{\rho}(\bar{r})$, the equilibrium single-particle density, i.e., $P_N(H_N) = P_N[\bar{\rho}(\bar{r})]$. Since $P_N(H_N)$, is a functional of the single-particle density, then in the frame of the density functional theory, all the functions describing the GCE could be expressed as functionals of $\bar{\rho}(\bar{r})$. Since all the thermodynamic functions of the system could be obtained with the help of $P_N(H_N)$, then they must be dependent of the equilibrium single-particle density [17]. In this way, we could define the intrinsic Helmholtz free energy, which is the Helmholtz free energy of the classical system of interests, but with the exclusion of the external field interaction, as [17]:

$$F[\bar{\rho}(\bar{r})] = \overline{K.E. + \Phi + kT \ln P_N}$$

where $\overline{K.E. + \Phi + kT \ln P_N}$, means average in the GCE. This definition is related with the rest of thermodynamics functions for the GCE, since as we know:

$$\overline{kT \ln P_N(H_N)} = -TS = n\mu - \bar{E} - kT \ln \Theta.$$

See Equation 1.28 and the definition of entropy in the GCE: $S = -k\overline{\ln P_N(H_N)}$ in Section 1.7.

Consequently, for a many-particle classical system immersed in an external potential, U_{ext}, arising, for instance, from the adsorption field happening when a fluid is confined in a pore, a function, $\Omega[\rho(\bar{r})]$, which reduces to the grand potential $\Omega = \Omega[\bar{\rho}(\bar{r})]$, when $\rho(\bar{r}) = \bar{\rho}(\bar{r})$, the equilibrium density, can be expressed with the help of the following unique functional of the density [16–18]:

$$\Omega[\rho(\bar{r})] = F[\rho(\bar{r})] - \int d\bar{r}\rho(\bar{r})[\mu - U_{ext}(\bar{r})] \qquad (1.44a)$$

which is obtained by means of a Legendre transformation [12] (see Appendix 1.1) of F [$\rho(\bar{r})$], which is the intrinsic Helmholtz free energy [17], and μ, the chemical potential of the studied system. To simplify Equation 1.44, it will now be defined:

$$u(\bar{r}) = \mu - U_{ext}(\bar{r}) \tag{1.44b}$$

and then:

$$\Omega[\rho(\bar{r})] = F[\rho(\bar{r})] - \int d\bar{r}\rho(\bar{r})u(r) \tag{1.45}$$

For a thermodynamic system of N classical particles, the true equilibrium density, $\bar{\rho}(\bar{r})$, is determined with the help of the Euler-Lagrange equation (see Appendix 1.4) [13,19]; that is, we must determine the minimum value of the functional $\Omega[\rho(\bar{r})]$. That is, the equilibrium density is those functions which made the functional $\Omega[\rho(\bar{r})]$ a minimum, so that we have:

$$\frac{\delta\Omega[\rho(\bar{r})]}{\delta\rho(\bar{r})} = 0 \tag{1.46}$$

i.e., $\bar{\rho}(\bar{r})$, is the solution of Equation 1.46, where

$$\frac{\delta}{\delta\rho(\bar{r})}$$

indicates the functional derivative (see Appendix 1.4). Now, combining Equations 1.44 and 1.46, we will obtain [17]

$$u(\bar{r}) = \mu - U_{ext}(\bar{r}) = \frac{\delta F[\rho(\bar{r})]}{\delta\rho(\bar{r})} \tag{1.47}$$

which is also the minimum condition, that is, the condition which will allow us to determine the equilibrium density. So the solution of Equation 1.47 is $\bar{\rho}(\bar{r})$, the equilibrium density distribution.

For a classical fluid with inhomogeneous density distribution, the functional, F [$\rho(\bar{r})$], representing the intrinsic Helmholtz free energy can be expressed as [16,18]:

$$F[\rho(\bar{r})] = F_{id}[\rho(\bar{r})] + F_{ex}[\rho(\bar{r})] \tag{1.48}$$

where:

$$F_{id}[\rho(\bar{r})] = \left[\int d\bar{r}\rho(\bar{r})\left\{\ln\left(\rho(\bar{r})\Lambda^3\right) - 1\right\}\right]kT \tag{1.49}$$

is the ideal-gas free energy functional, resulting from a system of noninteracting particles, where [1]:

$$\Lambda = \left(\frac{h^2}{2\pi mkT} \right)^{1/2}$$

is the thermal wavelength. $F_{ex}[\rho]$ represents the excess free energy for the classical system and is analogous to the interaction energy functional in the case of electronic quantum systems [2,16].

Now defining [16,17]:

$$c^1(\bar{r}) = \frac{\delta[\beta F_{ex}(\rho(\bar{r})]}{\delta\rho(\bar{r})} \tag{1.50}$$

from the variational principle, Equation 1.46, for the classical system of N particles, it follows that the equilibrium density satisfies [16,17]:

$$\rho(\bar{r}) = \Lambda^{-3}[\exp(\beta\mu)]\left[\exp-\left(\beta U_{ext} + c^1\left(\bar{r}, \rho(\bar{r})\right)\right)\right] \tag{1.51}$$

where $c^1(\bar{r})$ is also a functional of $\rho(\bar{r})$. This equation, when $c^1(\bar{r}) = 0$ (i.e., in the case of an ideal gas), reduces to the barometric law for the density distribution in the presence of an external field [7].

To proceed further, the excess intrinsic Helmholtz energy is split into contributions from the short-ranged repulsion and long-term attraction [18]:

$$\mathrm{F_{ex}}\ [\rho(\bar{r})] = F_{rep}[\rho(\bar{r})] + F_{att}[\rho(\bar{r})]$$

Details about this procedure will be given in Chapter 4.

1.11 THERMODYNAMICS OF IRREVERSIBLE PROCESSES

Let us provide now a brief summary of thermodynamics and statistical mechanics of irreversible processes [20–25]. To be definite and keep the exposition in a simple form, we will only consider the linear terms in all the equations describing the irreversible processes.

In an irreversible process, in conformity with the Second Law of Thermodynamics, the quantity that rules the time dependence of an isolated thermodynamic system is the entropy, S [6]. Only processes in the systems which lead to an increase in entropy are feasible. So the necessary and sufficient condition for a stable state in an isolated system is that the entropy has attained its maximum value [6]. Consequently, the most probable state is that in which the entropy is a maximum [6,7]. Irreversible processes are driven by generalized forces, X, and are characterized by

transport, or Onsager phenomenological coefficients, L [20–25]. The transport coefficients, L_{ij}, are defined by linear relations between the generalized flux densities, J_{iR}, which are the rates of change with time of state variables and the corresponding generalized forces X_i:

$$J_k = -\sum_{i=1}^{N} L_{ki} X_i \tag{1.52}$$

where the Onsager reciprocity relations, which are related with the principle of time reversal symmetry in mechanics: $L_{ij} = L_{ji}$, are valid. It is postulated that the rate of entropy production per unit volume, due to internal processes, may be expressed as:

$$\frac{ds}{dt} = -\sum_{i=1}^{N} J_i X_i \tag{1.53}$$

where s denote the specific value of S per unit volume of the system.

Familiar examples of the relation between generalized fluxes and forces are Fick's first law of diffusion, Fourier's law of heat transfer, Ohm's law of electricity conduction, and Newton's law of momentum transfer in a viscous flow.

Since diffusion means molecular, or in general, particle transport caused by a gradient of concentration (in more rigorous terms, this is a gradient of chemical potential), then Fick's first law can be expressed as [26–28]:

$$\bar{J} = -D\bar{\nabla}C \tag{1.54a}$$

where $\bar{J}$,is the matter flux, $\bar{\nabla}C$ is the concentration gradient, and D is the Fickean diffusion coefficient, or transport diffusion coefficient, which is the proportionality constant. The units of the above described parameters are: D [(longitude)^2/time], C [moles/volume], and J [moles/area·time]. In the International System (SI) the unit of D is [m^2/s], for the concentration, C could be expressed in [mol/m^3], and in this case the flux is expressed in [mol/m^2·s].

Now it is necessary to affirm that the flux, and therefore also the diffusion coefficient, has to be chosen relative to a frame of reference, since the diffusion flux, $\bar{J}$, gives the number of species crossing a unit area, fixed relative to the local center of mass, per unit of time [28].

Fick's second law:

$$\frac{\partial C}{\partial t} = -D\nabla^2 C \tag{1.54b}$$

is an expression of the law of conservation of matter, i.e.,

$$\frac{\partial C}{\partial t} = -D\bar{\nabla}\cdot\bar{J}$$

As was previously stated, the real driving force of mass transport is the gradient of chemical potential, in this sense in the absence of an external Newtonian force like those exerted in a charged species by an electric field, it is expresses as:

$$X_i = \bar{\nabla}\left(\frac{\mu_i}{T}\right) \tag{1.55}$$

for the transport of the type of particles, *i.*

On the other hand, heat conductivity means transfer of energy caused by temperature gradients. The Fourier law of heat transfer is expressed as:

$$\bar{Q} = -\kappa\bar{\nabla}T \tag{1.56}$$

where $\bar{Q}$ is the energy flux, $\bar{\nabla}T$ is the temperature gradient, and κ is the thermal conductance coefficient, which is the proportionality constant. In terms of the thermodynamics of irreversible processes, the generalized force for the energy flux is:

$$X_q = -\bar{\nabla}\frac{1}{T} = \frac{\nabla T}{T^2}. \tag{1.57}$$

Thus, for a problem with interest for us in the present book, i.e., single-component diffusion in an adsorbent under conditions of nonuniform temperature [27]:

$$J = -L_p\bar{\nabla}\left(\frac{\mu}{T}\right) - L_c\left(\frac{1}{T^2}\right)\nabla T$$

$$Q = -L_c\bar{\nabla}\left(\frac{\mu}{T}\right) - L_e\left(\frac{1}{T^2}\right)\nabla T$$

where L_p and L_e are the transport coefficients related with particle transport and energy transfer, respectively. L_c is the cross coefficient, which is only one because of the reciprocity relations. Since normally in adsorption systems, the energy transfer is faster than diffusion, the transport process of matter in an adsorbent may be considered an isothermal process, in this case for single-component diffusion under isothermal conditions in a porous adsorbent [27]:

$$J = -L\bar{\nabla}(\mu) \tag{1.58}$$

where $L = L_p/T$.

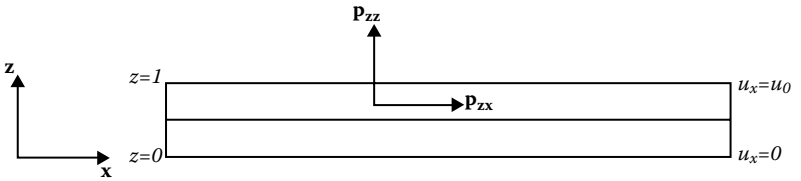

FIGURE 1.4 Viscous fluid flowing in the x direction.

This expression reduces to:

$$J = -L\frac{\partial \mu}{\partial x} = -D_0\left(\frac{\partial \ln P}{\partial \ln C}\right)\left(\frac{\partial C}{\partial x}\right) \tag{1.59}$$

If it is substituted, the following expression for the chemical potential [1,2]:

$$\mu = \mu^0 + RT \ln P$$

considers unidimensional diffusion.

Another relation between generalized fluxes and forces which is interesting for the purpose of the present monograph is the Newton's law of momentum transfer in a viscous flow. In this sense (see Figure 1.4), it is possible to express the transfer of momentum caused by a gradient of velocity in a viscous flow by [7]:

$$p_{zx} = -\eta\frac{\partial u_x}{\partial z} \tag{1.60}$$

where p_{zx} is the tangential force per unit area, or stress, between two parallel layers of the viscous flow, i.e., the index, *z,* indicates the orientation of the plane that is perpendicular to axis *z,* and the second index, *x,* designates the component of the force exerted across this plane, $\partial u_x/\partial z$ is the velocity gradient, and η, is the dynamic viscosity measured in [Pa·s].

Figure 1.4 shows a situation where the velocity of the layer of fluid adjacent to the plane located at z = 0, perpendicular to the z axis, is $u_x = 0$. The velocity of the layer of fluid placed at $z = l$ is $u_x = u_0$, that is, this reflects the existence of a velocity gradient, $\partial u_x/\partial z$.

1.12 STATISTICAL MECHANICS OF IRREVERSIBLE PROCESSES

Until the middle of the twentieth century, the typical way of calculating the response of a system to external perturbations consisted of trying the solution of the complete

dynamical equations of motion, such as the Liouville equation or the Boltzmann equation, incorporating the perturbation into the system Hamiltonian or evolution matrix. However, about fifty years ago Kubo [29,30] and others [29,31–34] introduced simplifications which are based in the possibility of the description of the effect of external perturbations in terms of a system's own correlation functions [25].

As was previously demonstrated, all the information to calculate the thermodynamic properties of macroscopic systems is included in the partition function or in the probability distribution function [6–8]. However, the probability distribution also contains nonthermodynamic information. Macroscopic magnitudes, such as the fluctuations of the thermodynamic magnitudes, and also the kinetics coefficients that characterize the linear response of a system to an external perturbation, such as the temperature gradient, the chemical potential gradient, the electric field, and others, could be calculated with the help of the correlation functions.

An external perturbation destroys the state of thermodynamic equilibrium of a system. This fact is expressed in the appearance of, for example, fluxes of energy, matter, electricity, and momentum, or in the time variation of the internal parameters of the system, such as polarization, magnetization, and other parameters. If the external perturbation is weak enough, then the departure of the system from the equilibrium state will be small, and consequently the system response will be linear, i.e., the system response will linearly depend on the perturbation.

This linear relation between the system response and the perturbation could be characterized by a set of kinetic coefficients, such as the diffusion coefficient, the thermal and electric conductivities, the electric and magnetic susceptibilities, and other coefficients. These coefficients normally depend on temperature, the external parameters, and the frequency of variation of the perturbation. The central result of the theory developed by Kubo and others [30–34] is that the kinetic coefficients could be calculated with the help of the correlation functions

1.12.1 Correlation Functions and Generalized Susceptibilities

Here will be considered a classical systems described in the, Γ-space, by the phase space coordinates, $q(t)$ and $p(t)$ [6], where:

$$q(t) = \{q_1, q_2, \ldots q_f\}, \text{ and } p(t) = \{p_1, p_2, \ldots p_f\}$$

where *f,* the number of degrees of freedom, is the number of generalized coordinates and momenta needed to describe the system [35]. If we now define two functions of the phase space coordinates [10]:

$$A\{q(t), p(t)\} = A(q,p,t) = A(t)$$

$$B\{q(t), p(t)\} = B(q,p,t) = B(t)$$

it is possible to define the time correlation functions $K_{AB}(t)$ by [5–7,10,24,25]:

$$K_{AB}(t) = \left\langle A(t)B(0)\right\rangle_{\Gamma} = \int \ldots \int A(q,p,t)B(q,p,0)\rho(q,p)dqdp \tag{1.61}$$

using the ensemble average in the Γ-space, with the equilibrium phase space density $\rho(q,p)$, which is the classical equilibrium distribution function in the phase space [6]. The obtained correlation function only depends on the time difference, t [7], since the ensemble average is taken in the equilibrium situation, where the distribution of systems in the ensemble is independent of the absolute value of time [7–10,24,25].

Assuming $A = B$, it is possible to define the autocorrelation function [5–7,10,25]

$$K_{AA}(t) = \langle A(t)A(0)\rangle_{\Gamma} = \int \ldots \int A(q,p,t)A(q,p,0)\rho(q,p)dqdp \tag{1.62}$$

Among the properties of the autocorrelation function is included the symmetry property, which could be expressed as [7]:

$$K_{AA}(t) = K_{AA}(-t) \tag{1.63}$$

One autocorrelation function of interest for the aims of the present book is the function $A(t) = v(t)$, where $v(t)$ is the velocity [10]

$$K_{vv}(t) = \langle v(t)v(0)\rangle = \int \ldots \int v(q,p,t)v(q,p,0)\rho(q,p)dqdp \tag{1.64}$$

As will be demonstrated later, it will help to calculate the self-diffusion coefficient and the Einstein relation [10,24], applying the generalized susceptibilities, which can be expressed as Fourier transforms of the correlation functions [6,7,10, 23–25]:

$$\sigma(\omega) = \int_0^{\infty} \exp(-i\omega t)\left\langle \dot{A}(t)\dot{B}(0)\right\rangle dt \tag{1.65}$$

For $\dot{A}(t) = \dot{B}(t)$ we will get the Fourier transforms of the autocorrelation functions [10,24]:

$$\sigma(\omega) = \int_0^{\infty} \exp(-i\omega t)\left\langle \dot{A}(t)\dot{A}(0)\right\rangle dt \tag{1.66}$$

For $\omega = 0$:

$$\sigma(0) = \int_0^{\infty} \left\langle \dot{A}(t)\dot{B}(0)\right\rangle dt \tag{1.67}$$

In the long-time limit, i.e., for $t \to \infty$, for the autocorrelation function [10,24]:

$$2t\sigma(0) = \left\langle [A(t) - A(0)]^2 \right\rangle \tag{1.68}$$

1.12.2 Calculation of the Mean Square Displacement and the Self-Diffusion Coefficient

1.12.2.1 Calculation of the Mean Square Displacement with the Help of the Velocity Autocorrelation Function

As an illustration of the utilization of the correlation functions, let us now calculate the mean square displacement, $\langle x^2(t) \rangle$, of the particle in time. We will consider here the situation where the system is in equilibrium in the absence of external forces [7]. Let $x(0) = 0$, at $t = 0$; then since $\dot{x} = v$, one has:

$$x(t) = \int_0^t v(\tau) d\tau \tag{1.69}$$

Then:

$$\left\langle x^2(t) \right\rangle = \left\langle \int_0^t v(\tau) d\tau \int_0^t v(\tau') d(\tau') \right\rangle = \int_0^t d\tau \int_0^t d(\tau') \left\langle v(\tau) v(\tau') \right\rangle \tag{1.70}$$

As we know, the velocity autocorrelation function, $\langle v(\tau) v(\tau') \rangle$, is dependent only on the time difference, $s = \tau' - \tau$; therefore:

$$\left\langle v(\tau) v(\tau') \right\rangle = \left\langle v(0) v(s) \right\rangle = K_v(s) \tag{1.71}$$

Now changing the integration limits:

$$\left\langle x^2(t) \right\rangle = \int_0^t ds \int_0^{t-s} d\tau K_v(s) + \int_{-t}^0 ds \int_{-s}^t d\tau K_v(s) = \int_0^t ds K_v(s)(t-s) + \int_{-t}^0 ds K_v(s)(t+s)$$

If we now put $s \to -s$ in the second integral and use the symmetry property of the autocorrelation function: $K_v(s) = K_v(-s)$, then [7]:

$$\left\langle x^2(t) \right\rangle = 2 \int_0^t ds (t-s) \left\langle v(0) v(s) \right\rangle \tag{1.72}$$

In the long-time limit, i.e., for $t \to \infty$, we will have $t >> s$, and consequently we will get:

$$\lim_{t\to\infty} \left\langle x^2(t) \right\rangle = 2t \int_0^t ds \left\langle v(0)v(s) \right\rangle \tag{1.73}$$

1.12.2.2 Langevin's Brownian Motion Model

An adequately small macroscopic particle immersed in a liquid shows a random type of motion called Brownian motion. In general, we designate by Brownian motion the movement of a particle arising from thermal agitation, i.e., the movement of small macroscopic particles, molecules, or atoms [36,37]. Consequently, there are a diversity of significant physical phenomena which are essentially analogous to Brownian motion. Therefore, this phenomenon could operate as a sample problem, whose study offers significant insight into the mechanism responsible for the analyzed problem [5,7,38]. The first theory explaining Brownian motion was developed by Einstein in 1905 [36]. Later, Langevin created another model to explain this phenomenon [37].

For the sake of simplicity, the problem will be treated here in one dimension, considering a particle of mass m, whose center of mass coordinate is located at $x(t)$ at time t, and whose velocity and acceleration are $v = \dot{x} = dx/dt$, and $a = \dot{v} = dv/dt$, respectively, where the particle is immersed in a liquid at temperature, T. Subsequently, the Langevin model is based on an expression of Newton's second law of motion [5,7]:

$$m\dot{v} = \Gamma(t) + F_{ext} - \alpha v = F(t) - \alpha v \tag{1.74}$$

where F_{ext} represents the external forces acting on the moving particle, the αv term accounts for drag forces, and the function $\Gamma(t)$ is a stochastic noise term which accounts for random collisions with the liquid at temperature T, and then $F(t) = \Gamma(t) + F_{ext}$.

The function $\Gamma(t)$ is truly a white noise, so that:

$$\left\langle \Gamma(t) \right\rangle = 0 \tag{1.75a}$$

and:

$$\left\langle \Gamma(t)\Gamma(\tau + s) \right\rangle = q\delta(s) \tag{1.75b}$$

We will now consider that the system is in the state of equilibrium, where $\langle x \rangle = 0$, because there is no preferred direction in space [7]. Now we will calculate the mean square displacement, i.e., $\langle x^2 \rangle$. Since $v = \dot{x} = dx/dt$ and $a = \dot{v} = dv/dt$, then multiplying Equation 1.74 by x, we will get [5,7]:

$$mx\frac{d\dot{x}}{dt} = m\left[\frac{d}{dt}\left(x\dot{x}\right) - \left(\dot{x}\right)^2\right] = -\alpha x\dot{x} + xF(t) \tag{1.76}$$

One can now calculate the ensemble average of both sides of Equation 1.76:

$$m\left\langle\left[\frac{d}{dt}\left(x\dot{x}\right) - \left(\dot{x}\right)^2\right]\right\rangle = -\alpha\left\langle x\dot{x}\right\rangle + \left\langle xF(t)\right\rangle \tag{1.77}$$

Thus Equation 1.77 becomes:

$$m\left\langle\left[\frac{d}{dt}\left(x\dot{x}\right)\right]\right\rangle = m\frac{d}{dt}\left\langle x\dot{x}\right\rangle = kT - \alpha\left\langle x\dot{x}\right\rangle \tag{1.78}$$

since $\langle xF(t)\rangle = \langle x\rangle\langle F(t)\rangle = 0$, because $\langle x\rangle = 0$, $\langle F(t)\rangle = 0$, and

$$\frac{1}{2}m\left\langle(\dot{x})^2\right\rangle = \frac{1}{2}kT,$$

on account of the equipartition theorem [6–8]. Then solving the differential Equation 1.78, we will get:

$$\left\langle x\dot{x}\right\rangle = C\exp\left(-\frac{\alpha t}{m}\right) + \frac{kT}{\alpha} \tag{1.79a}$$

since $x(0) = 0$, at $t = 0$; consequently,

$$0 = C + \frac{kT}{\alpha}.$$

Then Equation 1.79a becomes:

$$\left\langle x\dot{x}\right\rangle = \frac{1}{2}\frac{d\left\langle x^2\right\rangle}{dt} = \frac{kT}{\alpha}\left[1 - \exp\left(-\frac{\alpha t}{m}\right)\right] \tag{1.79b}$$

Integrating Equation 1.79b:

$$\left\langle x^2\right\rangle = 2\frac{kT}{\alpha}\left[t - \frac{m}{\alpha}\left\{1 - \exp\left(-\frac{\alpha t}{m}\right)\right\}\right] \tag{1.80}$$

If we evaluate Equation 1.80 for $t \to \infty$, we will obtain the following equation:

$$\left\langle x^2 \right\rangle = \frac{2kT}{\alpha} t \tag{1.81}$$

1.12.2.3 The Diffusion Equation

Consider now a random walker in one dimension, with probability R of moving to the right and L for moving to the left. At $t = 0$, we place the walker at $x = 0$, as indicated in Figure 1.5. The walker can then jump, with the above probabilities, either to the left or to the right for each time step. Every step has length $\Delta x = l$, and we have a jump either to the left or to the right at every time step. Let us now assume that we have equal probabilities for jumping to the left or to the right, i.e., $L = R = 1/2$. Then, the average displacement after N time steps is:

$$\left\langle x(N) \right\rangle = \left\langle \sum_{i=1}^{N} \Delta x_i \right\rangle = \sum_{i=1}^{N} \left\langle \Delta x_i \right\rangle = 0, \quad \text{for} \quad \Delta x_i = \pm l$$

Since we have an equal opportunity of jumping either to the left or to the right. The value of $\langle x(N)^2 \rangle$ is:

$$\left\langle x(N)^2 \right\rangle = \left\langle \left(\sum_{i=1}^{N} \Delta x_i \right)^2 \right\rangle = \left\langle \sum_{i=1}^{N} \Delta x_i \sum_{j=1}^{N} \Delta x_j \right\rangle = \sum_{i=1}^{N} \left\langle \Delta x_i^2 \right\rangle + \sum\nolimits_{i \neq j} \left\langle \Delta x_i \Delta x_j \right\rangle = l^2 N$$

Since the steps are not correlated, then: $\langle \Delta x_i \Delta x_j \rangle = \langle \Delta x_j \Delta x_i \rangle$, and:

$$\sum_{i \neq j} \left\langle \Delta x_i \Delta x_j \right\rangle = 0$$

and the time between jumps is τ; therefore, the jump frequency is: $\Gamma = 1/\tau$. Consequently, if $\Gamma = constant$, then for N steps where $N = t/\tau$, the mean square displacement is [7]:

$$\left\langle x^2(N) \right\rangle = Nl^2 = \left(\frac{l^2}{\tau} \right) t \tag{1.82}$$

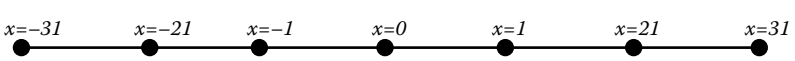

FIGURE 1.5 One-dimensional random walker which can jump either to the left or to the right.

On the other hand, a Markov processes is an stochastic process, where the time dependence of the probability, $P(x,t)dx$, that a particle position at time t lies between x and $x + dx$, depends only on the fact that $x = x_0$, at $t = t_0$, and not on the whole past history of the particle movement [5,7]. A very important application of the Markov dynamics is random walk, and the Fokker-Planck equation [5,38]:

$$\frac{\partial P(x,t)}{\partial t} = -\frac{\partial}{\partial x}\Big[f(x)P(x,t)\Big] + \kappa\frac{\partial^2}{\partial x^2}\Big[g(x)P(x,t)\Big]$$

accounts for the time development of a Markov process. For random walk, $f(x) = 0$, and $g(x) = 1$, then the diffusion equation for a random walk in one dimension is:

$$\frac{\partial P(x,t)}{\partial t} = D\frac{\partial^2 P(x,t)}{\partial x^2} \tag{1.83}$$

in which D is the self-diffusion coefficient, and $P(x,t)$, where

$$\int_{-\infty}^{\infty} P(x,t)dx = 1$$

is the probability density to find a diffusing particle at the position x, during the time t, if this particle was at $x = 0$, at $t = 0$.

The solution of this equation with the following initial and boundary conditions:

$$\left.\frac{\partial P}{\partial x}\right| = 0 \quad \left.\frac{\partial P}{\partial t}\right|_{\infty,t} \infty, t = 0$$

and $P(x,0) = \delta(x)$ is [39]:

$$P(x,t) = \left(\frac{1}{(4\pi Dt)}\right)^{1/2} \exp\left(-\frac{x^2}{4Dt}\right) \tag{1.84}$$

Therefore, it is very easy to show that the one-dimensional mean square displacement (MSD) is:

$$\left\langle x^2 \right\rangle = \int x^2 P(x,t)dx = 2Dt \tag{1.85}$$

Then, from Equations 1.72 and 1.73:

$$\lim_{t\to\infty}\left\langle x^2(t)\right\rangle = 2tD = 2t\int_0^t ds\left\langle v(0)v(s)\right\rangle \tag{1.86}$$

Consequently:

$$D = \int_0^t ds \left\langle v(0)v(s) \right\rangle \tag{1.87}$$

Furthermore, from Equation 1.81:

$$\left\langle x^2 \right\rangle = \frac{2kT}{\alpha} t = 2Dt \tag{1.88}$$

Then:

$$D = \frac{kT}{\alpha} \tag{1.89}$$

Also from Equation 1.82:

$$D = \frac{l^2}{2\tau}$$

Consequently in a more general form, the self-diffusion coefficient and the Einstein relation for three-dimensional self-diffusion are [10,24]:

$$D = \frac{1}{3} \int_0^\infty \left\langle \overline{v}(t)\overline{v}(0) \right\rangle dt \tag{1.90}$$

$$2tD = \frac{1}{3} \left\langle [\overline{r}(t) - \overline{r}(0)]^2 \right\rangle \tag{1.91}$$

REFERENCES

1. Atkins, P.W., *Physical Chemistry,* 6th ed., W.H. Freeman and Co., New York, 1998.
2. Levine, I., *Physical Chemistry,* Mc Graw Hill, New York, 2001.
3. Fowler, R.H. and E.A. Guggenheim, *Statistical Thermodynamics* (revised edition), Cambridge University Press, Cambridge, 1949.
4. Fowler, R.H., *Statistical Mechanics* (second edition), Cambridge University Press, Cambridge, 1955.
5. Kittel, C., *An Introduction to Statistical Physics,* J. Wiley & Sons, New York, 1949.
6. Landau, L. and Lifshits, E.M., *Statistical Physics,* Addison & Wesley, Reading, MA, 1959.

7. Reif, R., *Fundamentals of Statistical and Thermal Physics,* McGraw-Hill, Boston, MA, 1965.
8. Hill, T.L., *An Introduction to Statistical Thermodynamics,* Dover Publications, New York, 1986.
9. Lansberg, P.T., in *Problems in Thermodynamics and Statistical Physics*, Lansberg, P.T., Ed., London, 1974, chap. 2.
10. Haberlandt, R., Fritzche, S., and Vortler, H.-L., in *Handbook of Surfaces and Interfaces of Materials,* Vol. 5, Nalwa, H.S., Ed., Academic Press, New York, 2001, p. 357.
11. Davison, N., *Statistical Mechanics,* Dover Publications, New York, 2003.
12. Boas, M.L., *Mathematical Methods in the Physical Sciences,* J. Wiley & Sons, New York, 1966.
13. Arfken, G.B. and Weber, H.J., *Mathematical Methods for Physicists,* 5th ed., Academic Press, New York, 2001.
14. Hohemberg, P. and Kohn, W., *Phys. Rev.,* 136, B864, 1964.
15. Kohn, W. and Sham, L.J., *Phys. Rev.,* 140, A1441, 1965.
16. Ghosh, S.K., *Int. J. Mol. Sci.,* 3, 260, 2002.
17. Evans, R., in *Fundamentals of Inhomogeneous Fluids*, Henderson, D., Ed., Marcel Dekker, New York, 1992, p. 85.
18. Tang, Y. and Wu, J., *J. Chem. Phys.,* 119, 7388, 2003.
19. Forsyth, A.R., *Calculus of Variations,* Dover, New York, 1960.
20. Onsager, J., *Phys. Rev.,* 37, 405, 1931, and 38, 2265, 1931.
21. De Groot, S.R. and Mazur, P., *Nonequilibrium Thermodynamics,* Elsevier, Amsterdam, 1962
22. Prigogine, I., *Thermodynamics of Irreversible Process,* J. Wiley & Sons, New York, 1967.
23. McQuarrie, D.A., *Statistical Mechanics,* University Science Books, Sausalito, CA, 2000.
24. Kreuzer, H., *Nonequilibrium Thermodynamics, and Its Statistical Foundations,* Clarendon Press, Oxford, 1981.
25. Kubo, R., Toda, M., and Hashitsume, N., *Statistical Physics II. Nonequilibrium Statistical Mechanics,* Springer-Verlag, Berlin, 1991.
26. Manning, J.R., *Diffusion Kinetics for Atoms in Crystals,* Van Nostrand, Princeton, 1968.
27. Karger, J. and Ruthven, D.M., *Diffusion in Zeolites and Other Microporous Solids,* J. Wiley, and Sons, New York, 1992.
28. Kizilyalli, M., Corish, J., and Metselaar, R., *Pure Appl. Chem.,* 71, 1307, 1999.
29. Parris, P.E., Kus, M., Dunlap, D.H., and Kenkre, V.M., *Phys. Rev. E,* 56, 5295, 1997.
30. Kubo, R.S., *J. Phys. Soc. Japan.,* 12, 570, 1957.
31. Lax, M., *Phys. Rev.,* 109, 1921, 1958.
32. Peterson, R., *Rev. Mod. Phys.,* 39, 69, 1967.
33. Kenkre, V.M. and Dresden, M., *Phys. Rev. Lett.,* 6A, 769, 1971.
34. Kenkre, V.M., *Phys. Rev. A,* 7, 772, 1973.
35. Landau, L. and Lifshits, E.M., *Mecanique,* Mir, Moscou, 1966.
36. Einstein, A., *Investigations on the Theory of Brownian Movement,* Dower Publications, New York, 1956.
37. Langevin, P., Comptes Rendus de l'Academie de Sciences (Paris), 146, 530, 1908.
38. Risken, H., *The Fokker-Planck Equation,* 2nd ed., Springer-Verlag, New York, 1996.
39. Crank, J., *The Mathematics of Diffusion,* 2nd ed., Oxford University Press, Oxford, 1975.

APPENDIX 1.1 LEGENDRE TRANSFORMATIONS

The Legendre transformations [12] allow us to describe a function using a different set of variables. Given a function f(x,y), the total derivative of that function is given as:

$$df = \frac{\partial f}{\partial x}dx + \frac{\partial f}{\partial y}dy$$

The coefficients for the partial derivatives are defined as:

$$u = \frac{\partial f}{\partial x}, \text{ and } v = \frac{\partial f}{\partial y}$$

To change to a new representation, the function, $g(u,x)$ is defined as: $g(u,x) = f(x,y) - ux$, implying that:

$$dg = df - xdu - udx$$

Using the total derivative of $f(x,y)$ then:

$$dg = -xdu + vdy$$

where:

$$x = -\frac{\partial g}{\partial u}, \text{ and } v = \frac{\partial g}{\partial y}$$

Consequently the Legendre transformation construct, from a function $f = f(x,y)$, a function $g = g(u,y)$, which by definition depends on u and y.

APPENDIX 1.2 THE LAGRANGE MULTIPLIERS

If we wish to locate the maximum or minimum in, for example, the function: $F = F(x,y,z)$, we require that at the maximum or minimum [12]:

$$dF(x,y,z) = \left(\frac{\partial F}{\partial x}dx + \frac{\partial F}{\partial y}dy + \frac{\partial F}{\partial z}dz\right) = 0 \qquad \text{(A1.2-1)}$$

Since *dx, dy,* and *dz* are linearly independent, because they are independent variables, we have subsequently [12]:

$$\frac{\partial F}{\partial x} = \frac{\partial F}{\partial y} = \frac{\partial F}{\partial z} = 0 \tag{A1.2-2}$$

Now suppose that we want to locate the maximum, or minimum, in $F = F(x,y,z)$, not including all the values of x, y, and z, but only those values which satisfied the condition $G(x,y,z) = C$. In this case, dx, dy, and dz are not linearly independent, since only two of them are linearly independent, given that [12]:

$$dG(x,y,z) = \left(\frac{\partial G}{\partial x} dx + \frac{\partial G}{\partial y} dy + \frac{\partial G}{\partial z} dz \right) = 0 \tag{A1.2-3}$$

Lagrange developed a methodology to solve this problem, defining the following auxiliary function:

$$H = F + \alpha G \tag{A1.2-4}$$

where α is a Lagrange multiplier. Now, since $dF = 0$ and $dG = 0$, then $dH = 0$. Therefore,

$$dF(x,y,z) = dF + \alpha dG = 0 \tag{A1.2-5}$$

and consequently:

$$\left(\frac{\partial F}{\partial x} - \alpha \frac{\partial G}{\partial x} \right) dx + \left(\frac{\partial F}{\partial y} - \alpha \frac{\partial G}{\partial y} \right) dy + \left(\frac{\partial F}{\partial z} - \alpha \frac{\partial G}{\partial z} dz \right) = 0 \tag{A1.2-6}$$

at (x_0, y_0, z_0). Since α is an arbitrary parameter, we can evaluate α at (x_0, y_0, z_0) applying:

$$\frac{\partial F}{\partial z} - \alpha \frac{\partial G}{\partial z} dz = 0 \tag{A1.2-7}$$

Therefore the remaining terms are now linearly independent, and consequently:

$$\left(\frac{\partial F}{\partial x} - \alpha \frac{\partial G}{\partial x} \right) dx + \left(\frac{\partial F}{\partial y} - \alpha \frac{\partial G}{\partial y} \right) dy = 0 \tag{A1.2-8}$$

where

$$\frac{\partial F}{\partial x} - \alpha \frac{\partial G}{\partial x} = 0 \tag{A1.2-9}$$

and

$$\frac{\partial F}{\partial y} - \alpha \frac{\partial G}{\partial y} = 0 \qquad \text{(A1.2-10)}$$

Now with the help of Equations A1.2-7, A1.2-9, and A1.2-10, we have enough equations to solve how to locate the maximum or minimum.

Finally, it is necessary to affirm that the method could be easily generalized to more than one condition [12,13].

APPENDIX 1.3 METHODS OF COUNTING

If one thing can be done in N_1 ways, and after that, a second thing can be done in N_2 ways, the two things can be done, in succession, in that order in: $N_1 \times N_2$ ways. This principle, called the ***principle of counting***, could be extended to any number of things.

Therefore, following this principle of counting, if we have a set of n things lined up in a row, or a set of n objects in n boxes, or n people and n chairs to be seated, and we ask how many ways we can arrange or permute them to form different permutations, then the answer is in [12]:

$$P(n,n) = n.(n-1)(n-2)(n-3)\ldots 1 = n! \qquad \text{(A1.3-1)}$$

ways of arranging them.

On the other hand, if we have n objects but only r boxes, or n people and only r chairs, then there are:

$$P(n,r) = n.(n-1)(n-2)(n-r+1) = \frac{n!}{(n-r)!} \qquad \text{(A1.3-2)}$$

ways of arranging n objects from a population of n objects in $r < n$ boxes, because we have n ways to fill the first box, $n - 1$, ways to fill the second box, and finally, $(n - r + 1)$, ways of filling the r box.

If the objects in the previous case are indistinguishable or equal, the number of different ways of arranging from a population of n objects in r boxes is:

$$C(n,r) = \frac{P(n,r)}{P(r,r)} = \frac{n!}{(n-r)!r!} \qquad \text{(A1.3-3)}$$

Since the number that we are seeking, $C(n, r)$, is the number of ways for selecting, from the total number of objects, **r** objects and then arranging the r objects in r boxes in $P(r,r,)$ ways, then by applying the principle of counting, the total number of ways of selecting n objects to be located in r boxes is: $C(n,r)P(r,r) = P(n,r)$.

Similarly, the number of ways of putting N balls in N boxes, with N_1 in box **1,** N_2 in box **2,** etc., is:

$$W = \frac{N!}{N_1!N_2!N_3!\ldots N_n!} \tag{A1.3-4}$$

This equation allows us to find, for example, the distribution $\{N_i\}$ at equilibrium, i.e., the most probable macrostate distribution of N distinguishable particles over Ω energy levels: The number of ways to assign N_1 particles in the first level is:

$$C(N, N_1) = \frac{N!}{(N - N_1)!N_1!}$$

Now the number of ways to assign N_2 particles in the second level is:

$$C(N - N_1, N_2) = \frac{(N - N_1)!}{(N - N_1 - N_2)!N_2!}$$

Consequently:

$$W = C(N, N_1)C(N - N_1 - N_2)\ldots = \frac{N!}{N_1!N_2!N_3!\ldots N_n!}$$

APPENDIX 1.4 CALCULUS OF VARIATIONS

Suppose, $y(x)$, is defined on the interval, $[a,b]$, and so defines a curve on the (x,y) plane. Now assume that [12,13]:

$$F[y(x)] = \int_a^b f(y(x), y_x(x), x)dx \tag{A1.4-1}$$

where $y_x(x) = dy/dx$. A function like $F[y(x)]$ is called a functional; this name is used to distinguish $F[y(x)]$ from ordinary real-valued functions, whose domains consist of ordinary variables. The value of this functional will depend on the choice of the function, $y(x)$, and the basic problem of the calculus of variations is to find the form of the function which makes the value of the integral a minimum or maximum, normally a minimum.

In order to derive the extreme value conditions, we will require that the function, $f(y(x),y_x(x),x)$, in the integral have continuous partial derivatives of x, y, *and* y_x. We also require the continuity of the derivatives, because we will need to apply chain rules and the Leibniz rule for differentiation.

Now if $y(x)$ is a curve in $[a,b]$, which minimizes the functional:

$$F[y(x)] = \int_a^b f(y(x), y_x(x), x)dx \tag{A1.4-2}$$

then [13,19]:

$$\delta F[y(x)] = \delta \int_a^b f(y(x), y_x(x), x)dx = \int \left(\frac{\partial f}{\partial y}\delta y + \frac{\partial f}{\partial y_x}\delta y_x \right) = 0$$

Now it is easy to show that [13,19]:

$$\delta F[y(x)] = \int \left(\frac{\partial f}{\partial y} - \frac{d}{dx}\frac{\partial f}{\partial y_x} \right) \delta y(x)dx = 0$$

Or in terms of the so-called functional derivative:

$$\frac{\delta F[y(x)]}{\delta y(x)} = \int \left(\frac{\partial f}{\partial y} - \frac{d}{dx}\frac{\partial f}{\partial y_x} \right) dx = 0$$

Then the function, $y = y(x)$, which minimizes the functional, $F[y(x)]$, must obey the following differential equation:

$$\frac{\partial f}{\partial y} - \frac{d}{dx}\left(\frac{\partial f}{\partial y_x} \right) = 0 \tag{A1.4-3}$$

This equation is called the Euler-Lagrange equation [13,19].

The functional derivative is a generalization of the usual derivative that arises in the calculus of variations [13,19]. In a functional derivative, instead of differentiating a function with respect to a variable, one differentiates a functional with respect to a function. The formal definition of the functional derivative for the one-variable case is:

$$\frac{\delta F[y(x)]}{\delta y(x)} = \lim_{\varepsilon \to 0} \frac{F[y(x) + \varepsilon \delta y(x)] - F(y(x)]}{\varepsilon} \tag{A1.4-4}$$

2 General Introduction to Adsorption in Solids

2.1 DEFINITIONS AND TERMINOLOGY

2.1.1 What Is the Meaning of the Term Adsorption

The term "adsorption" was created by Kayser in 1881 to describe the increase in concentration of gas molecules in neighboring solid surfaces, a phenomenon previously noted by Fontana and Scheele in 1777.

The unpolluted surface of any solid is characterized by the fact that not all bonds of the atoms which compose the surface are saturated. This fact causes the existence of an adsorption field over this surface. This adsorption field causes the accumulation of molecules near the solid surface [1–11]. This adsorption is a general tendency, since during its occurrence, a decrease of the surface tension is experienced by the solid [1–11]. The term adsorption is used for the description of the direct process; for the reverse process the term desorption is used [1].

In the cases that will be treated in the present book, for gas–solid and liquid–solid interfaces, adsorption is defined as an increase in concentration of gas molecules in a solid surface, or an increase in the concentration of a dissolved substance at the interface of a solid and a liquid phase. These phenomena are caused, in both cases, because of the operation of surface forces.

2.1.2 Phases and Components Involved in the Adsorption Process

The adsorptive, sorptive, or adsorbate is the gas, or molecule dissolved in a liquid, adsorbed by the solid, that is, the adsorbent, whenever the gas or liquid is brought in contact with it [1,4,8].

In the case of gas–solid physical adsorption, the adsorptive (or adsorbate) is the gas adsorbed by the solid (the adsorbent) whenever the gas is brought in contact with it [1]. During physical adsorption of gases, the *adsorbed phase* is in thermodynamic equilibrium with the *gas phase.* That is, $\mu_a = \mu_g$, where μ_a and μ_g are the chemical potential of the adsorbed and gas phases, respectively. This fact allows the application of the *Gibbs phase rule* for adsorption systems [5]:

$$P + F = C + 2 + I$$

where F is the number of degrees of freedom of the thermodynamic system in equilibrium, I is the number of bidimensional or restricted phases, P is the number of phases, and C is the number of components. Then, for a single-component

gas–solid adsorption system, where the number of components is $C = 2$ (i.e., gas and solid), the number of restricted phases is $I = 1$ (i.e., the adsorbed phase), and the total number of phases is $P = 3$ (gas, solid, and adsorbed phase), then [5]:

$$F = C + 2 + I - P = 2 + 2 + 1 - 2 = 2$$

As a result, adsorption data are expressed as [1]:

$$n_a = F(P,T)$$

a relation between the amount adsorbed, n_a, which will be accurately defined in the next section, and the equilibrium adsorption pressure, P, and temperature, T.

In practice, it is measured as the relationship between the amount adsorbed, na, and the equilibrium pressure, P, at constant temperature, T (i.e., the adsorption isotherm) [1]:

$$n_a = F(P)_T \tag{2.1}$$

The gas adsorption process, in general, is considered as a physisorption process because the molecular forces involved are normally of the van der Waals type [3–5,8–12]. The physical adsorption of gases and vapors in solids could also be classified as mobile adsorption, which occurs when the adsorbed molecule behaves as a gas molecule in the adsorption space, and immobile adsorption, which occurs whenever the adsorbed molecule is forced to vibrate around an adsorption site [5,13].

For open surfaces, adsorption consists of a layer-by-layer filling process, where the first layer is filled when $\theta = n_a/N_m = 1$, where θ is the surface recovery, and N_m is the monolayer capacity. Consequently, we said that we have monolayer adsorption when $\theta = n_a/N_m < 1$, and multiplayer adsorption when $\theta = n_a/N_m > 1$.

Physical adsorption of gases in solid surfaces occurs in the case where no reaction involving exchange of electrons between the solid surface and the gas molecules with the formation of chemical bonds is required during the adsorption process [1,4,8]. In the case where a reaction by means of electron exchange between the solid surface and the gas molecules occurs during adsorption, the phenomenon is called chemical adsorption [1,4,8].

2.1.3 Porous Materials

Practical adsorbents are normally porous. The pore widths of porous adsorbents are classified by the International Union of Pure and Applied Chemistry (IUPAC) as micropores, which are those with pore diameters between 0.3 and 2 nm, mesopores with pore diameters between 2 and 50 nm, and macropores with pore diameters greater than 50 nm [1]. The pore width, D_p, is defined as the diameter, in the case of cylindrical pores, and as the distance between opposite walls, in the case of slit-shape pores.

The parameters which characterize a porous adsorbent are: the specific surface area, denoted by *S,* measured in [m^2/g]; the micropore volume, denoted by W^{MP}, measured in [cm^3/g]; the pore volume, denoted by *W,* which is the sum of the micropore and mesopore volumes of the adsorbent, measured in [cm^3/g]; and the pore size distribution (PSD) [1,8]. The PSD is a graphical representation of $\Delta V_p/\Delta D_p$ versus D_p, where V_p is the pore volume accumulated up to the pore of width D_p, measured in [cc-STP/g·Å] [1,8,14]. The unit, cc-STP, indicates the amount adsorbed measured in cubic centimeters at STP, that is, at standard temperature and pressure, namely 273.15 K and 760 Torr (1.01325×10^5 Pa). In this case, strictly speaking, the surface area is the outer surface, the area out of the micropores. If the adsorbent does not present micropores, the surface area and the outer surface area coincide.

2.2 INTERFACIAL LAYER, GIBBS DIVIDING SURFACE, AND GIBBS ADSORPTION

The *interfacial layer* is the inhomogeneous space intermediate between two bulk phases in contact, where properties are significantly different from, but related to, the properties of the bulk phases. Examples of such properties are: compositions; molecular density, orientation, or conformation; charge density; pressure tensor; electron density; etc. [4]. The interfacial properties vary in the direction normal to the surface. Complex profiles of interfacial properties occur in the case of multicomponent systems with coexisting bulk phases where attractive/repulsive molecular interactions involve adsorption or depletion of one or several components [4]. In the reference ideal system the concentration remains constant up to the *Gibbs dividing surface* (*GDS*) (Figure 2.1). However, in the actual system, concentration changes across the interface of thickness $\gamma = z_\beta - z_\alpha$, from phase α to phase β (Figure 2.1) [4].

The *surface excess amount, or Gibbs adsorption* of the *ith* component (i.e., n_i^σ) is defined as the excess of the amount of this component actually present in the

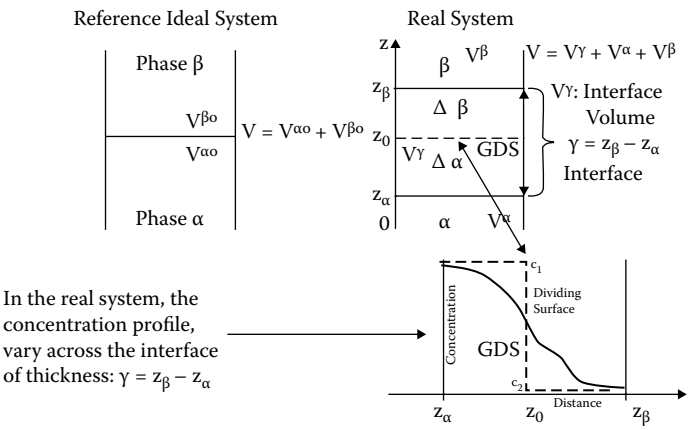

FIGURE 2.1 Gibbs dividing surface (GDS).

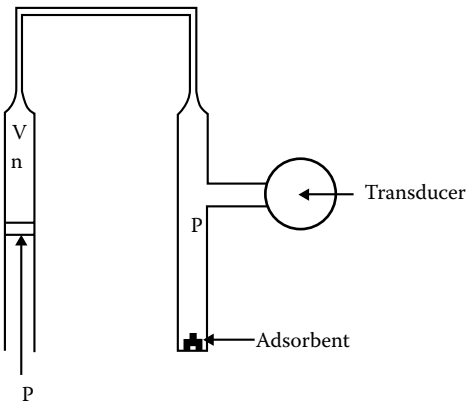

FIGURE 2.2 Schematic representation of a volumetric adsorption experiment.

system over that present in a reference ideal system of the same volume as the real system, and in which the bulk concentrations in the two phases remain uniform up to the Gibbs dividing surface. That is [4]:

$$n_i^{\sigma} = n_i - V^{\alpha_0} c_{\alpha}^i - V^{\beta_0} c_{\beta}^i \tag{2.2}$$

where n_i is the total amount of the component i in the system; c_{α}^i and c_{β}^i are the concentrations in the two bulk phases, α and β; and V^{α_0} and V^{β_0} are the volumes of the two phases defined by the Gibbs surface. The GDS is a geometrical surface chosen parallel to the interface and used to define the volumes of the bulk phases in the calculation of the extent of adsorption and of other surface excess properties.

For gas–solid adsorption (see Figure 2.1 and Figure 2.2 [1,4,8]), since $c^g = 0$ in the solid phase [8]:

$$n^{\sigma} = n - V^{\alpha_0} c^g = n - c^g (V^g + V^a) \tag{2.3}$$

in which $V^{\alpha_0} = V^g + V^a$. Now, if A is the adsorbent surface area, and t is the thickness of the adsorbed layer, then the volume of the adsorbed layer, or adsorption space is [8]:

$$V^a = At \tag{2.4}$$

We may define the amount adsorbed as [8]:

$$n^a = \int_0^{V^a} c dV = A \int_0^t c dz \tag{2.5}$$

The total amount of gas molecules in the system is:

$$n = n^a + V^g c^g \tag{2.6}$$

therefore:

$$n^a = n - V^g c^g \tag{2.6a}$$

Consequently, combining Equations 2.3 and 2.6, we get:

$$n^a = n^\sigma + V^a c^g \approx n^\sigma$$

since

$$V^a c^g \approx 0$$

Now we will define more precisely some surface parameters. If the mass of degassed adsorbent is defined as m_s and measured in *g,* then the specific surface area is:

$$S = \frac{A}{m_s}$$

which is measured in [m^2/g]. The specific surface excess amount is defined by:

$$n_a = \frac{n^\sigma}{m_s} \approx \frac{n^a}{m_s}$$

where n_a is the amount adsorbed measured in mol/g. The specific surface excess amount is what is usually measured in practice and is approximately equal to the amount adsorbed, n_a. This quantity is dependent on the equilibrium adsorption pressure, *P*, at constant adsorbent temperature, *T.* Consequently, gas adsorption data are, in practice, expressed by:

$$n_a = \frac{n^\sigma}{m_s} \approx \frac{n^a}{m_s} = F(P)_T$$

which is the gas-solid adsorption isotherm.

2.3 THERMODYNAMICS OF GAS–SOLID ADSORPTION

2.3.1 Adsorption Interaction Fields

As was previously stated, the fresh surface of a solid is distinguished by the fact that the atoms which compose it do not have all its bonds saturated. Then, when a molecule contacts the surface of a solid adsorbent, it becomes subject to divers interaction fields characterized by different potentials, such as the dispersion energy, ϕ_D, repulsion energy,

ϕ_R, polarization energy, ϕ_P, field dipole energy, $\phi_{E\mu}$, field gradient quadrupole energy, ϕ_{EQ}, sorbate–sorbate interaction energy, ϕ_{AA}, and the acid-base interaction with the active site, ϕ_{AB}, if the surface contains hydroxyl bridge groups [3,7–13].

The terms: $\phi_D + \phi_R$, for the potential energy of interaction of a molecule with a surface could be represented by the Lennard-Jones 12-6 potential [11]:

$$\phi_D + \phi_R = 4\varepsilon\left(\left(\frac{\sigma}{z}\right)^{12} - \left(\frac{\sigma}{z}\right)^{6}\right)$$

where ε is the potential energy minimum, and σ is the gas–solid separation at maximum interaction. This term is present in the interaction of all molecules with any adsorbent.

The electrostatic polarization term appears in the case of nonpolar molecules interacting with an adsorbent which possess a crystalline electric field. This term could be expressed as follows [3,7]:

$$\phi_P = -\frac{\alpha E^2}{2}$$

where α is the of the adsorbed molecule or atom, and E is the intensity of the adsorbent electric field.

The field dipole energy comes into view in the case of polar molecules interacting with an adsorbent which possess a crystalline electric field. This term could be written as follows [3,7]:

$$\phi_\mu = -\mu E \cos\varphi$$

where μ is the permanent dipole moment of the adsorbed molecule, and φ, is the angle between E, the electric field, and the dipole moment [3,7].

The field gradient quadrupole energy is [3,7]:

$$\phi_{EQ} = \frac{Q}{2}\left(\frac{\partial E}{\partial z}\right)$$

where Q is the quadrupole moment of the adsorbed molecule, and $(\partial E/\partial z)$ is the electric field gradient of the adsorbent.

2.3.2 Isosteric and Differential Heats of Adsorption

As was previously reported, adsorption is a general tendency of matter, since during its occurrence a decrease of the surface tension is experienced by the solid. Therefore, adsorption is a spontaneous process, where a decrease of the Gibbs free energy is observed (i.e., $\Delta G < 0$). During physical adsorption, molecules from a disordered bulk phase pass to a more ordered adsorbed state, because in this adsorbed state the molecules are restricted to move in a surface or a pore. Therefore, the whole system

experiences a decrease of entropy during adsorption (i.e., $\Delta S < 0$). Since $\Delta G = \Delta H - T\Delta S$, then $\Delta H = \Delta G + T\Delta S < 0$. Consequently, adsorption is an exothermic process and, therefore, is a process favored by a decrease in temperature.

As was stated in the first chapter, the fundamental equation of thermodynamics for a bulk mixture is:

$$dU = TdS - PdV + \sum_i \mu_i dn_i$$

in which U is the internal energy of the system, S its entropy, V its volume, T its temperature, μ_i the chemical potentials, and n_i the number of moles of the components contained in the system.

The thermodynamic approach applied here considers the adsorbent plus adsorbed gas or vapor as a solid solution (system aA). Using this description, it is possible to obtain the fundamental thermodynamic equation for the aA system [15]:

$$dU_{aA} = TdS_{aA} - PdV_{aA} + \mu_a dn_a + \mu_A dn_A$$

where U_{aA}, S_{aA}, and V_{aA} are the internal energy, entropy, and volume of the system *aA, and* μ_a, μ_A, n_a, and n_A are the chemical potentials and the number of moles of the adsorbate and the adsorbent in the system, aA.

If we define $\Gamma = n_a/n_A$, then $\mu_a = \mu_a(T,P,\Gamma)$, and $\mu_A = \mu_A(T,P)$; therefore [16]:

$$d\mu_a = -\bar{S}_a dT + \bar{V}_a dP + \left(\frac{\partial \mu_a}{\partial \Gamma}\right)_{T,P} d\Gamma$$

where $\bar{S}_a$ and $\bar{V}_a$ are the partial molar entropy and volume of the adsorbate in the system aA. During equilibrium, the chemical potential of the adsorbate in the aA phase and the gas phase are equal; then:

$$d\mu_a = d\mu_g = -\bar{S}_g dT + \bar{V}_g dP$$

Subsequently, for Γ = *constant* [16]:

$$\left[\frac{d\ln P}{dT}\right]_\Gamma = \frac{\bar{H}_g - \bar{H}_a}{RT^2} = \frac{q_{iso}}{RT^2} \tag{2.7}$$

where $\bar{H}_g$ and $\bar{H}_a$ are the partial molar enthalpies of the adsorbate in the gas phase and in the system aA. Now, using Equation 2.7, it is possible to define the isosteric enthalpy of adsorption [11]:

$$\Delta H(n_a) = -(\bar{H}_g - \bar{H}_a) = -q_{iso} \tag{2.7a}$$

where q_{iso} is the enthalpy of desorption, or isosteric heat of adsorption. The isosteric heat of adsorption is calculated with the help of adsorption isotherms. An example of the calculation of the isosteric heat of adsorption is given in the next chapter, in Section 3.5.

Another important adsorption heat is the differential heat of adsorption, which is defined as follows [5,16]:

$$q_{diff} = \frac{\Delta Q}{\Delta n_a} \tag{2.8}$$

where ΔQ is the evolved heat during the finite increment, Δn_a, in the magnitude of adsorption that provides the evolution of heat. The differential heat of adsorption is measured calorimetrically; an example will be given in Section 2.5.3. It can be also approximately calculated with the help of the following expression [5,16]:

$$q_{diff} \approx q_{iso} - RT \tag{2.8a}$$

However, it is necessary to acknowledge that the relation in (2.8a) is only exactly satisfied in the case of inert adsorbents, although porous adsorbents systems are not generally inert [15].

2.3.3 Some Relations between Adsorption Macroscopic and Microscopic Parameters

The molar integral change of free energy at a given temperature, *T,* during adsorption is [12]:

$$\Delta G^{ads} = \Delta H^{ads} - T\Delta S^{ads} \tag{2.9}$$

Furthermore, it is possible to show that the relation between the enthalpy of adsorption (ΔH^{ads}) and the differential heat of adsorption (q_{diff}) for porous systems is [12,15,16]:

$$\Delta H^{ads} \approx -q_{diff} - RT + \frac{T}{\Gamma}\left(\frac{\partial \vartheta}{\partial T}\right)_{\Gamma} \tag{2.10}$$

where $\Gamma = n_a/n_A$, $q_{diff} \approx q_{iso} - RT$, n_a and n_A are the number of moles of the adsorbate and the adsorbent, and ϑ, ın the system aA, is defined by [15,16]:

$$\vartheta = RT\int_0^P \Gamma d\ln P \tag{2.11}$$

Now assuming that the change in entropy on adsorption is negligible in comparison with the rest of the terms in Equation 2.9, and taking into account that the change in the free energy of adsorption (ΔG^{ads}) could be expressed by:

$$\Delta G^{ads} = RT \ln\left(\frac{P}{P_0}\right) \tag{2.12}$$

and that [5,12]:

$$-q_{diff} = U_0 + P_a - \Delta H^{ads} \tag{2.13}$$

where U_0 and P_a denote the adsorbate–adsorbent and adsorbate–adsorbate interaction energies, respectively (see Section 2.3.1), then from Equations 2.9, 2.10, 2.12, and 2.13, it is possible to get:

$$RT \ln\left(\frac{P}{P_0}\right) + \left(RT - \frac{T}{\Gamma}\left(\frac{\partial \vartheta}{\partial T}\right)\right) = U_0 + P_a \tag{2.14}$$

If we consider now that the adsorbed phase is ideal (i.e., if $\Gamma = KP$), then from the definition of ϑ, Equation 2.11:

$$\vartheta = RT \int_0^P \Gamma d \ln P = RTK \int_0^P \frac{P dP}{P} = RTKP \tag{2.15}$$

Consequently, from Equations 2.14 and 2.15:

$$RT \ln\left(\frac{P}{P_0}\right) + \left(RT - \frac{T}{\Gamma}(R\Gamma)\right) = U_0 + P_a$$

or:

$$RT \ln\left(\frac{P}{P_0}\right) = U_0 + P_a \tag{2.16}$$

2.4 GASES AND VAPORS ADSORPTION IN POROUS MATERIALS

2.4.1 Measurement of Adsorption Isotherms by the Volumetric Method

A real volumetric adsorption experiment [5] (see Figure 2.3 [1]) consists of a thermostated sample cell of volume V_g at the experimental temperature T, a container with an accurately determined volume, known as the calibrated volume, V_c, a connection to the gas reservoir, and a transducer for pressure measurement. The volume

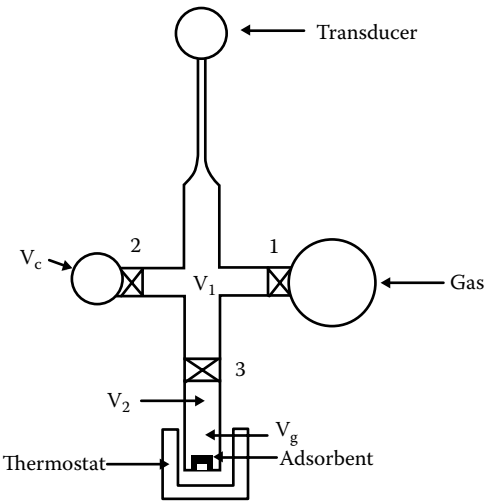

FIGURE 2.3 Schematic representation of volumetric adsorption experiment.

between stopcock 3, at ambient temperature, T_r, and the thermostat is called V_2, and the volume between stopcocks 1, 2, and 3, also at ambient temperature, T_r, is called V_1.

Gas from the container is introduced into the manifold or dose volume, V_1, of the previously evacuated vacuum system, and the resultant pressure, P_1, is measured with the transducer. Subsequently, stopcock 2 is opened, resulting in a pressure, P_2. Then [5]:

$$V_1 = \frac{V_c P_2}{P_1 - P_2}$$

When stopcock 3 is opened, the gas contacts with the adsorbent at temperature T. The volume of the sample-side is called the dead volume, V_d:

$$V_d = V_2 + \frac{V_g T_r}{T}$$

These volumes, V_2 *and* V_g, must be measured with the adsorbent present inside the sample cell, using He, which is a gas not adsorbed normally at the experimental temperature.

To measure V_d, the same methodology previously explained for the measurement of V_1 is applied. Further, in order to determine V_d, the volume, V_2, is experimentally made approximately zero ($V_2 \approx 0$).

The application of the volumetric method for the determination of an adsorption isotherm could be reduced to the application of the following procedure. First, adsorbate gas is introduced into the manifold volume,V_1, and the amount dosed is measured, generally in cubic centimeters at STP, that is, standard temperature and pressure, namely 273.15 K and 1.01325×10^5 Pa.

$$n_{dose}^{i} = \frac{P_1^i V_1}{RT_r} + \frac{P_2^{i-1} V_d}{RT_r}$$

where P_2^{i-1} is the equilibrium pressure of the previous adsorption step (i–1th step), T_r is ambient temperature, V_1 is dose volume, V_d is dead volume, P_1^i is initial pressure (ith step), and n_{dose}^i is initial number of moles during the ith adsorption step. Then, when equilibrium is attained the quantity of gas not adsorbed is calculated by:

$$n_{final}^{i} = \frac{P_2^i (V_1 + V_d)}{RT_r}$$

where P_2^i is the equilibrium pressure of the current measurement (ith step). The amount adsorbed in the ith isotherm point, $\Delta^i n_a$, is then calculated with the help of the following equation:

$$\Delta^i n_a = \frac{n_{dose}^i - n_{final}^i}{m_s}$$

in which m_s is the mass of degassed adsorbent. Finally, the isotherm is calculated with the sum of the different adsorption steps.

$$n_a^i = \sum_{j=1}^{i} \Delta^j n_a$$

where n_a^i is the magnitude of adsorption or amount adsorbed up to the ith adsorption step. Then the experimental isotherm is obtained by plotting n_a^i versus P_2^i.

2.4.2 Porous Materials Characterization by Vapor Adsorption Methods

Porous materials are of immense practical importance for applications in industrial and pollution abatement applications. Microporous materials, such as zeolites and related materials, are extensively used in the petrochemical industry as heterogeneous catalysts in cracking and other applications. Micro/mesoporous materials and mesoporous materials (e.g., silica gels, porous glasses, active carbon, and mesoporous titania (alumina) are widely used in separation processes, catalysis, and other applications [17]. The successful performance of the adsorption unitary operation in industry and pollution abatement requires a comprehensive characterization of these porous materials with regard to micropore volume, surface area, and pore size distribution [1–12,17–20].

Common porous materials, such as silica gels, active carbons, alumina, titania, and porous glasses are amorphous. In contrast, materials like zeolites are crystalline (i.e., every atom can be located in a microscopically sized unit cell) [17]. Mesoporous molecular sieves, such as MCM-41 and SBA-15, are not crystalline; however, they

are ordered [21,22]. Such order is not present in amorphous materials. Consequently, a more complete characterization can be performed in the case of crystalline and ordered materials, while for amorphous nanoporous materials, a complete and comprehensive characterization is more problematic. Nevertheless, typical properties, such as microporous volume, total pore volume, specific surface area, and pore size distribution, can still be determined, as will be discussed in Chapters 3 and 4.

During the adsorption of vapors in complex porous systems, the adsorption process occurs approximately as follows: Initially there is micropore filling, where the adsorption behavior is dominated almost entirely by the interactions of the adsorbate and the pore wall [3]. We will consider here that adsorption in the micropores could be considered as a volume filling of the microporous adsorption space, and not as a layer-by-layer surface coverage [7]. Afterward, at higher pressures, the adsorption process involves external surface coverage, consisting of monolayer and multilayer adsorption on the walls of mesopores and open macropores, and capillary condensation taking place in the mesopores [3,6,8].

Vapor adsorption in micropores is the main method for measuring the micropore volume using the Dubinin adsorption isotherm, the t-plot method, and other adsorption isotherms [3,6–8]. Surface coverage is generally described with the Brunauer-Emmett-Teller (BET) adsorption isotherm, which allows the specific surface area of the porous solid to be determined [1,6,8]. On the other hand, capillary condensation of vapors is the primary method of assessment of pore size distribution (PSD) in the range of mesopores [1,4,6,8]. Capillary condensation is associated with a shift of the vapor–liquid coexistence in pores compared to bulk fluid. This means that a confined fluid in a pore condenses at a pressure lower than the saturation pressure at a given temperature. This phenomenon, in the majority of systems, is accompanied by hysteresis [4,6,8].

In recent years the standard method for determining the PSD in the mesoporous range with the help of adsorption isotherms was the Barret-Joyner-Hallenda (BJH) method [8]. However, this methodology does not estimate the PSD properly. Consequently, a new methodology of adsorption isotherm assessment based on the nonlocal density functional theory, which originated in the density functional theory applied to inhomogeneous fluids, has revolutionized the methodology of PSD calculation in porous materials [14].

All these characterization methodologies will be described and illustrated with concrete experimental data in Chapters 3 and 4.

2.5 SOME EXAMPLES OF THE APPLICATION OF THE VOLUMETRIC METHOD

2.5.1 Volumetric Automatic Surface Area and Porosity Measurement Systems

The adsorbed amount as a function of pressure can be obtained by volumetric [5,8] (see Figure 2.4 [17]) and gravimetric methods [5,8] and, to a smaller extent, by carrier gas and calorimetric techniques [23,24]. The volumetric method to carry out the microporosity, surface area, and pore size analysis is based fundamentally on

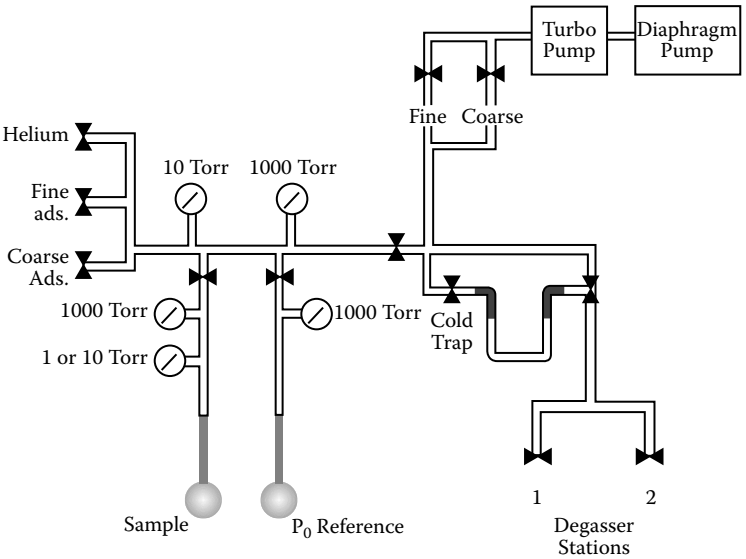

FIGURE 2.4 Representation of a commercial volumetric adsorption apparatus (taken from Thommes, M., in *Nanoporous Materials: Science and Engineering* [Lu, G.Q. and Zhao, X.S., Eds.]. Imperial College Press, London, 2004, Chapter 11, p. 317, reproduced with the author's permission).

nitrogen and argon adsorption isotherms obtained with the volumetric method at temperatures of liquid nitrogen (77.35 K) and liquid argon (87.27 K). As will be shown in Chapter 4, the shape of adsorption and desorption isotherms depends on pore size and temperature, as well as on the chemical and geometrical heterogeneity of the tested porous material.

A model of a volumetric adsorption apparatus is given in the graphic representation shown in Figure 2.4 [17]. The volumetric sorption equipment is set with pressure transducers in the dosing volume of the apparatus, with high-precision pressure transducers devoted to measure the pressure in the sample cell [17,25,26]. For this reason, the sample cell is isolated throughout equilibration, which guarantees a very small void volume and consequently a highly accurate determination of the adsorbed amount [17,25].

The vapor pressure of the adsorbate at the temperature of the adsorption experiment, P_0, is measured during the whole analysis by means of a saturation pressure transducer, which allows the vapor pressure to be monitored for each data point [17,25]. This produces great accuracy and precision in the determination of the relative pressure, $x = P/P_0$, and thus in the measurement of the pore size distribution [25].

Finally, it is necessary to state that the vacuum system of a standard commercial volumetric adsorption apparatus utilizes a diaphragm pump as a fore-pumping system for the turbomolecular pump, in order to guarantee a completely oil-free environment for the adsorption measurement and the outgassing of the sample, previous to the analysis [25].

2.5.2 Adsorption Isotherms of Nitrogen at 77 K in Zeolites

The study of zeolites as adsorbent materials began in earnest in 1938, when Prof. R. M. Barrer published a series of papers on the adsorptive properties of zeolites [27]. In the last 50 years, zeolites, both natural and synthetic, have become one of the most important materials in modern technology [27–38]. Today, the production and application of zeolites for industrial processes is a multimillion-dollar industry.

Zeolites have been shown to be good adsorbents for H_2O, NH_3, H_2S, NO, NO_2, SO_2, CO_2, linear and branched hydrocarbons, aromatic hydrocarbons, alcohols, ketones, and other molecules. However, adsorption is not only an industrial application of zeolites, it is also a powerful means of characterizing these materials [1–12], because the adsorption of a particular molecule gives information about the microporous volume, the mesoporous area and volume, the size of the pores, the heat of adsorption, and molecular transport.

The N_2 adsorption isotherm of a natural erionite, sample AP [32], at 77 K is shown in Figure 2.5. Sample AP contain 85% of erionite, the rest in all samples is composed of 15% of other minerals, such as montmorillonite (2–10 wt. %), quartz (1–5 wt. %), calcite (1–6 wt. %), feldspars (0–1 wt. %), magnetite (0–1 wt. %), and volcanic glass (3–6 wt. %) [34].

Figure 2.6 and Figure 2.7 show the N_2 adsorption isotherms at 77 K of the synthetic zeolites, Na-Y (CBV100, SiO_2/Al_2O_3 = 5.2) (Figure 2.6) [3] and Na-Y (SK-40, SiO_2/Al_2O_3 = 4.8) (Figure 2.7) [3].

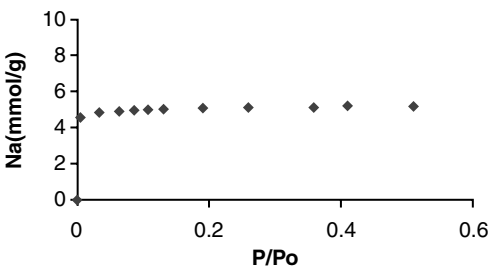

FIGURE 2.5 N_2 adsorption isotherm at 77 K of the natural erionite, sample AP.

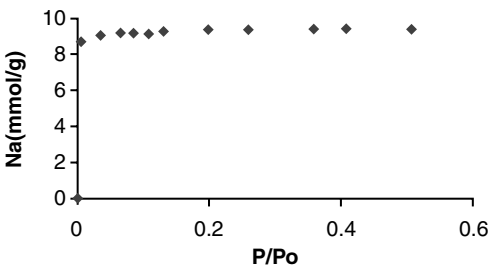

FIGURE 2.6 N_2 adsorption isotherm at 77 K of the synthetic zeolite Na-Y, sample CBV-100.

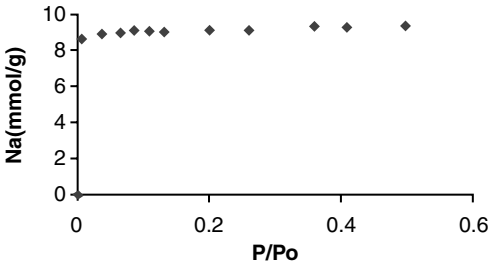

FIGURE 2.7 N_2 adsorption isotherm at 77 K of the the synthetic zeolite Na-Y, sample SK-40.

The N_2 adsorption isotherms at 77 K were measured with an accelerated surface area and Porosimetry System ASAP 2000 from Micromeritics [3,32], which is a volumetric automatic apparatus similar to those reported in Figure 2.4.

2.5.3 Calorimetry of Adsorption of NH_3 in $AlPO_4$-5 and FAPO-5 Molecular Sieves

$AlPO_4$-5 and FAPO-5 molecular sieves, synthesized using procedures previously described [39–42], were used for the study of the calorimetry of adsorption of NH_3. The occluded amine in both cases was triethylamine (TEA) [40]. The quantity of Fe included in the FAPO-5 molecular sieve was determined by X-ray fluorescence using a Camberra spectrometer equipped with a Si–Li detector [3,40]. The X-ray diffractograms of $AlPO_4$-5 and FAPO-5 were obtained in a Carl Zeiss TUR-M62 apparatus [40]. The crystallinity of the as-synthesized FAPO-5 and $AlPO_4$-5 molecular sieves was approximately 100%. The weigh percent of metal included in the framework of the FAPO molecular sieve was 1% [40]. The heat of adsorption of NH_3 in the $AlPO_4$-5 and FAPO-5 molecular sieves was measured in a heat flow calorimeter using the equation [32]:

$$\Delta Q = \kappa \int \Delta T dt$$

where ΔQ is the heat evolved during the finite increment, Δn_a, in the magnitude of adsorption, κ is a calibration constant, ΔT is the difference between thermostat temperature and the sample temperature during adsorption, and t is time.

The calorimeter was a high-vacuum line for adsorption measurements applying the volumetric method, consisting of a Pyrex glass, homemade vacuum system including a sample holder, a dead volume, a dose volume, a U-tube manometer, and a thermostat (see Section 2.4.1). In the sample holder the adsorbent (thermostated with 0.1% of temperature fluctuation) is in contact with a chromel–alumel thermocouple included in an amplifier circuit (amplification factor: 10), and connected with an x-y plotter [3,32]. The calibration of the calorimeter was performed using the reported data for the adsorption of NH_3 at 300 K in Na-X zeolite [38]. The differential heat of adsorption was calculated with the help of Equation 2.8 in increment form: $q_{diff} = \Delta Q/\Delta n_a$.

TABLE 2.1
Differential Heat of Adsorption, q_{diff}, of NH_3 at 300 K versus θ in $AlPO_4$-5 and FAPO-5

θ	q_{diff}($AlPO_4$-5) [kJ/mol]	q_{diff}($FAPO_4$-5) [kJ/mol]
0.02	65	111
0.03	63	81
0.04	62	63
0.06	58	60
0.08	49	58
0.10	40	56

The results obtained during the measurement of the differential heats of adsorption of NH_3 at 300 K in $AlPO_4$-5 and FAPO-5 molecular sieves are presented in Table 2.1. The error in q_{diff} is ±2 kJ/mol, $\theta = n_a/N_a$, n_a is the magnitude of adsorption, and N_a is the maximum magnitude of adsorption in the zeolite.

REFERENCES

1. Sing, K.S.W., Everett, D.H., Haul, R.A.W., Moscou, L., Pirotti, R.A., Rouquerol, J., and Siemieniewska, T., *Pure App. Chem.*, 57, 603, 1985.
2. Roque-Malherbe, R., *Physical Adsorption of Gases*, ENPES-MES, Havana, 1987, and *Physical Chemistry of Zeolites,* ENPES-MES, Havana, 1988.
3. Roque-Malherbe, R., *Mic. Mes. Mat.*, 41, 227, 2000.
4. Adamson, A.W. and Gast, A.P., *Physical Chemistry of Surfaces* (sixth ed,), J. Wiley & Sons, New York, 1997.
5. Ross, S. and Olivier, J.P., *On Physical Adsorption,* Wiley, New York, 1964.
6. Gregg, S.J. and Sing, K.S.W., *Adsorption Surface Area and Porosity*, Academic Press, London, 1982.
7. Dubinin, M.M., *Prog. Surface. Membrane Sci.*, 9, 1, 1975.
8. Rouquerol, F., Rouquerol, J., and Sing, K., *Adsorption by Powder Porous Solids*, Academic Press, New York, 1999.
9. Ruthven, D.W., *Principles of Adsorption and Adsorption Processes,* Wiley, New York, 1984.
10. Fraissard, J.P., *Physical Adsortion: Experiment, Theory and Applications,* Kluwer Academic Publishers, The Netherlands, 1997.
11. Rudzinski, W. and Everett, D.H., *Adsorption of Gases in Heterogeneous Surfaces,* Academic Press, London, 1992.
12. Rege, S.U. and Yang, R.T., in *Adsorption. Theory, Modeling and Analysis* (Toth, J., Ed.), Marcel Dekker, New York, 2002, p. 175.
13. Hill, T.L., *An Introduction to Statistical Thermodynamics,* Dover Publications Inc., New York, 1986.
14. Neimark, A.V. and Ravikovitch, P.I., *Mic. Mes. Mat.,* 44–45, 697, 2001.
15. Bering, B.P., Dubinin, M.M., and Serpinskii, V.V., *J. Coll. Int. Sci.*, 38, 185, 1972.
16. Roque-Malherbe, R., *J. Thermal Anal.,* 32, 1361, 1987.

17. Thommes, M., in *Nanoporous Materials: Science and Engineering* (Lu, G.Q. and Zhao, X.S., Eds.), Imperial College Press, London, 2004, p. 317.
18. Kiseliov, A., in *Curso de Fisica Quimica* (Gerasimov, I.I., Ed.), Editorial MIR, Moscow, 1971, p. 441.
19. Zhujovitskii, A. A., *Kolloidzschr* 66, 139, 1934.
20. Shchukin, E.D., Perzov, A.V. and Amelina, E.A., *Kolloidnaia Ximia,* Ximia, Moscow, 1982.
21. Kresge, C.T., Leonowicz, M.E., Roth, W.J., Vartuli J.C., and Beck, J.S., *Nature,* 359, 710, 1992.
22. Zhao, X.S., Lu, G.Q., and Millar, J.G., *Ind. Eng. Chem. Res.,* 35, 2075, 1996.
23. Kaneko, K., Ohba, T., Hattori, Y., Sunaga, M., Tanaka, H., and Kanoh, H., *Stud. Surf. Sci. Catal.*, 144, 11, 2002.
24. Keller, J.U., Robens, E., and du Fresne von Hohenesche, C., *Stud. Surf. Sci. Catal.*, 144, 387, 2002.
25. AUTOSORB-1, Manual, 2003.
26. Micromeritics, ASAP 2020. Description, 1992.
27. Barrer, R.M., *Zeolites and Clay Minerals as Sorbents and Molecular Sieves,* Academic Press, London, 1978.
28. Breck, D.W., *Zeolite Molecular Sieves,* J. Wiley, and Sons, New York, 1974.
29. Vansant, E.F., *Pore Size Engineering in Zeolites,* J. Wiley & Sons, New York, 1990.
30. Szostak, R., *Handbook of Molecular Sieves,* Van Nostrand-Reinhold, New York, 1992.
31. Tsitsisvili, G.V., Andronikashvili, T.G., Kirov, G.N., and Filizova, L.D., *Natural Zeolites,* Ellis Horwood, New York, 1992.
32. Roque-Malherbe, R., Lemes-Fernandez, L., Lopez-Colado, L., de las Pozas, C., and Montes-Caraballal, A., in *Natural Zeolites '93 Conference Volume International Committee on Natural Zeolites* (Ming, D.W. and Mumpton, F.A., Eds.), Brockport, New York, 1995, p. 299.
33. Corma, A., *Chem. Rev.*, 95, 559, 1995.
34. Roque-Malherbe, R., in *Handbook of Surfaces and Interfaces of Materials,* Volume 5, (Nalwa, H.S., Ed.), Academic Press, New York, Chapter 12, 2001, p. 495.
35. Guisnet, M. and Gilson, J.-P. (Eds.), *Zeolites for Cleaner Technologies,* Imperial College Press, London, 2002.
36. Auerbach, S.M., Corrado, K.A., and Dutta, P.K. (Eds.), *Handbook of Zeolite Science and Technology,* Marcell Dekker, Inc., New York, 2003.
37. Roque-Malherbe, R. and Marquez-Linares, F., *Facets-IUMRS Journal,* 3, 8, 2004.
38. Avgul, N.M., Aristov, B.C., Kiseliov, A.V., and Kurdiukova, L.Ya., *Zhurnal Fizicheskoi Ximii,* 62, 2678, 1968.
39. Lok, B.M., Messina, C.A., Patton, R.L., Gajek, R.T., Cannan, T.R., and Flanigen, E.M., *Amer. Chem. Soc.*, 106, 6092, 1984.
40. Roque-Malherbe, R., Lopez-Cordero, R., Gonzales-Morales, J.A., de Onate-Martinez, J., and Carreras-Gracial, M., *Zeolites,* 13, 481, 1993.
41. Martens, J.A. and Jacobs, P.A., in *Advanced Zeolites Science and Applications, Surface Science and Catalysis,* Vol 85, (Jansen, J.C., Stucker, M., Karge, H.G., and Eweitkamp, J., Eds.), Elsevier, Amsterdam, 1994, p. 653.
42. de las Pozas, C., Lopez-Cordero, R., Gonzales-Morales, J.A., Travieso, N., and Roque-Malherbe., R., *J. Mol. Catal.*, 83, 145, 1993.

3 Microporosity and Surface Area Evaluation Methods

3.1 INTRODUCTION

Gas adsorption measurements are widely used for the characterization of the surface and the porosity of porous materials [1–43]. This methodology is specifically applied for the calculation of the surface area, pore volume, and pore size distribution (PSD) of porous materials [3,4].

As was previously affirmed, during adsorption of vapors in complex porous systems, the adsorption process occurs approximately as follows [2,3,13,20]: initially, micropore filling, where the adsorption behavior is dominated almost entirely by the interactions of the adsorbate and the pore wall; afterward, at higher pressures, external surface coverage, consisting of monolayer and multilayer adsorption on the walls of mesopores and open macropores, and capillary condensation taking place in the mesopores.

This chapter will explain:

1. how adsorption in micropores is applied as a methodology for the measurement of the micropore volume using the Dubinin and other adsorption isotherms and the t-plot method [2,5–7]
2. how surface coverage is described with the BET adsorption isotherm, which also allows measurement of the specific surface area of the porous solid [3,4,15,20]
3. the Horvath-Kawazoe method of assessment of pore size distribution (PSD) in the range of micropores [4]

3.2 THE DUBININ AND OSMOTIC ADSORPTION ISOTHERMS

3.2.1 Dubinin Adsorption Isotherm

The adsorption process in the micropore volume is characterized by n_a, the magnitude of adsorption in the micropore volume, which is expressed in mol adsorbed/mass of dehydrated adsorbent. Additionally, the maximum adsorption magnitude (i.e., the amount adsorbed, which saturates the micropore volume of the adsorbent) is described by the parameter N_a, which is also expressed in mol adsorbed/mass of dehydrated adsorbent.

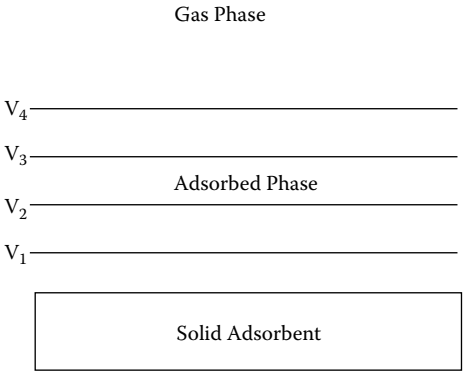

FIGURE 3.1 Polanyi adsorption model.

The Dubinin adsorption isotherm equation can be deduced using the Dubinin's theory of volume filling and the Polanyi's adsorption potential [5]. Polanyi, in 1914, developed possibly the first consistent adsorption theory. Dubinin, who was a disciple of Polanyi, took this theory, which fundamentally consists of the fact that a relation exists between the volume of the adsorption space, V_i, and the potential energy of the adsorption field, ε_i (see Figure 3.1) [4,30]:

$$\varepsilon_i = F(V_i)$$

Polanyi called this the characteristic function, which was considered independent of temperature. The following consideration of this theory was that [4]:

$$\mu_g = \mu_L + \varepsilon_i = \mu_a \tag{3.1a}$$

where μ_g is the chemical potential of the adsorbate in the gas phase, μ_L is the chemical potential of the adsorbate in the pure liquid phase, μ_a is the chemical potential of the adsorbate in the gas phase, and ε_i, as was previously affirmed, is the potential energy of the adsorption field. Therefore, with the help of Equation 3.1a, it is easy to show that [4,30]:

$$\varepsilon_i = RT \ln\left(\frac{P_0}{P_i}\right) \tag{3.1b}$$

where P_o is the vapor pressure of the adsorptive at the temperature, T, of the adsorption experiment, and P_i is the equilibrium adsorption pressure (ε could be also designed as the differential work of adsorption). It is necessary, at this point, to acknowledge that Equation 3.1a was justified in Chapter 2, Section 2.3.3.

Following the so-called Gurvich rule [40], it is possible to obtain the relation, $V_i = V^L n_a$, between the volume of the adsorption space, V_i, and the amount adsorbed,

where V^L is the molar volume of the liquid phase which conforms the adsorbed phase. Combining Equation 3.1b with the characteristic function and the relation between the volume of the adsorption space and the amount adsorbed, we will get [4,30]:

$$F(V_i) = f(n_a) = \varepsilon_i = RT \ln\left(\frac{P_0}{P_i}\right)$$

Now, applying the Weibull distribution function, the relation between the amount adsorbed, n_a, and the differential work of adsorption, ε, is defined by the following relation [5]:

$$n_a = N_a \exp\left(-\frac{\varepsilon}{E}\right)^n \tag{3.2a}$$

where E is a parameter named the characteristic energy of adsorption, N_a is the maximum amount adsorbed in the volume of the micropore, and n ($1 < n < 5$) is an empirical parameter.

Merging Equations 3.1b and 3.2a, it is possible to get the Dubinin adsorption isotherm equation [5] in the following form:

$$n_a = N_a \exp\left(-\frac{RT}{E} \ln\left[\frac{P_0}{P}\right]\right)^n \tag{3.2b}$$

It is possible, as well, to express the Dubinin adsorption isotherm equation in linear form:

$$\ln\left(n_a\right) = \ln\left(N_a\right) - \left(\frac{RT}{E}\right)^n \left(\ln\frac{P_0}{P}\right)^n \tag{3.3}$$

which is a very powerful tool for the description of the experimental data of adsorption in microporous material.

Figure 3.2 shows the Dubinin plot of the adsorption isotherm in the range: $0.001 < P/P_o < 0.03$, describing the adsorption of N_2, at 77 K, in a high-silica commercial HY zeolite, specifically, sample CBV-720, provided by PQ corporation. The isotherm was obtained in an Autosorb-1 gas adsorption system [27]. It is evident that, in the present case, the experimental data are accurately fitted by Equation 3.3.

The Dubinin plot shown in Figure 3.2 was carried out as a linear plot:

$$y = \ln\left(n_a\right) = \ln\left(N_a\right) - \left(\frac{RT}{E}\right)^n \ln\left(\frac{P_0}{P}\right)^n = b - mx$$

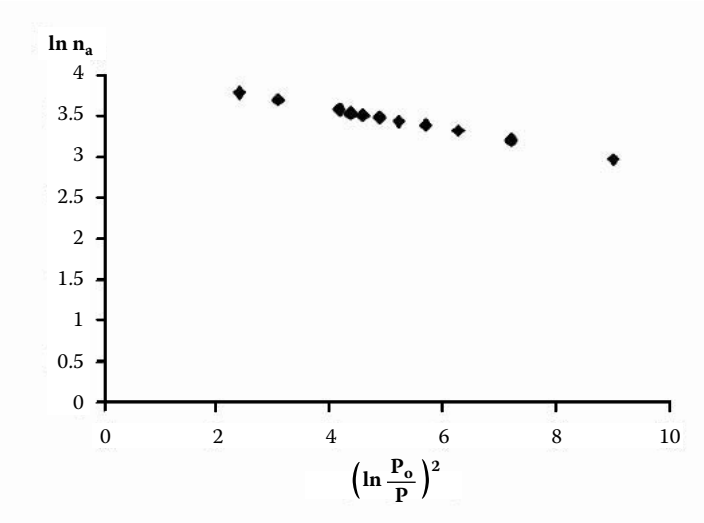

FIGURE 3.2 Dubinin plot for sample CBV-720 N_2 at 77 K.

where

$$y = \ln\left(n_a\right),\ \ b = \ln\left(N_a\right),\ \ m = \left(\frac{RT}{E}\right)^n, \text{ and } zx = \ln\left(\frac{P_0}{P}\right)^n$$

However, the fitting process of the Dubinin equation could be also carried out with the help of a nonlinear regression method [44]. The fitting process could be carried out with a program based on a least square procedure [44], which allows us to calculate the best fitting parameters of Equation 3.2b, i.e., N_a, E, and n, if this parameter is not taken as a constant, for example, $n = 2$. The program also calculates the regression coefficient and the standard errors.

When the Dubinin equation is applied, the additional output of the calculation process is the parameter, E, of the Dubinin equation, which is closely related with the adsorbate–adsorbent interaction. In the framework of the volume filling theory of adsorption, it is feasible to make an approximate estimation of q_{iso}, the isosteric heat of adsorption, using only one experimental isotherm. As we know (see Chapter 2, Section 2.3.2) [2,21,23]:

$$\left(\frac{d(\ln P)}{dT}\right)_\Gamma = \frac{\overline{H}_g - \overline{H}_a}{RT^2} = \frac{q_{iso}}{RT_2}$$

If we made the approximation that Γ = *constant* is equivalent to n_a = *constant,* it is possible to calculate the isosteric heat of adsorption employing the expression [2,37]:

$$q_{iso} = RT^2 \left(\frac{d(\ln P)}{dT} \right)_{n_a}$$

Then, substituting the Dubinin adsorption equation into the previous equation, it is possible to show that [2,37]:

$$q_{iso} \approx L + E \left[\ln \left(\frac{N_a}{n_a} \right) \right]^{1/n}$$

where L [kJ/mol] is the liquefaction heat of the adsorbate at the temperature of the adsorption experiment, and E and n are the parameters of the Dubinin adsorption equation.

3.2.2 Osmotic Adsorption Isotherm

In the osmotic theory of adsorption, the adsorption phenomenon in a microporous adsorbent, as for example a zeolite, is considered as the "osmotic" equilibrium between two solutions (vacancy plus molecules) of different concentrations. One of these solutions is created in the micropores, and the other in the gas phase, and the role of the solvent in the present model is carried out by the vacancies; this means by vacuum [5,7].

These solutions could only be in equilibrium when one of the solutions is immersed in an external field. The key assumption of the model is that the potential field can be virtually represented by an osmotic pressure, Π. That is, the effect of the adsorption field present in, for instance, the zeolite cavities and channels, can be formally represented by the difference in pressures between the gas and the adsorbed phase. Therefore, if we consider that the adsorption space is an inert volume, then the adsorption effect is caused by a virtual pressure applied to compress the adsorbed phase in this volume [5,7]. That is, we could delineate a mental experiment, where the micropore is dispossessed of its adsorption field. In this case we will have only a volume (i.e., an empty adsorption space), where the role of the adsorption field is taken by an external pressure, Π.

Following the hypotheses of the osmotic theory of adsorption developed by Bering and Serpinskii [7], it is possible to state that the volume occupied by the adsorbate, V_a, and the vacancies, V_x, or free volume is [5,7]:

$$V_a + V_x = V$$

Considering now that the volume occupied by an adsorbed molecule, b, and a vacancy is the same, then:

$$\frac{V_a}{b} + \frac{V_x}{b} = n_a + N^x = \frac{V}{b} = N_a$$

Multiplying this expression by $1/N_a$, we will get:

$$\frac{V_a}{N_a b} + \frac{V_x}{N_a b} = \frac{n_a}{N_a} + \frac{N^x}{N_a} = \frac{V}{N_a b} = X_a + X^x = 1$$

where X_a, and X^x are the molar fractions of adsorbed molecules and vacancies, respectively.

If we consider that adsorption in a micropore system could be described as an osmotic process, where vacuum (i.e., the vacancies) is the solvent, and the adsorbed molecules the solute, then by applying the methods of osmosis thermodynamics to the above described model [5,7], it is possible to obtain the following adsorption isotherm equation:

$$n_a = \frac{N_a K_0 P^B}{1 + K_0 P^B} \tag{3.4}$$

called the osmotic isotherm of adsorption. Equation 3.4 reduces, for $B = 1$, to a Langmuir-type isotherm equation describing a volume filling:

$$n_a = \frac{N_a K_0 P}{1 + K_0 P} \tag{3.4a}$$

Equation 3.4 is known in literature [21] as the Sips or Bradley's isotherm equation. This isotherm equation describes the experimental data of adsorption in zeolites and other micoroporous materials fairly well [5].

The linear form of the osmotic equation could be expressed as follows:

$$y = P^B = N_a \left(\frac{P^B}{n_a} \right) + \frac{1}{K} = mx + b \tag{3.4b}$$

where $y = P^B$, $x = P^B/n_a$, $m = N_a$, is the slope, and $b = 1/K$ is the intercept.

Figure 3.3 shows the plot of the linear form of the osmotic isotherm equation, with $B = 0.5$, using adsorption data of NH_3 adsorbed at 300 K in a homoionic magnesium natural zeolite sample labeled CMT, which is a mixture of clinoptilolite (42 wt. %) and mordenite (39 wt. %) and other phases (15 wt. %), where the other phases are: montmorillonite (2–10 wt. %), quartz (1–5 wt. %), calcite (1–6 wt. %), feldspars (0–1 wt. %), and volcanic glass [37]. The adsorption data reported in Figure 3.3 was determined volumetrically in a Pyrex glass [37] vacuum system, consisting of a sample holder, a dead volume, a dose volume, a U-tube manometer, and a thermostat (see Chapter 2, Section 2.4.1).

With this plot it was possible to calculate the maximum adsorption capacity of this zeolite, which is: $m = N_a = 5.07$ mmol/g, and $b = 1/K = -0.92$, $[(\text{Torr})^{0.5}]$. It is, as well, obvious that the experimental data is accurately fitted by Equation 3.4b.

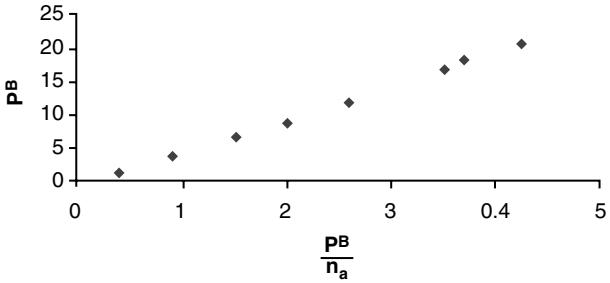

FIGURE 3.3 Linear osmotic plot, with B = 0.5 of the adsorption data of NH_3 at 300 K in magnesium homoionic CMT zeolite.

As was indicated previously, the fitting process of the osmotic isotherm equation could also be carried out with the help of a nonlinear regression method [44]. The fitting process allows us to calculate the best fitting parameters of Equation 3.4, i.e., N_a, K_0, and B, if this parameter is not taken as a constant (for example, $B = 1$). The program also calculates the regression coefficient, and the standard errors.

3.3 LANGMUIR AND FOWLER–GUGGENHEIM TYPE ADSORPTION ISOTHERM EQUATIONS

3.3.1 Introduction

Now we will apply the grand canonical ensemble methodology to deal with the adsorption process in zeolites and related materials [2,31,32].

Zeolites are three-dimensional microporous crystalline materials which are built from tetrahedra (simplified as TO_4) linked in the corners, sharing all oxygen atoms [45]. Zeolites belong to the group of molecular sieves, and about 150 structure types are known today.

Silicon and aluminum are the main tetrahedrically coordinated atoms (AlO_4 and SiO_4 tetrahedra) in aluminosilicate zeolites. However, elements such as: P, Pd, Ge, Ga, Fe, B, Be, Cr, V, Zn, Zr, Co, Mn, and others could also be tetrahedrically coordinated (TO_4) atoms incorporated into the zeolite [38,45]. Most zeolites and related materials are synthetic (more than 100 structure types), and this number is constantly increasing [45]. In addition, about 40 different natural zeolites have been found in the Earth's crust.

Aluminosilicate zeolites are three-dimensional microporous crystalline aluminosilicates. The zeolite framework is built from AlO_4 and SiO_4 tetrahedra, linked in the corners, sharing all oxygen atoms. The presence of tetracoordinated Al generates negative charge that must be balanced by extra-framework cations (one per Al). The chemical composition of aluminosilicate zeolites can be expressed as: $M_{x/n}[(AlO_2)_x(SiO_2)_y]\cdot zH_2O$, where M are the balancing cations (charge +n) compensating the charge from the T(III) atom in tetrahedral coordination, and z is the water contained in the voids of the zeolite. The balancing cation can be an inorganic (metal), or an

organic or inorganic species, for example ammonium. If this cation is located within the zeolite channel it can be exchanged, giving the zeolite its ion-exchange property.

Zeolite dimensions are determined during the synthesis procedure, revealing cages, channels, and pores of very different sizes depending on the zeolitic structure. These dimensions depend on the arrangement of the tetrahedra to form substructures.

Thus, a zeolite is a microporous crystalline material with selective adsorption, ionic exchange, catalytic, and other properties on the basis of its structure and composition. As was previously stated, zeolites belong to the group of molecular sieves, a term coined by McBain in 1932. Molecular sieves also include clays, porous glasses, microporous charcoals, active carbons, and other materials. Therefore, to simplify the nomenclature, when we refer here to zeolites we are also including the related materials.

3.3.2 Application of the Grand Canonical Ensemble Methodology to Describe Adsorption in Zeolites

In order to get isotherm equations to handle the adsorption process in zeolites and related materials, using the grand canonical ensemble methodology, we will conceive the zeolite as a grand canonical ensemble (GCE). That is, we will consider the zeolite cavities or channels as independent open subsystems belonging to the GCE (see Chapter 1, Section 1.6). In this case, it is possible to use statistical thermodynamics to describe the adsorption of gases in zeolites.

The zeolite is considered in the frame of the current model, as a grand canonical ensemble, where the cavities or channels are the systems belonging to the ensemble. The adsorption space is believed energetically homogeneous; that is, the adsorption field is the same in any place within the adsorption space. With the help of the laws of statistical thermodynamics, it will be relatively easy to describe the adsorption of gases in zeolites [2,31–36].

In the frame of this model, developed in different steps by different authors [31–36], the zeolite is considered as a system composed of M cavities or channels. Consequently, we have M independent open subsystems belonging to the GCE. If each cavity or channel can accommodate a maximum of m molecules (where $m = w/b$, w is the channel or cavity volume, and b the sorbate molecular volume), then the cavity or channel could be considered as an independent subsystem, and the grand canonical partition function for the zeolite will be [2,36] (see Chapter 1, Sections 1.7 and 1.8):

$$\Theta = [1 + \lambda Z(1) + \lambda^2 Z(2) + \ldots \lambda^m Z(m)]^M = \bar{Z}^M \tag{3.5}$$

in which:

$$\bar{Z} = \sum_{N=0}^{m} \lambda^N Z(N) \tag{3.5a}$$

is the grand canonical partition function of the cavity or channel, $Z(N)$ is the canonical partition function for N molecules in the cavity or channel ($0 < N < m$),

$$\lambda = \exp\left(\frac{\mu}{RT}\right)$$

is the absolute activity, and μ is the chemical potential. On that account, the expression for the average number of molecules adsorbed, $\bar{N}$, in the zeolite is [2,36].

$$\bar{N} = \frac{\partial \ln \Theta}{\partial \ln \lambda} = RT\left(\frac{\partial \ln \Theta}{\partial \mu}\right) \tag{3.6}$$

In the present case we are expressing Equation 3.6 in molar terms, since, $R = N_A k$, in which $N_A = 6.02214 \times 10^{23}$ [mol^{-1}], and $k = 1.38066$ [JK^{-1}] is the Boltzmann constant, and $R = 8.31451$ [JK^{-1}mol^{-1}] is the ideal gas constant.

If the condition, $m >> 1$, is fulfilled, it is possible to make the calculations with the grand canonical partition function of the cavity or channel (G.C.P.F.C.C.). In this case, the average number of molecules ($\bar{N}$) in the zeolite cavity or channel is [2,36]:

$$\bar{N} = \frac{\partial \ln \bar{Z}}{\partial \ln \lambda} = RT\left(\frac{\partial \ln \bar{Z}}{\partial \mu}\right) \tag{3.7}$$

Thereafter, the volume coverage can be calculated with the help of the following expression:

$$\theta = \frac{\bar{N}}{Mm} = \frac{M\bar{N}}{Mm} = \frac{\bar{N}}{m} \tag{3.7a}$$

where θ is the micropore volume recovery.

3.3.2.1 Immobile Adsorption

In the case of immobile adsorption in a homogeneous field, and considering lateral interactions between neighboring molecules, the canonical partition function for $N < m$ molecules in the cavity or channel is [2,34,36]:

$$Z(N) = \frac{m!}{N!(m-N)!}\left(Z_a^I\right)^N \exp\left(-\frac{N(E_0^a + \eta E_i)}{RT}\right) \tag{3.8}$$

where, as is very well-known [36]:

$$Z(N) = \frac{m!}{N!(m-N)!}X^N \tag{3.8a}$$

and

$$X \approx Z_a^I \exp\left(-\frac{(E_0^a + \eta E_i)}{RT}\right) \tag{3.8b}$$

where m is the number of adsorption sites in the cavity or channel, N is the number of adsorbed molecules, and Z_a^i is the canonical partition function for the internal degrees of freedom of the adsorptive in the adsorbed phase. In addition, E_o^a is the reference energy state for the adsorbed molecule in the homogeneous adsorption field inside the cavity or channel. Moreover,

$$\eta E_i = \frac{cN}{2m} E_i$$

is the interaction energy of an adsorbed molecule with neighboring adsorbed molecules, assuming a random distribution of neighbors, where c is the number of nearest neighbors to an adsorption site in the cavity [36].

In order to get the isotherm equation, it is necessary to carry out the following approximation:

$$\frac{cN}{2m} E_i \approx \frac{c\overline{N}}{2m} E_i$$

in Equation 3.9 [2,36]:

$$Z(N) = \frac{m!}{N!(m-N)!}\left(Z_a^I\right)^N \exp\left(-\frac{\left[NE_0^a + \left(\frac{c\overline{N}}{2m}\right)E_i\right]}{RT}\right) \tag{3.9}$$

To calculate the adsorption isotherm, we use Equations 3.5a, 3.7, and 3.9 and Newton's binomial polynomial expansion [34]:

$$B = (1+\lambda X)^m = \sum_{N=0}^{m} \frac{m!}{N!(m-N)}(\lambda X)^N$$

to get the following equation [2,34,36]:

$$\overline{N} = \frac{\partial \ln \overline{Z}}{\partial \ln \lambda} = \lambda \frac{\partial \ln \overline{Z}}{\partial \lambda} = \frac{A}{B}$$

where

$$A = m\lambda X(1+\lambda X)^{m-1}$$

and

$$X = Z_a^I \exp\left(-\frac{N(E_0^a + \left(\frac{c\overline{N}}{2m}\right)E_i)}{RT} \right)$$

Consequently, the adsorption isotherm is [2,36]:

$$\theta = \frac{\overline{N}}{m} = \frac{K_I P}{1+K_I P} \tag{3.10}$$

$$K_I = \left\{\frac{Z_a^I}{Z_g^I}\right\}\left[\frac{1}{RT\Lambda}\right]\exp\left(\frac{[(E_0^g - E_0^a)+\Omega\theta)]}{RT}\right) \tag{3.10a}$$

or

$$K_I = K_o^I \exp\left(\frac{\Omega\theta}{RT}\right) \tag{3.10b}$$

in which Z_g^i is the canonical partition function for the internal degrees of freedom of the adsorptive in the gas phase, E_o^g is the reference energy state for the gas molecule, and

$$\Omega = \frac{cE_i}{2}.$$

In addition,

$$\Lambda = \left(\frac{2\pi MRT}{h^2}\right)^{3/2},$$

where $M = N_A m$ is the molar mass of the adsorptive molecule, m is the mass of the adsorptive molecule, N_A is the Avogadro number, and h is the Planck constant.

Finally, it is necessary to affirm that the average adsorption field in the volume filled by the adsorbed molecules, in the present case of immobile adsorption, is: $\xi(\theta) \approx -[(E_0^g - E_0^a) + \Omega\theta]$ [2,35].

3.3.2.2 Mobile Adsorption

Let us consider again the zeolite as a grand canonical ensemble. Then, employing the hypothesis of mobile adsorption in a homogeneous adsorption field, and taking into account lateral interactions between neighboring molecules, the canonical partition function for $N < m$ molecules in the cavity or channel could be expressed as follows [2,36]:

$$Z(N) = \frac{w^N}{N!}[\Lambda]^N (Z_a^I)^N \exp\left(-\frac{N\left(E_0^a - \alpha \frac{N}{w} \right)}{RT} \right) \tag{3.11}$$

in which

$$\Lambda = \left(\frac{2\pi MRT}{h^2} \right)^{3/2},$$

where M is the molar mass of the adsorptive molecule, h is the Planck constant, $\alpha \approx B_2 RT$ [31], and B_2 is the second virial coefficient.

To calculate the adsorption isotherm, we use Equations 3.5a, 3.7, and 3.11 and the exponential series expansion [2,36]:

$$B = \sum_{N=0}^{m} \frac{1}{N!}(\lambda X)^N \approx \exp(\lambda X) \approx \left(1 + \frac{\lambda X}{m} \right)^m$$

to get:

$$\bar{N} = \frac{\partial \ln \bar{Z}}{\partial \ln \lambda} = \lambda \frac{\partial \ln \bar{Z}}{\partial \lambda} = \frac{A}{B}$$

where

$$A = \lambda X \left(1 + \frac{\lambda X}{m} \right)^{m-1}.$$

After that, we get the following isotherm equation [2,36]:

$$\theta = \frac{K_M P}{1 + K_M P} \tag{3.12}$$

where

$$K_M = \left\{ \frac{Z_a^I}{Z_g^I} \right\} \left[\frac{b}{RT} \right] \exp\left(\frac{[(E_0^g - E_0^a) + \Phi\theta)]}{RT} \right) \tag{3.12a}$$

$$K_M = K_0^M \exp\left(\frac{\Phi\theta}{RT} \right). \tag{3.12b}$$

In the present case, Z_a^i and Z_g^i are the canonical partition functions for the internal degrees of freedom of the adsorptive in the adsorbed phase and the gas phase, respectively. E_o^g is the reference energy state for the gas molecule, and E_o^a is the reference energy state for the adsorbed molecule in the homogeneous adsorption field inside the cavity or channel. Furthermore, $\Phi = \alpha/b$ is a parameter characterizing lateral interactions, and b, the sorbate volume, is expressed in molar units.

Finally, for mobile adsorption, the average adsorption field in the volume filled by the adsorbed molecules is: $\xi(\theta) \approx -[(E_0^g - E_0^a) + \Phi\theta]$ [2,35].

3.3.3 Some Remarks in Relation with the Langmuir Type and Fowler–Guggenheim Type Adsorption Isotherm Equations

If $c \approx 0$ or $\alpha \approx 0$, Equations 3.10 and 3.12 reduce to a Langmuir type (LT) adsorption isotherm equation:

$$\theta = \frac{K_L P}{1 + K_L P} \tag{3.13}$$

where, depending on the case (i.e., immobile, or mobile), $K_L = K_0^I$, or $K_L = K_0^M$.

Equations 3.10 and 3.12 are of the Fowler–Guggenheim type (FGT) adsorption isotherm equations *describing a volume filling rather than a surface coverage.* Likewise, Equation 3.13 is of the Langmuir Type (LT) adsorption isotherm equation, also *describing a volume filling rather than a surface coverage.* This is also the case for the adsorption isotherm Equation 3.4, which reduces to the LT isotherm Equation 3.4a, *describing a volume filling rather than a surface coverage.*

In addition, an adsorption isotherm equation for the description of the adsorption process in zeolites and related materials was obtained with the help of the modified lattice gas model and quantum statistical methods [9]:

$$\frac{\theta}{1-2\theta}=\left(1-\frac{1}{m}\right)\left[\frac{1}{\left(\frac{P_1}{P}\right)\left(\exp\left[\beta\varepsilon_2(1-2\theta)\right]-1\right)}\right] + \left(\frac{1}{m}\right)\left[\frac{1}{\left(\frac{P_1}{P}\right)\left(\exp\left[\beta\varepsilon_1(1-2\theta)\right]-1\right)}\right] \tag{3.14}$$

where:

$$P_1 = P_0\exp\left(\beta\varepsilon_0\right),\ \varepsilon_0=\varepsilon+\frac{U}{2},\ \varepsilon_1=t+\frac{U}{2},\ \varepsilon_0=\frac{U}{2}-\frac{t}{m-1},\ \beta=\frac{1}{RT}$$

and where m is the maximum number of molecules adsorbed in a cavity or channel, ε is the interaction energy between the zeolite framework and the molecule located in one adsorption site, U is the interaction energy between adsorbed molecules, and t is the probability of jumping between adsorption sites [9]. Equation 3.14 reduces to an LT isotherm equation if the condition $\varepsilon_1 = \varepsilon_2 = 0$ is observed (i.e., in the case of immobile adsorption without interactions), because $U = 0$ and $t = 0$ [9]:

$$\theta=\frac{1}{1+\frac{P_1}{P}} \tag{3.14a}$$

Thus, a variety of different approaches for describing the adsorption process in zeolites all lead to LT and FGT isotherms, describing adsorption as a volume filling effect. Consequently, it is possible to conclude that the LT and FGT adsorption isotherm equations describing volume filling must be useful in the characterization of the adsorption properties of zeolites and related materials [2], for systems where the lateral interactions between the adsorbed molecules are not considered isotherms of the following LT type:

$$\theta=\frac{K_L P}{1+K_L P},$$

and for systems which have the lateral interactions:

$$\theta=\frac{K_{FG} P}{1+K_{FG} P},$$

where K_L and K_{FG} are respectively functions of temperature, and temperature, and magnitude of adsorption whose specific form depends on the concrete model describing the physical situation.

As a result, the preceding isotherm equations, that is Equations 3.4a, 3.10, 3.12, 3.13, and 3.14a, obtained with completely different model descriptions of the adsorption process in microporous materials, all have a similar mathematical appearance. Therefore, it is possible to infer that these adsorption isotherm equations describing volume filling in micropore materials could be useful in the evaluation of the micropore volume of micropore materials. To show the usefulness of the obtained isotherm equations, an experimental test was carried out.

The test was carried out using Ar adsorption at 87 K in the following commercial zeolites: Na-Y (CBV100, SiO_2/Al_2O_3= 5.2) provided by the PQ Corporation, Na-X (13X, SiO_2/Al_2O_3 = 2.2) provided by Micromeritics, and Na-Y (SK-40, SiO/Al_2O_3 = 4.8) provided by the Linde Division of Union Carbide [2]. The experiments were carried out with a Micromeritics ASAP 2000 analyzer for adsorption isotherm determination [2,28].

The experimental data was fitted with the linear form of the FGT isotherm equation type:

$$\ln\left(\frac{\theta}{1-\theta}\right) = \ln K + \frac{k\theta}{RT} \tag{3.15}$$

which reduces to the LT isotherm equation type for $k = 0$. It is evident from Figure 3.4 that the LT isotherm equation fits Ar adsorption in the range $0.01 < \Theta < 0.4$, for Na-Y (SK-40), Na-Y(CBV100), and Na-X(13 X).

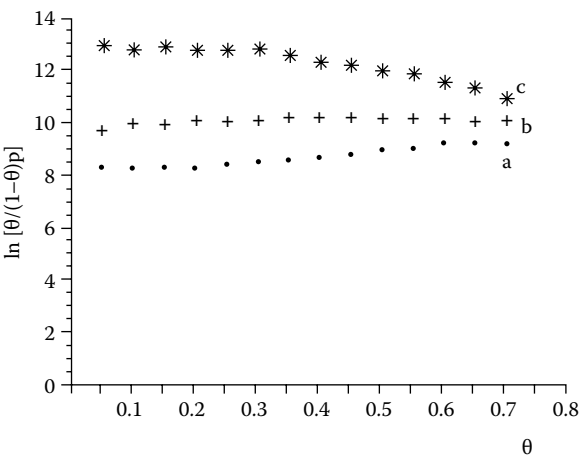

FIGURE 3.4 Plot of ln [Θ/(1 – Θ)P] versus Θ where $\Theta = n_a/N_a$ for the following commercial zeolites: (a) Na-Y (CBV-100), (b) Na-Y(SK-40), and (c) Na-X (13X).

TABLE 3.1
Micropore Volume, W^{Ar}, Measured with the Adsorption Isotherm of Ar at 87.3 K

Zeolite	W^{Ar} [cm³/g]
Na-Y (CBV100)	0.319
Na-Y (SK-40)	0.311
Na-X(13X)	0.192

Since Equation 3.15, with $k = 0$, describes the adsorption of Ar at 87 K in the above referred zeolites, then the linear form of the LT isotherm:

$$P = N_a\left(\frac{P}{n_a}\right) + \frac{1}{K} \tag{3.15a}$$

allows a reliable measurement of the micropore volume (W^{Ar}) for the studied zeolites (see Table 3.1 [2]). The calculation of W^{Ar} is carried out with the equation: $W^{Ar} = N_a \times b$, where N_a is determined with Equation 3.15a. The value for the parameter b (volume occupied by one mole of adsorbed Ar molecules) was $b = 32.19$ cm³/mol.

A methodology that, by applying the Dubinin isotherm in combination with LT, osmotic, and FGT isotherm equations, permits calculation of the micropore volume and other characteristics of zeolites and related materials will be described later, in Section 3.5.

As was specified previously, the fitting process of the LT and FGT isotherm equations could also be carried out with the help of a nonlinear regression method [44].

3.4 THE t-PLOT METHOD

Halsey, de Boer, and coworkers developed the t-plot method [4,27–29,39]. The method is based on the concept, introduced by Frenkel-Halsey-Hill [4,30], which states that it is possible to calculate t, which is the width (in [Angstrom]) of the adsorbed layer [4,28–30] or multilayer thickness. This method considers the adsorbed phase as a liquid adhered film over the solid surface, similar to what is shown in Figure 3.1. This model is valid for a multilayer adsorption (i.e., when

$$\frac{n_a}{N_m} > 2,$$

where N_m is the monolayer capacity). The surface liquid film is considered of uniform width, t, with density equal to the bulk liquid adsorbate, ρ_L, and in contact with a uniform surface, which creates an attraction adsorption field over the solid surface. Then, according with the previous suppositions, the adsorption magnitude will be [4]:

$$n_a = \rho_L t.$$

On the other hand, the attraction a adsorption field could be described by [4,30]:

$$V(z) = \frac{A}{z^9} - \frac{B}{z^m}.$$

Then, following a model similar to those proposed in the Polanyi theory [4,30], where the entropy contribution to the free energy is considered to be small in comparison with the large change of enthalpy, we will have [4]:

$$\mu - \mu_L = RT \ln\left(\frac{P}{P_0}\right)$$

and [4,30]:

$$\mu - \mu_L = V(z) \tag{3.16}$$

where Equation 3.16 was previously justified in Chapter 2, Section 2.3.3. Subsequently, since the adsorption process considered in the present model is a multilayer one, then,

$$V(z) \approx -\frac{B}{z^m};$$

consequently:

$$RT \ln\left(\frac{P}{P_0}\right) = -\frac{B}{z^m} = -\frac{C}{t^m}$$

where this equation shows a correlation between t and the relative pressure:

$$x = \frac{P}{P_0}.$$

The t-plot methodology suggests that, for multilayer adsorption, the shape of the adsorption isotherm is less dependent on the adsorbent structure than in the case of monolayer adsorption [4]. This means that t depends fundamentally on

$$x = \frac{P}{P_0}$$

and hardly on the nature of the adsorbent surface. Therefore, this thickness could be evaluated after normalizing an adsorption isotherm for an adsorbent that does

not possess micropores or mesopores. The multilayer thickness, *t,* can be calculated by the following relation [4]:

$$t = \frac{n_a}{N_m} d_0$$

where d_0 is the effective thickness of monolayer. Now, assuming, as was previously done, that the surface liquid film is considered of uniform width, *t,* and its density is equal to the bulk liquid adsorbate, ρ_L, then [4]:

$$d_0 = \frac{M}{\sigma N_A \rho_L}$$

where N_A is the Avogadro number, and σ is the cross-sectional area (i.e., the average area occupied by each molecule in a completed monolayer). Taking, for example, that $\sigma(N_2) = 0.162$ nm^2 for N_2 at 77 K, $M(N_2) = 28.1$ g/mol, and $\rho_L(N_2) = 0.809$ g/cm^3, we will obtain $d_0 = 0.354$ nm.

Lippens and de Boer [39] experimentally showed, by measuring *t* versus

$$x = \frac{P}{P_0}$$

plots (i.e., t-plots) of nitrogen at 77 K in different nonporous oxides, the existence of a "universal multilayer thickness curve," because of the similarity of the obtained t–plots [4,39]. In practice, the "universal multilayer thickness curve" is not currently accepted [4]. Conversely, for example, the following relations between *t* and (x^{-1}) are used to carry out the t-plot [27,29]:

$$t = 3.54\left(\frac{5}{2.303\log\left(\frac{P_0}{P}\right)}\right)^{1/3} \tag{3.17a}$$

which is the Halsey equation, valid for N_2 at 77 K; or the equation used by de Boer [27]:

$$t = \left(\frac{13.99}{\log\left(\frac{P_0}{P}\right) + 0.034}\right)^{1/2} \tag{3.17b}$$

Or in more general terms, the equation [27]:

$$t = a\left(\frac{1}{\ln\left(\frac{P_0}{P}\right)}\right)^{1/b} \tag{3.17c}$$

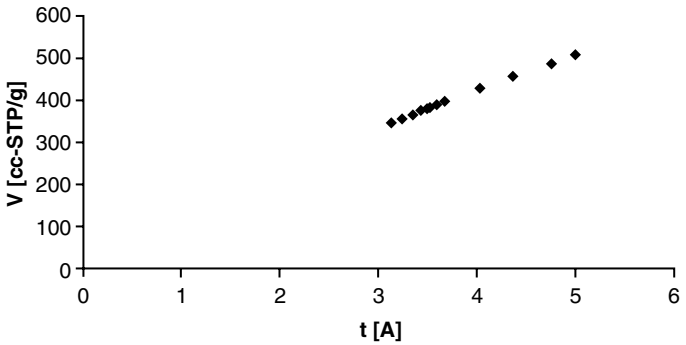

FIGURE 3.5 t-plot 70bs2-25C.

valid for other adsorbates and/or temperatures, in which, $a = 6.053$, and $b = 3$, for N_2 at 77 K. In all the Equations 3.17, P is the equilibrium adsorption pressure, and P_o the vapor pressure of the adsorptive at the temperature, T, of the adsorption experiment.

To carry out the calculation of the microporous volume and the area of the secondary porosity or outer area with the help of the t-plot method, it is necessary to plot n_a versus t (in [Angstrom]). A typical t-plot ($0.01 < P/P_0 < 0.3$) for the adsorption of N_2 at 77 K in a silica material, specifically in the sample 70bs2 [26], is presented in Figure 3.5. The t-plot is carried out with the help of Equation 3.17a or 3.17b to calculate t for a concrete value of $x = P/P_0$, and the amount adsorbed is taken from the experimental isotherm, for the same value of $x = P/P_0$, and then the plot of n_a versus t is carried out.

The method to calculate W, the microporous volume (in [cm^3/g]), and S (in [m^2/g]), the outer surface, applying the t–plot method is as follows. After the elimination of the points that do not fit a linear plot (see Figure 3.5), with the help of the following linear equation:

$$y = n_a = Rt + N_a = mx + b$$

the linear regression is carried out, and the intercept, $b = N_a$, and the slope, $m = R$, are calculated. The intercept is related with the microporous volume, W^{MP}. Then, applying the Gurvich rule [4,40] through the following relation:

$$W^{MP} = N_a V_L$$

where V_L is the molar volume of the adsorptive at the temperature, T, of the adsorption experiment, the volume of the micropores is calculated.

The outer surface will be [27,28]:

$$S = RV_L$$

TABLE 3.2
Micropore Volume, W^{MP}, Measured Using the N_2 Adsorption Isotherm at 77 K, and Applying the t-Plot Method

Zeolite	W_2^N [cm³/g]
Na-Y (CBV100)	0.305
Na-Y (SK-40)	0.303

since

$$n_a V_L = RV_L t + N_a V_L.$$

Then the term:

$$RV_L t = St$$

is equal to the contribution of the adsorption in the outer surface to the volume of the whole adsorbed phase.

Table 3.2 [2] reports values of the micropore volume, W^{MP}, of two commercial zeolites, specifically, Na-Y (CBV100, SiO_2/Al_2O_3= 5.2) provided by the PQ Corporation, and Na-Y (SK-40, SiO/Al O = 4.8) provided by the Linde Division of Union Carbide.

The reported micropore volumes were calculated with the help of the t-plot method, using N_2 adsorption isotherms at 77 K. The experiments were carried out with a Micromeritics ASAP 2000 analyzer for adsorption isotherm determination [2,28].

If we made a comparison between the results reported in Table 3.1 and Table 3.2, a similarity is evident between the results obtained by both methodologies. These results are also consistent with the crystallographic void volume [46] corresponding to the framework FAU [45] of zeolite Y.

3.5 ADDITIONAL COMMENTS ABOUT THE APPLICATION OF THE DUBININ AND OSMOTIC ISOTHERMS, THE LT AND THE FGT ISOTHERM EQUATION TYPES, AND THE t-PLOT METHOD IN THE MEASUREMENT OF THE MICROPORE VOLUME

Generally in porous materials, micropores, mesopores, and macropores are integrated. Then, the correct value of the micropore volume, W^{MP}, is extremely difficult to establish correctly, since in the majority of cases, it is difficult to determine the point where adsorption in the micropores ends and the adsorption in the mesopores starts [20].

For zeolites, which are primarily composed of micropores, in order to calculate the micropore volume, the author proposes a methodology consisting of fitting the

experimental adsorption data to the Dubinin isotherm equation and the LT, osmotic, or FGT isotherm equations using a least-square-fitting computer program [2]. During the fitting process, different parameters are tested, for example, *n, E,* and K and *B,* if the Dubinin and osmotic isotherm equations were applied. The fitting process is stopped when all the applied equations give the same value for N_a, the maximum adsorption magnitude. Then the micropore volume is calculated with the help of the following equation: $W = N_a V_L$, where V_L is the molar volume of the adsorptive used in the adsorption experiment [40].

The previously described methodology for the determination of the micropore volume in zeolites can be verified using NH_3 as adsorptive at 300 K. This gas is perfect for this application, because its boiling point (240 K) and its molecular kinetic diameter (σ = 3.08 A [46]) ensure that it is not adsorbed in the outer surface and easily penetrates through the microporosity [2,37].

Some examples of the use of this methodology, applying the Dubinin and the Osmotic adsorption isotherm equations, for the calculation of the micropore volume of natural zeolites are reported in Table 3.3. This table (Table 3.3) reports the following parameters: N_a, [mmol/g], the characteristic energy of adsorption, E [kJ/mol], and the micropore volume W^{MP} in [cm^3/g], for the adsorption of NH_3 at 300 K on different natural zeolites [37].

The maximum adsorption magnitude, N_a, is given in mmol of NH_3 adsorbed per gram of dehydrated zeolitic rock, and the microporous volume, W^{MP}, in cm^3 per g of dehydrated zeolitic rock. The errors in N_a, W, and E are ±0.2 (mmol/g), ±0.005 (cm^3/g), and ±0.4 (kJ/mol), respectively [37,47]. The NH_3 adsorption data were obtained in a Pyrex glass vacuum system consisting of sample holder, a dead volume, a dose volume, a U-tube manometer, and a thermostat [37] (see Chapter 2, Section 2.4.1).

The chemical composition (in oxide wt. %.), and the mineralogical composition (in wt. %), of the natural zeolite rocks employed to illustrate the micropore volume measurement method are reported in Table 3.4 and Table 3.5, respectively [37,47]. The sample identification (label: deposit name, location) is: HC: Castillas, Havana, Cuba; MP: Palmarito, Santiago de Cuba, Cuba; SA: AD, Aguas Prietas, Sonora,

TABLE 3.3
Parameters of the Dubinin Equation for NH_3 Adsorption at 300 K on Some Natural Zeolitic Rocks and Two Commercial Synthetic Zeolites

Sample	N_a [mmol/g]	W^{MP} [cm^3/g]	E [kJ/mol]	N
HC	6.2	0.130	28	2
MP	6.8	0.143	25	2
AP	6.9	0.145	31	2
CMT	6.1	0.128	22	2
Na-A	9.8	0.204	23	2
Na-X	10.1	0.210	24	2

TABLE 3.4
Chemical Composition (in Oxide Wt. %) of Some Natural Zeolite Rocks Used to Illustrate Distinct Properties and Applications of These Materials

Sample	SiO_2	Al_2O_3	Fe_2O_3	CaO	MgO	Na_2O	K_2O	H_2O
HC	66.8	13.1	1.3	3.2	1.2	0.6	1.9	12.1
MP	66.9	11.6	2.7	4.4	0.8	1.8	0.8	12.1
AP	59.6	14.2	2.3	2.2	1.5	2.4	3.3	13.8
CMT	66.6	12.5	2.0	2.7	0.7	1.7	0.8	12.9

TABLE 3.5
Mineralogical Composition (in Wt. %) of Specific Natural Zeolite Rocks Employed to Illustrate Some Properties and Applications of These Materials

Sample	Clinoptilolite	Mordenite	Erionite	Others
HC	85	0	0	15
MP	5	80	0	15
AP	0	0	85	15
CMT	42	39		19

Mexico; and CMT, Tasojeras, Ville Clara, Cuba [37,47]. The synthetic zeolite sample NaA was provided by Degussa, and the sample Na-X was provided by Laporte [37,47]. In Table 3.5, others are: montmorillonite (2–10 wt. %), quartz (1–5 wt. %), calcite (1–6 wt. %), feldspars (0–1 wt. %), magnetite (0–1 wt. %), and volcanic glass (3–6 wt. %).

In the case of natural zeolites, this information could be very helpful to find out the quantity of zeolite present in the natural zeolite rock [2]. The micropore volume for pure clinoptilolite and mordenite is: $W_{HEU} \approx W_{MOR} \approx 0.16$ cm^3/g [48], and the microporous volume of erionite could be estimated to be $W_{ERI} \approx 0.18$–0.19 cm^3/g [46].

Consequently, with the reported values for W and the micropore volume of the zeolitic phases present in a rock (W_{XXX}), it is feasible to calculate a fairly accurate value for the fraction of zeolitic phases present in the rock with the help of the equation:

$$f = \frac{W^{MP}}{W_{XXX}}.$$

This relation is valid if all the zeolite phases present in the rock exhibit approximately the same value for W_{XXX} and also if the quantity of molecules adsorbed by the impurity phases could be neglected.

TABLE 3.6
Micropore Volume (W_{Mic}) Corresponding to Some Silica Samples and an MCM-41 Mesoporous Material

Sample	W^{MP} [cm^3/g]
70bs2	0.18
68bs1E	0.27
75bs1	0.16
79BS2	0.21
74bs5	0.14
68C	0
MCM-41	0

On the other hand, adsorption isotherms of N_2 at 77 K are also used to measure the micropore volume. Some examples of the use of this methodology for the calculation of the micropore volume of amorphous silica materials are reported in Table 3.6 [26].

The silica samples tested were degassed at 200°C, for 3 h, in high vacuum (10^{-6} Torr), before analysis [26]. The micropore volume accessible to the N_2 molecule at 77 K (W^{MP}, [cm^3/g]) was measured using the t-plot method [4,5], which is a powerful tool for the measurement of the micropore volume in porous materials such as silica and active carbons, which could be composed of micropores, mesopores, and macropores. The condition to be successful in this task is to carefully select a proper range of relative pressures to find the linear zone (see Figure 3.5). In general, this range should be found around: $0.00001 < P/Po < 0.02$.

The Gurvich rule [40] was also applied, in the present case, for the calculation of the micropore volume. However, the adsorbate in the micropore does not necessarily have the same density as the adsorptive in the liquid state, as is needed for the fulfillment of this rule [49]. This is one of the facts that make it difficult to arrive to an unequivocal measurement of the micropore volume. Another factor that makes it difficult to get an unequivocal evaluation of the micropore volume, as was previously stated, is that in the present case (i.e., adsorption of N_2 at 77 K in amorphous silica) it is very difficult to determine the point where adsorption in the micropores finishes and the external surface coverage begins [26], since pore filling is observed at pressures very close to the pressure range where monolayer–multilayer formation on the pore walls occurs [20].

3.6 THE BET METHOD

The BET theory of multilayer adsorption for the evaluation of specific surface area, *S,* was developed by Brunauer, Emmett, and Teller [4,15]. However, it will be used here for the deduction of the isotherm equation the grand canonical ensemble approach, applying a methodology developed by Hill [31].

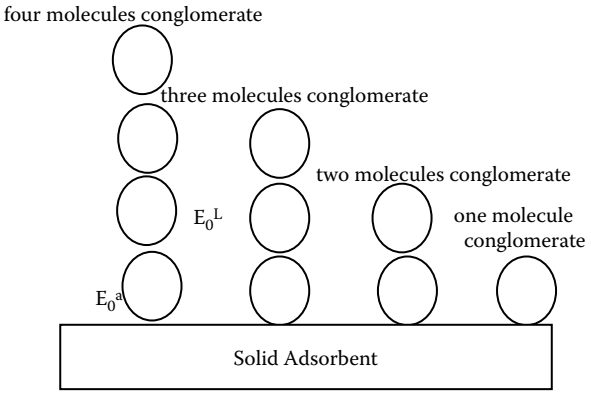

FIGURE 3.6 BET adsorption model.

The adsorption process, within the frame of the BET theory, is viewed as a layer-by-layer process. The surface is assumed to be energetically homogeneous; that is, the adsorption field is the same in any place within the surface. In addition, the adsorption process is considered immobile (i.e., each molecule is adsorbed in a concrete adsorption site in the surface). Then, the first layer of adsorbed molecules has an energy of interaction with the adsorption field, E_0^a, and the vertical interaction between molecules after the first layer is E_0^L (i.e., similar to the liquefaction heat of the adsorbate; see Figure 3.6). In addition, adsorbed molecules do not interact laterally.

The construction of the grand canonical partition function is a complex process, where the concepts of independent distinguishable systems will be applied (see Chapter 1, Sections 1.7 and 1.8) for each of the *s* molecules which form a conglomerate (see Figure 3.6). Specifically, each conglomerate has a variable number of molecules, which do not interact laterally with the neighboring conglomerates. Consequently, the adsorbed phase forms a grand canonical ensemble (GCE) of conglomerates. Since all the conglomerates form the adsorbed phase, then the adsorbed phase could be considered as a GCE, where the canonical partition function for a molecule adsorbed in an adsorption site the first layer is:

$$Z_1 = K_1 \exp\left(-\frac{E_0^a}{RT}\right) = q_1 \tag{3.18}$$

Similarly, for the next layers the molecular canonical partition function will be:

$$Z_2 = Z_3 = \ldots = Z_s = K_L \exp\left(-\frac{E_0^L}{RT}\right) = q \tag{3.19}$$

Since a_s is the number of conglomerates with *s* molecules, then *N,* the number of adsorption sites in the surface, is:

$$N = \sum_{s=0}^{m} a_s \tag{3.20}$$

Consequently, the number of adsorbed molecules will be:

$$N_a = \sum_{s=0}^{m} s a_s \tag{3.21}$$

The grand canonical partition function of an arbitrary conglomerate having m molecules will be:

$$\xi = q_0 + \lambda q(1) + \lambda^2 q(2) + \ldots + \lambda^m q(m) \tag{3.22}$$

where q_0 is the molecular canonical partition function of the empty site, and $q(s)$ is the molecular canonical partition function of the site with a conglomerate of s molecules adsorbed:

$$q(s) = \prod_{i=1}^{s} q_i \tag{3.23}$$

Finally, the grand canonical partition function of the adsorbed phase is:

$$\Theta = \xi^N \tag{3.24}$$

Defining now:

$$C = \frac{K_1}{K_L} \exp\left(\frac{E_0^a - E_0^L}{RT} \right) \tag{3.25}$$

Subsequently, we will have:

$$q_1 = Cq, \text{ and } q(s) = q^s C$$

for $s > 1$. In this way:

$$\Theta = (1 + \lambda Cq + \lambda^2 Cq^2 + \ldots + \lambda^m Cq^m)^N = \left(\frac{1 + (C-1)\lambda q}{1 - \lambda q} \right)^N \tag{3.26}$$

Now since:

$$\bar{n}_a = \frac{\partial \ln \Theta}{\partial \ln \lambda}$$

and

$$\lambda q = \frac{P}{P_0} = x$$

then we could get [31]:

$$\frac{\bar{n}_a}{N_m} = \frac{Cx}{(1-x+Cx)(1-x)} \tag{3.27}$$

where $\bar{n}_a = n_a$ is the amount adsorbed, N_m, is the monolayer capacity, and the other terms have the previously explained meaning.

In order to apply the BET isotherm equation to real adsorption data, it is habitual to use Equation 3.27 in linear form:

$$y = \frac{x}{n_a(1-x)} = \left(\frac{1}{N_m C}\right) + \left(\frac{C-1}{CN_m}\right)x = b + mx \tag{3.27a}$$

where

$$b = \left(\frac{1}{N_m C}\right),\ m = \left(\frac{C-1}{CN_m}\right),\ y = \frac{x}{n_a(1-x)}, \text{ and } x = \frac{P}{P_0}$$

in the region: $0.05 < x < 0.4$ [4].

If the term

$$\frac{C-1}{C} \approx 1,$$

then the slope, m, of the linear regression is:

$$m \approx \frac{1}{N_m}.$$

Consequently, the monolayer capacity, N_m, is determined, and the specific surface area can be calculated as:

$$S = N_m N_A \sigma$$

where N_A is the Avogadro number, and σ is the cross-sectional area (i.e., the average area occupied by each molecule in a completed monolayer), where $(N_2) = 0.162$ nm^2 for N_2 at 77 K, and $\sigma(Ar) = 0.138$ nm^2 for argon at 87 K [4].

In the general case where the condition,

$$\frac{C-1}{C} \approx 1,$$

is not fulfilled,

$$b = \left(\frac{1}{N_m C}\right), \quad m = \left(\frac{C-1}{CN_m}\right),$$

must be calculated. Thereafter, we will have two equations with two unknowns that could be solved to get N_m and C. After that, S is calculated following the procedure previously explained.

Figure 3.7 shows the BET plot ($0.04 < P/Po < 0.3$) for the adsorption of N_2 at 77 K in a silica material, specifically in the sample 70bs2 (see Table 3.7) [26].

The fitting process of the BET isotherm equation, as was repeatedly stated before, could be also carried out with the help of a nonlinear regression method [44].

The BET methodology must be very carefully applied in order to get proper results [4,15,20]. The method is really useful in cases where the sorbates do not penetrate in the primary porosity, and then the adsorption process takes place only in the outer surface. Therefore, the BET equation is truly valid for surface area analysis of nonporous and mesoporous materials consisting of pores of wide pore diameter. However, it is not strictly applicable in the case of microporous adsorbents [20], because the BET theory describes a surface recovery, and adsorption in the primary porosity of zeolites is a volume filling [2].

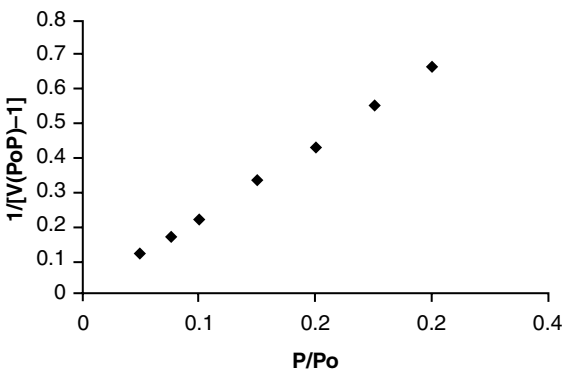

FIGURE 3.7 BET plot of sample 70bs2-25C.

TABLE 3.7
BET-Specific Surface Area (S) Corresponding to Some Silica Samples and an MCM-41 Mesoporous Material

Sample	S [m^2/g]
70bs2	1600
68bs1E	1500
75bs1	1400
79BS2	1300
74bs5	1200
68C	320
MCM-41	800

Note: Silica materials with such a high surface area, as those reported here, are normally unstable and in the course of time will, as a rule, reduce its specific surface area, because of the coalescence of the particles composing the material [50].

It also appears that the BET method is inexact for the calculation of the surface area of mesoporous molecular sieves of pore widths less than about 4 nm [20], since pore filling is observed at pressures very close to the pressure range where monolayer–multilayer formation on the pore walls occurs, which may lead to a significant overestimation of the monolayer capacity in case of a BET analysis [20]. However, the BET surface area is widely taken as a reproducible parameter for the characterization of the surface of porous materials, notwithstanding the fact that in some cases it lacks a precise physical meaning.

Another source of error in the application of the BET equation is related to the surface chemistry of the sample under test. For example, in the case of silica samples, the cross-sectional area of nitrogen on hydroxylated surfaces [51], such as silica, is not always $\sigma\ (N_2) = 0.162\ nm^2$, as is normally considered for the calculation of the BET surface area [5].

One more cause of error in the application of the BET equation during adsorption experiments is the determination of the adsorbent mass. Consequently, the adsorbent mass must be very carefully measured with an analytical balance [4].

To end this section, it is necessary to state that, following the previous discussion, it is evident that different causes exist for the spreading of the specific surface area measured in an adsorption experiment. As a result, it is estimated by repeatedly measuring the tested samples, that the relative error in the BET surface area measurements of the adsorption parameters is normally around 20% [15]. For samples of very large surface area, the relative error could be even 30% [26].

3.7 HORVATH-KAWAZOE METHOD

The Horvath-Kawazoe (HK) method for determining the micropore size distribution was introduced by Horvath and Kawazoe in 1983 [52]. It is based on the idea that the relative pressure,

$$x = \frac{P}{P_0},$$

required for the filling of micropores of a concrete size and shape is directly related to the adsorbate–adsorbent interaction energy [4]. This means that the micropores are progressively filled with an increase in adsorbate pressure. More concrete, in the HK method it is understood that only pores with dimensions lower than a particular unique value will be filled for a given relative pressure of the adsorbate [53]. Thus, the HK method allows the calculation of the pores size distribution in the micropore range at low pressures [27].

As in the previously analyzed instance of the Frenkel-Halsey-Hill (FHH) model, the entropy contribution to the free energy is small in comparison with the large change of enthalpy [4,53]. Consequently, the following equation is also valid in the present case:

$$RT \ln\left(\frac{P}{P_0}\right) = U_0 + P_a \tag{3.28}$$

which was previously justified in Chapter 2, Section 2.3.3. The HK method is based on Equation 3.28, including only van der Waals interactions, calculated with the help of the Lennard-Jones (L-J) potential [52–54].

Halsey and coworkers [55] applied the 6-12 L-J potential to the case of the interaction of one adsorbate molecule with an infinite layer plane of adsorbent molecules, obtaining [56]:

$$\varepsilon(z) = \frac{N_{AS}A_{AS}}{2\sigma^4}\left[\left(-\left(\frac{\sigma}{z}\right)^4 + \left(\frac{\sigma}{z}\right)^{10}\right)\right] \tag{3.29}$$

Later Everett and Paul [57] extended the Halsey and coworkers result to two infinite lattice planes separated by a distance, *L,* valid for the specific case of a slit pore (see Figure 3.8):

$$\mathrm{E}(z) = \frac{N_{AS}A_{AS}}{2\sigma^4}\left[\left(-\left(\frac{\sigma}{z}\right)^4 + \left(\frac{\sigma}{z}\right)^{10}\right) + \left(-\left(\frac{\sigma}{L-z}\right)^4 + \left(\frac{\sigma}{L-z}\right)^{10}\right)\right] \tag{3.30}$$

where N_{AS} is the number of solid molecules/surface unit, and L is the distance between the layers (Figure 3.8) [52]. In Equation 3.30, $\sigma = 0.858d$, where

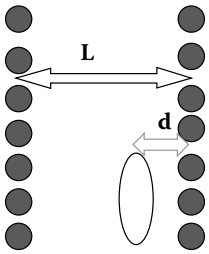

FIGURE 3.8 Adsorption in a slit pore.

$$d = \frac{d_s + d_a}{2},$$

and d_s is the diameter of the adsorbent molecule, and d_a is the diameter of the adsorbate molecule. Further, z is the internuclear distance between the adsorbate and adsorbent molecules, $(L - d_s)$ is the effective pore width, and A_{AS} is the dispersion constant, which takes into account the adsorbate–adsorbent interaction.

The term, A_{AS}, is calculated with the help of the Kirkwood-Muller formula [53]:

$$A_{AS} = \frac{6mc^2\alpha_S\alpha_A}{\left(\frac{\alpha_S}{\chi_S} + \frac{\alpha_A}{\chi_A}\right)}$$

where m is the mass of an electron, c is the speed of light, α_A and α_S are the polarizabilities of the adsorbate and the adsorbent molecules, and χ_A and χ_S are the magnetic susceptibilities of the adsorbate and the adsorbent.

Later Horwath and Kawazoe proposed that the potential is increased by the adsorbate–adsorbate interaction, suggesting the following potential [52]:

$$\Phi(z) = \frac{N_{AS}A_{AS} + N_{AA}A_{AA}}{2\sigma^4}\left[\left(-\left(\frac{\sigma}{z}\right)^4 + \left(\frac{\sigma}{z}\right)^{10}\right) + \left(-\left(\frac{\sigma}{L-z}\right)^4 + \left(\frac{\sigma}{L-z}\right)^{10}\right)\right] \quad (3.31)$$

where N_{AA} is the number of adsorbed molecules/surface unit, L is the distance between the layers (Figure 3.8) [52,53], and σ = 0.858d. As a final point, A_{AA}, calculated with the help of the Kirkwood-Muller formula, is the constant characterizing adsorbate–adsorbate interaction [53]:

$$A_{AA} = \frac{3mc^2\alpha_A\chi_A}{2}$$

The next step is to obtain the average interaction energy. This is made by volumetrically averaging the potential expressed by Equation 3.31 as follows [52–54]:

$$\xi(L) = \int_{d}^{L-d} \frac{\Phi(z)dz}{(L-2d)} = \left(\frac{N_{AS}A_{AS} + N_{AA}A_{AA}}{\sigma^4(L-2d)} \right) \left(\frac{\sigma^4}{3\left(L-d\right)^3} - \frac{\sigma^{10}}{9\left(L-d\right)^9} - \frac{\sigma^4}{3d^3} + \frac{\sigma^4}{9d^9} \right) \tag{3.32}$$

where $\xi(L)$ is the average potential in a given pore obtained by the integration across the effective pore width [52,53], and $\Phi(z)$ is the adsorption field inside the slit pore (see Figure 3.8) [52,53].

Finally, the average energy is related to the free energy change upon adsorption:

$$\Delta G^{ads} = RT \ln\left(\frac{P}{P_0} \right)$$

obtaining [52–54]:

$$RT \ln\left(\frac{P}{P_0} \right) = N_A \left(\frac{N_{AS}A_{AS} + N_{AA}A_{AA}}{\sigma^4(L-2d)} \right) \left(\frac{\sigma^4}{3\left(L-d\right)^3} - \frac{\sigma^{10}}{9\left(L-d\right)^9} - \frac{\sigma^4}{3d^3} + \frac{\sigma^4}{9d^9} \right) \tag{3.33}$$

where N_A is the Avogadro number, since in molar units [53]:

$$RT \ln\left(\frac{P}{P_0} \right) = U_0 + P_a = N_A \xi(L)$$

The HK method is a tool for the characterization of microporous materials that allows an estimation of the pore size of the studied materials [4,27,28,58]. To calculate the micropore size distribution, the relative pressure,

$$x = \frac{P}{P_0},$$

is calculated first, corresponding with a concrete pore width, L, using Equation 3.33. Then, with the help of experimental adsorption isotherm, the amount adsorbed, n_a, corresponding to this value of

$$x = \frac{P}{P_0}$$

is estimated. After that, by differentiating the amount adsorbed with respect to the pore width, dn_a/dL, the pore size distribution in the micropore range is obtained [27].

Table 3.8 shows a set of values for the parameters α, χ, d, and N_s for nitrogen and argon, as adsorbates, and carbon and the oxide ion (a zeolite, for example), as adsorbents [52–54,59,60]. Then, with the help of the Kirkwood-Muller formulas and

TABLE 3.8
Physical Properties of Nitrogen, Argon as Adsorbate, and Carbon and the Oxide Ions as Adsorbents

Atomic Species	Polarizability α [10^{-24} cm^3]	Magnetic Susceptibility χ [10^{-29} cm^3]	Diameter d [nm]	Surface Density N_s [10^{18} atoms/m^2]
Nitrogen	1.46	2.00	0.30	6.70
Argon	1.63	3.25	0.34	8.52
Carbon	1.02	13.5	0.34	38.4
Oxide Ion	2.50	1.30	0.28	13.1

Equation 3.33, Horwath and Kawazoe obtained the following equation to describe the adsorption of N_2 at 77 K in carbon molecular sieves [4,52]:

$$\ln\left(\frac{P}{P_0}\right)=\left(\frac{61.23}{(L-0.64)}\right)\left(\frac{1.895x10^{-3}}{(L-0.32)^3}-\frac{2.709x10^{-7}}{(L-0.32)^9}-0.05014\right) \quad (3.33a)$$

where L is in nm.

Equation 3.33 also incorporates the physical parameters (see Table 3.8) for the oxide as adsorbent and nitrogen as adsorbate, but uses for nitrogen $d = 0.36$ nm and $\alpha = 1.74 \times 10^{-24}$ cm^3 [60]. The following equation describes the adsorption of N_2 at 77 K in oxide adsorbents [60]:

$$\ln\left(\frac{P}{P_0}\right)=\left(\frac{21.77}{(L-0.64)}\right)\left(\frac{1.847x10^{-3}}{(L-0.32)^3}-\frac{2.540x10^{-7}}{(L-0.32)^9}-0.04981\right) \quad (3.33b)$$

Figure 3.9 provides an HK plot of micropore size distribution for a zeolite ZSM-5-5020, provided by Zeolyst. The isotherm was obtained in a Quantachrome Autosorb-1 gas adsorption system, and the calculation was carried out by the equipment software [27].

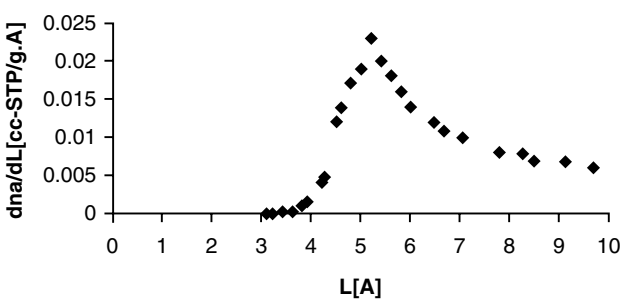

FIGURE 3.9 Horwath-Kawazoe micropore size distribution plot of a ZSM-5 zeolite.

It is evident from Figure 3.9 that the maximum of the PSD coincides fairly well with the crystallographic value of the pore diameter corresponding to the MFI framework of the analyzed ZSM-5 zeolite [45].

To finish the present section, it is necessary to state that the HK method was criticized by Lastoskie and collaborators, and a modified Horvath-Kawazoe pore size analysis method was relatively recently presented [61]. The proposed new HK model is generalized so as to account for the effect of the temperature and the solid–fluid interaction potential strength on the adsorbed fluid density within a slit-shaped pore [61]. In addition, two descriptions of the local adsorbate density profile are taken into account in the proposed HK model: an unweighted version analogous to the original HK method, in which a uniform density profile is assumed, and a weighted version [61]. The pore filling correlations forecasted by the two HK models were compared with density functional theory (DFT) results calculated using the same solid–fluid potential and potential parameters [60]. It is found that the pore filling correlation of the unweighted HK model agrees unexpectedly well with the DFT correlation for argon and nitrogen adsorption at 77 K. Ironically, the weighted HK pore filling correlation does not agree as well with DFT results, even though the weighted HK model more realistically represents the local density profile than does the unweighted HK approach [60].

REFERENCES

1. Roque-Malherbe, R., *Adsorcion Fisica de Gases,* ENPES-MES, Havana, 1987; and *Fisica Quimica de las Zeolitas,* ENPES-MES, Havana, 1988.
2. Roque-Malherbe, R., *Mic. Mes. Mat.*, 41, 227, 2000.
3. Sing, K.S.W., Everett, D.H., Haul, R.A.W., Moscou, L., Pirotti, R.A., Rouquerol, J., and Siemieniewska, T., *Pure App. Chem.*, 57, 603, 1985.
4. Rouquerol, J., Rouquerol, F., and Sing, K., *Adsorption by Powder and Porous Solids,* Academic Press, New York, 1999.
5. Dubinin, M.M., *Prog. Surf. Memb. Sci.*, 9, 1, 1975; and *American Chemical Society Symposium Series*, 40, 1, 1977.
6. Bering, B.P., Dubinin, M.M., and Serpinskii, V.V., *J. Coll. Int. Sci.*, 38, 185, 1972.
7. Bering, B.P. and Serpinskii, V.V., *Ixv. Akad. Nauk, SSSR, Ser. Xim.*, 2427, 1974.
8. Keller, J.U. and Staudt, R., *Gas Adsorption Equilibria: Experimental Methods and Adsorptive Isotherms,* Springer-Verlag, New York, 2004.
9. de la Cruz, J., Rodriguez, C., and Roque-Malherbe, R., *Surface Sci.,* 209, 215, 1989.
10. Yang, R.T., *Adsorbents, Fundamentals, and Applications,* J. Wiley & Sons, New York, 2003.
11. Neimark, A.V. and Ravikovitch, P.I., *Mic. Mes. Mat.*, 44–45, 697, 2001.
12. Ravikovitch, P.I. and Neimark, A.V., *Colloids Surf. A*, 187–188, 11, 2001.
13. Thommes, M., Kohn, R., and Froba, M., *J. Phys. Chem. B,* 104, 7932, 2000.
14. Barrer, R.M., *Zeolites and Clay Minerals as Sorbents and Molecular Sieves,* Academic Press, London, 1978.
15. Gregg, S.J. and Sing, K.S.W., *Adsorption Surface Area and Porosity,* Academic Press, London, 1982.
16. Ruthven, D.W., *Principles of Adsorption and Adsorption Processes,* Wiley, New York, 1984.

17. Rudzinskii, W., Steele, W.A., and Zgrablich, G., *Equilibria and Dynamic of Gas Adsorption on Heterogeneous Solid Surfaces,* Elsevier, Amsterdam, 1996.
18. Loos, J.B., *Modeling of Adsorption and Diffusion of Vapors in Zeolites,* Coronet Books, Philadelphia, 1997.
19. Fraissard, J.P., Ed., *Physical Adsortion: Experiment, Theory and Applications,* Kluwer Academic Publishers, The Netherlands, 1997.
20. Thommes, M., in *Nanoporous Materials: Science and Engineering*, Lu, G.Q. and Zhao, X.S., Eds., Imperial College Press, London, 2004, p. 317.
21. Rudzinski, W. and Everett, D.H., *Adsorption of Gases in Heterogeneous Surfaces,* Academic Press, London, 1992.
22. Bansal, R.C. and Meenakshi, G., *Activated Carbon Adsorption,* CRC Press, Boca Raton, FL, 2005.
23. Ross, S. and Olivier, J.P., *On Physical Adsorption,* Wiley, New York, 1964.
24. Roque-Malherbe, R. and Marquez-Linares, F., *Mat. Sci. Semicond. Proc.,* 7, 467, 2004; and *Surf. Interf. Anal.,* 37, 393, 2005.
25. Roque-Malherbe, R. and Marquez-Linares, F., U.S. Provisional Patent Application No. 10/982,798, filed on November 8, 2004.
26. Marquez-Linares, F. and Roque-Malherbe, R., *J. Nanosci. Nanotech.,* 6, 1114, 2006.
27. Quantachrome, AUTOSORB-1, Manual, 2003.
28. Micromeritics, ASAP 2000, Description, 1992.
29. Halsey, G.D., *J. Chem. Phys.*, 16, 931, 1948.
30. Young, D.M. and Crowell, A.D., *Physical Adsorption of Gases,* Butterworth, London, 1962.
31. Hill, T.L., *An Introduction to Statistical Thermodynamics,* Dover Publications Inc., New York, 1986.
32. Bakaev, V.A., *Dokl. Akad. Nauk SSSR,* 167, 369, 1966.
33. Ruthven, D.M., *A.I.Ch.E. J.,* 22, 753, 1976 and *Zeolites,* 2, 242, 1982.
34. Dupont-Pavlovskii, M., Barriol, J., and Bastick, J., Colloques Internes du CNRS, No. 201 (Termochemie), 1972.
35. Schirmer,W., Fiedler, K., and Stach, H., *ACS Symposium Series,* 40, 305, 1977.
36. Roque-Malherbe, R., *KINAM,* 6, 35, 1984.
37. Roque-Malherbe, R., Lemes, L., López-Colado, L., and Montes, A., in *Zeolites '93 Full Papers Volume*, Ming, D. and Mumpton, F.A., Eds., International Committee on Natural Zeolites Press, Brockport, New York, 1995, p. 299.
38. Marquez-Linares, F. and Roque-Malherbe, R., *Facets-IUMRS J.*, 2, 14, 2003; and 3, 8, 2004.
39. Lippens, B.C. and de Boer, J.H., *J. Catalysis* 4, 319, 1965.
40. Gurvich, L., *J. Phys. Chem. Russ.*, 47, 805, 1915.
41. Kiseliov, A., in *Curso de Fisica Quimica,* Gerasimov, I.I., Ed., Editorial Mir, Moscow, 1971, p. 441.
42. Zhujovitskii, A.A., *Kolloidzschr,* 66, 139, 1934.
43. Shchukin, E.D., Presov, A.V., and Amelina, E.A., *Kolloidnaia Ximia,* Ximia, Moscow, 1982.
44. Draper, N.R. and Smith, H., *Applied Regression Analysis* (third edition), Wiley, New York, 1998.
45. Baerlocher, C., Meier, W.M., and Olson, D.M., *Atlas of Zeolite Framework Types,* 5th ed., Elsevier, Amsterdam, 2001.
46. Breck, D.W., *Zeolite Molecular Sieves,* J. Wiley & Sons, New York, 1974.
47. Roque-Malherbe, R., in *Handbook of Surfaces and Interfaces of Materials,* Vol. 5, Nalwa, H.S., Ed., Academic Press, New York, 2001, p. 495.

48. Dubinin, M.M., Zhukovskaya, E.F., Lukianovich, V.M., Murrdmaia, K.O., Polstiakov, E.F., and Senderov, E.E., *Izv. Akad. Nauk SSSR,* 1500, 1965.
49. Balbuena, P.B. and Gubbins, K.E., in *Characterization of Porous Solids,* Rouquerol, I.J., Rodriguez-Reynoso, P., Sing, K.S.W., and Unger, K.K., Eds., Elsevier, Amsterdam, 1994, p. 41.
50. Rogue-Malherbe, R., Morquez, F., dil volle, W. and Thommes, M., paper in progress.
51. Galarneau, A., Desplantier, D., Dutartre, R., and Di Renzo, F., *Mic. Mes. Mat.*, 27, 297, 1999.
52. Horvath, G. and Kawazoe, K., *J. Chem. Eng. Japan*, 16, 470, 1983.
53. Rege, S.U. and Yang, R.T., in *Adsorption. Theory, Modeling and Analysis,* Toth, J., Ed., Marcel Dekker, New York, 2002, p. 175.
54. Saito, A. and Foley, H.C., *A.I.Ch.E. J.*, 37, 429, 1991.
55. Sams, J.R., Contabaris, G., and Halsey, G.D., *J. Phys. Chem.*, 64, 1689, 1960.
56. Everett, D.H. and Powl, J.C., *J. Chem. Soc. Faraday Trans.*, 72, 619, 1976.
58. Vaughan, D.E.W., Treacey, M.M.J., and Newsam, J.M., *NATO-ASI Ser. B Phys.*, 221, 99, 1990.
59. Thommes, M., personal communication.
60. Parent, M.A. and Moffat, J.B., *Langmuir,* 11, 4474, 1996.
61. Dombrowski, R.J., Lastoskie, C,M., and Hyduke, D.R., *Colloids Surf. A*, 187–188, 23, 2001.

4 Nanoporous Materials Mesoporosity Evaluation

4.1 INTRODUCTION

Porous materials have found great application as catalysts, adsorbents, separation materials, and other industrial applications. The large surface areas of these materials enhance their catalytic, sorptive, and separation activity.

As previously acknowledged, gas and vapor adsorption measurements are widely used for the characterization of porous materials [1–20]. In the previous chapter, we explained the use of this methodology for determining the micropore volume, the surface area of porous materials, and the micropore size distribution. IUPAC [2] classified pores by their inner pore width, where the mesopore pores are those with internal width between 2 and 50 nm. In modern terms, this is the nanoporous region. In the present chapter, we will study the mesoporosity characterization of nanoporous materials, applying basically the capillary condensation of vapors, which is the primary method of assessment of the mesoporosity of nanoporous materials [3,6–15].

4.2 CAPILLARY CONDENSATION

Capillary condensation in mesopores is generally associated with a shift in the vapor–liquid coexistence in pores compared to the bulk fluid. That is, a fluid confined in a pore condenses at a pressure lower than the saturation pressure at a given temperature, since the condensation pressure depends on the pore size and shape, and also on the strength of the interaction between the fluid and pore walls [11–15] (see Figure 4.1 [16]).

To be precise, pore condensation represents a confinement-induced shifted gas–liquid phase transition. Specifically, condensation occurs at a pressure, P, less than the saturation pressure, P_0, of the fluid [8]. The $x = P/P_0$ value where pore condensation takes place depends on the liquid–interfacial tension, the strength of the attractive interactions among the fluid and pore walls, the pore geometry, and the pore size. It is assumed that, for pores of a given shape and surface chemistry, there exists a one-to-one correspondence between the condensation pressure and the pore diameter. Thus, adsorption isotherms contain unequivocal information about the pore size distribution of the sample under analysis [8–15].

Capillary condensation of vapors in the pores of solids is a prominent example of phase transitions in confined fluids [12]. When a porous solid contacts the vapor of a wetting fluid, the later condenses in pores at a vapor pressure lower than the saturation pressure at the given temperature. The pressure of condensation is related to the liquid–vapor interfacial tension, the attraction interaction between the solid

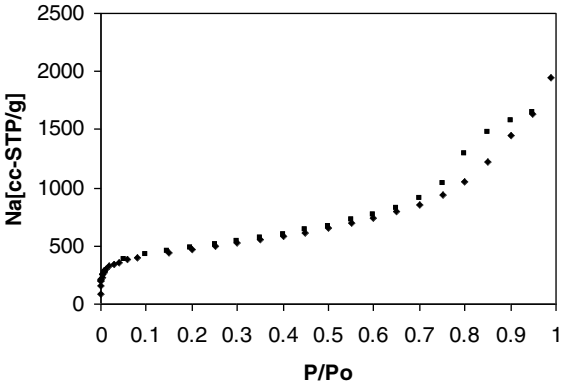

FIGURE 4.1 Adsorption isotherm of N_2 at 77 K, in the high specific surface area silica sample 70bs2 (♦: adsorption branch, ■: desorption branch).

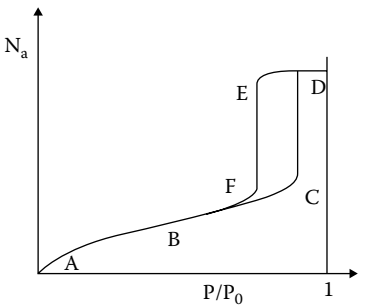

FIGURE 4.2 Diagrammatic representation of an adsorption isotherm in a single mesopore of cylindrical shape.

and the fluid, and the pore geometry, its size and shape [9,12]. Capillary condensation is typically characterized by a step in the adsorption isotherm; in materials with a uniform pore size distribution, the capillary condensation step is notably sharp [8,9]. A graphic representation of a sorption isotherm, as it is expected for adsorption/desorption of a pure fluid in a single mesopore of cylindrical shape, is shown in Figure 4.2.

The graphic isotherm (Figure 4.2) exposes a vertical pore condensation step. On the contrary, a real isotherm, such as those shown in Figure 4.1, which is the result of an adsorption process in a real porous material with an existent pore-size distribution, shows a less sharp pore condensation transition.

As is schematically shown in Figure 4.3 [8], the adsorption mechanism in mesopores is at low relative pressures completely similar to the adsorption process on planar surfaces. Subsequent to the completion of the monolayer formation (**A**), multilayer adsorption commences (**B**). Subsequently, after the attainment of a critical film thickness (**C**), capillary condensation occurs, fundamentally in the core of the pore; that is, the transition from configuration **C** to **D**.

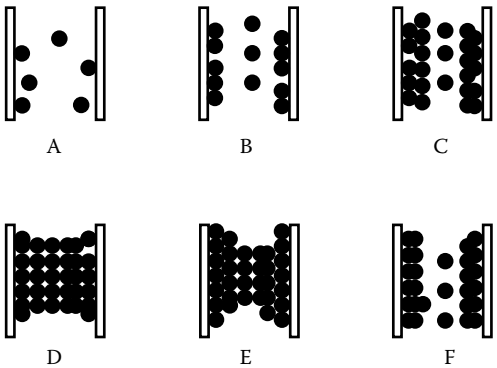

FIGURE 4.3 Graphic representation of multilayer adsorption and pore condensation in a single mesopore.

The plateau section of the isotherm reproduces the situation of a pore completely filled with liquid; the pore liquid is separated from the bulk gas phase by a hemispherical meniscus, and pore evaporation then takes place by a thinning meniscus (**E**) at a pressure which is less than the pore condensation pressure (see Figure 4.2 and Figure 4.3) [8].

The pressure where the hysteresis loop finishes matches the situation of an adsorbed multilayer film that is in equilibrium with a vapor in the core of the pore and the volume gas phase. In the relative pressure range between (**F**) and (**A**), adsorption and desorption are reversible [8].

Therefore, in pores wider than approximately 5 nm, capillary condensation is connected with hysteresis [12]. This means that, as the vapor pressure decreases, the desorption occurs at a pressure lower than the pressure of adsorption. The hysteresis loop is reproducible in adsorption experiments carried out with enough equilibration time [12]. But, as the pore size decreases, the experimental hysteresis loop gradually narrows and finally disappears for pores smaller than about 4 nm [12].

Pore condensation indicates a first-order phase transition between an inhomogeneous gas configuration, consisting of vapor in the core region of the pore in equilibrium with a liquidlike adsorbed film (arrangement **C** in Figure 4.3), and a liquid configuration, where the pore is filled with liquid (pattern **D** in Figure 4.3) [8]. At the critical point of the confined fluid, these two hitherto distinct fluid configurations will become indistinguishable (i.e., a pore condensation step cannot be observed anymore) [8].

In practice, hysteresis is observed in materials consisting of slitlike pores, cylindrical-like pores, and spherical pores (i.e., ink-bottle pores) [13–15]. The H1 type is associated with porous materials formed of properly defined cylindrical-like pore channels or agglomerates of compacts of roughly homogeneous spheres [2,3,5,8,9] (see Figure 4.4 [2]). It was also established that materials that give rise to H2 hysteresis are frequently disordered, and their pore size distribution (PSD) is not well defined [2,3,5,8] (see Figure 4.4 [2]).

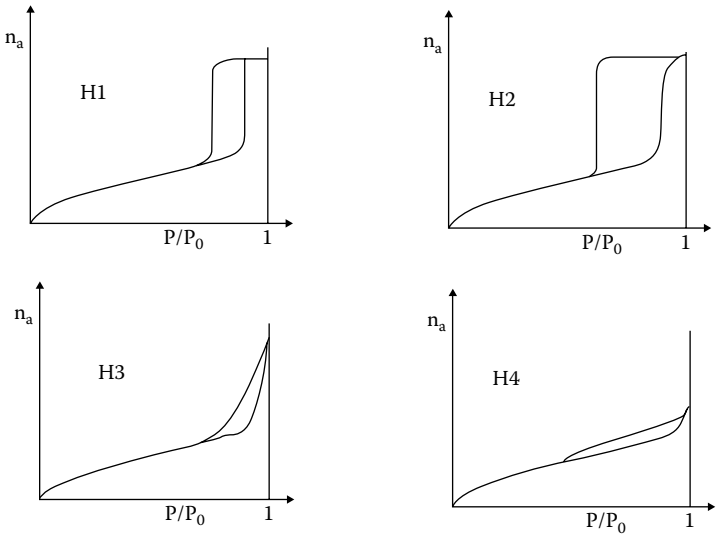

FIGURE 4.4 IUPAC classification of adsorption hysteresis.

Systems revealing type H3 hysteresis do not show any limiting adsorption at high relative pressure. This is observed in nonrigid aggregates of platelike particles giving rise to slit-shaped pores [2,3,5,8,9] (see Figure 4.4 [2]). Likewise, type H4 loops are also frequently associated with thin slit pores, but also including pores in the micropore region [2,3,5,8,9] (see Figure 4.4 [2]).

Network models take into consideration that in many materials the pores are connected and form a three-dimensional network [8,9]. A significant characteristic of the network model is the possibility of pore-blocking effects during evaporation. This occurs if a pore has access to the external gas phase only via narrow constrictions, as for example, an ink-bottle pore [8,9]. Therefore, the desorption branch of the hysteresis loop does not occur at thermodynamic equilibrium, as is the case in the single-pore model. In such a case the desorption branch of the hysteresis loop is much steeper as compared to the adsorption branch leading to H2 hysteresis [8].

4.3 MACROSCOPIC THEORIES TO DESCRIBE PORE CONDENSATION

4.3.1 The Kelvin-Cohan Equation

During capillary condensation the pore walls are first covered by a multiplayer adsorbed film at the beginning of pore condensation (see Figure 4.3 and Figure 4.4), and thereafter, at a certain critical thickness, t_c, pore condensation occurs in the core of the pore, controlled by intermolecular forces in the core fluid [8]. For pores of regular shape and width, as for example ideal slitlike or cylindrical pores (see Figure 4.5), pore condensation can be described on the basis of the Kelvin-Cohan equation [17]. That is, the shift of the gas–liquid phase transition of a confined fluid

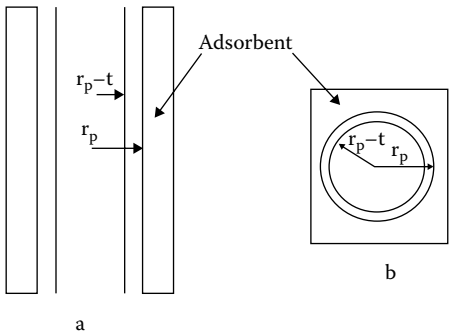

FIGURE 4.5 Slablike (a) and cylindrical (b) pores during pore condensation.

from bulk coexistence is expressed in macroscopic quantities like the surface tension, γ, of the bulk fluid and the densities of the coexistent liquid, ρ_l, and gas, Δ_g ($\Delta\rho = \rho_l - \rho_g$) [8]. The adsorbed multilayer film, of thickness *t*, shown in Figure 4.5, is wide enough to be considered as a slab of liquid under the action of the adsorption field [6,7].

The Kelvin-Cohan or modified Kelvin equation is derived from the Kelvin equation, which is based on the effect of the curvature of the surface on vapor pressure. This effect of curvature is best understood in terms of the pressure drop, ΔP, across an interface which is described by the well-known Young-Laplace equation [7]:

$$P^{II} - P^{I} = \gamma\left(\frac{1}{r_I} + \frac{1}{r_{II}}\right)$$

where γ is the surface tension, and r_I and r_{II} are the two curvature radii describing the surface (see Figure 4.6).

From thermodynamics, the effect of a change in mechanical pressure at constant pressure on the chemical potential of a substance is [7]:

$$\Delta\mu = \int V_L dP$$

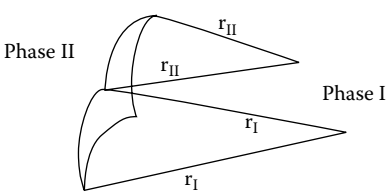

FIGURE 4.6 Sector of radius r_I and r_{II} separating phase I and phase II.

where V_L is the molar volume of the fluid substance. If V_L is constant, then applying the Young-Laplace equation produces [7]:

$$\Delta\mu = \gamma V_L \left(\frac{1}{r_I} + \frac{1}{r_{II}} \right)$$

since:

$$\mu = \mu^0 + RT \ln(P)$$

then:

$$RT \ln\left(\frac{P}{P_0} \right) = \gamma V_L \left(\frac{1}{r_I} + \frac{1}{r_{II}} \right)$$

which is the Kelvin equation. Now it is possible to state that, for a cylindrical pore, the modified Kelvin equation or the Kelvin-Cohan equation [17] is given by:

$$RT \ln\left(\frac{P_A}{P_0} \right) = \frac{\gamma V_L}{r_P - t_A} \tag{4.1}$$

while the evaporation/desorption process is associated with the formation of a hemispherical meniscus between the condensed fluid and vapor [17]:

$$RT \ln\left(\frac{P_D}{P_0} \right) = \frac{2\gamma V_L}{r_P - t_D} \tag{4.2}$$

where r_p is the pore radius, $x_A = P_A/P_0$ and $x_D = P_D/P_0$ are the relative pressures of adsorption and desorption, respectively, γ is the surface tension, V_L is the molar volume of the bulk liquid, and t_A and t_D are the thickness of an adsorbed multilayer film, which is formed prior to pore condensation at the relative pressures x_A and x_D [13–15]. In Equations 4.1 and 4.2 the modification made to the Kelvin equation was to consider that the curvature radius for cylindrical and spherical pores is the core radius, $r_c = r_P - t$ [6–9].

The Kelvin-Cohan equation gives a correlation between the pore diameter and the pore condensation pressure. It predicts that pore condensation shifts to a higher relative pressure with increasing pore diameter and temperature. Consequently, the Kelvin-Cohan equation serves as the basis for the traditional methods applied for mesopore analysis, such as the Barret-Joyner-Halenda method (BJH) [21], which is extensively used.

In order to account for the preadsorbed multilayer film, the Kelvin-Cohan equation is combined with a standard isotherm or t-curve, which typically refers to

adsorption measurements on a nonporous solid [6–8,10,21]. The preadsorbed multilayer film is assessed by the statistical thickness of an adsorbed film on a nonporous solid of a surface similar to that of the sample under consideration [6–8,10,21].

We will now describe the details of the BJH method [21] to determine the pore size distribution (PSD), which, as was explained in Chapter 2, is a graphical representation of $\Delta V_p/\Delta D_p$ versus D_p, where V_p is the pore volume accumulated up to the pore of width D_p, measured in [cc-STP/g·Å], and where cc-STP indicates the amount adsorbed measured in cubic centimeters at STP; that is, at standard temperature and pressure, namely 273.15 K and 760 Torr (i.e., 1.01325×10^5 Pa). The pore volume denoted by W is the sum of the micropore and mesopore volumes of the adsorbent measured in [cm^3/g] [2,3,5,8].

As was indicated in Figure 4.5, the pore of radius r_p has a physically adsorbed layer of adsorbate molecules, normally nitrogen at 77 K, of thickness t. Within this thickness is an inner capillary radius, $r_K = r_p - t$, from which evaporation occurs as $x = P/P_0$ is lowered. This is the *core of the pore* [6,10,21].

The BJH method, in addition to the previous assumptions related with the Kelvin-Cohan equation, supposes that at the initial relative pressure of the desorption process, which is close to unity (i.e., in the range: $0.9 < P/P_0 < 0.95$), all the pores are filled with the adsorbate fluid [10,21]. Therefore, the first step ($j = 1$) (see Figure 4.7 [16]) in the desorption process only involves removal of capillary condensate. However, the next step involves both removal of condensate from the cores of a group of pores and the thinning of the multilayer in the larger pores (i.e., in the pores already emptied of condensate) [6].

In the present description of the BJH method, the core volume will be designated by V_{Kj}, and the pore volume will be designated by V_{pj}. The corresponding radii are r_K and r_p. The BJH method is normally related to the desorption of nitrogen at 77 K.

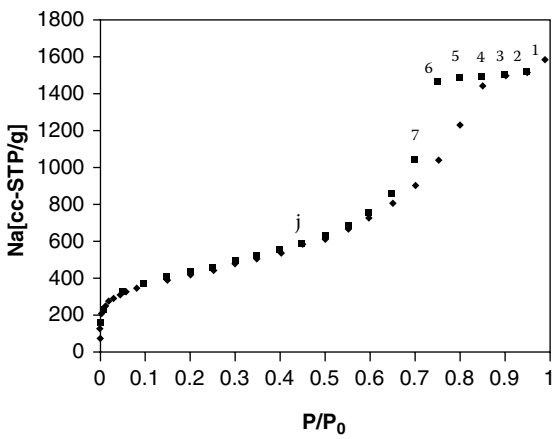

FIGURE 4.7 Adsorption isotherm (obtained in a Quantachrome Autosorb-1, gas analysis system) of N_2 at 77 K, in the high specific surface area silica sample 68bs1E (♦: adsorption branch, ■: desorption branch), where are designated the different steps in the desorption branch of the isotherm for the calculation of the BJH-PSD.

Then the amount of nitrogen removed in each desorption step, *j,* is $\Delta n_a(j)$; however in the present case, this amount is expressed as the volume $\Delta V(j)$ of liquid nitrogen.

As was previously stated, in the first step ($j = 1$) the initial removal is the result of capillary evaporation alone, and consequently the volume of core space removed is equal to the volume of nitrogen removed, i.e., $\Delta V_K(1) = \Delta V(1)$ [6,21].

For the first group of mesopores, the relationship between the core volume, V_{K1}, and the pore volume, V_p, if the pores are of cylindrical shape, is given by [10,21]:

$$V_{p1} = \frac{V_{K1}\bar{r}_{p1}^{-2}}{\bar{r}_{K1}^{-2}}$$

where $\bar{r}_{p1}$ and $\bar{r}_{K1}$ are the mean pore and core radii [6].

When the relative pressure, *x,* is lowered from $(P/P_0)_1$ to $(P/P_0)_2$, a volume, $\Delta V(1)$, will be desorbed from the pores. This fluid volume, $\Delta V(1)$, represents not merely emptying the largest pore of its condensate, but a decrease in the thickness of the physically adsorbed layer by an amount Δt_1. Consequently, across this relative pressure reduction the average change in thickness is: $\Delta t_1/2$ [21]. Thereafter, the pore volume of the largest pore may be expressed as [10,21]:

$$V_{p1} = \Delta V(1)\left(\frac{r_{p1}}{r_{K1} + \dfrac{\Delta t_1}{2}}\right)^2$$

When the relative pressure, *x,* is again lowered to $(P/P_0)_3$, the volume of liquid desorbed comprises not only the condensate from the next larger size pores but also the volume from a second thinning of the physically adsorbed layer left behind in the pores of the largest size. Therefore, the volume, V_{p2}, desorbed from pores of the smaller size is given by [10,21]:

$$V_{p2} = \left(\frac{r_{p2}}{r_{K2} + \dfrac{\Delta t_2}{2}}\right)^2 \left(\Delta V(2) - \Delta V_t(2)\right)$$

where:

$$\Delta V(2) = \Delta V_K(2) + \Delta V_t(2)$$

and the volume desorbed from multilayer is [10]:

$$\Delta V_t(2) = \Delta t_2 A c_1$$

and Ac_1 is the area exposed by the previously emptied pores from which physically adsorbed gas is desorbed. Next, the previous equation could be generalized to symbolize any step of a stepwise desorption by writing:

$$\Delta V_t(n) = \Delta t_n \sum_{j=1}^{n-1} Ac_j$$

This summation term in the previous equation is the sum of the average area in unfilled pores down to but not including the pore that was emptied in the concrete desorption step [10]. Substituting the general value of $\Delta V_t(n)$ into the equation defining V_{p2}, we will get:

$$V_{pn} = \left(\frac{r_{pn}}{r_{Kn} + \frac{\Delta t_n}{2}} \right)^2 \left(\Delta V(n) - \Delta t_n \sum_{j=1}^{n-1} Ac_j \right)$$

which is an exact expression for calculating the pore volumes at various relative pressures [10,21].

In the BJH approach to the PSD calculation, it is assumed that all pores emptied of their condensate during a relative pressure decrement have an average radius, $\overline{r}_p$, calculated from the Kelvin-Cohan equation radii at the upper and lower values of the relative pressure, *x,* in the desorption step. Then the average core radius is expressed as [10]:

$$\overline{r}_c = \overline{r}_p - t_{\overline{r}}$$

where $t_{\overline{r}}$ is the thickness of the adsorbed layer at the average radius in the interval in the current decrement calculated from the equation [22]:

$$t(A) = \left(\frac{13.9}{\ln\left(\frac{P}{P_0} \right) + 0.034} \right)$$

which is an equation proposed by de Boer and collaborators for estimating *t* in the case of nitrogen at 77 K.

Now, the term, *c,* could be calculated by [10]:

$$c = \frac{\overline{r}_c}{\overline{r}_p} = \frac{\overline{r}_p - t_{\overline{r}}}{\overline{r}_p}$$

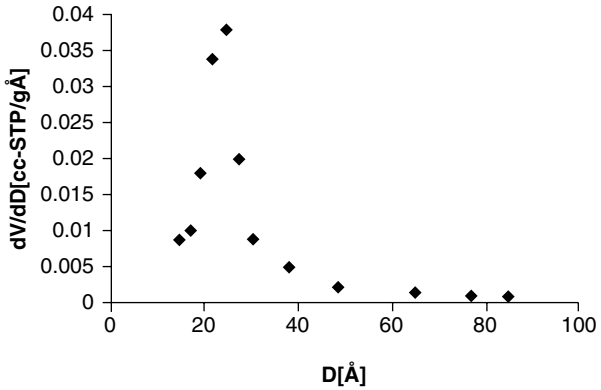

FIGURE 4.8 BJH-PSD, (dV/dD) [cc-STP/g. Å] versus pore width [Å] of an MCM-41 mesoporous molecular sieve sample [16]. The calculations were carried out by means of the adsorption isotherm of N_2 at 77 K obtained in a Quantachrome Autosorb-1 gas analysis system, applying the system software [10].

Then, with the previous equation and the expression for V_{pn}, it is possible to calculate the Barret-Joyner-Halenda pore size distribution (BJH-PSD) [6,10,21].

The BJH-PSD of an MCM-41 mesoporous molecular sieve is represented in Figure 4.8. The MCM-41 is a member of the M41S family of mesoporous ordered silicas with hexagonal and cubic symmetry and pore sizes ranging from 20 to 100 Å [23]. These materials are characterized by an ordered, not crystalline, pore wall structure, presenting sharp pore size dispersions. The original members of the M41S family consisted of MCM-41 (hexagonal phase), MCM-48 (cubic phase), and MCM-50 (a stabilized lamellar phase) [23]. The MCM-41 structure is proposed to have a hexagonal stacking of uniform-diameter porous tubes, whose size can be varied from about 15 to more than 100 Å [23].

Notwithstanding the ample use that was made of the BJH method for the PSD determination, it is necessary to recognize that it is based on a simplified macroscopic description of the capillary condensation process [17] with limitations at the microscopic level [12–15].

These limitations made the method inaccurate, especially for materials with pore sizes of 2–4 nm (20–40 Å) [13,14]. The BJH method, as is evident from the comparison of Figure 4.8 and Figure 4.9, underestimates the pore size by about 1 nm (10 Å) in relation with the nonlocal density functional theory method [13,14]. This fact made it necessary to use more accurate methods, as will be seen in the next sections; especially in Section 4.4 [12–15].

4.3.2 The Derjaguin-Broeckhoff-de Boer Theory

The Derjaguin-Broeckhoff-de Boer (DBdB) theory is similar to the Derjaguin approach [15]. According to the DBdB theory, the equilibrium thickness of the adsorbed film, *t,* in a cylindrical pore of radius r_P is determined from the balance of capillary and disjoining pressures: [19]

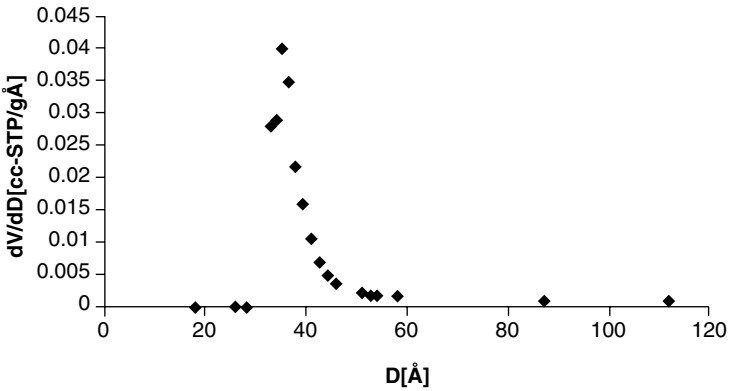

FIGURE 4.9 NLDFT-PSD (dV/dD) [cc-STP/g. Å] versus pore width [Å] corresponding to an MCM-41 mesoporous molecular sieve sample [16]. The calculations were carried out by the use of the adsorption isotherm of N_2 at 77 K obtained in a Quantachrome Autosorb-1 gas analysis system, applying the system software [10].

$$RT \ln\left(\frac{P_0}{P}\right) = \Pi(t)V_L + \frac{\gamma V_L}{r_P - t} \tag{4.3}$$

Here, P is the equilibrium adsorption pressure, P_0 is the vapor pressure of the adsorbate at the temperature of the adsorption experiment, γ and V_L are the surface tension and the molar volume of liquid, and $\Pi(t)$ is the disjoining pressure of the adsorbed film. Note that, by omitting the disjoining pressure term, we obtain the Kelvin-Cohan equation for a spherical interface.

Equation 4.3 could be explained as follows: the chemical potential difference, $\Delta\mu$, between the gas and the adsorbed phase could be given by [8]:

$$\Delta\mu = \Delta\mu_a + \Delta\mu_c$$

where the first term, $\Delta\mu_a$, is associated with multilayer adsorption. This term rules the process during multilayer adsorption. In contrast, when the adsorbed film turns out to be thicker, the adsorption potential will become less important. Subsequently, $\Delta\mu$ will be controlled virtually completely by the curvature contribution, $\Delta\mu_c$, particularly the Laplace term, as was formerly stated (see Section 4.3.1) [7], which is given for a cylindrical pore [7]:

$$\Delta\mu_c = \frac{\gamma V_L}{r_P - t}$$

On the other hand [18,19], $\Delta\mu_a = \Pi(t)V_L$, a relation which is based on the concept of disjoining pressure, Π, introduced by Derjaguin in 1936, could be obtained with the help of the relation [7]:

$$\Delta\mu = \int V_L dP$$

In the DBdB approach, the disjoining pressure, $\Pi(t)$, accounts for the sum of fluid–solid intermolecular interactions. That is, this pressure is equivalent to the action of the adsorption field. In the case of dominant attractive potential, as was previously studied in the case of the Frenkel-Halsey-Hill (FHH) model (see Chapter 3, Section 3.4) [20]:

$$\Pi(t) \propto \frac{1}{t^m}$$

Dubinin and coworkers recommended the standard N_2 isotherm, at 77.4 K, on nonporous oxides in FHH form as [13]:

$$\ln\left(\frac{P_0}{P}\right) = \frac{\Pi(t)V_L}{RT} = \frac{C}{t^m} \tag{4.4}$$

with the parameters $C = 44.54$, and $m = 2.241$, to get t in Å [13].

The stability condition for the wetting film was formulated earlier by Derjaguin and coworkers as [13]:

$$\left(\frac{d\Pi(t)}{dt}\right) < 0 \tag{4.5}$$

Certainly, it is supposed that during adsorption the isotherm draws a sequence of metastable states of the adsorption film, and the capillary condensation take places spontaneously when the film thickness approaches the limit of stability. The critical thickness of metastable films is determined from the condition [18]:

$$-\left(\frac{d\Pi(t)}{dt}\right)_{t=t_\alpha} = \frac{\gamma}{(r_P - t_{critical})^2} \tag{4.6}$$

where $t_{critical}$ is the critical adsorbed film thickness parameter, which establishes the limit of stability of the adsorbed film [13,15]. Thus, the conditions of capillary condensation in a cylindrical pore are determined by the system of both Equation 4.3 and Equation 4.6 [13].

Desorption from a cylindrical capillary is determined by the condition of formation of the equilibrium meniscus given by the enhanced Kelvin-Cohan equation recognized as the Derjaguin equation [18]:

$$RT\ln\left(\frac{P}{P_0}\right) = \frac{2\gamma V_L + \dfrac{2V_L}{(r_P - t_e)^2}\displaystyle\int_{t_e}^{r_P}(r_P - t)^2\Pi(t)dt}{r_P - t} \tag{4.7}$$

where t_e is the thickness of the adsorbed film in equilibrium with the meniscus given by Equation 4.3. Thus, the conditions of desorption are determined by the system of both Equation 4.3 and Equation 4.7.

As was stated in a previous paragraph, the film thickness cannot expand without limit in pores. The stability of the multilayer adsorbed film is determined by the long-range van der Waals interactions and by the surface tension and curvature of the liquid–vapor interface [8,13]. The chemical potential difference, $\Delta\mu$, is given by [8]: $\Delta\mu = \Delta\mu_a + \Delta\mu_c$. When the adsorbed film turns out to be thicker, the adsorption potential becomes less important, and $\Delta\mu$ will be controlled virtually completely by the curvature contribution, $\Delta\mu_c$. Then at a certain critical thickness, $t_{critical}$, pore condensation occurs in the core of the pore, controlled by intermolecular forces in the core fluid [8,13].

It is necessary to point out that the DBdB method has not received the widespread acceptance given to the BJH method, which was implemented in the majority of commercial automated surface area and porosity analyzers [10].

4.3.3 Some Concluding Remarks about the Macroscopic Theories to Describe Multilayer Adsorption and Pore Condensation

The DBdB theory [18,19] and also the Saam-Cole theory [24], not explained here, describe the mechanism of pore condensation and hysteresis as it is described in Figure 4.3 [8,13,15]. These theories take into consideration the influence of the adsorption potential on the equilibrium and stability of the adsorbed multilayer film [8,13,15]. In agreement with experimental studies, these theories anticipate that a growth in the strength of the adsorbate–adsorbent interaction, a decrease of the experimental temperature, or diminishing the pore size will move the pore condensation transition to lower relative pressures [8,13].

There have been many efforts to revise the DBdB theory to take into account the effects of the pore wall curvature, which are expected to be appreciable in very narrow pores [13]. Other authors introduced corrections for the liquid–vapor surface tension; further studies calculated the fluid–solid potential accounting for the substrate curvature [13]. However, only the density functional theory of inhomogeneous fluids bridges the gap between molecular-level and macroscopic approaches [13].

The macroscopic theories do not describe the individuality of the critical region [8,13,15]. The Kelvin-Cohan methodology contemplates pore condensation as a gas–liquid phase transition in the core of the pore between two homogeneous, bulk-like gas and liquid phases, where the density difference, $\Delta\rho = \rho_l - \rho_g$, is considered to be the difference in orthobaric densities of coexisting bulk phases [8]. That is to say, pore condensation and hysteresis are anticipated to happen up to the bulk critical point, where $\Delta\rho = 0$. On the contrary, microscopic approaches, such as the density functional theory [12–15] and other microscopic methods [8], propose that a fluid confined to a single pore can exist with two possible density profiles, corresponding to inhomogeneous gas and liquid configurations in the pore [8,12–15].

4.4 DENSITY FUNCTIONAL THEORY

4.4.1 The Density Functional Theory Methodology in General

Molecular models, as for instance the density functional theory (DFT), provide a more comprehensive representation of phase transitions in pores than the classical thermodynamic methods [11–15,25–43]. As was explained in Chapter 1, Section 1.10, the basic variable in DFT is the single-particle density, $\rho(\bar{r})$. For a many-particle classical system immersed in an external potential, U_{ext} (arising, for instance, from the adsorption field happening when a fluid is confined in a pore), a function, $\Omega[\rho(\bar{r})]$, which reduces to the grand potential, $\Omega = \Omega[\bar{\rho}(\bar{r})]$, when $\rho(\bar{r}) = \bar{\rho}(\bar{r})$ is the equilibrium density, can be defined with the help of the following unique functional of the density [26,27]:

$$\Omega[\rho(\bar{r})] = F[\rho(\bar{r})] - \int d\bar{r}\rho(\bar{r})[\mu - U_{ext}(\bar{r})] \tag{4.8}$$

which is obtained by means of a Legendre transformation (see Appendix 1.1) of $F[\rho(\bar{r})]$, which as was previously defined, in Chapter 1, Section 1.10, is the intrinsic Helmholtz free energy [26], where μ is the chemical potential of the studied system. To simplify Equation 4.8, it will be now defined:

$$u(\bar{r}) = \mu - U_{ext}(\bar{r}) \tag{4.9}$$

and then:

$$\Omega[\rho(\bar{r})] = F[\rho(\bar{r})] - \int d\bar{r}\rho(\bar{r})u(r) \tag{4.10}$$

The ground energy and all other properties of a ground state molecule are uniquely determined by the ground state electron probability density of the system. Therefore, for a thermodynamic system of N classical particles, the true equilibrium density, $\bar{\rho}(\bar{r})$, is determined with the help of the Euler-Lagrange equation (see Appendix 1.4). That is, we must determine the minimum value of the functional $\Omega[\rho(\bar{r})]$:

$$\frac{\delta\Omega[\rho(\bar{r})]}{\delta\rho(\bar{r})} \tag{4.11}$$

i.e., $\bar{\rho}(\bar{r})$ is the solution of Equation 4.11, where

$$\frac{\delta}{\delta\rho(\bar{r})}$$

indicates the functional derivative (see Appendix 1.4). Now, combining Equations 4.8 and 4.11, we will obtain [26,27]

$$u(\bar{r}) = \mu - U_{ext}(\bar{r}) = \frac{\delta F[\rho(\bar{r})]}{\delta \rho(\bar{r})} \tag{4.12}$$

which is also the minimum condition.

In order to get $\bar{\rho}(\bar{r})$, as is normally done in the solution of statistical mechanical problems, the studied system is reduced to simpler components. Then, for a classical fluid with inhomogeneous density distribution, the functional F $[\rho(\bar{r})]$ representing the intrinsic Helmholtz free energy can be expressed as [26,39]:

$$\mathrm{F}\,[\rho(\bar{r})] = F_{id}[\rho(\bar{r})] + F_{ex}[\rho(\bar{r})] \tag{4.13}$$

where:

$$F_{id}[\rho(\bar{r})] = kT \int d\,\bar{r}\rho(\bar{r}) \left\{ \ln\left(\rho(\bar{r})\Lambda^3\right) - 1 \right\} \tag{4.14}$$

is the ideal-gas free energy functional, resulting from a system of noninteracting particles, where

$$\Lambda = \left(\frac{h^2}{2\pi mkT} \right)^{1/2}$$

is the thermal wavelength. In Equation 4.13, $F_{ex}[\rho]$ represents the excess free energy for the classical system.

Now defining [26,27]:

$$c^1(\bar{r}) = \frac{\delta[\beta F_{ex}(\rho(\bar{r})]}{\delta \rho(\bar{r})} \tag{4.15}$$

From the variational principle equation for the classical system of N particles, it follows that the density profile satisfies [26,27,39]:

$$\rho(\bar{r}) = \Lambda^{-3}[\exp(\beta\mu)][\exp -(\beta U_{ext} + c^1(\bar{r}, \rho(\bar{r})))] \tag{4.16}$$

where $c^1(\bar{r})$ is also a functional of $\rho(\bar{r})$, and $\beta = 1/kT$. When $c^1(\bar{r}) = 0$ (i.e., in the case of an ideal gas), this equation reduces to the barometric law for the density distribution in the presence of an external field.

To continue, the studied system is additionally reduced to simpler components. Then, the excess intrinsic Helmholtz energy is split into contributions from the short-ranged repulsion and long-term attraction [39]:

$$F_{ex}\ [\rho(\bar{r})] = F_{rep}[\rho(\bar{r})] + F_{att}[\rho(\bar{r})] \tag{4.17}$$

4.4.2 Calculation of the Pore Size Distribution

In the frame of the present book, we are interested in modeling capillary condensation and desorption of nitrogen and argon in slit pores [32,33], cylindrical pores [13,14], and spherical cavities [15]. Consequently, to compute the pore size distribution (PSD) of slit pores, cylindrical, and spherical cavities, the experimental isotherm is described as a combination of theoretical isotherms in individual pores. The theoretical isotherm is obtained, for example, with the help of a DFT approach [12–15,32,33,43]. That is, the experimental isotherm is the integral of the single-pore isotherm multiplied by the PSD [40], specifically, the Fredholm-type integral equation:

$$N_{\exp}\left(\frac{P}{P_0}\right) = \int_{D_{\min}}^{D_{\max}} N_V^{ex}\left(D, \frac{P}{P_0}\right)\varphi_V(D)dD \tag{4.18}$$

Here,

$$N_V^{ex}\left(D, \frac{P}{P_0}\right)$$

is a kernel of the theoretical isotherm in pores of different diameters, $\varphi_V(D)$ is the PSD function [8,10,12–15,40], and D is the pore diameter. Different kernels are used to carry out the calculations of the PSD from the experimental isotherms [10,12–15]. To find a PSD from the experimental isotherm function,

$$N_{\exp}\left(\frac{P}{P_0}\right),$$

it is first necessary to calculate

$$N_V^{ex}\left(D, \frac{P}{P_0}\right),$$

with the help of $\bar{\rho}(\bar{r})$, as will be explained below. Then, the integral equation is represented as a matrix equation with pores spanning logarithmically in different ranges [10]. The procedure is to expand $\varphi_V(D_{in})$ with the help of, for example, the γ-distribution, with multiple modes, as follows [37,40]:

$$\varphi_V(D) = \sum_{i=1}^{m} \frac{\alpha_i(\gamma_i, D)^{\beta_i}}{\Gamma(\beta_i)D}\left(\exp\left[-\gamma_i D\right]\right)$$

where m is the number of modes of the distribution, $\Gamma(\beta_i)$, is the gamma function [44], and α_i, β_i, and γ_i are adjustable parameters that define the amplitude, mean, and variance of the mode, i, of the distribution. Then, a solution, i.e., the PSD, $\varphi_V(D)$, is found using multilinear least-square fitting procedures [45] for the parameters defining the assumed PSD, so as to match the experimental isotherm [40].

4.4.3 The Nonlocal Density Functional Theory for the Description of Adsorption in Slit Pores, Cylindrical Pores, and Spherical Cavities

The Evans and Tarazona nonlocal density functional theory (NLDFT) model [28,34] will be used here to find $\bar{\rho}(\bar{r})$. This model has been shown to provide reliable results in quantitative agreement with molecular simulations and experimental data on regular different model systems [12–15,35–37].

In the NLDFT approach, the adsorption and desorption isotherms in pores are calculated based on the intermolecular potentials of fluid–fluid and solid–fluid interactions, assuming that each individual pore has a fixed geometry and is open and in contact with the bulk adsorbate fluid. The local density of the adsorbate, confined in a pore at a given chemical potential, μ, volume, V, and temperature, T, is determined by the minimization of the grand thermodynamic potential Ω [12–15,32,33]. Specifically, the NLDFT proceeds by considering that the adsorbed fluid in a pore is in equilibrium with a bulk gas phase. The local fluid density of the adsorbate confined in the pore, in the presence of a spatially varying external potential, U_{ext}, at a given chemical potential, volume, and temperature, is determined by the minimization of the grand potential [12–15,32,39,40]:

$$\Omega[\rho(\bar{r})] = F_{id}[\rho(\bar{r})] + F_{\text{rep}} + F_{att}[\rho(\bar{r})] - \int d\bar{r}\rho(\bar{r})[\mu - U_{ext}(\bar{r})] \qquad (4.18a)$$

As was previously stated, in Equation 4.18a, the intrinsic free energy, is divided in a perturbative fashion into the ideal gas free energy, F_{id}, given by an exact expression [27,28,39], and the excess free energy, F_{ex}, which takes into account the interparticle interactions. The term F_{ex} consists of two components. F_{rep} represents the repulsive forces between molecules and is commonly described as a reference system of hard spheres; then $F_{rep} = F_{HS}$ and the free energy arising from the attractive interactions, i.e., F_{att} [39,41–43], where F_{att} is the mean-field free energy due to the Lennard–Jones (LJ) attractive interactions [13–15,28,32,39,41–43].

To take into consideration the repulsive forces, several functionals for hard sphere fluids have been developed, among them are the so-called weighted density approximation [31], the so-called fundamental measure theory [36], and the smoothed density approximations [28, 34]. The smoothed density approximation,

developed by Evans, Tarazona, and collaborators, is applied in nearly all NLDFT versions presently used for pore size characterization. Then the free energy of the hard sphere system is calculated with the help of [32]:

$$F_{rep}[\rho(\bar{r})] = F_{HS}[\rho(\bar{r})] = kT \int \rho(\bar{r}) d\bar{r} f_{ex}[\bar{\bar{\rho}}(\bar{r})] \tag{4.19}$$

where the hard sphere diameter, d_{HS}, is [43]:

$$d_{HS} = \int_0^{\sigma} \left\{1 - \exp\left[-\beta u_{rep}(r)\right]\right\} dr$$

and $f_{ex}[\bar{\bar{\rho}}(\bar{r})]$, the excess free energy per molecule, is [32,36,37]:

$$f_{ex}[\bar{\bar{\rho}}(\bar{r})] = \mu[\bar{\bar{\rho}}(\bar{r})] - \frac{P[\bar{\bar{\rho}}(\bar{r})]}{\bar{\bar{\rho}}(\bar{r})} - kT\{\ln[\Lambda^3 \bar{\bar{\rho}}(\bar{r})] - 1\}$$

In the previous equation, $\mu[\bar{\bar{\rho}}(\bar{r})]$ and $P[\bar{\bar{\rho}}(\bar{r})]$ are the chemical potential and the pressure, in that order, of a uniform hard sphere fluid, and $\bar{\bar{\rho}}(\bar{r})$ is a smoothed density profile. The smoothed density profile, which is introduced into the $f_{ex}[\bar{\bar{\rho}}(\bar{r})]$ functional is defined as follows [28,34]:

$$\bar{\bar{\rho}}(\bar{r}) = \int d\bar{R} \rho(\bar{R}) W\left(\left|\bar{r} - \bar{R}\right|, \bar{\bar{\rho}}(\bar{r})\right) \tag{4.20}$$

where $W(|\bar{r} - \bar{R}|, \bar{\bar{\rho}}(\bar{r}))$ is a weighting function which takes into account nonlocal effects [28]. The idea behind the smoothed, or weighted density approximations is to construct a smoothed density, $\bar{\bar{\rho}}(\bar{r})$, which is an average of the true density profile, $\rho(\bar{r})$, over a local volume that is determined by the range of the interatomic forces. Several types of weigh functions have been proposed to study confined fluids [27]. The Tarazona prescription for the weighting functions uses a power expansion in the smoothed density, truncating the expansion in the second order, which yields [28,34]:

$$W_{nonlocal}\left(\left|\bar{r} - \bar{R}\right|\right) = W_0\left(\left|\bar{r} - \bar{R}\right|\right) + W_1\left(\left|\bar{r} - \bar{R}\right|\right)\bar{\bar{\rho}}(\bar{r}) + W_2\left(\left|\bar{r} - \bar{R}\right|\right)\left(\bar{\bar{\rho}}(\bar{r})\right)^2 \tag{4.21}$$

The expansion coefficients, W_0, W_1, and W_3, are [28,34]:

$$W_0(r) = \frac{3}{4\pi\sigma^3} \qquad \text{for } r < \sigma,$$

$$W_0(r) = 0 \qquad \text{for } r > \sigma.$$

$$W_1(r) = 0.475 + 0.648\left(\frac{r}{\sigma}\right) + 0.113\left(\frac{r}{\sigma}\right)^2 \qquad \text{for } r < \sigma,$$

$$W_1(r) = 0.288\left(\frac{\sigma}{r}\right) - 0.924 + 0.764\left(\frac{r}{\sigma}\right) - 0.187\left(\frac{r}{\sigma}\right)^2 \qquad \text{for } \sigma < r < 2\,\sigma,$$

$$W_1(r) = 0 \qquad \text{for } r > \sigma.$$

and

$$W_2(r) = \left(\frac{5\pi\sigma^3}{144}\right)\left(6 - 12\left(\frac{r}{\sigma}\right) + 5\left(\frac{r}{\sigma}\right)^2\right) \qquad \text{for } r < \sigma,$$

$$W_2(r) = 0 \qquad \text{for } r > 2\sigma.$$

where $r = \left|\bar{r} - \bar{R}\right|$.

To calculate the hard sphere excess free energy, the Carnahan-Starling equation of state [46] is normally used:

$$P_{HS}[\bar{\bar{\rho}}] = \bar{\bar{\rho}}kT\left(\frac{1 + \bar{\bar{\xi}} + \bar{\bar{\xi}}^2 - \bar{\bar{\xi}}^3}{\left(1 - \bar{\bar{\xi}}\right)^3}\right)$$

$$\mu_{HS}[\bar{\bar{\rho}}] = kT\left[\ln(\Lambda^3\bar{\bar{\rho}} + \left(\frac{8\bar{\bar{\xi}} - 9\bar{\bar{\xi}}^2 + 3\bar{\bar{\xi}}^3}{\left(1 - \bar{\bar{\xi}}\right)^3}\right)\right]$$

where

$$\bar{\bar{\xi}} = \frac{\pi}{6}\bar{\bar{\rho}}d_{HS}^3,$$

and the hard sphere diameter can be calculated with the help of the Barker-Handerson diameter [47] and

$$\frac{d_{HS}}{\sigma_{ff}} = \frac{\frac{\eta_1 kT}{\varepsilon_{ff}} + \eta_2}{\frac{\eta_3 kT}{\varepsilon_{ff}} + \eta_4}$$

where $\eta_1 = 0.3837$, $\eta_2 = 1.305$, $\eta_3 = 0.4249$, and $\eta_4 = 1$ [37] are fitting parameters.

In addition,

$$F_{att}[\rho(\bar{r})]=(1/2)\iint d\bar{r}d\bar{r'}\rho(\bar{r})\rho(\bar{r'})\Phi_{atr}\left(\left|\bar{r}-\bar{r'}\right|\right) \tag{4.22}$$

where the attractive fluid–fluid potential, Φ_{attr}, is calculated according to the Weeks-Chandler-Andersen scheme (WCA) [48]:

$$\Phi_{attr}\left(\left|\bar{r}-\bar{r'}\right|\right)=\phi_{ff}\left(\left|\bar{r}-\bar{r'}\right|\right) \quad \text{for} \quad \left|\bar{r}-\bar{r'}\right|>r_m \tag{4.23a}$$

$$\Phi_{attr}\left(\left|\bar{r}-\bar{r'}\right|\right)=-\varepsilon_{ff} \quad \text{for} \quad \left|\bar{r}-\bar{r'}\right|<r_m \tag{4.23b}$$

where $r_m = 2^{1/6}\sigma_{ff}$, and ϕ_{ff} is the Lennard-Jones potential of a pair of adsorbate molecules whose centers of mass are separated by a distance, *r,* and [37,43]:

$$\phi_{ff}=4\varepsilon_{ff}\left[\left(\frac{\sigma_{ff}}{r}\right)^{12}-\left(\frac{\sigma_{ff}}{r}\right)^{6}\right] \tag{4.24}$$

where r is the separation distance between a pair of molecules, and the parameters σ_{ff} and ε_{ff} are the Lennard-Jones molecular diameter and well depth for the adsorbate–adsorbate pair potential, and r_m reflects the minimum of the potential [32,37,43] of the fluid–fluid Lennard-Jones 12-6 pair potential.

The external potential imposed by the pore walls depends on the assumed pore model, and the chemical composition of the adsorbent. No we will compute the external adsorptive-adsorbent potential.

The solid-fluid potential, $U_{ext}(\mathbf{r})$, in the case of spherical silica pores, is the result of Lennar-Jones interactions with the outer layer of oxygen atoms in the wall of a spherical cavity of radius *R,* measured to the centers of the first layer of atoms in the pore wall. The potential at a distance, *x,* from the wall is obtained by integrating the Lennard Jones, 12-6, potential over the spherical surface [15]:

$$\begin{aligned} U_{ext}(x,R)=2\pi\rho_s^O\varepsilon_{sf}\sigma_{sf}^2\Bigg\{&\frac{2}{5}\sum_{j=0}^{9}\left(\left(\frac{\sigma_{sf}^{10}}{R^j x^{10-j}}+(-1)^j\frac{\sigma_{sf}^{10}}{R^j(x-2R)^{10-j}}\right)\right)\\ &-\sum_{j=0}^{3}\left(\frac{\sigma_{sf}^{4}}{R^j x^{4-j}}+(-1)^j\frac{\sigma_{sf}^{4}}{R^j(x-2R)^{4-j}}\right)\Bigg\}\end{aligned} \tag{4.25}$$

Here, ε_{sf} and σ_{sf} are the energetic, and scale parameters of the potential, respectively. Moreover, ρ_s^O is the number of oxygen atoms per unit area of the pore wall,

or oxygen surface density. The parameters of the adsorptive-adsorptive, and adsorptive-adsorbent intermolecular potentials, necessary to evaluate Equations 4.23, 4.24, and 4.25 are reported in Tables 4.1 and 4.2 [13,50–52].

In a slit pore of physical pore width H (Fig. 4.10) located between two homogeneous carbon slabs, the external potential U_{ext} depends only upon one spatial coordinate. z (Fig. 4.10.) is given by [44]:

$$U_{ext}(z) = \phi_{sf}(z) + \phi_{sf}(H - z)$$

The potential of the adsorbate interaction with one of the bounding slabs, ϕ_{sf}, is the in the case of graphite layers well described by the Steele potential [53]:

$$\phi_{sf} = 2\pi\rho_s\varepsilon_{sf}\sigma_{sf}^2\Delta\left[\frac{2}{5}\left(\frac{\sigma_{sf}}{z}\right)^{10} - \left(\frac{\sigma_{sf}}{z}\right)^{4} - \left(\frac{\sigma_{sf}^4}{3\Delta([z+0.61\Delta]^3)}\right)\right]\Bigg\} \quad (4.25a)$$

where, ε_{sf}, and, σ_{sf}, are the Lennard-Jones parameters for the adsorbate molecule interaction with a carbon atom in the porous solid. Moreover, $\rho_s = 0.114$ Å^{-3}, is the atomic bulk density of graphite, and, $\Delta = 3.34$ Å, is the distance between graphite layers [38]. In Tables 4.1, and 4.2 [13, 50-52] are reported the parameters of the adsorptive-adsortive, and adsorptive-adsorbent intermolecular potentials necessary to evaluate Equations 4.23, 4.24, and 4.25a. It is necessary to state that: $\rho_s \times \Delta = \rho_s^C$ 0.114 Å^{-3} × 3.34 Å = 0.381 Å^{-2} = 3.81 × 10^{19} m^{-2} is the number of carbon atoms per unit area of the pore wall, or carbon surface density.

TABLE 4.1
Adsorptive–Adsorptive Intermolecular Potentials Parameters

Gas	ε_{ff}/k [K]	σ_{ff} [nm]	d_{HS} [nm]
Nitrogen	94.45	0.3575	0.3575
Argon	118.05	0.3305	0.3380

TABLE 4.2
Adsorptive–Adsorbent Intermolecular Potentials Parameters

Gas/Solid	ε_{sf}/k [K]	σ_{sf} [nm]	Surface Density
Nitrogen/carbon	53.22	0.3494	Carbon: $\rho_s^C = 3.819 \times 10^{19}$ m^{-2}
Nitrogen/silica	147.3	0.3170	Silica: $\rho_s^O = 1.53 \times 10^{19}$ m^{-2}
Argon/silica	171.24	0.3000	Silica: $\rho_s^O = 1.53 \times 10^{19}$ m^{-2}

Theoretical adsorption isotherms for a pore of a particular width, and geometry are constructed by solving for the equilibrium adsorbate density profile. The density profile that minimize the Grand Potential Function of the adsorbed fluid for a range of chemical potentials, μ; that is the equilibrium density profile which fulfills:

$$u(\bar{r}) = \mu - U_{ext}(\bar{r}) = \frac{\delta F[\rho(\bar{r})]}{\delta\rho(\bar{r})} = \frac{\delta(F_{id} + F_{HS})}{\delta\rho} + \frac{\delta\left\{(1/2)\iint d\bar{r}.d\bar{r}'\,\rho(\bar{r})\rho(\bar{r}')\Phi_{atr}\left(\left|\bar{r}-\bar{r}'\right|\right)\right\}}{\delta\rho}$$

where introducing Equations 4.14 and 4.19 is obtained:

$$\mu - U_{ext}(\bar{r}) = kT\ln(\Lambda^3\rho(\bar{r})) + \frac{\delta\left\{kT\int \rho(\bar{r}) f_{ex}[\bar{\bar{\rho}}(\bar{r})]d\bar{r}\right\}}{\delta\rho} + \frac{\delta\left\{(1/2)\iint d\bar{r}.d\bar{r}'\rho(\bar{r})\rho(\bar{r}')\Phi_{atr}\left(\left|\bar{r}-\bar{r}'\right|\right)\right\}}{\delta\rho} \tag{4.26}$$

The previous equation is an implicit expression, whose functional inversion yields the density profile in terms of the chemical potential, the attractive, and external potentials, and the geometry of the system and particles. The inversion of the Euler-Lagrange equation, expression "4.26", requires the calculation of a series of convolution integrals, such as:

$$\int f(\bar{r})\phi\left(\left|\bar{r}-\bar{r}'\right|\right)d\bar{r},$$

where $\phi(|\bar{r}-\bar{r}'|)$ is an arbitrary isotropic kernel, and, $f(\bar{r})$, is an arbitrary function [53]. The inversion of these convolution integrals depends on the symmetry of the concrete pore, which normally reduces the problem to a one-dimensional one, as is the case in the slit, cylindrical, and spherical pore geometries. These convolutions are calculated by repeated one-dimensional integration taking advantage of the Gaussian quadrature [44] to increase the velocity of the numerical evaluation [53]. If we consider, for example [44]:

$$g(x) = \int \phi(z-x)f(z)dz.$$

The integral, in principle, can be evaluated by the Gaussian quadrature method. Then the numerical quadrature replaces the integral by a summation:

$$g(x_i) = \sum_{k=1}^{n} B_k \phi(z_k - x_i) f(z_k),$$

or in matrix notation:

$$g_i = \sum_{k=1}^{n} B_{ik} f_k.$$

Then inverting the matrix (B_{ik}) we will have:

$$f(x_k) = f_k = \sum_{i=1}^{n} B_{ki}^{-1} g_i$$

which allow the numerical evaluation of the unknown function, $f(x)$.

For the case of a slit pore [43] the specific excess adsorption

$$N_V^{ex}\left(H, \frac{P}{P_0}\right)$$

is a kernel of the theoretical isotherm in slit like pores of different diameters:

$$N_V^{ex}\left(H, \frac{P}{P_0}\right) = \frac{1}{H}\int_0^H (\rho(z) - \rho_{bulk}) dz, \tag{4.27}$$

where $\rho(z)$ is the density profile that minimize the grand potential functional of the adsorbed fluid over a range of chemical potential values, ρ_{bulk}, is the bulk gas density at a given relative pressure, P/P_0 at chemical potential, μ. Where H and z have the meaning explained in Figure 4.10.

We consider, for the case of cylindrical pores a cylindrically symmetric density profile, $\rho(r)$, that minimize the grand potential functional of the adsorbed fluid over a range of chemical potential values. For a this cylindrically symmetric density distribution, $\rho(r)$, where, r, is a cylindrical coordinate from the pore center, the excess adsorption per unit area of a cylindrical pore is calculated from [13,14]:

$$N_V^{ex}\left(D, \frac{P}{P_0}\right) = \frac{2}{D}\int_0^{D/2} \rho(r) r dr - \frac{D_{in}}{4}\rho_{bulk}$$

where, ρ_{bulk}, is the bulk gas density at a given relative pressure, P/P_0, $D_{in} = D - \sigma_{ss}$, is the internal pore diameter, which is the diameter of the cylindrical layer formed

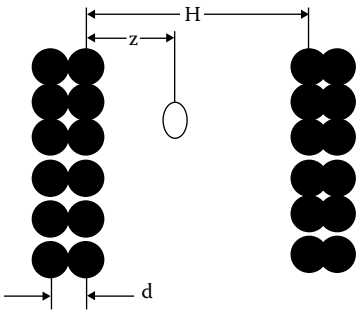

FIGURE 4.10 Schematic representation of a slit pore.

by the centers of the atoms present in the pore wall, D, less the effective diameter of the atom.

For the situation of spherical pores (specifically, ink-bottle pores, considered as spherical cavities connected by narrow cylindrical necks windows) spherically symmetric density distributions, then for a spherically symmetric density distribution, $\rho(r)$, where $r = R - x$ is a radial coordinate from the pore center, in this case, the specific excess adsorption per unit of internal pore volume is calculated as [15]:

$$N_V^{ex} = \frac{3\int_0^R \rho(r) r^2 dr}{\left(R - \frac{\sigma_{OO}}{2}\right)^3} - \rho_{bulk},$$

where, $\sigma_{OO}/2$, is the effective radius of an atom in the pore wall; ρ_{bulk} ., is the bulk gas density at a given relative pressure, P/P_0. The pore diameters reported below are internal, $D_{in} = 2R - \sigma_{OO}$, when expressed in dimensional units and crystallographic when expressed in units of the molecular diameter of the adsorbate, $2R/\sigma_{ff}$.

As was formerly expressed, the whole adsorption isotherm,

$$N_{\exp}\left(\frac{P}{P_0}\right),$$

that is, the experimental isotherm, is the integral of the single pore isotherm multiplied by the pore size distribution $\varphi_V(D)$ (PSD) [41],

$$\int_{D_{\min}}^{D_{\max}} N_V^{ex}\left(D, \frac{P}{P_0}\right)\sigma_V\left(D\right)dD.$$

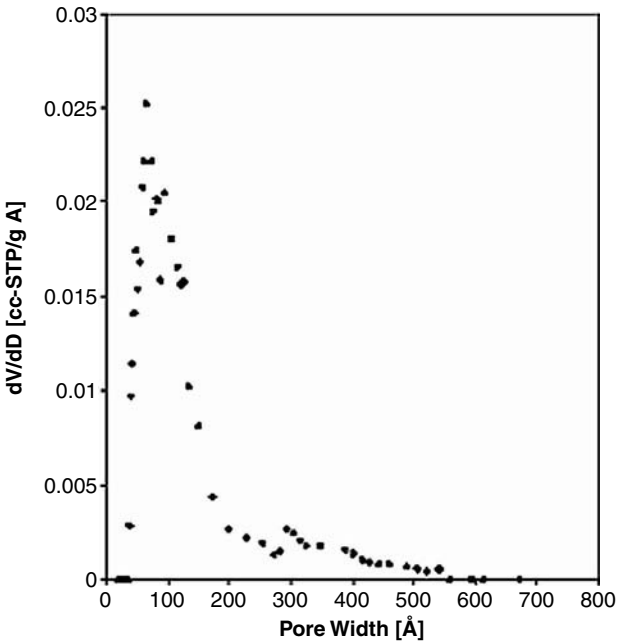

FIGURE 4.11 NLDFT-PSD (dV/dD) [cc-STP/g _] versus pore width [_] corresponding to the sample 70bs2.

In order to calculate the PSD, a theoretical single pore isotherm,

$$N_V^{ex}\left(D, \frac{P}{P_0}\right),$$

which correctly describe the relationship between the isotherm, and the pore size distribution is needed [12–15,33,33,43].

In Figure 4.11 [16] is presented the complete NLDFT-PSD (dV/dD), corresponding to the sample 70bs2. The sample tested in the adsorption experiment was degassed at 200°C, for 3 h, in high vacuum (10^{-6} Torr), previous to analysis. The measurement of the adsorption isotherm was carried out in a Quantachrome Instruments Autosorb-1 [10] applying the nitrogen-silica at 77 K adsorption branch kernel [16] included in the software of the Autosorb-1 [10]. This methodology is applicable in the pore range from 18 to 1000 Å. In Table 4.3. [16] the mode of the DFT-PSD distribution (d) and the NLDFT-pore volume (W) are reported.

4.4.4 Some Concluding Remarks about the Molecular Models to Describe Adsorption

The molecular models, specifically the density functional theory (DFT) approaches, provide a comprehensive representation of physical adsorption in porous solids

TABLE 4.3
DFT-Pore Volume (W) and DFT-Pore Width Mode (d) Corresponding to Some Silica Samples and the MCM-41 Mesoporous Material

Sample	W [cm^3/g]	d [ ]
70bs2	3.0	65
68bs1E	2.4	81
75bs1	2.7	125
79BS2	1.6	31
74bs5	1.4	61
68C	0.46	21
MCM-41	1.7	35

[12–15,41–43]. During the last 100 years the theory of adsorption was developed thermodynamically, kinetically, and statistically, and also using empirical isotherm equations. All these methods describe real adsorption systems for certain materials in a certain range of pressure and temperature. However, each of the reported methods fails when applied outside of its range of soundness. The DFT approaches allow us to calculate the equilibrium density profile, and integrating the density profile over the pore geometry, we could obtain a theoretical kernel, which allows us to generate the experimental isotherm if we know the PSD, or vice versa to get the PSD if we know the experimental isotherm.

In contrast to the classical methods, this methodology allows us to describe the complete range of pressures and temperatures. However, the classical methods generally bring a quantifiable functional dependence between the magnitude of adsorption and equilibrium pressure and temperature. On the other hand, the molecular methods such as the DFT approach only give a numerical kernel, which could only be calculable with the help of computers; besides the kernel is only useful for one adsorbate–adsorbent system and for the adsorption or desorption branch of the isotherm [10].

Regarding capillary condensation the DFT approaches give the option to make a precise analysis of the process. The NLDFT revealed that, in principle, both pore condensation and pore evaporation can be associated with metastable states of the pore fluid [8,13]. This is consistent with the classical van der Waals representation, which predicts that the metastable adsorption branch end at a vaporlike spinodal, where the threshold of stability for the metastable states is attained and the fluid spontaneously condenses into a liquidlike state [8,13]. Therefore, the desorption branch would end at a liquidlike spinodal, which is compatible with spontaneous evaporation. Nevertheless, metastabilities take place merely on the adsorption branch [8]. Assuming a pore of limited length, vaporization can take place by means of a thinning meniscus, a nucleation problem, and therefore metastability is not expected to occur during desorption. Neimark and Ravikovitch [13] have shown that the

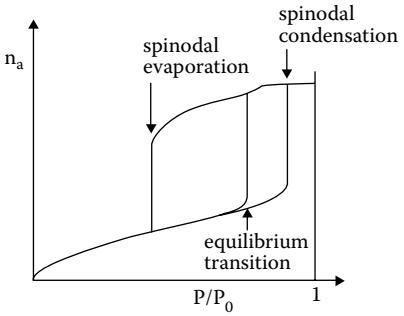

FIGURE 4.12 NLDFT description of capillary condensation.

experimental desorption branch is associated with the equilibrium gas–liquid transition, while the experimental condensation step corresponds to the spinodal spontaneous transition, and the spinodal evaporation is not experimentally observed [8,13] (see Figure 4.12).

REFERENCES

1. Everett, D.H., in *The Solid-Gas Interface*, Vol. 2, Flood, E.A., Ed., Marcel Decker, New York, 1967.
2. Sing, K.S.W., Everett, D.H., Haul, R.A.W., Moscou, L., Pirotti, R.A., Rouquerol, J., and Siemieniewska, T., *Pure App. Chem.*, 57, 603, 1985.
3. Gregg, S.J. and Sing, K.S.W., *Adsorption Surface Area and Porosity,* Academic Press, London, 1982.
4. Lowell, S. and Shields, J.E., *Powder Surface Area and Porosity,* Chapman Hall, London, 1991.
5. Rouquerol, J., Avnir, D., Fairbridge, C.W., Everett, D.H., Haynes, J.H., Pernicone, N., Ramsay, J.D.F., Sing, K.S.W., and Unger, K.K., *Pure Appl. Chem.*, 66, 1739, 1994.
6. Rouquerol, J., Rouquerol, F., and Sing, K., *Adsorption by Powder, and Porous Solids,* Academic Press, New York, 1999.
7. Adamson, A.W. and Gast, A.P., *Physical Chemistry of Surfaces,* 6th ed., J. Wiley & Sons, New York, 1997.
8. Thommes, M., in *Nanoporous Materials: Science and Engineering,* Lu, G.Q. and Zhao, X.S. Eds., Imperial College Press, London, 2004, p. 317.
9. Thommes, M., Kohn, R., and Froeba, M., *J. Phys. Chem. B,*. 104, 7932, 2000; and *App. Surf. Sci.*, 196, 239, 2002.
10. AUTOSORB-1, Manual, 2003.
11. Ravikovitch, P.I. and Neimark, A.V., *Colloids Surf, A,* 187–188, 11, 2001.
12. Neimark, A.V., Ravikovitch, P.I. and Vishnyakov, A., *J. Phys. Condens. Matter,* 15, 347, 2003.
13. Neimark, A.V. and Ravikovitch, P.I., *Mic. Mes. Mat.*, 44–45, 697, 2001.
14. Ravikovitch, P.I. and Neimark, A.V., *J. Phys. Chem. B,* 105, 6817, 2001.
15. Ravikovitch, P.I. and Neimark, A.V. *Langmuir,* 18, 1550, 2002.
16. Marquez-Linares, F. and Roque-Malherbe, R., *J. Nanosci. Nanotech.*, 6, 1114, 2006.
17. Cohan, L.H., *J. Amer. Chem. Soc.*, 60, 433, 1938.
18. Broekhoff, J.C.P. and de Boer, J.H., *J. Catal.*, 9, 8, 1967; and 9, 15, 1967.

19. Broekhoff, J.C.P. and de Boer, J.H., *J. Catal.*, 10, 153, 1968; and 10, 377, 1968.
20. Hill, T.L., *Adv. Catal.*, 4, 211, 1952.
21. Barret, E.P., Joyner, L.G., and Halenda, P.H., *J. Amer. Chem. Soc.*, 73, 373, 1951.
22. de Boer, J.H., Lippens, B.C., Broekhoff, J.C.P., van den Heuvel, A., and Osinga, Th.V., *J. Colloid Interface Sci.*, 21, 405, 1966.
23. Barton, T.J., Bull, L.M., Klemperer, G., Loy, D.A., McEnaney, B., Misono, M., Monson, P.A., Pez, G., Scherer, G.W., Vartulli, J.C., and Yaghi, O.M., *Chem. Mater.*, 11, 2633, 1999.
24. Cole, M.W. and Saam, W.F., *Phys. Rev. Lett.*, 32, 985, 1974.
25. Hohenberg, P. and Kohn, W., *Phys. Rev.*, 136, B864, 1964.
26. Ghosh, S.K., *Int. J. Mol. Sci.*, 3, 260, 2002.
27. Evans, R., in *Fundamentals of Inhomogeneous Fluids,* Henderson, D., Ed., Marcel Dekker, New York, 1992, p. 85.
28. Tarazona, P., *Phys. Rev. A,* 31, 2672, 1985.
29. Rosenfeld, Y., Schmidt, M., Lowen, H., and Tarazona, P., *Phys. Rev. E,* 55, 4245, 1997.
30. Davis, H.T., *Statistical Mechanics of Phases, Interfaces, and Thin Films,* J. Wiley & Sons, New York, 1996.
31. Curtin, W.A. and Ashcroft, N.W., *Phys. Rev. A,* 32, 2909, 1985.
32. Pan, H., Ritter, J.A. and Balbuena, P.B., *Ind. Eng. Chem. Res.*, 37, 1159, 1998.
33. Nguyen, T.X. and Bhatia, S.K., *J. Phys. Chem. B,* 108, 14032, 2004.
34. Tarazona, P., Marconi, U.M.B., and Evans, R., *Mol. Phys.*, 60, 573, 1987.
35. Neimark, A.V., Ravikovitch, P.I., and Vishnyakov, A., *Phys. Rev. E,* 62, R1493, 2000; and *Phys. Rev. E,* 64, 011602, 2001.
36. Kierlik, E. and Rosinberg, M., *Phys. Rev. A,* 42, 3382, 1990.
37. Lastoskie, C., Gubbins, K. E., and Quirke, N., *J. Phys. Chem.,* 97, 4786, 1993.
38. Gonzales, A., White, J.A., Roman, F.L., and Evan, R., *J. Phys. Condens. Matter,* 9, 2375, 1997; and *J. Chem. Phys.*, 109, 3637, 1998.
39. Tang, Y. and Wu, J., *J. Chem. Phys.*, 119, 7388, 2003.
40. Rege, S.U. and Yang, R.T., in *Adsorption. Theory, Modeling and Analysis,* Toth, J. Ed., Marcel Dekker, New York, 2002, p. 175.
41. Neimark, A.V., Ravikovitch, P.I., Grun, M., Schuth, F., and Unger, K., *J. Colloid Interface Sci.*, 207, 159, 1998.
42. Ravikovitch, P.I., Haller, G.L., and Neimark, A.V., *Adv. Colloid Interface Sci.*, 77, 203, 1998.
43. Dombrokii, R.J., Hyduke, D.R., and Lastoskie, C.M., *Langmuir,* 16, 5041, 2000.
44. Arfken, G.B. and Weber, H.J., *Mathematical Methods for Physicists,* 5th ed., Academic Press, New York, 2001.
45. Draper, N.R. and Smith, H., *Applied Regression Analysis, Third Edition,* J. Wiley & Sons, New York, 1998.
46. Carnahan, N. F. and Starling, K.E., *J. Chem. Phys.*, 51, 635, 1969.
47. Barker, J.A. and Henderson, D.J., *J. Chem. Phys.*, 47, 4714, 1967.
48. Week, J.D., Chandler, D., and Andersen, H.C., *J. Chem. Phys.*, 54, 5237, 1971.
49. Thommes, M., personal communication.
50. Ravikovitch, P.I., Vishnyakov, A., Russo, R., and Neimark, A.V., *Langmuir,* 16, 23, 2000.
51. Ravikovitch, P., Vishnyakov, A., and Neimark, A.V., *Phys. Rev. E.*, 64, 011602, 2001.
52. Steele, W.A., *The Interaction of Gases with Solid Surfaces,* Pergamon Press, Oxford, 1974.
53. Figueroa-Gerstenmaier, S., Development, and Application of Molecular Modeling Techniques for the Characterization of Porous Materials, Ph.D. Dissertation, Departament d'Enginyeria Quimica, Universitat Rovira I Virgili, Tarragona, Oct. 2002.

5 Diffusion in Porous Materials

5.1 INTRODUCTION

Diffusion is the random migration of molecules or small particles, arising from motion due to thermal energy [1–19]. It is a general property of matter related to the tendency of systems to occupy all of the accessible states. In a more simple way, diffusion is a spontaneous tendency of all systems to equalize concentration, if any external influence does not impede this process. That is, atoms, molecules, or any particle moves chaotically in the direction where fewer elements of its own type are located. Diffusion of gases in porous materials is a very important topic, since this effect is crucial in catalysis, gas chromatography, and gas separation processes.

From an industrial standpoint, it is significant to be able to predict and describe the mass transfer through the packed-bed reactors used in the chemical industries [7,14]. A better comprehension of this phenomenon will aid in the optimization and development of industrial applications of these materials in separation, catalytic processes, and kinetics-based pressure swing adsorption. In separation processes, for example, the necessity of an understanding of diffusion phenomena is evident [8]. Membrane-based separations also rely on the diffusion properties of the applied membrane. Therefore, to advance practical applications diffusion must be accurately described.

5.2 FICK'S LAWS

The quantitative study of diffusion started in 1850–1855 with the works of Adolf Fick and Thomas Graham. As a conclusion of his studies, Fick understood that diffusion obeys a law isomorphic to the Fourier law of heat transfer [17]. This fact allowed him to propose his first equation in order to describe macroscopically the diffusion process. Fick's first equation (see also Chapter 1, Section 1.11) is a linear relation between the matter flux, $\bar{J}$, and the concentration gradient, $\bar{\nabla}C$:

$$\bar{J} = -D\bar{\nabla}C \tag{5.1}$$

where D is the Fickean diffusion coefficient or transport diffusion coefficient, which is the proportionality constant. The units of the above described parameters are: D [(longitude)^2/time]; C [moles/volume]; and J [moles/area·time]. In the International System (SI), the unit of D is expressed in [m^2/s]; the concentration, C, could be expressed in [mol/m^3]; in this case the flux is expressed in [mol/m^2·s]. The flux

and, consequently, also the diffusion coefficient must be chosen relative to a frame of reference, since the diffusion flux, $\bar{J}$, gives the number of species crossing a unit area in the medium per unit of time [13].

Under the influence of external forces the particles move with an average drift velocity, v_F, which gives rise to a flux, Cv_F. Here, C is the concentration of diffusing species, and the total flux is given by the relation [4,13]:

$$J = -D\nabla C + Cv_F \tag{5.1a}$$

As diffusion is not anything more than the macroscopic expression of the tendency of a system to move toward equilibrium, the real driving force should be the gradient of the chemical potential, μ. Using irreversible thermodynamics, produces the relation (see Chapter 1, Section 1.11) [12,18]:

$$\bar{J} = -L\bar{\nabla}\mu \tag{5.2}$$

which is applicable for a porous material, where L is the phenomenological Onsager coefficient. This equation clearly identifies the cause for diffusive flow and will prove later to be helpful when trying to link the transport diffusion coefficient to a self-diffusion coefficient.

Fick's second equation:

$$\frac{\partial C}{\partial t} = -D\nabla^2 C \tag{5.3}$$

is an expression of the law of conservation of matter, i.e.:

$$\frac{\partial C}{\partial t} = -D\bar{\nabla}\cdot\bar{J}$$

if D does not depend on C.

As was formerly affirmed, diffusion is the random migration of molecules or small particles arising from motion due to thermal energy. A very simple derivation of Fick's first law, based on the random walk problem (see Chapter 1, Section 1.12), could be obtained in one dimension [4]. In this case, $J_x(x,t)$ (i.e., the number of particles that move across unit area in unit time) could be defined as:

$$J_x(x,t) = \frac{\mathrm{N}}{A\tau}$$

because the number of particles at position x and $(x + \Delta)$ at time t is $N(x)$ and $N(x + \Delta)$ (see Figure 5.1), respectively. Subsequently, half of the particles at x at time t move to the right (i.e., to $x + \Delta$), at the same time as the other half move to

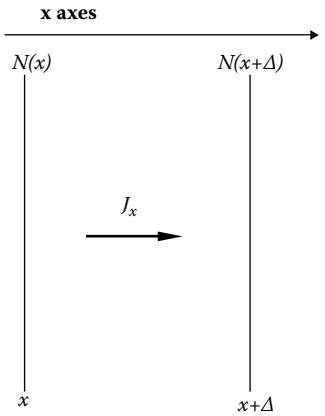

FIGURE 5.1 One-dimension diffusion.

the left (i.e., to $x - \Delta$) during the time-step τ. Likewise, half of the particles at $x + \Delta$ at time t move to the right (i.e., to $x + 2\Delta$), while the other half move to the left (i.e., to x). Subsequently, the net number of particles that move from x to $x + \Delta$, when $t = t + \tau$, is:

$$\mathrm{N} = -\frac{[N(x+\Delta,t) - N(x,t)]}{2}$$

Now:

$$J_x(x,t) = -\frac{\Delta^2}{2\tau}\left(\frac{1}{\Delta}\right)\left(\frac{N(x+\Delta,t)}{A\Delta} - \frac{N(x,t)}{A\Delta}\right) = -D\frac{[C(x+\Delta) - C(x,t)]}{\Delta}$$

For $\Delta \to 0$:

$$J_x(x,t) = \lim_{\Delta\to 0} -D\frac{[C(x+\Delta) - C(x,t)]}{\Delta} = -D\frac{\partial C(x,t)}{\partial x}$$

5.3 TRANSPORT, SELF-DIFFUSION, AND CORRECTED COEFFICIENTS

5.3.1 Transport Diffusion and Self-Diffusion

Transport diffusion simply results from a gradient concentration [9] (see Figure 5.2a [12]). On the other hand, self-diffusion is the diffusion which takes place in the absence of a chemical potential gradient, describing the uncorrelated movement of a particle [13] (see Figure 5.2b [12]). This process is described by following the molecular trajectories of a large number of molecules and determining their mean

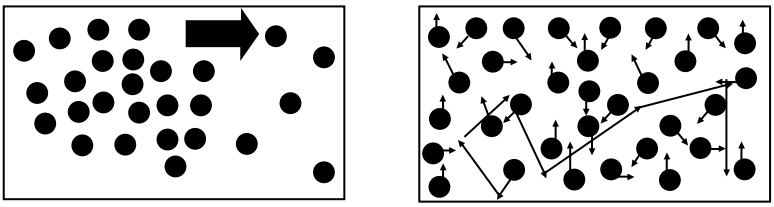

FIGURE 5.2 (a) Transport diffusion and (b) self-diffusion.

square displacement [13]. The differences in the microphysical situations between the transport diffusion, represented in Figure 5.2a, and self-diffusion, represented in Figure 5.2b, implies that D, the transport diffusion coefficient, and D^*, the self-diffusion coefficient, are generally different [12].

5.3.2 Interdiffusion and the Frame of Reference for Porous Materials

As was previously commented, the flux, as well as the diffusion coefficient, has to be chosen relative to a frame of reference. Pores are typical in materials such as microporous and mesoporous molecular sieves, silica, alumina, and activated carbons, among others. A solid framework, as a porous solid media, provides a convenient and unambiguous frame of reference against which to measure the diffusive flux. Then, given that the framework atoms are not transported, the coordinates to measure the molecular motion of the mobile species are the fixed coordinates of the solid [12,13].

The interdiffusion coefficient occurs when two atomic or molecular species mix together [4,13]. Consequently, for the interdiffusion in one dimension of two components, A and B [4,12]:

$$J_A = -D_A \frac{\partial C_A}{\partial x} \tag{5.4}$$

and:

$$J_B = -D_B \frac{\partial C_B}{\partial x} \tag{5.4a}$$

If the partial molar volume of the species A and B are different ($V_A \neq V_B$), the interdiffusion of the two species will lead to a net flow relative to a fixed coordinate frame of reference; consequently, the total volumetric flux is [12]:

$$J = V_A D_A \frac{\partial C_A}{\partial x} + V_B D_B \frac{\partial C_B}{\partial x} \tag{5.5}$$

The plane across which there is no net transfer of volume is given by:

$$J = 0 \tag{5.6}$$

In the case where there is no volume change during the mixing process [4,12]:

$$V_A C_A + V_B C_B = 0 \tag{5.7a}$$

and:

$$V_A \frac{\partial C_B}{\partial x} + V_B \frac{\partial C_B}{\partial x} = 0 \tag{5.7b}$$

To comply with Equations 5.5 and 5.7b, under the condition 5.6, and given that V_A and V_B are finite, then [4,12]:

$$D_A = D_B$$

Subsequently, interdiffusion can be described by a single diffusivity, provided that the fluxes, and therefore the diffusivity, are defined relative to the plane of no net volumetric flow, if we consider diffusion into a porous solid as a special case of binary diffusion, where the diffusivity of the solid atoms is zero. In the present case, the fixed coordinates of the porous solid are the frame of reference. Consequently, the interdiffusion coefficient is simply the diffusivity of the mobile species [12].

5.3.3 Relation between the Transport, *D*, the Corrected, D_0, and the Diffusion Coefficients

As was previously stated in Chapter 1, Section 1.11, the driving force of diffusion is the gradient of the chemical potential [18]. The chemical potential can be related to the concentration by considering the equilibrium vapor phase:

$$\mu_A = \mu_A^0 + RT \ln P_A \tag{5.8}$$

in which P_A is the partial pressure of the component A, and μ_A^0 is the chemical potential of the standard state of component A. Mass transport is described by an atomic or molecular mobility, b_A, which is defined by [13]:

$$\bar{v}_A = b_A \bar{F}_A \tag{5.9}$$

where $\bar{v}_A$ is the average drift velocity, and

$$\bar{F}_A = -\nabla \mu_A \tag{5.9a}$$

is the force on particle *A,* in the case where the only driving force is a concentration gradient.

In addition, it is known that [4]:

$$J_A = v_A C_A \tag{5.10}$$

Now, with the help of the previous relations we could get, for one-dimensional diffusion [4,12,13]:

$$J_A = RTb\left(\frac{d\ln P_A}{d\ln C_A}\right)\left(\frac{dC_A}{dx}\right) \tag{5.11}$$

Consequently:

$$D_A = RTb\left(\frac{d\ln P_A}{d\ln C_A}\right) = D_0\left(\frac{d\ln P_A}{d\ln C_A}\right) = D_0\Psi \tag{5.12}$$

in which $D_0 = RTb$. We will now discuss two extreme situations, to be precise, the case of microporous and macroporous materials.

In a microporous adsorbent, there is no clear distinction between molecules on the surface and the molecules in the gas phase, since adsorption in microporous adsorbents is a volume filling process [20]. In this case, D_0 is usually referred to as the corrected diffusion coefficient, and Ψ is called the thermodynamic correction factor, which rectifies for the nonlinearity between the pressure and the concentration of the microporous adsorbent [10]. P_A is the sortive gas pressure, and C_A the concentration of the sorbed phase in the microporous material [10].

However, in the case of macroporous materials, there is an obvious distinction between molecules on the surface and molecules in the gas phase. Consequently, it is possible to consider that adsorption does not affect the diffusion process. Then, if we consider that the gas phase is an ideal gas, we will have:

$$C_A = \frac{n_A}{V} = \frac{P_A}{RT}$$

where n_A is the number of moles of the species A in the volume V at constant temperature T and partial pressure P_A. Hence, it is very easy to show that $\psi = 1$, and:

$$D = RTb = D_0 \tag{5.13}$$

5.3.4 Relation between the Transport, D, the Corrected, D_0, and the Self-Diffusion Coefficients in Zeolites

Experimental studies of diffusion in zeolites have been carried out by different methods [21–33]. The Fickean diffusion coefficients can be measured with the help of steady-state methods [21] and uptake methods [23–32]; on the other hand, the self-diffusion coefficient can be measured directly with the help of microscopic methods [21,33].

The corrected diffusivity is calculated in experimental studies where the transport diffusion is measured [28]. In this case the obtained Fickean diffusion coefficients, *D,* are rectified to obtain the corrected diffusion coefficients, D_0. That is, the Fickean diffusion coefficient, *D,* is calculated with the help of a particular solution of the Fick's second equation. With this parameter, it is possible to obtain, with the help of Equation 5.12, the corrected diffusion coefficient, D_0. After that, since the corrected diffusion coefficient is approximately equal to the self-diffusion coefficient (i.e., $D^* \approx D_0$) [34], then the calculations are carried out with the help of the following equation [35]:

$$D^* = D(1-\theta) \tag{5.14}$$

where $\theta = n_a/N_a$ is the fractional saturation of the adsorbent, in which n_a is the amount adsorbed, and N_a is the maximum amount adsorbed. The calculation of θ could be carried out, for example, with the help of the osmotic adsorption isotherm equation (see Chapter 3, Section 3.2) [28].

5.4 MEAN SQUARE DISPLACEMENT, THE RANDOM WALKER, AND GASEOUS DIFFUSION

5.4.1 The Mean Square Displacement (MSD)

The general solution of the Fick's second equation in one dimension [5] (see also Chapter 1, Section 1.12) is:

$$\frac{\partial C}{\partial t} = D\frac{\partial^2 C(x,t)}{\partial x^2} \tag{5.15}$$

with the following initial and boundary conditions: $C(\times,t) = 0$, $C(-\times, t) = 0$, and $C(x,0) = M\delta(x)$,

$$\left.\frac{\partial C}{\partial x}\right|_{x=-\sigma,t} = 0 \text{ and } \left.\frac{\partial C}{\partial x}\right|_{x=-\sigma,t} \quad [5,6]$$

is:

$$\frac{C(x,t)}{M} = \left(\frac{1}{4\pi Dt}\right)^{1/2} \exp\left(-\frac{x^2}{4Dt}\right) \tag{5.16}$$

Now it is possible to define:

$$P(x,t) = \frac{C(x,t)}{M} \tag{5.17}$$

where [5]:

$$M = \int_{-\infty}^{\infty} C(x,t)dx \tag{5.18}$$

as the probability to find a diffusing particle at the position, *x,* during the time, *t,* if this particle was at $x = 0$ at $t = 0$. Therefore, it is very easy to show that the one-dimensional mean square displacement (MSD) is [19]:

$$\left\langle x^2 \right\rangle = \int x^2 P(x,t)dx = 2Dt \tag{5.19}$$

The equivalent result for isotropic diffusion from a point source in three-dimensional space is:

$$P(\bar{r},t) = \frac{C(\bar{r},t)}{M} = \left(\frac{1}{4\pi Dt}\right)^{3/2} \exp\left(-\frac{\bar{r}^2}{4Dt}\right) \tag{5.20}$$

i.e., $P(\bar{r},t)$ is the probability to find a diffusing particle at the position $\bar{r}$ during the time t if this particle was at $\bar{r} = 0$ at $t = 0$. This magnitude is called the propagator, and it is a Gaussian function [2]. Consequently, it is simple to show that the three-dimensional mean square displacement [19] (MSD) is:

$$\left\langle \bar{r}^2 \right\rangle = \int \bar{r}^2 P(\bar{r},t)dxdydz = 6Dt \tag{5.21}$$

5.4.2 Gaseous Diffusion and the Random Walker

In the simple case when the steps of the one-dimensional random walker are ±l in the x direction [2,4] (see also Chapter 1, Section 1.12), and the time between jumps is τ, the jump frequency is

$$\Gamma = \frac{1}{\tau}$$

(see Chapter 1, Section 1.12). Consequently, if Γ = *constant,* and the direction of the jumps are not correlated, then for N steps, where $N = t/\tau$, the MSD is [2,4]:

$$\left\langle x^2(N) \right\rangle = \left\langle \sum l_i \right\rangle^2 = \sum \left\langle l_i^2 \right\rangle + \sum \left\langle l_i l_j \right\rangle = \sum \left\langle l_i^2 \right\rangle \tag{5.22}$$

since because of randomness there is no correlation [6]:

$$\sum \left\langle l_i l_j \right\rangle = 0.$$

Therefore:

$$\left\langle x^2(N) \right\rangle = Nl^2 = \frac{tl^2}{\tau} \tag{5.23}$$

Hence:

$$\left\langle x^2(N)\right\rangle = 2D^* t \tag{5.24}$$

where

$$D^* = \frac{l^2}{2\tau}$$

is the self-diffusion coefficient, which is generally different from the transport diffusion coefficient (i.e., $D \neq D^*$), because the described processes are physically different, as was previously explained.

During gaseous diffusion, the successive displacement of the diffusing particle between collisions are statistically independent; then, we can denote the z component of the *ith* displacement of the diffusing particle by ξ_i [2]. If the starting point of the diffusion process is $z = 0$, then the z component of the gaseous molecule during the diffusion process is [2]:

$$z = \sum_{i=1}^{N} \xi_i \tag{5.25}$$

By virtue of the random direction of each displacement, the mean of the distances between collisions is: $\langle \xi_i \rangle = 0$, so that the mean displacement is: $\langle z \rangle = 0$. The mean square displacement in the z direction is:

$$\left\langle z^2 \right\rangle = \left\langle \sum_{1}^{N} \xi_i \right\rangle^2 = \sum_{1}^{N} \left\langle \xi_i^2 \right\rangle + \sum_{i} \sum_{j} \left\langle \xi_i \xi_j \right\rangle = \sum_{1}^{N} \left\langle \xi_i^2 \right\rangle \tag{5.26}$$

because of the statistical independence $\langle \xi_i \xi_j \rangle = \langle \xi_j \xi_i \rangle = 0$.

Now: $\langle \xi_i^2 \rangle = \langle \xi^2 \rangle$, where $\langle \xi^2 \rangle$ is the mean square displacement per step, then:

$$\left\langle z^2 \right\rangle = N \left\langle \xi^2 \right\rangle \tag{5.27}$$

Since $\xi = v_z\, t$, then:

$$\left\langle \xi^2 \right\rangle = \left\langle v_z^2 \right\rangle \left\langle t^2 \right\rangle \tag{5.28}$$

Now, in the frame of the collision time approximation, $\tau = \langle t \rangle$, the mean time between collisions or the relaxation time of the molecule is calculated by [2]:

$$\left\langle t \right\rangle = \tau = \int_0^\infty \frac{t \exp(-t/\tau)}{\tau} dt \tag{5.29}$$

Consequently [2]:

$$\left\langle t^2 \right\rangle = \int_0^\infty \frac{t^2 \exp(-t/\tau)}{\tau} dt = 2\tau^2 \tag{5.30}$$

by symmetry [2]:

$$\left\langle v_z^2 \right\rangle = \frac{1}{3}\left\langle v^2 \right\rangle.$$

For this reason

$$\left\langle \xi^2 \right\rangle = \frac{2}{3}\left\langle v^2 \right\rangle \tau^2 \tag{5.31}$$

Now since: $N = \frac{t}{\tau}$, and applying Equation 5.27, we have:

$$\left\langle z^2 \right\rangle = \left(\frac{2}{3}\left\langle v^2 \right\rangle \tau \right) t \tag{5.32}$$

Using the definition of mean square displacement (MSD) for the self-diffusion of a gaseous molecule (i.e., $\langle z^2 \rangle = \int z^2 P(z,t) dz = 2D^* t$), produces an equation for the self-diffusion coefficient for a diffusing gas [2]:

$$D^* = \frac{1}{3}\left\langle v^2 \right\rangle \tau \tag{5.33}$$

5.5 TRANSPORT MECHANISMS IN POROUS MEDIA

As was earlier affirmed, according to the classification scheme proposed by the International Union of Applied Chemistry (IUPAC) pores are divided into three categories on the basis of size: macropores (more than 50 nm), mesopores (from 2 to 50 nm), and micropores (less than 2 nm). This arrangement is based on the difference in the types of forces controlling adsorption performance. In the micropore size, the overlapping surface forces of opposed pore walls are predominant. In the mesopore range, surface forces and capillary forces turn out to be significant, while for the macropores, the contribution of the pore walls is very small.

There are four well-known types of diffusion [10]:

- gaseous or molecular diffusion [2,3]
- Knudsen diffusion [36–39]
- liquid diffusion [10]
- atomic diffusion in solids [4,13]

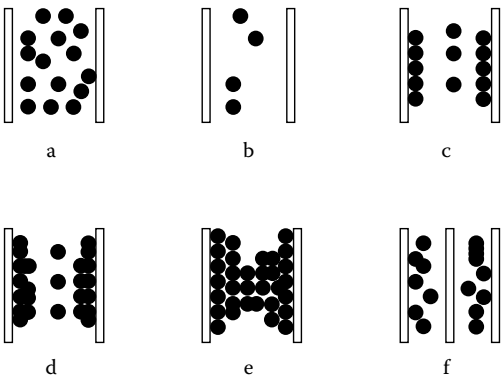

FIGURE 5.3 Transport mechanisms in porous media: (a) molecular or gaseous flow, (b) Knudsen flow, (c) surface diffusion, (d) multilayer diffusion, (e) capillary condensation, and (f) configurational diffusion.

The possible transport mechanisms in porous media are schematically shown in Figure 5.3 [36]. Gaseous flow (Figure 5.3a) takes place when the pore diameter is larger than the mean free path of the fluid molecule. Then, collisions between molecules are more frequent than those between molecules and the pore surfaces [36,40]. As the pore dimension decreases (Figure 5.3b), or the mean free path of the molecule increases, owing to pressure lowering, the flowing species tend to collide more and more with the pore walls than among themselves; then molecules are flowing almost independently from one another according to the Knudsen flow [38,40].

In addition, surface flow (Figure 5.3c) is attained when the diffusing molecules can preferentially be adsorbed on the pore surfaces [21,39,41]. An extension of this mechanism is multilayer diffusion (Figure 5.3d) [42], which could be considered as a transition flow regime between the capillary and surface flows. Now if capillary condensation is attained (Figure 5.3e) [36], if the diffusing component is condensed within the pore, then the flow fills the pore and then evaporates at the other end of the pore [36]. The last mechanism (Figure 5.3f) is configurational diffusion, which is active when pore diameters are small enough to allow only small molecules to diffuse along the pores, while preventing the larger ones from getting into the pores [10,21].

Configurational diffusion is the term coined to describe diffusion in zeolites and related materials and is characterized by very small diffusivities (10^{-12} to 10^{-18} m^2/s) with a strong dependence on the size and the shape of the guest molecules, high activation energies (10 to 100 kJ/mol), and strong concentration dependence [9]. Zeolites and related materials are microporous crystalline solids of special interest in the chemical and the petroleum industries as catalysts and sorbents. For these applications, migration or diffusion of sorbed molecules through the pores and cages within the crystals plays a dominant role.

If the diffusion process takes place at high enough temperatures, as is normally the case in applications, we will have essentially three regimes with different diffusivities according to the pore diameter (see Figure 5.4 [9]). For macropores (i.e.,

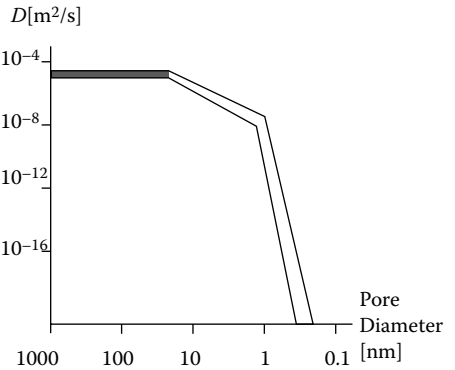

FIGURE 5.4 Relation between diffusivity and pore diameter.

pores with diameters of 50 nm or larger), collisions between the molecules generally occur much more frequently than collisions with the wall, and molecular diffusion is the dominant mechanism. At the same time as the size of the pores decreases, the number of collisions with the wall increases; at this point, Knudsen diffusion takes over, and the mobility starts to depend on the dimensions of the pore. At even smaller pore sizes, in the range of 2 nm or less (i.e., when the pore diameter turns out to be similar to the size of the molecules), the molecules will constantly experience the interaction with the pore surface. Consequently, diffusion in the micropores of a zeolite or related materials, as was previously stated, typically takes place in the configurational diffusion regime [10].

5.6 VISCOUS, KNUDSEN, AND TRANSITION FLOWS

For an ideal gas modeled as rigid spheres, the mean free path of the molecules, λ, can be related to the temperature, T, and pressure, P, via the following equation [2,3,43,44]:

$$\lambda = \frac{kT}{\sqrt{2}\sigma_c^2 P} = \frac{1}{\sqrt{2}\sigma_c^2 C} \tag{5.34}$$

where σ_c is the collision diameter of the molecules, k is the Boltzmann constant, and C is the gas concentration.

To classify the different types of gas-phase flow, the ratio between the mean free path, λ, and the characteristic length of the flow geometry, L, commonly referred to as the Knudsen number, K_n, defined as [39,43,44]:

$$K_n = \frac{\lambda}{L} \tag{5.35}$$

is applied. That is, according to the magnitude of K_n, three main flow regimes can be defined: viscous flow when $K_n << 1$, Knudsen flow for $K_n >> 1$, and transition flow for $K_n \approx 1$ [39].

More precisely, for $K_n < 10^{-2}$, the continuum hypothesis is correct; on the other hand, for $K_n > 10$, the continuum approach fails completely, and the regime can then be described as being a free molecular flow [43,44]. In such situations, the mean free path of the molecules is far greater than the characteristic length scale, and as a result, molecules reflected from a solid surface travel, on average, many lengths scales previous to colliding with other molecules [43,44]. In conclusion, in the large K_n region, continuum models, such as the compressible Navier-Stokes equation do not hold [14,45]. In other words, when λ becomes comparable to L, the linear transport relationship for mass, diffusion, viscosity, and thermal conductivity is no longer valid [45]. For this reason, discrete models are proposed to examine the behavior of the rarefied gas flow [45]. A method to treat the large K_n region is the so-called direct simulation Monte Carlo (DSMC) method, which gives a solution to the Boltzmann equation without any assumptions on the form of the distribution function [46].

Now we will analyze the physical reasons for the transition from the gaseous to the Knudsen flow [2]. To calculate the mean free path, the kinetic theory of gases assumes that molecules collide primarily with other molecules, and not with the walls of the gas container; this hypothesis is valid if C, the gas concentration, is sufficiently large [2]. If the gas is made too dilute, this condition is no longer valid.

If the total collision probability per unit time, $1/\tau_T$, is [2]:

$$\frac{1}{\tau_T} = \frac{1}{\tau} + \frac{1}{\tau_S} \tag{5.36}$$

in which $1/\tau$ is the collision probability per unit time between molecules, and $1/\tau_S$ is the collision probability per unit time between molecules and the container surface, the kinetic theory of gases states that [2,3]:

$$\frac{1}{\tau} = \frac{\langle v \rangle}{\lambda}. \tag{5.37}$$

On the other hand [2]:

$$\frac{1}{\tau_S} = \frac{\langle v \rangle}{L}. \tag{5.38}$$

where L is the smallest dimension of the container, or as was previously affirmed, the characteristic length of the flow geometry. If we define now a resultant mean free path, λ_0, as [2]:

$$\lambda_0 = \langle v \rangle \tau_T \tag{5.39}$$

then, substituting Equations 5.37, 5.38, and 5.39 in Equation 5.36, we will get:

$$\frac{1}{\lambda_0} = \frac{1}{\lambda} + \frac{1}{L} = \sqrt{2}\pi C \sigma_c + \frac{1}{L}.$$

In the expression for the viscosity of an ideal gas [2]:

$$\eta = \frac{1}{3} C \langle v \rangle M \lambda = \frac{M \langle v \rangle}{3(2)^{1/2} \sigma_c} = \frac{M \langle v \rangle}{3\sqrt{2}\sigma_c} \tag{5.40}$$

it is evident that η is independent of C. However, if we use λ_0 instead of λ in Equation 5.40, an approximate description of the role of the collision on the walls will be obtained where, when $C \to 0$, then $\lambda_0 \to L$, and consequently, $\eta \propto C$. This fact means that, for Knudsen gas, the concept of viscosity tends to lose its meaning [2].

5.7 VISCOUS AND KNUDSEN FLOWS IN MODEL POROUS SYSTEMS

5.7.1 Viscous Flow in a Straight Cylindrical Pore

The gaseous self-diffusion coefficient is (see Section 5.4.2) [2,3]:

$$D^* = \frac{1}{3} \langle v^2 \rangle \tau = \frac{1}{3} \langle v \rangle \lambda$$

since $\langle v^2 \rangle = \langle v \rangle^2$, and $\langle v \rangle \tau = \lambda$.

Now since:

$$\langle v \rangle = \left(\frac{8kT}{\pi M} \right)^{1/2}$$

is the mean velocity, where M is the molecular weight of the gas molecule, and:

$$\lambda = \frac{kT}{2^{1/2} \pi \sigma_c^z P} = \frac{1}{2^{1/2} \pi \sigma_c^z C} \to \frac{kT}{\sqrt{2}\pi \sigma_c^z P} = \frac{1}{\sqrt{2}\pi \sigma_c C}$$

is, as well, an expression for the mean free path, then as a result [2,10]:

$$D^* = \frac{2}{3\pi\sigma_c^z} \left(\frac{kT}{P} \right) \left(\frac{kT}{\pi M} \right)^{1/2} = D^* = \frac{2}{3\pi\phi_c^z} \left(\frac{kT}{P} \right) \left(\frac{kT}{\pi M} \right)^{1/2} \tag{5.41}$$

where ϕ_c is the molecular diameter.

If the formerly discussed conditions for viscous diffusion are satisfied for a cylindrical macropore (i.e., a pore of diameter larger than 50 nm), as soon as the pore diameter is large relative to the mean free path, collisions between diffusing molecules will take place considerably more often than collisions between molecules and the pore surface [2,10,43–45]. Under these circumstances, the pore surface effect is negligible, and consequently diffusion will take place by basically the same mechanism as in the bulk gas. Therefore, the pore diffusivity is subsequently equal to the molecular gaseous diffusivity (Equation 5.41).

The previous situation for gaseous flow is always valid for a liquid phase [12]. Consequently, since the diffusion coefficient in liquid phase is [10]:

$$D^* = \left(\frac{8kT}{\pi M}\right)^{1/2} \left(\alpha_T \sigma_m T\right) \tag{5.42}$$

where σ_m is the Lennard-Jones length constant for the diffusing molecule, and α_T is the thermal expansion coefficient, the pore diffusivity is therefore equal to the molecular liquid diffusivity, Equation 5.42.

5.7.2 Knudsen Flow in a Straight Cylindrical Pore

In the Knudsen regime, the rate at which momentum is transferred to the pore walls surpasses the transfer of momentum between diffusing molecules. The rate at which molecules collide with unit area of the pore wall is [2]:

$$\omega = \frac{C\langle v \rangle}{4}.$$

If the average velocity in the flow direction is $\langle v_z \rangle$, then the momentum flux per unit time, to an element of area of the wall in the z direction is (see Figure 5.5) [12]:

$$F_z = \frac{c\langle v \rangle}{4}\left(m\langle v_z \rangle\right)(2\pi r dz).$$

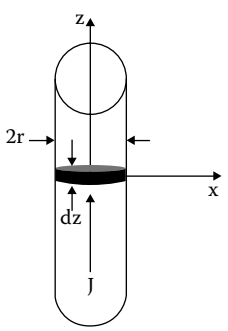

FIGURE 5.5 Knudsen flow in a straight cylindrical pore of diameter $d_P = 2r$.

Now, as this force must be equalized:

$$F_z = -\pi r^2 dP$$

where P is the gas pressure in the element of volume (see Figure 5.5), it is possible to calculate the flux in the pore with the following expression:

$$J = C\langle v_z \rangle = -D_K \frac{\partial C}{\partial z}$$

in which D_K is the Knudsen diffusivity [39]. It is easy to calculate D_K, knowing from the kinetic theory of gases the value of

$$\langle v \rangle = \left(\frac{8kT}{\pi M} \right)^{1/2},$$

and that $P = kCT$ [2,3]. Consequently:

$$D_K^* = \frac{d_P}{2} \left(\frac{\pi kT}{2M} \right)^{1/2} \tag{5.43}$$

where d_P, is the pore diameter. Then if the formerly discussed conditions for Knudsen diffusion are satisfied for a mesopore (i.e., a pore of diameter in the range between 20 and 50 nm), then the diffusion coefficient for the Knudsen flow in a straight cylindrical mesopore is described by Equation 5.43.

5.8 TRANSPORT IN REAL POROUS SYSTEMS: MEMBRANES

5.8.1 Membranes

Membranes have been employed for the treatment of a diversity of fluids including gases, waste water, seawater, milk, yeast suspensions, and other fluids [47–58]. A membrane is a perm-selective barrier between two phases capable of being permeated owing to a driving force, such as pressure, concentration, or electric field gradient [49,50]. From the standpoint of the basic material for their production, membranes are categorized as organic or inorganic. These membranes are classified as porous and microporous, and symmetric and asymmetric [36,48,50]. Porous membranes are those with pores in the microporous (with pore diameters of 0.3 to 2 nm), mesoporous (2 to 50 nm), and macroporous (greater than 50 nm) domain [49].

Porous inorganic membranes are made of alumina, silica, carbon, zeolites, and other materials [48]. They are generally prepared by the slip coating method, ceramic technique, and sol-gel method [49,50]. Inorganic membranes are employed in gas

separation [48–50], catalytic reactors [36,52], gasification of coal [49], water decomposition [49] and other applications [22,53,55,56]. The materials used for inorganic porous membrane synthesis undergo phase transformations, structural changes, and sinterization at high temperature [49,51]. As a result, the maximum temperature at which porous inorganic membranes could be used is 400–1000°C [48].

Macroporous and mesoporous membranes are applied in microfiltration, ultrafiltration [49,50], and as supports for microporous material layer [48], such as a zeolite thin film [53]. Also, macroporous and mesoporous membranes are used as a support for the synthesis of asymmetric membranes with a dense thin film [36,52]. The mechanical strength of self-supported microporous inorganic membranes is normally inadequate [48,53]. As a result, mechanically strong porous substrates are used as supports. The macro- and/or mesopores of the support are covered with films of a micropore material. The support gives mechanical strength, while the zeolite is intended to carry out selective separations [48,53]. Different methods have been used to deposit microporous thin films, including sol-gel, pyrolysis, and deposition techniques in particular [36,48].

The synthesis and characterization of perm-selective membranes is a blossoming activity in materials science [47,52]. Nevertheless, for the commercial utilization of membranes, much work remains to be done [52]. It is necessary to raise the membrane permeance, to resolve the brittleness problems, to be capable to scale up the process, and to increase the membrane area per unit volume [52]. It is also necessary to know and model the process of gas transport through macroporous, mesoporous [10,36,49,50,56,59–62], and microporous [10,12,20,22,28,53,57,63–68] membranes.

5.8.2 Permeation Mechanisms in Porous Membranes

The permeation rate and selectivity of porous membranes depends on their microstructure (i.e., pore size and pore size distribution), tortuosity, permeating molecules and membrane–pore walls interactions, and permeating species mass and size [48–50]. In the course of the transport of gases through porous (macropous, mesoporous, and microporous) membranes, when pressure is the driving force of the process, the gaseous molecules will be transported from the high-pressure to the low-pressure side of the membrane (see Figure 5.6 [58]). For single gases and a linear pressure drop across the porous media, this transport process follows the Darcy law [49,56]:

$$J = B\left(\frac{\Delta P}{l}\right) = \Pi\,\Delta P \tag{5.44a}$$

$$J = \frac{Q}{V_m A} \tag{5.44b}$$

$$\Pi = \frac{B}{l} \tag{5.44c}$$

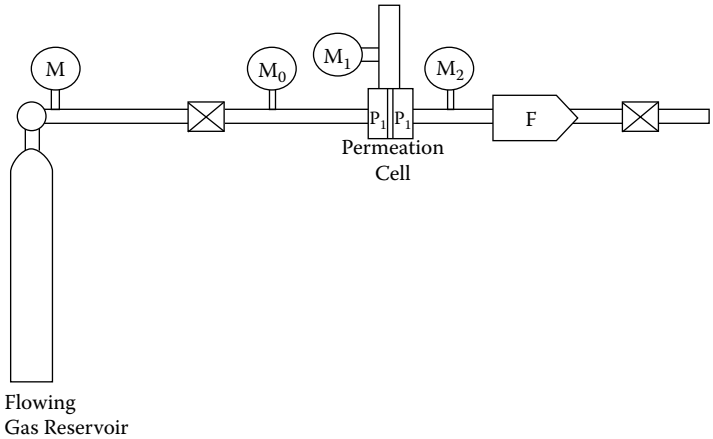

FIGURE 5.6 Schematic diagram of a permeation test facility. The permeation cell is coupled with two pressure transducers (M1 and M2) to measure P1, the reject pressure, and P2, the permeate pressure, and a mass flow meter (F) to measure the flux (J) passing through the membrane.

where A is the effective membrane area, B the permeability [mol/m·s·Pa], J the molar gas flow [mol/m^2 s], l the membrane thickness, $\Delta P = P_1 - P_2$ the transmembrane pressure [Pa], Π the gas permeance [mol/m^2·s·Pa], Q the gas filtrate flux [m^3/s], and V_m the molar volume of the flowing gas [m^3/mol], since for an ideal gas

$$V_m = \frac{V}{n} = \frac{RT}{P}.$$

As already stated, during the transport of gases through porous membranes, various mechanisms can take place, depending on the temperature, pressure, and membrane pore diameters. Gaseous laminar flow can occur in wide pores, Knudsen flow in narrower pores, as well as surface diffusion, multilayer diffusion, and capillary condensation [36,49]. Finally in microporous membranes, configurational diffusion is the transport mechanism [57].

In the case of a gaseous flow in a pore, if a difference between the pressures of the gas at the ends of the pore is present, as is the situation in membrane transport, then a laminar flow is established, if some conditions are fulfilled [12,14,69]. A viscous flow, that is a flow where the effects of viscosity are significant, can be classified as either a laminar flow or a turbulent flow [69]. A laminar flow is one with no significant mixing of neighboring fluid particles, except by molecular motion. In a turbulent flow the quantities that characterize the flow show a random variation with time and space coordinates.

The quantity used to predict the flow regime is the Reynold number (Re), which is a dimensionless parameter defined as [69]:

$$\mathrm{Re} = \frac{vL}{\eta}$$

where L is the characteristic length, for example the pipe diameter, that is the length scale of the flow field, v is the flow velocity, and η is the dynamic viscosity. If Re < 2000, then the flow is laminar [69].

In the case of Knudsen flow in a pore, the number [39,43,44] $K_n = \lambda/L$, where λ is the mean free path, and L is the characteristic length of the flow geometry for $K_n >> 1$, is established as the Knudsen flow [39].

The flow in microporous materials will be explained in the Section 5.9.

5.8.3 Viscous Flow in Membranes

In the simplest case of a flow through a straight cylindrical pore, the form of the Darcy law, based in the Hagen-Poiseuille equation describes the process by means of the following equation [14]:

$$J_v = \left(\frac{r^2}{8\eta V_m}\right)\left(\frac{\Delta P}{l}\right)$$

where r is the pore radius.

The Darcy law for laminar flow in a real macroporous membrane is described by the following equation [56]:

$$J_v = B_v\left(\frac{\Delta P}{l}\right) \tag{5.45a}$$

where:

$$B_v = \frac{k}{\eta V_m} \tag{5.45b}$$

in which k is the permeation factor in [m^2], and η is the dynamic viscosity of the gas in [Pa·s]. For the description of this flow, the Carman-Kozeny equation [49,56] can be employed, because the Hagen-Poiseuille equation is not valid, since inorganic macroporous and mesoporous membranes are normally obtained by the sinterization of packed quasi-spherical particles, then forming a random pore structure. In that case, the Carman-Kozeny equation for the permeability factor for a membrane formulated with pressed spherical particles is [56]:

$$k = \frac{\varepsilon\, d_v^2}{16\, C} \tag{5.46}$$

where:

$$\varepsilon = 1 - \frac{\rho_A}{\rho_R}.$$

Therefore [56]:

$$k \approx \frac{\varepsilon\, d_v^2}{77}$$

in which $C = 4.8 \pm 0.3$ is the Carman-Kozeny constant, d_v is the membrane pore diameter, ε is membrane porosity, ρ_A the apparent membrane density [g/cm^3], and ρ_R the real membrane density [g/cm^3] [58].

The "dusty gas model" (DGM) developed by Mason and collaborators also accounts for the viscous mechanisms in real porous systems [59]. Within the frame of this model, the permeability for the viscous flow is given by the following expression [59,60]:

$$B_v = \frac{\varepsilon d_p^2}{8\tau\eta V_m}$$

where ε is the porosity, τ is the tortuosity, and d_p is the average pore diameter of the porous medium.

Since the viscous diffusion mechanism is also valid for transport process in the liquid phase, then if we have a liquid filtration process through a porous (i.e., macroporous or mesoporous) membrane, the following form of the Carman-Kozeny equation [49]:

$$J_v = \left(\frac{\varepsilon^2 \rho}{K\eta S^2 (1-\varepsilon)^2}\right)\left(\frac{\Delta P}{l}\right)$$

in which ε is the porosity, S the pore area, K a constant, and ρ the molar density, could be applied.

5.8.4 Knudsen Flow in Membranes

As the membrane pore dimensions decrease, or the mean free path of the molecules increases, the permeating particles tend to collide more with the pore walls than among themselves [2,10,39,43,44]. The Knudsen flow regime is then established; in that case, the molar gas flow, J, for the Knudsen flow in a straight cylindrical mesopore of length l and $\Delta P = P_1 - P_2$, transpore pressure is [39]:

$$J_K = D_K\left(\frac{\Delta P/kT}{l}\right).$$

Now Equation 5.43,

$$\left(D_K^* = \frac{d_P}{2}\left(\frac{\pi kT}{2M}\right)^{1/2}\right)$$

expresses the diffusivity of a Knudsen gas in the simple case of a straight cylindrical mesopore [10,39]. For a real mesoporous membrane, which is formed by a complicated pore network, the expression for the permeation flux across the membrane is given by [36]:

$$J_K = \left(\frac{G}{(2MkT)^{1/2}}\right)\left(\frac{\Delta P}{l}\right) \tag{5.47}$$

in which G is a geometrical factor. If M is expressed in molar units, then:

$$J_K = \left(\frac{G}{(2\mathrm{M}RT)^{1/2}}\right)\left(\frac{\Delta P}{l}\right) \tag{5.47a}$$

The geometrical factor, G, could be calculated, with the help of a simple model where it is assumed [12,49] that the diffusivity in a porous material, D, can be linked to the diffusivity (in analogous physical conditions) inside a straight cylindrical pore, D_K, with diameter equal to the mean pore diameter of the pore network, by a simple factor,

$$\left(\frac{\varepsilon_P}{\tau}\right),$$

explicitly:

$$D = \left(\frac{\varepsilon}{\tau}\right)\left(D_K\right) \tag{5.48}$$

where ε is the porosity, which takes into consideration the fact that transport only takes place throughout the pore and not through the solid matrix. The other effects are grouped together into a parameter called the tortuosity factor, τ. Consequently:

$$G = \frac{d_P \varepsilon(\pi)^{1/2}}{2\tau} \tag{5.49}$$

5.8.5 Transition Flow

As soon as the mean free path of the gas molecules is similar to the pore diameter, transfers of momentum between diffusing molecules and between molecules and the pore wall are both significant. In these conditions, transition flow takes places by the mutual effects of both the viscous and Knudsen mechanisms [39]. For single gases and a linear pressure drop across the porous media, the total flux, J_t, can be written as [39]:

$$J_t = J_v + J_K = \left(\frac{kP}{\eta RT}\right)\left(\frac{\Delta P}{l}\right) + \left(\frac{G}{(2\mathrm{M}RT)^{1/2}}\right)\left(\frac{\Delta P}{l}\right) \tag{5.50}$$

where

$$V_m = \frac{V}{n} = \frac{RT}{P}.$$

Subsequently, the expression for the total permeability, B_t, can be obtained from:

$$B_t = \frac{J_t}{\left(\frac{\Delta P}{l}\right)} = aP + b \tag{5.51}$$

As can be seen from Equation 5.51, the relation between B_t and P has a positive intercept, which is related with the Knudsen flow permeability, while the slope is controlled by the gaseous viscous flow. Consequently, the increase of the permeability with pressure is a sign that gaseous viscous flow might be responsible for mass transfer [39].

5.8.6 Surface Flow in the Adsorbed Phase

When the temperature of the gas is lowered to such a degree that adsorption on the pore surface is important, then supplementary flow should be added to the previous laws for gaseous flow [39,70,71]. The mechanism of surface flow is complex; the main mechanisms to explain surface flow include [71] the hopping model, which takes into account that the gas molecules move on the surface by jumping from site to site with a specific velocity. However, the mechanism mainly applied is the random walk model, which uses the two-dimensional form of Fick's law. Finally the hydrodynamic model supposes that the adsorbed gas can be considered as a liquid layer that slides along the surface under the effect of a pressure gradient [39]. For a low surface concentration, the surface flux can generally be [39]:

$$J_s = -D_s\left(\frac{dC_s}{dx}\right) \tag{5.52}$$

in which D_s is the surface diffusivity, which is a function of the surface concentration, C_s. It is usually established that the surface diffusion coefficient, D_s, follows the Arrhenius equation with the activation energy, E_s, for surface diffusion [39]. Since the diffusion process is supposed to take place by hopping from one site to another, the activation energy for diffusion is related to the heat of adsorption; this fact implies that strongly adsorbed molecules are less mobile than weakly adsorbed molecules [39].

In general, it is currently established that the surface flux makes an additional contribution to the gas-phase transport, and that the total permeation is a linear combination of gas and surface permeation [39,71,72]. In the case of very low pressure, where gaseous viscous flow is very small and the adsorption isotherm is

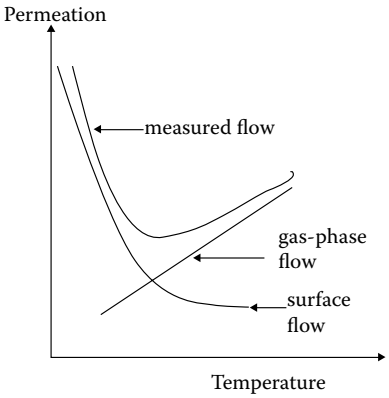

FIGURE 5.7 Graphic representation of the total flow as a function of temperature for the mix of gas and surface flow.

linear, then the total flux is the sum of the Knudsen flux and the surface diffusion flux [39].

$$J_{Ks} = J_K + J_s = \left(\frac{G}{(2\mathrm{M}RT)^{1/2}} \right) \left(\frac{\Delta P}{l} \right) + D_s K \frac{\Delta P}{l} \tag{5.53}$$

The permeability for this combined Knudsen and surface diffusions is [39]:

$$B_{Ks} = \frac{J_{Ks}}{\left(\frac{\Delta P}{l} \right)} = \left(\frac{G}{(2\mathrm{M}RT)^{1/2}} \right) + D_s K \tag{5.54}$$

Figure 5.7 [72] shows a schematic representation of the total permeation as a function of temperature for the combination of gas phase and surface flows, where it can be seen that the reduction of the surface diffusivity with temperature is more rapid than that of Knudsen diffusion [72]. This is because the heat of adsorption is bigger than the activation energy for surface diffusion; consequently, if surface diffusion is to be removed, experiments are usually carried out at high temperatures [39].

5.8.7 Experimental Permeation Study of Zeolite-Based Porous Ceramic Membranes

Porous zeolite-based membranes were synthesized using a ceramic methodology. These membranes were produced by a thermal transformation of natural clinoptilolite at 700 and 800°C [58]. In order to carry out a permeation test of these membranes, the permeability [B] and permeance [P] of H_2 were measured using the Darcy law correlation [58].

As was previously reported, gas transport mechanisms in macroporous, mesoporous, and microporous membranes are laminar gas flow, Knudsen flow, surface diffusion, multilayer diffusion, capillary condensation, and configurational diffusion. In the present permeation study, we will consider that configurational diffusion is not possible, because during the zeolite thermal treatment to obtain the ceramic membrane, the clinoptilolite framework collapsed [58]. Furthermore, since the particles used for the sintering process to produce the tested membranes are 220 and 500 μm, then it was shown that only macropores were present in these membranes [58]. In addition, since adsorption and capillary condensation in the surface of the membrane will be very weak, due to the relatively high temperature (300 K) and the somewhat low pressures (0.2–1.4 MPa) [58], it was also possible to exclude surface diffusion, multilayer diffusion, and capillary condensation. Consequently, in the present permeation test only Knudsen or gaseous flow could occur.

Figure 5.8 and Figure 5.9 show the results of two experiments of H_2 permeation in membranes obtained using two particle diameters (220 and 500 μm). The permeation cell used to make the permeation study is shown in Figure 5.10 [58]. In addition,

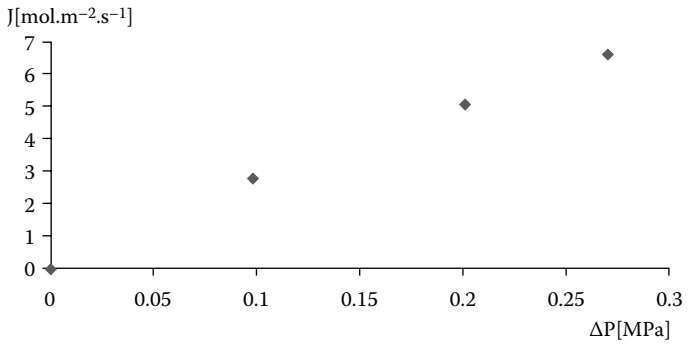

FIGURE 5.8 Permeation study of H_2 in a membrane produced by a thermal treatment at 800°C during 1 hour of a clinoptilolite powder of 500 μm of particle diameter.

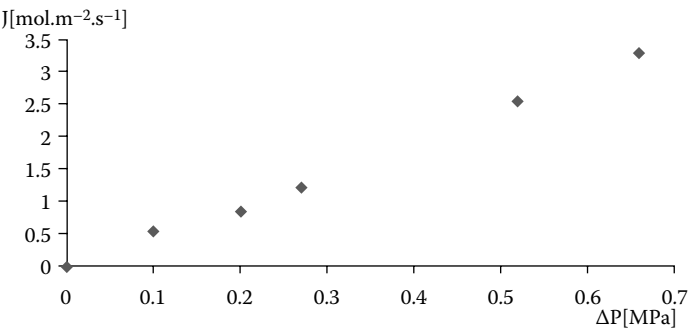

FIGURE 5.9 Permeation study of H_2 in a membrane produced by a thermal treatment at 800°C during 1 hour of a clinoptilolite powder of 220 mm of particle diameter.

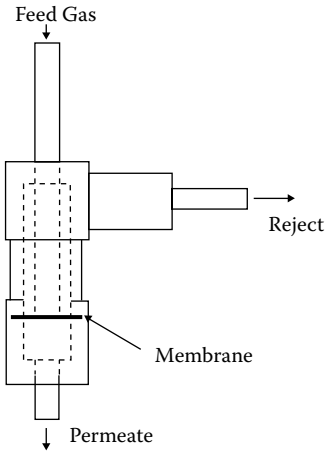

FIGURE 5.10 Permeation cell.

TABLE 5.1
Hydrogen Permeability [B] and Permeance [P] in the Studied Membranes

Sample d_p [μm]	Sample Treatment Temp. [°C]	Sample Treatment Time [h]	$B \times 10^8$ $\left[\frac{mol}{m^1 s\ Pa}\right]$	$\Pi \times 10^6$ $\left[\frac{mol}{m^2 s\ Pa}\right]$
220	700	2	1.1	4.1
500	700	2	4.9	18.1
220	800	1	1.4	5.2
500	800	1	6.8	25.1

the measured permeability [B] and permeance [P] of the two samples under study at two different temperatures are reported in Table 5.1. The permeability [B] and permeance [P] were calculated with the help of the Darcy law, Equation 5.44a [58].

In Table 5.2, the estimated [58] pore diameters of the membranes are reported. The mean free path of H_2 at the temperatures and pressures of the permeation experiment is reported in Table 5.3. These results indicate that Knudsen flow was not possible, since $d_v >> \lambda$, where d_v is the pore diameter. As a result, the determining process in the present case is gaseous laminar flow through the membrane pores [58]. It is therefore feasible to apply the Darcy law for gaseous laminar flow [56], Equations 5.45a and 5.45b.

In addition, for the description of this flow it is necessary to employ the Carman–Kozeny relation, Equation 5.46, since the Hagen-Poiseuille equation is not suitable, because the membranes were obtained by the sinterization of packed quasi-spherical particles [58].

TABLE 5.2
Estimated Membrane Pore Diameters, d_v

Sample d_P [μm]	Sample Treatment Temp. [°C]	Sample Treatment Time [h]	d_v [μm]
220	700	2	35
500	700	2	79
220	800	1	36
500	800	1	82

TABLE 5.3
Mean Free Path (λ) of Hydrogen at T = 300 K and Different Pressures

Pressure [MPa]	λ [nm]
0.2	55.4
0.4	27.7
0.6	18.4
0.8	13.9
1.0	11.1

TABLE 5.4
Hydrogen Permeation [k] and Membrane Average Pore Diameter [dv]

Sample d_P [μm]	Sample Treatment Temp. [°C]	Sample Treatment Time [h]	$k \times 10^{12}$ [m^2]	d_v [μm]
220	700	2	4.41	32
500	700	2	12.7	69
220	800	1	5.5	38
500	800	1	27.0	83

Equations 5.45a, 5.45b, and 5.46 were used to measure the membrane pore diameter (d_v) (see Table 5.4). The results coincided fairly well with the values previously estimated (see Table 5.2) [58].

5.9 DIFFUSION IN MICROPOROUS MATERIALS: ZEOLITES AND RELATED MATERIALS

Zeolites and related materials are inorganic, microporous, crystalline solids widely used in the chemical and the petroleum industries as catalysts, sorbents, and ion

exchangers [73,74]. For these applications, migration or diffusion of sorbed molecules and exchanged cations through the pores and cages within the crystals plays a dominant role [7,9,10,12,21,23–35,63–68,75–78]. The crystal lattice of the zeolites and related materials is formed by four connected tridimensional frameworks of T atoms bridged by oxygen atoms (where T is aluminum, silicon, phosphorus, or a similar atom in the TO_4 tetrahedron) [79–82]. These structural elements form a framework with cavities and channels of molecular dimensions [82]. These frameworks, in the majority of cases, are negatively charged [81]. For charge compensation of the negative charge arising in these frameworks, cations are located at different sites in the cavities and channels of the zeolite [81]. These properties make zeolites attractive materials for many new industrial processes [73–75,83]. However, our capability to select and adapt zeolites for particular processes is restricted by a deficient knowledge of the molecular-level interactions and their effect on macroscopic phenomena [75].

In a lot of processes using zeolites, the rate of diffusion of adsorbed molecules inside the zeolite pore system plays an important, sometimes critical, role in determining the overall observed performance of the whole process [73,83]. However, diffusion in zeolites is inadequately understood, owing to the sensitivity of zeolite diffusivities to the dimensions of the diffusing molecules and zeolite pores and cavities, as well as energetic interactions, such as those between adsorbates and the zeolitic framework, and charge-compensating cations [75]. In particular, multicomponent diffusion has not received the necessary consideration in comparison to single-component diffusion, even though it is, certainly, such multicomponent behavior that is of importance in the practical applications of zeolites and related materials [26,27,30,75].

5.9.1 Model Description of Molecular Diffusion in Zeolites and Related Materials

In the case of microporous materials, specifically zeolites, configurational diffusion is the term coined to describe molecular transport [10]. This diffusion regime is characterized by very small diffusivities (10^{-12} to 10^{-18} m^2/s), a strong dependence on the size and shape of guest molecules, high activation energies (10–100 kJ/mol), and a strong concentration dependence [9,10,28]. The strong interactions between the adsorbed species and the zeolite lattice give rise to configurational diffusion [75].

Mass transport in microporous media takes place in an adsorbed phase. When a molecule diffuses inside a zeolite channel, it becomes attracted to and repelled by different interactions, such as the dispersion energy, repulsion energy, polarization energy, field dipole energy, field gradient quadrupole, sorbate–sorbate interactions, and the acid–base interaction with the active site if the zeolite contains hydroxyl bridge groups [20,84]. Consequently this transport can be pictured as an activated molecular hopping between fixed sites [10,28,85–87]. Therefore, during the transport of gases through zeolites, both diffusion between localized adsorption sites and the activated gas translation diffusion will contribute to the overall process [10,28,85–87].

Subsequently, it is possible to consider that the adsorbate–adsorbent interaction field inside these structures is characterized by the presence of sites of minimum

potential energy for the interaction of adsorbed molecules with the zeolite framework and charge compensating cations. A simple model of the zeolite–adsorbate system is that of the periodic array of interconnected adsorption sites, where molecular migration at adsorbed molecules through the array is assumed to proceed by thermally activated jumps from one site to an adjacent site and can be envisaged as a sort of lattice-gas.

In order to describe the adsorption and diffusion in the zeolites in the frame of a modified lattice-gas, which takes into account the crystalline structure of the zeolite, the interaction between adsorbed molecules, and the possibility of a transition of adsorbed molecules between different adsorption sites in the same unit cell and between different unit cells, the following model description of molecular diffusion in zeolites was previously proposed [28,88].

In the frame of the present model description of diffusion, the zeolite is considered to be a three-dimensional array of N identical cells, i, centered at R_i, each containing N_O identical sites localized at $R_{i\alpha} = R_i + U_\alpha$, where the potential energy is a minimum (see Figure 5.11 [88]). If a molecule is localized at $R_{i\alpha}$, its energy would be $-\varepsilon$, and the interaction energy between molecules localized at different sites (i.e., at $R_{i\alpha}$ and $R_{i\beta}$) is $-U_{\alpha\beta}$ (see Figure 5.10 [88]). The motion of molecules between sites (i.e., the jumping of molecules inside a cell) is considered, and the motion between cells, through zeolite channels and cavities is also taken into account [28,88]. The solution of the motion equation for a molecule in the present system leads to the energy which consists of an $N(N_0–1)$-fold degenerate state, E_2, where molecules are adsorbed in a site, and N delocalized states, E_1, where the molecule moves through the zeolite, jumping from site to site through the zeolite channels and cavities [88]. Between adsorption and delocalized states (i.e., diffusion states), there exists an energy gap [28,88]. For low coverage of the adsorption space (i.e., at low pressures in the Henry's law region of adsorption), $E_g = E_1 - E_2$, which means that diffusion is an activated process in the frame of the present model [28,88].

The delocalized state can be considered to be a transition state, and transition state theory [89], a well-known methodology for the calculation of the kinetics of events [12,28,90–92], can be applied. In the present model description of diffusion in a zeolite, the transition state methodology is applied for the calculation of the self-diffusion coefficient of molecules in zeolites with linear channels and different dimensionalities of the channel system [28].

The transition state defined by the delocalized state of movement of molecules adsorbed in zeolites was established during the solution of the equation of motion of molecules whose adsorption is described by a model Hamiltonian, which describes the zeolite as a three-dimensional array of N identical cells, each containing N_O identical sites, as already described [88]. This result is very interesting, since adsorption and diffusion states are found in zeolites.

Consider an arrangement of adsorption sites in a linear channel in which each site is an energy minimum with respect to the neighboring space [28]. The number of adsorbed molecules is supposed to be small relative to the number of sites, so that each molecule could be considered to be an independent subsystem with enough free sites for jumping [28]. The canonical partition function for a molecule considered

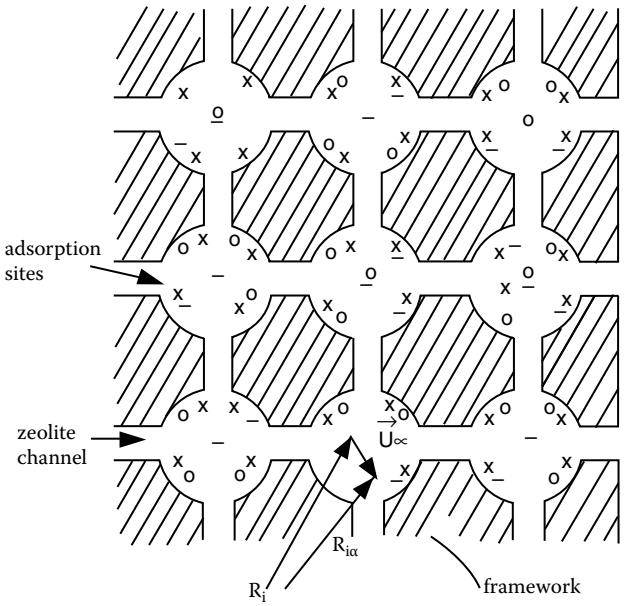

FIGURE 5.11 Schematic representation of the zeolite, or related material.

to be an independent subsystem in one of the adsorption sites with energy E_2 is (see Chapter 1, Sections, 1.5, 1.8, and 1.9) [91,92]:

$$Z_a = Z_x^a Z_y^a Z_z^a Z_i^a \exp\left(-\frac{E_2}{RT}\right) \tag{5.55}$$

where Z_x^a, Z_y^a, and Z_z^a represent the canonical partition functions for the movement in the directions *x, y,* and *z* of the adsorbed molecule, and Z_i^a represents the partition function for the internal degrees of freedom of the molecule, and E_2 is the energy of the adsorption state.

We will now deal with the translation of the molecule in the *z* direction, through the transition state, that is, through the delocalized state of movement. The partition function for a molecule in the transition state becomes [12]:

$$Z^* = Z_x^* Z_y^* \left(\frac{2\pi MRT}{h^2}\right)^{1/2} \Delta z Z_i^* \exp\left(-\frac{E_1}{RT}\right) \tag{5.56}$$

in which Z_x^* and Z_y^* are the partition functions for the movement in the directions *x* and *y* of the molecule in the transition state, Δz is the distance of movement in the transition state, in which $\Delta z = l$, where *l* is the jump distance. In addition, *M* is the molecular weight, *R* is the gas constant, *h* is Planck's constant, and *T* is the absolute temperature.

If we suppose now, as is the case in classical transition state theory, that the molecules in the ground (adsorbed) state and transition states (delocalized movement state) are in equilibrium, it is easily shown that the equilibrium constant for this equilibrium process is [12,93]:

$$K = \frac{N^*}{N_a} = \frac{L^*}{L}\exp\left(-\frac{E_g}{RT}\right)\left(\frac{2\pi MRT}{h^2}\right)^{1/2}\frac{\Delta z}{Z_z^a} \tag{5.57}$$

If

$$\left(\frac{Z_x^* Z_y^*}{Z_x^a Z_y^a}\right)\left(\frac{Z_i^*}{Z_i^a}\right) \approx 1,$$

Equation 5.57 is a good approximation, and N^* is the number of molecules in the transition state, N_a is the number of adsorbed molecules, L^* is the maximum number of transition states, L is the maximum number of adsorption sites, and Z_z^a is the partition function for the motion of the molecule in the z direction in the adsorption state [12,28].

The average velocity of translation of the molecule through the transition state is [89]:

$$\langle v_z \rangle = \left(\frac{2RT}{\pi M}\right)^{1/2}.$$

Consequently, the time of residence of the molecule in the transition state [28] is:

$$\mathrm{T} = \left(\frac{\langle v_z \rangle}{\Delta z}\right) = \frac{\langle v_z \rangle}{l}.$$

Now it is possible to state that the number of molecules passing through the transition state per unit time is [28]:

$$\vartheta = \left(\frac{dN^*}{dt}\right) = \frac{N^*}{\mathrm{T}} \tag{5.58}$$

In addition, the jump frequency of the molecules through the transition state is [28]:

$$\Gamma = \frac{\vartheta}{N_a} \tag{5.59}$$

Considering now dynamic equilibrium between the adsorbed state and the diffusion state [12], Γ, the jump frequency of molecules between sites is [12]:

$$\Gamma = \frac{L^*}{L}\left(\frac{2RT}{h}\right)\exp\left(-\frac{E_g}{RT}\right)\frac{1}{Z_z^a} \tag{5.60}$$

where $L^*/L = 1$, 2, or 3, depending on the dimensionality of the channel system [12]. Now the self-diffusion coefficient for a molecule in a zeolite is [4]:

$$D^* = \left(\frac{l^2}{2k\tau}\right) \tag{5.61}$$

in which 1 is the jump distance, $k = 1$, 2, or 3 is the dimensionality, and

$$\tau = \frac{1}{\Gamma}$$

is the time between jumps [4,13].

We must now take into account two extreme situations; the first one is where the adsorption in the site is very strong, that is, localized adsorption, and the partition function for the movement in the z direction in the adsorption site is a vibrational partition function for a molecule in a potential energy well [94]:

$$Z_z^a = \left(\frac{kT}{h\upsilon}\right)^{1/2} \tag{5.62}$$

where υ is the vibration frequency, and k is the Boltzmann constant. The second situation is where the adsorption is delocalized; specifically, the molecule could move in the neighborhood of the site, and the partition function for the movement in the z direction in the adsorption site is the translational partition function [93,95]:

$$Z_z^a = \left(\frac{2\pi MRT}{h^2}\right)l \tag{5.63}$$

We can obtain a diffusion coefficient for the case of localized adsorption on the sites by introducing in Equation 5.61 the expression for τ, described in Equation 5.60, and using, for Z_z^a, the vibrational partition function, Equation 5.62 [28].

$$D_i^* = \nu l^2 \exp\left(-\frac{E_g}{RT}\right) \tag{5.64}$$

The diffusion coefficients for mobile adsorption can also be calculated by introducing, in Equation 5.61, the expression for τ described in Equation 5.60 and using, for Z_z^a, the translational partition function, Equation 5.63 [28]:

$$D_i^* = \frac{1}{2}\left(\frac{RT}{\pi M}\right)^{1/2} l \exp\left(-\frac{E_g}{RT}\right) \tag{5.65}$$

Equations formally similar to Equations 5.64 and 5.65 for the self-diffusion coefficients were calculated using different approaches, and they result in [10]:

$$D^* = gul \exp\left(-\frac{E}{RT}\right) \tag{5.66}$$

in which

$$g = \frac{1}{z},$$

where z is the coordination number, u is the velocity at which the molecule travels, where $u = \upsilon\, l$, for localized adsorption, and

$$u = \left(\frac{8RT}{\pi M}\right)^{1/2}$$

for mobile adsorption. Finally, l is the jump distance or diffusional length [10].

5.9.2 Anomalous Diffusion

In the case where the geometry of the channels, which enclose the diffusing molecules, is such that the individual molecules are unable to pass each other, single-file diffusion (SFD) occurs, a process which leads to an elevated extent of mutual interaction of the diffusing molecules. SFD provokes important departure from the prototype of what is called normal diffusion, which is described by the Fick's laws, or by the Einstein relation [12,15,29,30,65–68,96–112]. This non-Fickean, or anomalous behavior could be justified as a result of constraints imposed by the system which force the molecules to move in a highly correlated manner. This is, potentially, the case for the diffusion of molecules with diameters comparable to the channel width of molecular sieves with structures consisting of one-dimensional channel networks. Some examples of these structures are: $AlPO_4$-5, $AlPO_4$-8, $AlPO_4$-11, SSZ-24, Omega, ZSM-12, ZSM-22, ZSM-23, ZSM-48, VPI-8, and MCM-41 [30].

The proportionality between the observation time, t, and the mean square displacement (MSD), $\langle x^2 \rangle$, existing in the Einstein equation, $\langle x^2 \rangle = 2D^*t$, where D^* is the self-diffusivity, is a consequence of the essential assumption of normal diffusion. To be precise, it is a result of assuming that it is feasible to divide the total observation time into identical time intervals, so that the probability distribution of molecular displacement is equal for each of these time intervals, and additionally, the displacement probability is independent of previous displacements [15]. Consequently, the random walk of each individual particle may be taken into account as a Markovian process, specifically, a process whose further progress is solely determined by the specified state, and not by the former, or past [15].

On the other hand, if the conditions for anomalous diffusion are operating in the diffusion system, successive displacements are correlated, and as an immediate consequence, the MSD cannot be expected to increase in proportion to time, t [65,101]. Then in the case of SFD, this correlation leads to an enlarged probability for subsequent displacements to be directed reverse to each other [15]. Meticulous study shows that under the conditions of SFD in the long-time limit, the MSD increases with the square root of the observation time (i.e., $\langle x^2 \rangle = 2Ft^{1/2}$), where F denotes the single-file mobility [65,101,107], with a probability distribution given by a Gaussian function, in complete analogy to the case of normal diffusion [65,101,107,108]. Consequently, for SFD the mean square displacement (i.e., $\langle x^2 \rangle$), for large time of observation is proportional to, $t^{1/2}$, if the condition that molecules must be always in the same order during the transport process is satisfied; that is, if the mutual passage of random walkers is excluded [65,101]. This tendency may be comprehended by rationalizing that, as a result of SFD, molecular displacement in one direction will more probably lead to an increased concentration of particles ahead of it than at the back of it [15].

SFD should be the rate-controlling mechanism in a large variety of processes [97]. In this sense, diffusion studies with zeolitic systems, which were supposed to ensure the circumstances of SFD, have been carried out by pulsed-field gradient–nuclear magnetic resonance (PFG-NMR) [97], quasi-elastic neutron scattering (QENS) [110], the tracer zero-length-column (T-ZLC) technique [111], and the frequency response method [112]. Nevertheless, there is a need for more experimental results to provide evidence about this phenomenon. For example, for methane in $AlPO_4$-5, single-file behavior was claimed to be experimentally observed by PFG-NMR [97]. However this was contradicted by other findings, which claim ordinary diffusion behavior for this system [29,109,110]. Additionally, the self-diffusion transport of propane in $AlPO_4$-5 was studied with the help of the tracer ZLC method, and was established as a fast one-dimensional Fickean diffusion, with no evidence of single-file behavior, in contrast with the PFG-NMR results [111].

In summary, the results obtained in the investigations described are in part contradictory and far from complete. This fact mainly originates in both the diverging temporal and spatial ranges of observation of these techniques and the deviations of the systems under study from ideal structures [15,29].

If the zeolite channel network contains communicated cages and/or interconnected channels, as is the case, for example, for the MFI, MEL, LTA, and FAU framework types [82], where molecules could exchange places during the transport process [65,101], then the merge of molecules during diffusion is produced [29,30]. Since this is the prerequisite that leads to an MSD proportional to time, in this instance the transport process is not of the SFD type, since statistically the molecules have time enough to be exchanged during the transport process; therefore, in this case ordinary diffusion is the transport mechanism [30].

On the other hand, if the zeolite channel network contains noninterconnected channels, as is the case, for example, for the AFI, AET, AEL, MAZ, MTN, TON, and MTT framework types [82], where molecules, in general, could not exchange places during the transport process [65,101], the merge of molecules during diffusion and counter-diffusion is not produced [29,30]. As a result, since this is the prerequisite

that leads to a SFD type of diffusion, we should experimentally observe this regime. However, since the crystals of these materials are finite, then statistically the molecules have time enough to be exchanged during the transport process. Consequently, in this instance, ordinary diffusion is the observed transport mechanism [30]. In conclusion, single-file diffusion should be a rare effect in molecular transport in zeolites and related materials.

To recapitulate about normal and anomalous diffusion, it is possible to assert that in a variety of physical systems the simple scaling (i.e., $\langle x^2 \rangle \propto t$) corresponding to Fickian diffusion is violated [113,114]; then the MSD will grow as $\langle x^2 \rangle \propto t^{\alpha}$, where the coefficient $\alpha \neq 1$ [115]. A consistent generalization of the diffusion equation could still be second order in the spatial coordinates and have a fractional order temporal derivative, for example [115]:

$$\frac{\partial^{\alpha} P(\bar{r},t)}{\partial t^{\alpha}} = \kappa_{\alpha} \nabla^2 P(\bar{r},t) \tag{5.67}$$

where $P(\bar{r},t)$ is the probability of finding the diffusing particle in the point $(\bar{r},t)$ where the particle concentration is $C(\bar{r},t)$, and $P(r,t) \propto C(x,t)$; thus the diffusion equations holds when probabilities are substituted for concentrations. Then anomalous transport phenomena could have sub-diffusion if $\alpha < 1$, and super-diffusion if $\alpha > 1$ [115].

The time derivative of Equation 5.67 is a fractional derivative, which is properly defined in a branch of mathematics called fractional calculus [116,117]. A fractional integral, of order α, in the variable x, is defined as [115–117]:

$${}_a D_x^{-\alpha} = \frac{1}{\Gamma(\alpha)} \int_0^x (x-y)^{\alpha-1} f(y) dy \quad \text{valid for } x > a$$

where $\Gamma(\alpha)$ is the gamma function. The fractional derivative is defined then by [115–117]:

$${}_a D_x^{\alpha} = \frac{d^n}{dx^n} \left({}_a D_x^{\alpha-n} \right).$$

In another notation:

$${}_0 D_x^{-\alpha} \left(f(x) \right) = \frac{d^{-\alpha}}{dx^{-\alpha}} \left(f(x) \right) \quad \text{valid for } x > 0$$

and:

$${}_0 D_x^{\alpha} \left(f(x) \right) = \frac{d^{\alpha}}{dx^{\alpha}} \left(f(x) \right).$$

Equation 5.67 handles boundary problems in the same way as its normal counterpart does [115]. Consequently it is a valuable tool for solving diffusion in some complex systems.

In a previous work the author, following a Gaussian probability distribution, treated single-file diffusion analytically on the basis of Fick's relations of normal diffusion by merely considering its dependence on the square root of the time instead of time itself [30]:

$$\frac{\partial C(x,t)}{\partial t^{1/2}} = F\frac{\partial^2 C(x,t)}{\partial x^2} \tag{5.68}$$

where F is the SFD mobility [65]. Equation 5.68 is within the spirit of Equation 5.67. However, it was affirmed [15] that Equation 5.68 is only valid for an infinitely extended single-file system, and as soon as this condition of infinite extension has to be abandoned, and boundary conditions are imposed, this analogy leads to erroneous conclusions [15]. Nevertheless, if Equation 5.67 is a consistent generalization of the diffusion equation, as was previously firmly acknowledged [115], then it is an expression of the existence of real physical systems which exhibit anomalous diffusion. Subsequently, these systems should be finite systems, in order to be real systems, and consequently, as was previously stated, boundary conditions could be imposed to Equation 5.67, and then also to Equation 5.68.

As was previously discussed, SFD in zeolites should be a rare effect, since the zeolite crystals are very small in general, and the conditions for the establishment of the SFD regime are not fulfilled in actual systems. However for a large enough crystal, possibly the temporal, and spatial conditions for SFD could be satisfied. If this is the case, an equation similar to 5.67 and 5.68 with proper boundary conditions should describe the system.

5.9.3 Experimental Methods for the Study of Diffusion in Zeolites

As was previously commented, the experimental studies of diffusion in zeolites have been carried out by different methods [9,12,21,26–28,97,110–112]. For instance, the Fickean diffusion coefficients can be measured with the help of steady-state methods such as membrane permeation (MP), and also by uptake methods [9,12,21], such as the zero-length column (ZLC) method [23], the frequency response (FR) [24,25,112], and the Fourier transform infrared (FTIR) method of measuring the kinetics of sorption [26–32]. On the other hand, the self-diffusion coefficient can be measured directly with the help of pulsed field gradient nuclear magnetic resonance (PFG-NMR) method, or with quasi-elastic neutron scattering (QENS) [12,21,33,97,110].

The MP, ZLC, FR, PFG-NMR, and QENS methods are well explained in literature [9,12,21,33], and will not be explained here. The FTIR method is not always broadly discussed in textbooks. Consequently, we will discuss the measurement of the Fickean diffusion coefficient with the FTIR method developed by Karge and Niessen [26,27].

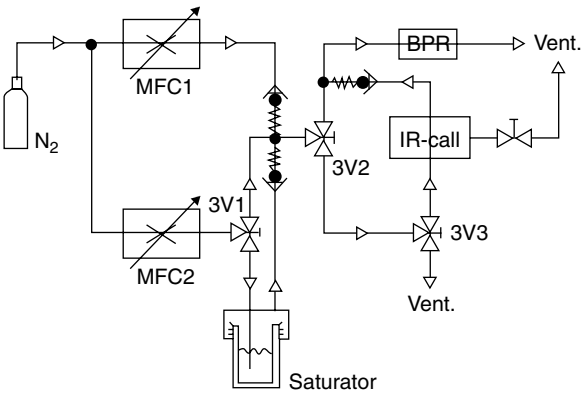

FIGURE 5.12 Schematic representation of an experimental facility to perform measurements of the Fickean diffusion coefficient by the FTIR method.

An experimental facility to carry out measurements of the Fickean diffusion coefficient by the FTIR method (see Figure 5.12 [28,30]) is, in general, composed of the IR cell connected through stainless steel pipes to a manifold containing the thermostated saturator. The system has two gas inlets, for the carrier gas (helium [26,27] or nitrogen [28–32], with grade of purity of 99.99%). Through inlet 1, the carrier gas bubbles through the saturator in which the adsorbate is located. The carrier gas coming from inlet 2, which is saturated with the corresponding hydrocarbon, is mixed with a measured flow of pure carrier gas coming from inlet 1. Sensitive mass flow controllers must be used for both inlets. The simultaneous variations of both flow controls enable us to vary the relative partial pressure of the hydrocarbon in the range: $0.01 < P/P_0 < 0.9$.

Recapitulating, the measurements were carried out as follows: the compound to be tested was filled in the stainless steel saturator, which was held thermostatically at 25°C. A flow of the gas carrier was divided in two, and each of these streams was passed through a flow controller [28,118]. One stream went through a tube with a sinterplate in the base into the saturator where the carrier gas bubbles in the liquid adsorbate. This gas flow (i.e., the stream that has passed through the saturator, and became saturated with the substance in test) was then mixed with the bypass stream of pure carrier gas at the outlet of the saturator, and the unified stream was then passed through the IR-cell [118].

The measurement process is normally carried out by monitoring the change in the intensity, specifically the absorbance, of a band of the sorbate molecule in a FTIR spectrometer, obtaining spectra consisting of 1 scan per spectrum, and for example, 0.85 seconds per scan, without delay between scans, analyzing the proper range for the tested adsorbate. For example [28], from 1450 to 1550 cm^{-1}, and using the band around 1482 cm^{-1} for benzene and the range from 1477 to 1517 cm^{-1}, and the band around 1497 cm^{-1} for both toluene and ethylbenzene. The range from 1550 to 1650 cm^{-1} and the band around 1613 cm^{-1} for m-xylene and the double peak with

bands at 1467 and 1497 cm^{-1} and the range from 1420 to 1520 cm^{-1} for o-xylene were used [28].

The key equipment in the testing facility is the water-cooled IR high-temperature cell (see Figure 5.11 [28,30]). In these cells demountable parts are normally fitted with Viton O-rings to minimize leaking. The temperature of the sample holder is controlled electronically with very low variation of temperature, normally $\Delta T < 1°C$ [28–32]. Self-supported wafers obtained by pressing 7–9 mg/cm^2 of the zeolite sample powder at 400 MPa are placed in the sample holder and introduced in the cell. These wafers fulfill the condition of the absence of macroporous limitations for the transport of the diffusing molecules during the sorption process, enabling measurement of intracrystalline diffusion [26–28].

Prior to the measurement of the diffusion coefficient, the samples must be carefully degassed at 450°C during 2 h in a flow of the pure carrier gas. After degassing, the sample is cooled to the desired temperature and kept at this temperature with the help of the temperature control. The flow rate is then adjusted to get the desired relative partial pressure. A background spectrum of the pure degassed zeolite is obtained as a reference, and then the flow coming from the saturator after mixing with the flow of pure carrier gas is admitted at a precisely defined pressure to the IR cell. The collection of the set of IR spectra is started at the same moment of the admittance of the diffusing molecule, and the spectra are stored as the difference spectra obtained by subtracting from each measurement [26–32].

The Fickean diffusion coefficient could be evaluated using a solution of Fick's second law for a geometry appropriate for the experimental setup [26–32]. For spherical geometry, which is the case if the zeolite crystals that form the wafer are approximately spherical, (Figure 5.13a), with variable surface concentration and initial concentration inside the sphere equal to zero, the solution of Fick's second law is [5]:

$$\frac{M_t}{M_\infty} = 1 - 3\frac{D}{\beta a^2}\exp(-\beta t)\left\{1 - \left(\frac{\beta a^2}{D}\right)^{1/2}\cot\left(\frac{\beta a^2}{D}\right)^{1/2}\right\} + \left(\frac{6\beta a^2}{D\pi^2}\right)\sum_1^\infty\left(\frac{\exp\left(\frac{-Dn^2\pi^2 t}{a^2}\right)}{n^2\left(n^2\pi^2 - \left(\frac{\beta a^2}{D}\right)\right)}\right) \tag{5.69}$$

where M_t, which is proportional to the absorbance A (where A is reported in arbitrary units [a.u.] (i.e., $M_t \sim A^T_t$), is the amount of sorbate taken at time t, and M_∞, also proportional to the absorbance, A (i.e., $M_\infty \sim \boldsymbol{A}^{\boldsymbol{T}}_\infty$), is the equilibrium sorption value, and D is the Fickean diffusion coefficient in the case of single-component diffusion [26–28]. In addition, $r = a$ is the radius of the zeolite crystallite, and β is a time constant

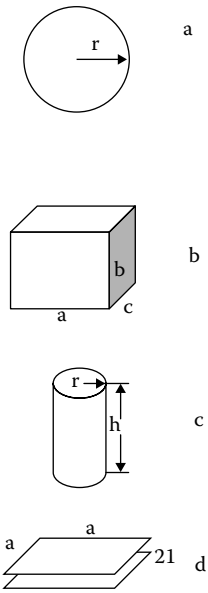

FIGURE 5.13 (a) Sphere, (b) coffin, (c) cylinder, and (d) plate crystal geometries.

which describes the evolution of the sortive partial pressure in the dead space of the IR cell, i.e.,

$$P = P_0[1 - \exp(-\beta t)]$$

where P_o is the steady-state partial pressure, and P is the partial pressure at time t [5,26,27]. Consequently, the initial nonstationary partial pressure of the sorbate in the gas stream is accounted for with the help of the parameter β [5,26,27].

Cutting the series, included in Equation 5.69, and using only the first four terms, it is obtained an approximation to Equation 5.69, which is numerically fitted [28,30] to experimental data (see Figure 5.14a–b [30]).

Then for each experiment, the numerical values of the Fickean diffusion coefficient, *D,* are calculated with the help of a nonlinear regression method [119]. The fitting process could be carried out with a program based on a least-square procedure [119], which allows us to calculate the best-fitting parameters of the approximation to Equation 5.69, i.e., the numerical values of the Fickean diffusion coefficient *D,* the equilibrium absorbance *A*, the parameter β, the regression coefficient, and the standard errors [28] (see Table 5.5).

The use of Equation 5.69 is completely justified only for a set of uniform spherical particles of radius, *a.* This is the case, for example, for the diffusion in beta zeolite [28]. However, this fact must be experimentally confirmed with the help of a scanning electron microscope; for instance, a beta zeolite material has been studied, showing round-shaped crystals with, $a = 0.45$ μm [28]. In the case of ZSM-5 [28] and ZSM-11 [30] zeolites, it is possible to define an equivalent spherical radius by means of the equation [80]:

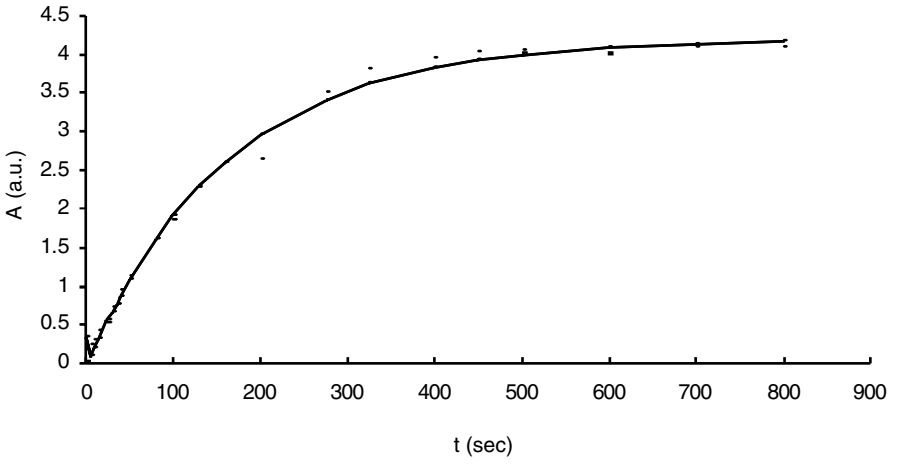

(a)

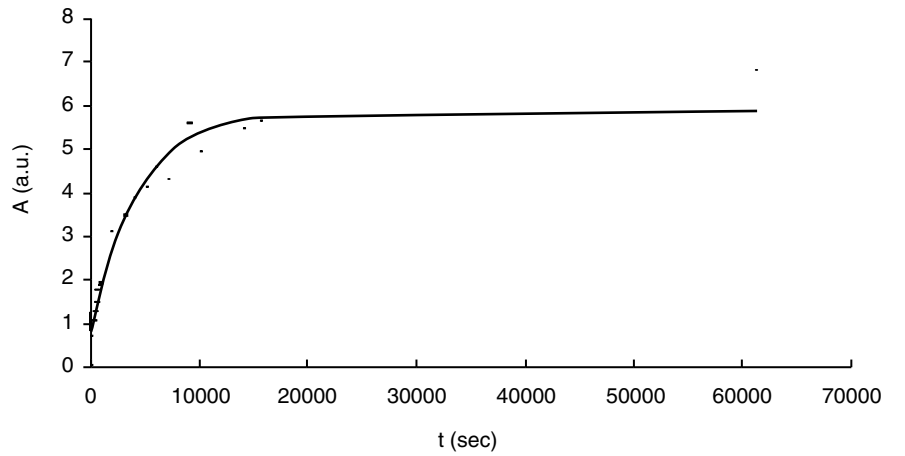

(b)

FIGURE 5.14 (a) Diffusion kinetics of para-xylene in H-ZSM-11 at 400 K, experimental points (-) fitted with the continuous theoretical curve. (b) Diffusion kinetics of ortho-xylene in H-ZSM-11 at 400 K, experimental points (-) fitted with the continuous theoretical curve.

$$r = \frac{2}{3}\left(\frac{1}{a} + \frac{1}{b} + \frac{1}{c}\right) \tag{5.70}$$

since the ZSM-5 and ZSM-11 zeolites, in general, show very regular "coffin"-shaped crystals (see Figure 5.13b) with the following average size: $a \times b \times c$ [28,30].

For a cylindrical geometry, which is the case if the zeolite crystals that form the wafer are approximately cylindrical (Figure 5.13c), then for diffusion through the

TABLE 5.5
Corrected Diffusion Coefficients ($D_0 \times 10^9$ [cm²/s]) of Benzene, Toluene, and Ethylbenzene in H-ZSM-5 and H-Beta Zeolites at Different Temperatures

Sortive	H-ZSM-5	H-Beta	T [°C]
Benzene	0.5	0.6	300
	2	3.2	350
	8	8.2	400
		13	450
Toluene	1	0.2	300
	4	0.9	350
	6	10	400
	16	18	450
Ethylbenzene	0.6	0.1	300
	1.5	0.2	350
	5	2.5	400
	17	26	450

cylindrical surface of the cylindrical shape particle with variable surface concentration, and initial concentration inside the cylinder equal zero, the solution of the Fick's second law is [5]:

$$\frac{M_t}{M_\infty} = 1 - \frac{2J_1\left(\left(\frac{\beta a^2}{D}\right)^{1/2}\right)\exp(-\beta t)}{\left(\frac{\beta a^2}{D}\right)^{1/2} J_0\left(\left(\frac{\beta a^2}{D}\right)^{1/2}\right)} + \left(\frac{4}{a^2}\right)\sum_1^\infty \left(\frac{\exp\left(-D\alpha_n t\right)}{\alpha_n^2\left\{\frac{D\alpha_n^2}{\beta} - 1\right\}}\right) \tag{5.71}$$

where $J_0(x)$ is the Bessel function of the first kind of order zero; α_n are the roots of $J_0(a\alpha_n) = 0$; $J_1(x)$ is the Bessel function of the first order; M_t, which is proportional to the absorbance A (where A is reported in arbitraty units [a.u.], i.e., $M_t \sim A^T_t$), is the amount of sorbate taken at time t; and M_∞, also proportional to the absorbance A (i.e., $M_\infty \sim \boldsymbol{A}^{\boldsymbol{T}}{}_\infty$), is the equilibrium sorption value; and D is the Fickean diffusion coefficient in the case of single component diffusion [26–28]. In addition, $r = a$ is the radius of the zeolite cylindrical crystallite, and β is a time constant which describes the evolution of the sortive partial pressure in the dead space of the IR cell.

For a plate-like geometry, which is the case if the zeolite crystals that form the wafer are approximately parallel slabs (Figure 5.13d), then for diffusion through the surface of the slab-shape particles, with variable surface concentration and initial concentration inside the sphere equal zero, the solution of Fick's second law is [5]:

$$\frac{M_t}{M_\infty} = 1 - \exp(-\beta t)\left(\frac{D}{\beta l^2}\right)^{1/2}\left\{\tan\left(\frac{\beta l^2}{D}\right)^{1/2}\right\} + \left(\frac{8}{\pi^2}\right)\sum_{1}^{\infty}\left(\frac{\exp\left(\frac{-(2n+1)^2\pi^2 Dt}{4l^2}\right)}{(2n+1)^2\left[1-(2n+1)^2\left(\frac{D\pi^2}{4\beta l^2}\right)\right]}\right) \quad (5.72)$$

where M_t, which is proportional to the absorbance, A, (where A is reported in arbitraty units [a.u.], i.e., $M_t \sim A^T_t$), is the amount of sorbate taken at time t; M_∞, also proportional to the absorbance, A (i.e., $M_\infty \sim \boldsymbol{A}^{\boldsymbol{T}}{}_\infty$), is the equilibrium sorption value; and D is the Fickean diffusion coefficient in the case of single component diffusion [26–28]. In addition, $2l$ is the length of the zeolite slablike crystallite (Figure 5.13d), and β is a time constant which describes the evolution of the sortive partial pressure in the dead space of the IR cell.

For the MCM-22 zeolite, the shapes of the crystallites are normally platelike with dimensions: $a \times a \times l = 0.5 \times 0.5 \times 0.05$ μm^3 [28] (see Figure 5.13D). For this zeolite, diffusion is impossible in the [001] crystallographic direction, because in this direction are stacked the cavities, corresponding to the MWW framework of the MCM-22 zeolite, which are joined by double 6-membered-rings [82]. In this case we should consider two possibilities for the disposition of the [001] direction, i.e., parallel (parallel-sided slab model, Figure 5.13d) or perpendicular (cylindrical model, Figure 5.13C) to the surface of the platelike crystal [28]. If we consider the [001] direction to be parallel to the crystallite face with area, $a \times a = 0.5 \times 0.5$ μm (Figure 5.13D), the diffusion will be through the surface of the slab. Then, using the model of a parallel-sided slab with thickness, 2l = 0.05 μm [28] for the solution of Fick's second law, Equation 5.72, the results obtained for the diffusion coefficients are very small [28]. Nevertheless, if we consider the [001] direction to be perpendicular to the crystal face with area, $a \times a$, and use a model of diffusion in a cylinder with radius, $r = a/2 = 0.25$ μm, and use Equation 5.71 or Equation 5.69, with an equivalent spherical radius, $a = (3/2)0.25 = 0.375$ μm, the results are in good agreement with the figures reported for the diffusion in H-ZSM-5 [28]. The previous results indicated that the MCM-22 have truncated cavities in its surface, showing that it is possible to get structural information from diffusion data [28,32].

In all the situations, the obtained Fickean diffusion coefficients, D, must be corrected in order to obtain the self-diffusion coefficients, D^*, with the help of Equation 5.14 [35], i.e., $D^* = D(1 - \theta)$, in which $\theta = n_a/N_a$ is the fractional saturation of the adsorbent, where n_a is the amount adsorbed, and N_a is the maximum amount adsorbed. The calculation of θ could be carried out, for example, with the help of the osmotic adsorption isotherm equation,

$$\frac{n_a}{N_a} = \frac{K_0 P^B}{1 + K_0 P^B},$$

where K and B are constants, fitting the experimental isotherms obtained with the equilibrium sorption values, A, which are proportional to n_a (see Chapter 3, Section 3.2) [28].

In Table 5.5 [28] reports the corrected diffusion coefficients, D_0, of benzene, toluene, ethylbenzene, o-xylene, and m-xylene in H-ZSM-5 and H-Beta zeolites calculated with the help of Equation 5.69 and Equation 5.14 [35] using the uptake data measured with the FTIR spectrometer, and taking into account the zeolite crystal geometry.

It must be noted that, in the interpretation of the uptake data for all the considered systems, additional transport mechanisms superimposed on the intracrystalline diffusion were not considered [9].

On the other hand, the Eyring equation:

$$D^* = D_0^* \exp\left(-\frac{E_a}{RT}\right)$$

was used for the calculation of the activation energy (E_a) and the preexponential factor, (D_0^*). The calculated values for the diffusional activation energy (Ea) and the preexponential factor are reported in Table 5.6 for all the studied systems.

The numerical evaluation of the preexponential factors in Equations 5.64 and 5.65 was possible because all the terms included in the equations are well defined; that is, R = 8.3 [kJ/(mol K)], T = 300–400 [K], M = 80–100 [g/mol], l = 10 [Å] [28], and $\nu = 10^{12}$–10^{13} s^{-1} [35]. The calculations result in a preexponential term for

TABLE 5.6
Diffusional Activation Energies and Preexponential Factors of the Eyring Equation for the Diffusion of Benzene, Toluene, and Ethylbenzene in H-ZSM-5 and H-Beta Zeolites [28]

Zeolite	Sortive	E_a [kJ/mol]	$D_0^* \times 10^4$ [cm²/g]
H-ZSM-5	Benzene	28	0.3
	Toluene	21	0.05
	Ethylbenzene	26	0.2
H-Beta	Benzene	32	2.2
	Toluene	36	3.3
	Ethylbenzene	41	9

localized adsorption in the range 10^{-1} [cm²/s] < D_0^* < 10^{-2} [cm²/s], and a preexponential term for mobile adsorption in the range 4×10^{-4} [cm²/s] < D_0^* < 6×10^{-4} [cm²/s] [28].

If the approximation, $D^* = D_0$, [34], is made, then it is possible to compare the values reported in Table 5.6 and the calculated values. The comparison indicates that the preexponential term for localized adsorption does not agree with the experimentally obtained preexponential terms, and consequently, we can conclude the diffusion of aromatic hydrocarbons in highly siliceous acid zeolites is not related to strong adsorption [28]. This conclusion was also reached by others [120,121] for the diffusion of benzene and toluene in ZSM-5 zeolite.

REFERENCES

1. Jost, W., *Diffusion in Solids, Liquids and Gases,* Academic Press, New York, 1960.
2. Reif, R., *Fundamentals of Statistical and Thermal Physics,* McGraw-Hill, Boston, 1965.
3. Kauzmann, W., *Kinetic Theory of Gases,* Addison-Wesley, Reading, 1966.
4. Manning, J.R., *Diffusion Kinetics for Atoms in Crystals,* Van Nostrand, Princenton, 1968.
5. Crank, J., *The Mathematics of Diffusion,* 2nd ed., Oxford University Press, Oxford, 1975.
6. Bokstein, B.S., Mendelev, M.I. and Srolovitz, D.J., *Thermodynamics and Kinetics in Materials Science,* Oxford University Press, Oxford, 2005.
7. Ruthven, D.M., *Principles of Adsorption, and Adsorption Processes,* John Wiley & Sons, New York, 1984.
8. Yang, R.T., *Gas Separation by Adsorption Processes,* Butterworths, Boston, 1987.
9. Post, M.F.M., *Stud. Surf. Sci. Catal.*, 58, 391, 1991.
10. Xiao, J. and Wei, J., *Chem. Eng. Sci.*, 47, 1123, 1992.
11. Chen, N.Y., Degnan, T.F., Jr., and Smith, C.M., *Molecular Transport and Reaction in Zeolites,* VCH Publishers, New York, 1994.
12. Karger, J. and Ruthven, D.M., *Diffusion in Zeolites and Other Microporous Solids,* J. Wiley & Sons, New York, 1992.
13. Kizilyalli, M., Corish, J., and J. Metselaar, J., *Pure Appl. Chem.,* 71, 1307, 1999.
14. Bird, R.B., Stewart, W.E., and Lightfoot, E.N., *Transport Phenomena,* 2nd ed., J. Wiley & Sons, New York, 2002.
15. Brauer, P., Fritzsche, S., Karger, J., Schutz, G., and Vasenkov, S., *Lect. Notes Phys.,* 634, 89, 2004.
16. Heitjans, P. and Karger, J., (Eds.), *Diffusion in Condensed Matter,* Springer, Berlin, 2005.
17. Fick, A., *Ann. Phys.*, 94, 59, 1855.
18. Onsager, L., *Phys. Rev.*, 37, 405, 1931; and 38, 2265, 1932.
19. Einstein, A., *Ann. Phys.*, 17, 549, 1905.
20. Roque-Malherbe, R., *Mic. Mes. Mat.*, 41, 227, 2000.
21. Karger, J., Vasenkow, S., and Auerbach, S.M., in *Handbook of Zeolite Science and Technology,* Auerbach, S., Carrado, K.A. and Dutta, P.K., Eds., Marcell Dekker Inc., New York, 2003, p. 341.
22. Burggraaf, A.J., *J. Membrane Sci.*, 155, 45, 1999.
23. Ruthven, D.M. and Eic, M., *ACS Symp. Ser.*, 388, 362, 1988; and *Zeolites,* 8, 40, 1988.

24. Yasuda, Y., *J. Phys. Chem.,* 86, 1913, 1982.
25. Van den Begin, N.G. and Rees, L.V.C., *Stud. Surf. Sci. Catal.*, 49B, 915, 1989.
26. Karge, H.G. and Niessen, W., *Catal. Today,* 8, 451, 1991.
27. Niessen, W. and Harge, H.G., *Stud. Surf. Sci. Catal.*, 60, 213, 1991.
28. Roque-Malherbe, R., Wendelbo, R., Mifsud, A., and Corma, A., *J. Phys. Chem.*, 99, 14064, 1995.
29. Roque-Malherbe, R., *Mic. Mes. Mat.*, 56, 321, 2002.
30. Roque-Malherbe, R. and Ivanov, V., *Mic. Mes. Mat.*, 47, 25, 2001.
31. Sastre, G., Raj, N., Richard, C., Catlow, C., Roque-Malherbe, R., and Corma, A., *J. Phys. Chem. B,* 102, 3198, 1998.
32. Wendelbo, R. and Roque-Malherbe, R., *Mic. Mat.*, 10, 231, 1997.
33. Pfeifer, H., in *NMR Basic Principles,* Diehl, P., Fluck, E., and Kosfeld, R., Eds., Springer, Berlin, 1972, p. 53
34. Karger, J., *Surf. Sci.*, 36, 797, 1973.
35. Barrer, R.M. and Jost, W., *Trans. Faraday Soc.*, 45, 928, 1949.
36. Saracco, G. and Specchia, V., *Catal. Rev. Sci. Eng.*, 36, 305, 1994.
37. Satterfield, C.N., *Heterogeneus Catalysis in Practice,* Mc Graw-Hill, New York, 1980.
38. Wang, M.R. and Li, Z.X. *Phys. Rev. E,* 68, 046704, 2003.
39. Choi, J.-G., Do, D.D., and Do, H.D., *Ind. Eng. Chem. Res.*, 40, 4005, 2001.
40. Hwang, S.-T. and Kammermeyer, K., *Techniques in Chemistry: Membranes in Separation,* J. Wiley & Sons, New York, 1975.
41. Kapoor, A., Yang, R.T., Wong, C., *Catal. Rev. Sci. Eng.*, 31, 129, 1989.
42. Ulhorn, R.J.R., Keizer, K., and Burggraaf, A.J., *J. Membrane Sci.*, 66, 271, 1992.
43. Barber, R.W. and Emerson, D.R., *Advances in Fluid Mechanics IV,* Rahman, M., Verhoeven, R., and Brebbia, C.A., Eds., WIT Press, Southampton, UK, 2002, p. 207.
44. Schaaf, S.A. and Chambre, P.L., *Flow of Rarefied Gases,* Princeton University Press, 1961.
45. Mizuseki, H., Jin, Y., Kawazoe, Y., and Wille, L.T., *J. App. Phys.*, 87, 6561, 2000.
46. Bird, G., *Annu. Rev. Fluid Mech.*, 10, 11, 1978.
47. Hsieh, H.P., *Inorganic Membranes for Separation, and Reaction,* Membrane Science and Technology Series 3, Elsevier, Amsterdam, 1996.
48. Morooka, S. and Kusakabe, K., MRS Bulletin, March 25, 1999.
49. Mulder, M., *Basic Principles of Membrane Technology,* Kluver Academic Publishers, Dordrecht, The Netherlands, 1996.
50. Baker, R.W., *Membrane Technology and Applications,* Wiley, New York, 2004.
51. Goosen, M.F., Sablani, S.S., and Roque-Malherbe, R., in *Handbook of Membrane Separations: Chemical, Pharmaceutical, and Biotechnological Applications,* Pabby, A.K., Sastre, A.N., and Rizvi, S.S., Eds., Marcel Dekker, New York, 2007.
52. Saracco, G., Neomagus, H.W.J.P., Versteeg, G.F., and Swaaij, W.P.M., *Chem. Eng. Sci.*, 54, 1997, 1999.
53. Sankar, N. and Tsapatsis, M., in *Handbook of Zeolite Science, and Technology,* Auerbach, S., Carrado, K.A., and Dutta, P.K. Eds., Marcell Dekker, New York, 2003, p. 867.
54. Vankelecom, I.F.J., *Chem. Rev.*, 102, 3779, 2002.
55. Boissiere, C., Martines, M.A.U., Kooyman, P.J., de Kruijff, T.R., Larbot, A., and Prouzet, E., *Chem. Mater.*, 15, 460, 2003.
56. Mauran, S., Rigaud, L., and Coudeville, O., *Transp. Porous Media,* 43, 355, 2001.
57. Krishna, R., in *Handbook of Zeolite Science and Technology,* Auerbach, S., Carrado, K.A., and Dutta, P.K., Eds., Marcell Dekker Inc., New York, 2003, p. 1105.
58. Roque-Malherbe, R., del Valle, W., Marquez, F., Duconge, J., and J. Goosen, J., *Sep. Sci. Tech.*, 41, 73, 2006.

59. Mason, E.A. and Malinauskas, A.P., *Gas Transport in Porous Media. The Dusty Gas Model,* Elsevier, Amsterdam, The Netherlands, 1983.
60. Papavassiliou, V., Lee, C., Nestlerode, J., and Harold, M.P., *Ind. Eng. Chem. Res.*, 36, 4954, 1997.
61. Rutherford, S.W. and Do, D.D., *Ind. Eng. Chem. Res.*, 38, 565, 1999.
62. Nicholson, D. and Cracknell, R., *Langmuir,* 12, 4050, 1996.
63. Wei, J., *Ind. Eng. Chem. Res.*, 33, 2467, 1994.
64. Weisz, P.B., *Ind. Eng. Chem. Res.*, 34, 2692, 1995.
65. Hahn, K. and Karger, J., *J. Phys. Chem. B,* 100, 316, 1996.
66. Bhide, S.Y. and Yashonath, S., *J. Phys. Chem. B,* 104, 11977, 2000.
67. Tepper, H.L., Hoogenboom, J.P., van der Vegt, N.F.A., and Briels, W.J., *J. Chem. Phys.*, 110, 11511, 1999.
68. Nelson, P.H. and Auerbach, S.M., *J. Chem. Phys.*, 110, 9235, 1999.
69. Potter, M.C. and Wiggert, D.C., *Mechanics of Fluids,* 3rd ed., Brooks/Cole-Thomson Learning, Pacific Groove, CA, 2002.
70. Okazaki, M., Tamon, H., and Toei, R., *AIChE J.*, 27, 262, 1981.
71. Uhlhorn, R.J.R. and Burggraaf, A.J., in *Inorganic Membranes,* Bhave, R.R., Ed., Van Nostrand Reinhold, New York, 1990, p. 155.
72. Burggraaf, A.J. and Cot, L., *Fundamentals of Inorganic Membrane Science and Technology,* Elsevier, New York, 1996.
73. Corma, A., *Chem. Rev.*, 97, 2373, 1997.
74. Marquez-Linares, F. and Roque-Malherbe, R., *Facets-IUMRS J.*, 2, 14, 2003; and 3, 8, 2004.
75. Snurr, R. and Karger, J., *J. Phys. Chem. B,* 101, 6469, 1997.
76. Ramanan, H., Auerbach, S.M., and Tsapatsis, M., *J. Phys. Chem. B,* 108, 17171, 2004.
77. Skoulidas, A.I. and Sholl, D.S., *J. Phys. Chem. B,* 105, 3151, 2001.
78. Valyon, J., Onyestyak, G. and Rees, L.V.C., *Langmuir,* 16, 1331, 2000.
79. Breck, D.W., *Zeolite Molecular Sieves,* J. Wiley & Sons, New York, 1974.
80. Barrer, R.M., *Zeolite and Clay Minerals as Sorbents and Molecular Sieves,* Academic Press, 1978.
81. Mortier, W.J., *Compilation of Extraframework Sites in Zeolites,* Butterworth, London, 1982.
82. Baerlocher, Ch., Meier, W.M., and Olson, D.M., *Atlas of Zeolite Framework Types,* 5th ed., Elsevier, Amsterdam, 2001.
83. Chen, N.Y., Degnan, T.F., Jr., and Smith, C.M., *Molecular Transport and Reaction in Zeolites,* VCH: New York, 1994.
84. Corma, A., *Chem. Rev.*, 95, 559, 1995.
85. Theodorou, D.N. and Wei, J., *J. Catal.*, 83, 205, 1983.
86. Nelson, P.H., Kaiser, A.B., and Bibby, D.M., *J. Catal.*, 127, 101, 1991.
87. Snurr, R.O., Bell, A.T., and Theodorou, D.N., *J. Phvs. Chem.*, 97, 13742, 1993.
88. de la Cruz, J., Rodriguez, C., and Roque-Malherbe, R., *Surf. Sci.*, 209, 215, 1989.
89. Glasstone, S., Laidler, K.J., and Eyring, H., *The Theory of Rate Process,* McGraw-Hill, New York, 1964.
90. Karger, J., Heifer, H., and Haberlandt, R., *Chem. Soc. Faraday Trans.*, 76, 1569, 1980.
91. Ruthven, D.M. and Derrah, R.I., *J. Chem. Soc.*, Faraday Trans., 68, 2322, 1972.
92. Larry, R.L., Bell, A.T., and Theodorou, D.N., *J. Phys. Chem.*, 95, 8866, 1991.
93. Hill, T.L., *An Introduction to Statistical Thermodynamics,* Dover Publications Inc., New York, 1986.
94. Rudzinskii, W. and Everett, D.H., *Adsorption of Gases on Heterogeneous Surfaces,* Academic, New York, 1992.

95. Ross, S. and Olivier, J.P., *On Physical Adsorption,* J. Wiley & Sons, New York, 1964.
96. Karger, J., Petzold, M., Pfeiffer, H., Ernst, S., and Weitkamp, J., *J. Catal.*, 136, 283, 1992.
97. Kukla, V., Kornatowski, J., Demuth, D., Girnus, I., Pfeifer, H., Rees, L.V.C., Schunk, S., Unger, K., and Karger, J., *Science,* 272, 702, 1996.
98. Brandini, S., Ruthven, D.M., and Karger, J., *Microporous Materials,* 9, 193, 1997.
99. Qureshi, W. and Wei, J., *J. Catal.*, 126, 147, 1990.
100. Tsikoyannis, J.G. and Wei, J., *Chem. Eng. Sci.*, 46, 233, 1991.
101. Hahn, K. and Karger, J., *J. Phys. A,* 28, 3061, 1995.
102. Shen, D. and Rees, L.V.C., *J. Chem. Soc. Faraday Trans.*, 92, 487, 1996.
103. Rodenbeck, C. and Karger, J., *J. Chem. Phys.*, 110, 3970, 1999.
104. Hahn, K. and Karger, J., *J. Phys. Chem. B,* 102, 5766, 1998.
105. Hoogenboom, J.P., Tepper, H.L., Van der Vegt, N.F.A., and Briels, W.J., *J. Chem. Phys.*, 113, 6875, 2000.
106. Radajhyaksksha, R.A., Pitale, K.K., and Tambe, S.S., *Chem. Eng. Science,* 45, 1935, 1990.
107. Karger, J., *Phys. Rev. A,* 45, 4173, 1992.
108. Karger, J., *Phys. Rev. E,* 47, 1427, 1993.
109. Nivarthi, S.S., Mc Cormick, A.V., and Davis, H.T., *Chem. Phys. Lett.*, 229, 298, 1994.
110. Jobic, H., Hahn, K., Karger, J., Bee, M., Tuel, A., Noak, M., Girnus, I., and Kearly, G., *J. Phys. Chem.*, 110, 5834, 1997.
111. Brandani, S., Ruthven, D.M., and Karger, J., *Micropor. Mater.*, 9, 193, 1997.
112. Song, L. and Rees, L.V.C., *Micropor. Mesopor. Mater.*, 41, 193, 2000.
113. Bouchard, J.P. and Georges, A., *Phys. Rep.*, 127, 127, 1990.
114. Schlesinger, M.F., Zaslavsky, G.M., and Klafter, J., *Nature,* 363, 31, 1993.
115. Sokolov, I.M., Klafter, J., and Blumen, A., *Physics Today,* 55, 48, 2002.
116. Oldham, K.B. and Spanier, J., *The Fractional Calculus,* Academic Press, San Diego, CA, 1974.
117. Miller, K.S. and Ross, B., *An Introduction to Fractional Calculus and Fractional Differential Equations,* J. Wiley & Sons, New York, 1993.
118. Roque-Malherbe, R. and Wendelbo, R., *Thermochimica Acta,* 400, 165, 2003.
119. Draper, N.R. and Smith, H., *Applied Regression Analysis, Third Edition,* Wiley, New York, 1998.
120. Xiao, J. and Wei, J., *J. Chem. Eng. Sci.*, 47, 1143, 1992.
121. Karge, H. and Niessen, W., *Mic. Mat.*, 1, 1, 1993.

6 The Plug-Flow Adsorption Reactor

6.1 DYNAMIC ADSORPTION

To apply adsorption, in most cases, a reactor where a dynamic adsorption process will occur is packed with a concrete adsorbent. The adsorbents normally used for these applications are: active carbons, zeolites and related materials, silica, mesoporous molecular sieves, alumina, titanium dioxide, magnesium oxide, clays, and pillared clays.

Dynamic adsorption is a mass-transfer problem that could be treated with complicated mass-transfer models, where many parameters are needed, which must be determined by independent batch kinetic studies, or estimated by suitable correlations [1,2].

We will discuss here the simplest application of dynamic adsorption, that is, the use of adsorbents to clean gas or liquid flows by the elimination of a low-concentration impurity by the use of a plug-flow adsorption reactor (PFAR) (see Figure 6.1), where the output of the operation of the PFAR is a breakthrough curve (see Figure 6.2) [3–18]. In Figure 6.2, C_o is the initial concentration, C_e is the breakthrough concentration, V_e is the fed volume of the aqueous solution of the solute A to breakthrough, and V_b is the fed volume to saturation. This is a response curve where the relation between concentration, at the exit of the packed bed adsorption reactor, and fed volume is shown through time.

An aqueous solution with an initial concentration, C_0 [mass/volume], of a trace solute A, or a gas flow with a low concentration, C_0 [mass/volume], of the gas component A is passing through this reactor with a volumetric flow rate:

$$F = \frac{\Delta V}{\Delta t} = \frac{volume}{time}$$

The volume of the empty bed is $V_B = \varepsilon V$, where V is the bed volume, and ε is the fraction of free volume in the bed. The interstitial fluid velocity, u, is defined as [15]:

$$u = \frac{F}{S}$$

where S is the reactor cross sectional. In addition, the contact or residence time of the fluid passing though the reactor, τ, is calculated with the equation [15]:

$$\tau = \frac{V_B}{F}$$

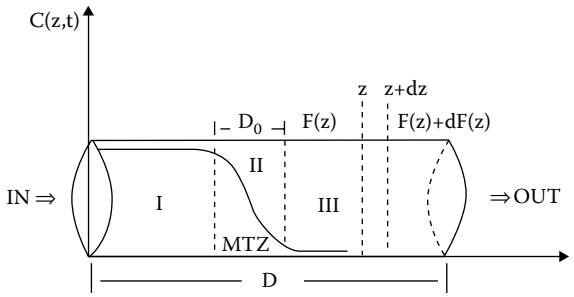

FIGURE 6.1 Packed bed adsorption reactor.

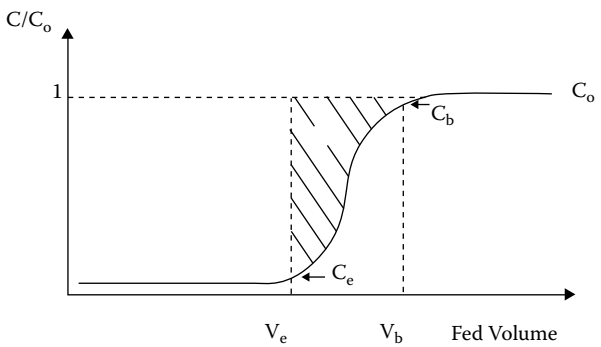

FIGURE 6.2 Breakthrough curve showing the relation between concentration at the exit of the packed bed adsorption reactor, and fed volume, which is proportional to time.

In order to work properly, the dynamic adsorption reactor should, as a rule, satisfy the following points [12]:

1. ***Residence time:*** Since adsorption could be a slow process; the fluid contact or residence time should be long enough for molecular transport to the adsorption sites to take place. As a rule of thumb in the present case, it is possible to try out residence times around the following figures: 0.05 sec $< \tau <$ 0.1 sec, for gaseous dynamic adsorption, and 0.5 sec $< \tau <$ 1 sec, for liquid-phase dynamic adsorption.
2. ***Particle size:*** If the particle size is small enough, there will be a considerable pressure drop inside the reactor. Consequently, granular particles with big enough particle size should be used. The particular particle size depends on the size of the reactor; therefore, a rule of thumb is to construct the reactor following the approximate relation: $d_R/d_P \geq 10$, where d_R is the reactor diameter, and d_P is the particle size. For a laboratory test of a material, which is the principal aim of the present book, $d_R/d_P \approx 10$ is a good choice.

3. ***Reactor longitude:*** Since residence times are relatively long, large facilities are sometimes required to attain the needed treatment capacities. Then in order to keep the proportions in the reactor dimensions, the following rule could be applied: $D/d_R \geq 10$, where D is the reactor length, and d_R is the reactor diameter. For a laboratory trial of a material, $D/d_R \approx 10$ is an excellent option.

Obviously, the above points are only very rough design criteria, which are solely justified for laboratory tests of materials, not in general, for the design of industrial reactors, which is not the aim of the present book.

6.2 THE PLUG-FLOW ADSORPTION REACTOR MODEL

The plug-flow model means that the fluid velocity profile is "plug shaped" (i.e., is uniform at all radial positions), a fact which generally involves turbulent flow conditions, such that the fluid constituents are well mixed [3]. In addition, it is assumed that the fixed-bed adsorption reactor is packed randomly with adsorbent particles that are fresh or just regenerated [8]. In addition, a rate process and a thermodynamic equilibrium occur in this adsorption separation process, where individual parts of the system react so rapidly that, for practical purposes, local equilibrium can be assumed [3]. The adsorption process is supposed to be very fast relative to the convection and diffusion effects; subsequently, local equilibrium will exist close to the adsorbent beads [6,8]. Additional assumptions are that no chemical reactions occur in the column, and that only mass transfer by convection is significant.

Finally, it is necessary to emphasize that the adsorbent is contacted with a binary mixture, one component of which is selectively adsorbed by the solid adsorbent. That is, in the flowing fluid a trace of an adsorbable species is adsorbed from an inert carrier. Furthermore, the heat effects could be disregarded; therefore, isothermal conditions will be taken [3,8]. The flow is fed to the top of the bed, at a constant flow rate, and under conditions such that mass-transfer resistance is negligible [6,8].

The reactor has a cross-sectional area S, column length D, and adsorbent mass in the bed M, (see Figure 6.1). The adsorbent bed in the PFAR could be divided in three zones: (1) the equilibrium zone, (2) the mass-transfer zone (MTZ) with a length D_o, and (3) the unused zone [4,10,11]. The length of the mass-transfer zone (MTZ), D_o, could be calculated with the following expression (see Figure 6.2) [11]:

$$D_0 = 2D\frac{V_b - V_e}{V_b + V_e} \tag{6.1}$$

The physical process of adsorption is fast relative to other slow steps, such as diffusion within the solid. Then in and near the solid adsorbent, the general form for the equilibrium isotherm is [3]:

$$q = KC^* \tag{6.2}$$

in which q is the equilibrium value of the adsorbate concentration, expressed as moles solute adsorbed per unit volume of the solid particle, and C^* denotes the solute composition, in moles of solute per unit volume of fluid, which could exist at equilibrium, and K is the linear partition coefficient.

Taking into account all previously acknowledged assumptions, then the mass balance equation for the PFAR is:

$$\text{IN} - \text{OUT} = \text{ACCUMULATION}$$

which could be expressed as follows [6,8]:

$$FC(z) - FC(z+dz) = \varepsilon \frac{\partial C}{\partial t} Sdz + (1-\varepsilon) \frac{\partial q}{\partial t} Sdz$$

where the first term is related to the fluid flow, and the two terms on the other side of the equation are related to the accumulation in the fluid phase and the solid phase, respectively. Then, dividing by Sdz, we will get [6]:

$$\frac{\partial C}{\partial t} + u \frac{\partial C}{\partial z} + \frac{1-\varepsilon}{\varepsilon} \frac{\partial q}{\partial t} = 0 \tag{6.3}$$

in which ε is the void fraction of the bed (i.e., the volume between particles), $(1 - \varepsilon)$ denotes the fractional volume taken up by the solid, u is the interstitial velocity of the carrier fluid, t is the operating time, z is the distance from the inlet of the mobile phase, $C(z,t)$ is the flowing solute composition, and q is the solute concentrations in the stationary phase.

To complete the necessary set of equations, it is necessary to include the adsorption rate of the solute or contaminant, which can be described by the linear driving force model in terms of the overall liquid-phase mass-transfer coefficient [6,8,9]:

$$\frac{\partial q}{\partial t} = k'(C - C^*) \tag{6.4}$$

where C^* is the mobile-phase concentration in equilibrium with the stationary-phase concentration, q, and k' is the rate coefficient, which is a lumped mass-transfer coefficient where

$$k' = \frac{k_c a}{(1-\varepsilon)},$$

in which k_c is the mass-transfer coefficient per unit interfacial area, $k_c a$ is the mass-transfer coefficient per unit volume, and a is the total interfacial area per unit volume of packed column [3,8].

The model of the system now comprises three equations (Equations 6.2, 6.3, and 6.4). That is, three equations and three unknowns (q, C, and C^*). Consequently, it is possible to eliminate q, with the help of Equation 6.2, and obtain [3]:

$$\frac{\partial C}{\partial t} + u\frac{\partial C}{\partial z} + \frac{1-\varepsilon}{\varepsilon}K\frac{\partial C}{\partial t} = 0 \tag{6.5a}$$

$$\frac{\partial C^*}{\partial t} = \frac{k_c a}{(1-\varepsilon)K}(C - C^*) \tag{6.5b}$$

The initial and boundary conditions associated with the simultaneous couple partial differential equations (PDE) describing the operation of the plug-flow adsorption reactor (PFAR) are [3,8]:

1. $C(z,0) = 0$, and $C^*(z,0) = 0$, initially clean interstitial fluid, for $0 \le z \le D$
2. $C(0, t) = C_0$ (i.e., constant composition at bed access)

To calculate the breakthrough curve, analytical solutions of the system of Equations 6.5a and 6.5b can be obtained using the Laplace transform method [3] (see Appendix 6.1).

The Laplace method could be used directly to solve the couple PDE describing the operation of the PFAR Equations 6.5a and 6.5b. However to simplify the solution, it is better to change the form of these equations [3]. First, a new variable is introduced:

$$\theta = t - \frac{z}{u}$$

which is the difference between the real time and the local fluid residence time. Now, it is necessary to introduce this new variable:

$$C(z,t) = C(z,\theta) \tag{6.6a}$$

$$C(z,t) = C(z,\theta) \tag{6.6b}$$

since [3]:

$$\left.\frac{\partial C}{\partial z}\right|_t dz + \left.\frac{\partial C}{\partial t}\right|_z dt = \left.\frac{\partial C}{\partial z}\right|_\theta dz + \left.\frac{\partial C}{\partial \theta}\right|_z d\theta \tag{6.7}$$

and:

$$d\theta = dt - \frac{dz}{u} \tag{6.8}$$

Then substituting Equation 6.8 in Equation 6.7 and equating the coefficients of *dt* and *dz,* we will get [3]:

$$\left.\frac{\partial C}{\partial z}\right|_t = \left.\frac{\partial C}{\partial z}\right|_\theta - \frac{1}{u}\left.\frac{\partial C}{\partial \theta}\right|_z \tag{6.9}$$

and

$$\left.\frac{\partial C}{\partial t}\right|_z = \left.\frac{\partial C}{\partial \theta}\right|_z \tag{6.10}$$

Similarly, it is possible to show that:

$$\left.\frac{\partial C^*}{\partial t}\right|_z = \left.\frac{\partial C^*}{\partial \theta}\right|_z \tag{6.11}$$

Now substituting Equations 6.9, 6.10, and 6.11 into Equations 6.5a and 6.5b, we will get:

$$u\left.\frac{\partial C}{\partial z}\right|_\theta = -\frac{k_c a}{\varepsilon}(C - C^*) \tag{6.12a}$$

$$(1-\varepsilon)K\frac{\partial C^*}{\partial \theta} = k_c a(C - C^*) \tag{6.12b}$$

To make the system of coupled Equations 6.12a and 6.12b more compact, the following two variables will be defined: the dimensionless distance:

$$\xi = \frac{k_c a}{\varepsilon}\left(\frac{z}{u}\right)$$

and the dimensionless relative time:

$$\tau = \frac{k_c a}{K(1-\varepsilon)}(\theta)$$

When these variables are substituted in Equations 6.12a and 6.12b, the following system of couple equations is obtained:

$$\frac{\partial C}{\partial \xi} = -(C - C^*) \tag{6.13a}$$

$$\frac{\partial C}{\partial \tau} = (C - C^*) \tag{6.13b}$$

At this time, the initial and boundary conditions will be:

$$C(\xi, 0) = 0, \; C^*(\xi, 0) = 0, \text{ and } C(0, \tau) = C_0$$

Taking Laplace transforms with respect to τ (see Appendix 6.1), we will get:

$$\frac{dC(\xi, s)}{d\xi} = -[C(\xi, s) - C^*(\xi, s)] \tag{6.14a}$$

$$sC^*(\xi, s) = [C(\xi, s) - C^*(\xi, s)] \tag{6.14b}$$

Solving the system from Equation 6.14b for C^* gives:

$$C^*(\xi, s) = \frac{C(\xi, s)}{s+1}$$

and Equation 6.14a yields:

$$\frac{dC(\xi, s)}{d\xi} = -C(\xi, s) + \frac{C(\xi, s)}{s+1} = -C(\xi, s)\frac{s}{s+1} \tag{6.15}$$

Now, integrating Equation 6.15, we will get:

$$C(\xi, s) = A(s)\exp\left(-\frac{s}{s+1}\xi\right) = A\exp(-\xi)\exp\left(\frac{\xi}{s+1}\right) \tag{6.16}$$

where $A(s)$ is the integration constant.

The transform of the step change at the bed entrance is [3]:

$$L[C(0, \tau) = L[C_0] = \frac{C_0}{s} \tag{6.17}$$

Consequently, it is possible to evaluate the integration constant $A(s)$*:*

$$A(s) = \frac{C_0}{s} \tag{6.18}$$

and the function that will be inverted is:

$$C(\xi,s)=\left(\frac{C_0}{s}\right)\exp(-\xi)\exp\left(\frac{\xi}{s+1}\right) \tag{6.19}$$

This function could be inverted with the help of the shifting theorem, except for the presence of the term 1/*s* [3]. In a Laplace transform table [19,20], it is possible to find the following transform:

$$L\left[J_0\left(2\sqrt{kt}\right)\right]=F(s)=\frac{e^{-\frac{k}{s}}}{s}=\int_0^\infty e^{-st}J_0\left(2\sqrt{kt}\right)dt \tag{6.20}$$

where J_0 is the zero-order Bessel function of the first kind [21], which is applicable to the solution of the current problem, if we could replace *s* for *s* + 1 in Equation 6.19. This can be done with the help of the following equation [3]:

$$\int_0^\xi \exp(-\beta)\exp\left(\frac{\beta}{s+1}\right)d\beta=\left(\frac{s+1}{s}\right)\left[1-\exp(-\xi)\exp\left(\frac{\xi}{s+1}\right)\right]$$

Then it is possible to express the exponential, in Equation 6.19, in integral form:

$$C(\xi,s)=C_0\left[\frac{1}{s}-\int_0^\xi \frac{\exp(-\beta)\exp\left(\frac{\beta}{s+1}\right)}{s+1}d\beta\right]$$

and finally, using the shifting theorem (see Appendix 6.1), the Laplace transform expressed in Equation 6.19, and noting that:

$$J_0\left(2\sqrt{-kt}\right)=J_0\left(2i\sqrt{kt}\right)=I_0\left(2\sqrt{kt}\right)$$

it is possible to get (see Figure 6.2)[3]:

$$C(\xi,\tau)=C_0u(\tau)\left[1-\exp(-\tau)\int_0^\xi \exp(-\beta)I_0\left(2\sqrt{\beta\tau}\right)d\beta\right]$$

where I_0 is the modified Bessel function, and $u(\tau)$ is the step function [20].

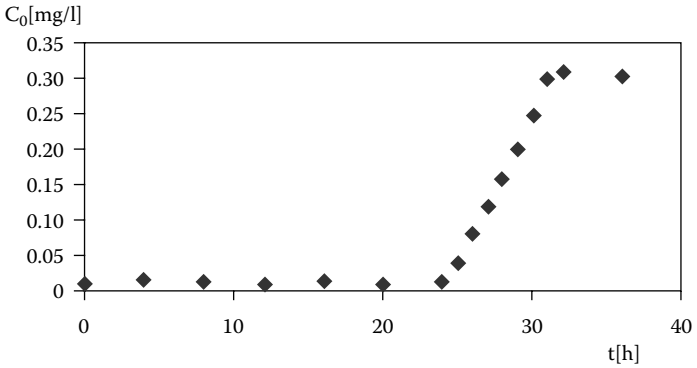

FIGURE 6.3 Breakthrough curve resulting from the dynamic adsorption of H_2O from a CO_2–H_2O mixture by Na-X synthetic zeolite.

The above reported analytical solution of the simultaneous couple partial differential equations (PDE) describing the operation of the plug-flow adsorption reactor (PFAR) is an elegant example of the use of the Laplace transform methodology in the solution of PDEs. More important, in the frame of the applications of adsorption, it is valuable in uses where the relation between q, the equilibrium value of the adsorbate concentration, and C^*, the solute composition, is linear (see Equation 6.2). However, numerical solutions offer more rigorous results, because of a smaller amount of simplifications implicated in the original model, and represent a more flexible line of attack, since their use is not limited by the type of adsorption isotherm, or initial and boundary conditions applied [22].

As an example of an application of a PFAR in a dynamic adsorption process of gas cleaning, Figure 6.3 shows the breakthrough curve following from the dynamic adsorption of H_2O from a CO_2–H_2O mixture by a Na-X synthetic zeolite provided by Laporte [23,24].

The water concentration in the mixture prior to breakthrough was 0.32 mg/l, which was reduced, after the passage of the gas flow through the adsorption reactor, to 0.02 mg/l. The reactor had a cross-sectional area, $S = 10.2$ cm^2, column length, $D = 6.9$ cm, adsorbent mass in the bed, $M = 30$ g. The volume of the bed was 70 cm^3, the volume free of adsorbent in the bed was about 35 cm^3, and the volumetric flow rate was $F = 7$ [cm^3/s] [23,24].

REFERENCES

1. Slaney, A.J. and Bhamidimarri, R., *Water Sci. Technol.*, 38, 227, 1998.
2. Wolborska, A., *Chem. Eng. J.*, 37, 85, 1999.
3. Rice, R.G., and Do, D.D., *Applied Mathematics and Modeling for Chemical Engineers,* John Wiley & Sons, New York, 1995.
4. Droste, R., *Theory and Practice of Water and Wastewater Treatment,* J. Wiley & Sons, New York, 1997.

5. Scott-Fogler, H., *Elements of Chemical Reaction Engineering,* Prentice-Hall, Upper Saddle River, New Jersey, 1999.
6. Ruthven, D.W., *Principles of Adsorption and Adsorption Processes,* Wiley, New York, 1984.
7. Helfferich, F.G. and Klein, G., *Multicomponent Chromatography: Theory of Interference,* Marcel Dekker, New York, 1970.
8. Chern, J.-M., and Chien, Y.-W., *Ind. Eng. Chem. Res.*, 40, 3775, 2001.
9. Sherwood, T.K., Pigford, R.L., and Wilke, C.R., *Mass Transfer,* McGraw-Hill, New York, 1975.
10. Pansini, M., *Mineral. Deposita,* 31, 563, 1996.
11. Michaels, A.C., *Ind. Eng. Chem.*, 44, 1922, 1952.
12. Rodriguez-Reinoso, F. and Sepulveda-Escribano, A., in *Handbook of Surfaces and Interfaces of Materials,* Volume 5, Nalwa, H.S., Ed., Academic Press, New York, 2001, p. 309.
13. Helfferich, F., *Ion Exchange,* Dover Publications Inc., New York, 1962.
14. Suzuki, M., *Adsorption Engineering,* Elsevier Science, Amsterdam, 1990.
15. Levenspiel, O., *Chemical Reaction Engineering,* 3rd ed., J. Wiley & Sons, New York, 1998.
16. Thomas, W.J. and Crittenden, B., *Adsorption Technology, and Design,* Elsevier Science and Technology, Amsterdam, 1998.
17. Seader, J.D. and Henley, E.J., *Separation Process Principles,* J. Wiley & Sons, New York, 1998.
18. Bansal, R.C. and Meenakshi, G., *Activated Carbon Adsorption,* CRC Press, Boca Raton, FL, 2005.
19. Oberhettinger, F. and Badii, L., *Tables of Laplace Transforms,* Springer-Verlag, New York, 1980.
20. Churchill, R.V., *Operational Mathematics,* Mc-Graw-Hill, New York, 1958.
21. Arfken, G.B. and Weber, H.J., *Mathematical Methods for Physicists,* 5th ed., Academic Press, New York, 2001.
22. Tien, C., *Adsorption Calculation and Modeling,* Butterworth-Heineman, Boston, 1994.
23. Roque-Malherbe, R., Lemes, L., Autie, M., and Herrera, O., in *Zeolite or the Nineties, Recent Research. Reports,* 8th International Zeolite Conference, Amsterdam, July 1989, Hansen, J.C., Moscou, L., and Post, M.F.M., Eds., IZA, 1989, p. 137.
24. Roque-Malherbe, R., Lemes, L., López-Colado, L., and Montes, A., in *Zeolites '93 Full Papers Volume,* Ming, D. and Mumpton, F.A., Eds., International Committee on Natural Zeolites, Brockport, New York, 1995, p. 299.

APPENDIX 6.1 LAPLACE TRANSFORMS

The Laplace transform converts integral and differential equations into algebraic equations, simplifying, in some cases, the calculation of the solutions of a differential equation. There are two versions of Laplace tranforms: the one sided and the two sided. Usually the one-sided transform is used when we are dealing with causal systems and signals. The one-sided transform is the type of Laplace transform that will be used here. In this case, it is assumed that $f(t) = 0$ for $t < 0$ [3]. Then, Laplace transform of a function, $f(t)$, is a function, $L[f(t)]=F(s)$, of the complex variable, $s = \sigma + i\omega$, and the transforms are defined as follows [20,21]:

$$L[f(t)] = F(s) = \int_0^\infty e^{-st} f(t) dt \tag{A6.1-1}$$

Of course, these transformations are only defined for those values of s for which the integrals converge. The condition for convergence is [3]:

$$\int_0^\infty \left| e^{-st} f(t) \right| dt < \infty$$

The set of values, s, for which the above condition is satisfied is called the region of convergence (ROC) of the Laplace transform.

The operator L is linear; then [20,21]:

$$L[ag(t) + bh(t)] = aL[g(t)] + bL[h(t)] \tag{A6.1-2}$$

In the most elementary function where the operator L could be applied, that is, a constant, $f(t) = C$:

$$L[C] = \int_0^\infty Ce^{-st} dt = C\left(\frac{e^{-st}}{-s} \Big|_0^\infty \right) = \frac{C}{s} \tag{A6.1-3}$$

Another simple function is $f(t) = t$

$$L[Ct] = \int_0^\infty Cte^{-st} dt = C\left(\frac{e^{-st}}{s^2}(-st - 1) \Big|_0^\infty \right) = \frac{C}{s^2} \tag{A6.1-4}$$

A higher-level function we can consider is the power function, $f(t) = Ct^n$, where n is a natural number:

$$L[Ct^n] = \int_0^\infty Ct^n e^{-st} dt = \frac{Cn!}{s^{n+1}} \tag{A6.1-5}$$

Let now $f(t) = Ce^{kt}$

$$L[Ce^{kt}] = \int_0^\infty Ce^{-st} e^{kt} dt = C\left(\frac{e^{-(s-k)t}}{-(s-k)} \Big|_0^\infty \right) = \frac{C}{s-k} \tag{A6.1-6}$$

Similarly [20,21]:

$$L[Ce^{-bt}] = \int_0^\infty Ce^{-st}e^{-bt}dt = C\left(\frac{e^{-(s+b)t}}{-(s+b)}\Big|_0^\infty\right) = \frac{C}{s+b} \tag{A6.1-7}$$

Now since:

$$f(t) = C\cosh kt = C\left(\frac{1}{2}(e^{kt} + e^{-kt})\right)$$

and

$$f(t) = Csenhkt = C\left(\frac{1}{2}(e^{kt} - e^{-kt})\right)$$

we then have [20,21]:

$$L[C\cosh kt] = \int_0^\infty Ce^{-st}(\cosh kt)dt = \frac{Cs}{s^2 - k^2} \tag{A6.1-8}$$

and:

$$L[Csenhkt] = \int_0^\infty Ce^{-st}(senhkt)dt = \frac{Ck}{s^2 - k^2} \tag{A6.1-9}$$

Similarly [20,21]:

$$L[C\cos\omega t] = \int_0^\infty Ce^{-st}(\cos\omega t)dt = \frac{Cs}{s^2 + \omega^2} \tag{A6.1-10}$$

and

$$L[C\sin\omega t] = \int_0^\infty Ce^{-st}(\cos\omega t)dt = \frac{C\omega}{s^2 + \omega^2} \tag{A6.1-11}$$

In addition, [20,21]:

$$L\left[\frac{df}{dt}\right] = sF(s) - f(0) \tag{A6.1-12}$$

and [20,21]:

$$L\left[\frac{d^2f}{dt^2}\right] = s^2F(s) - sf(0) - f'(0) \tag{A6.1-13}$$

In the case of a partial derivative of the variable *t,* we will have [3]:

$$L\left[\frac{\partial f(x,t)}{\partial t}\right] = sF(x,s) - F(x,0) \tag{A6.1-14}$$

in which,

$$F(x,s) = \int_0^\infty e^{-st} f(x,t)\, dt.$$

In the case of a partial derivative of the variable, *x,* the Laplace transform will be [3]:

$$L\left[\frac{\partial f(x,t)}{\partial x}\right] = \frac{dF(x,s)}{dx} \tag{A6.1-15}$$

Similarly [20,21]:

$$L\left[\int_0^t f(\tau)d\tau\right] = \frac{F(s)}{s} \tag{6-1-16}$$

Another important result is the shifting theorem [20,21].

$$L[e^{-at} f(t)] = F(s+a) \tag{A6.1-17}$$

The Laplace transform of the unitary step function, which is a function that takes the value $u(t) = 1$ for $t > 0$, is:

$$L[u(t)] = \frac{1}{s} \tag{A6.1-18}$$

If the step function is delayed such that $u(t - T) = 1$, for $t > T$, then the Laplace transform will be:

$$L[u(t-\mathrm{T})] = \int_0^{\mathrm{T}} 0e^{-st}dt + \int_{\mathrm{T}}^{\infty} 1e^{-st}dt = \frac{e^{-\mathrm{T}s}}{s} \tag{A6.1-19}$$

Finally, it is necessary to define the inverse Laplace transform, L^{-1}, as [21]:

$$f(t) = L^{-1}\{F(s)\} = \frac{1}{2\pi i}\lim_{\omega\to\infty}\left[\int_{\sigma_0-i\omega}^{\sigma_0+i\omega} e^{st}F(s)ds\right] \tag{A6.1-20}$$

7 Amorphous Porous Adsorbents: Silica and Active Carbon

7.1 BASIC FEATURES OF AMORPHOUS SILICA

The study of silica materials has been a field of enormous interest for a long time, because this is an inert and very stable material [1]. Following the discovery of silica sols and gels in the 1920s and the invention of pyrogenic silica in the 1940s, finely dispersed and porous silica became a subject of intensive research [1–9]. Porous silica is one of the various forms of amorphous silica. It can be prepared by acidification of basic aqueous silicate solutions, and when reaction conditions are properly adjusted, porous silica gels are obtained [1]. If water is evaporated from the pores of silica hydrogels prepared in this fashion, porous xerogels are obtained [6,9]. Using this methodology, high-surface-area catalysts and catalyst supports, chromatographic stationary phases, and adsorbents are commercially prepared [6,9].

An alternative route for the production of amorphous silica involves the reaction of alkoxides with water. In this case [3], silicic acid is first produced by hydrolysis of a silicon alkoxide, formally a silicic acid ether. The silicic acids formed in this reaction can undergo either self-condensation or condensation with the alkoxide. The global reaction continues as a condensation polymerization to form high-molecular-weight polysilicates. These polysilicates then connect together to form a network, whose pores are filled with solvent molecules, that is, a gel is formed [3,9]. Hence the name sol-gel polymerization of alkoxides.

Other forms of silica, such as pyrogenic silica and mineral opals, are nonporous [8]. Pyrogenic silica is composed of silica particles with a very narrow particle size distribution. This material is obtained by vaporizing SiO_2 in an arc or a plasma jet, or by the oxidation of silicon compounds [7].

Artificial opals are materials characterized by the presence of SiO_2 microspheres. They are obtained by self-assembly methods (i.e., are periodically arranged forming close-packed structures) [10]. Artificial opals are colloidal "crystals." These materials have been the subject of numerous investigations. This enormous interest is mainly due to the interesting behavior imposed by the high order of the silica microspheres. In fact, these materials are dielectrics with periodic structures in which the refractive index varies in three dimensions (3D) [10].

7.2 AMORPHOUS SILICA MORPHOLOGY AND SURFACE CHEMISTRY

Silica is one of the most abundant chemical substances on earth; it can be either crystalline or amorphous. The crystalline forms of silica are quartz, critobalite, and tridymite [11]. The amorphous forms are precipitated silica, silica gel, colloidal silica sols, and pyrogenic silica [11]. Amorphous silicas play an important role in many different fields, since siliceous materials are used as adsorbents and for ultrafiltration membrane synthesis, catalyst, nanomaterials supports, and other large surface and porosity-related applications [1,4,6,9,12–16].

Porous silica is one of the different forms of amorphous silica. These materials can be prepared by acidification of basic aqueous silicate solutions, and when reaction conditions are properly adjusted, porous silica gels are obtained [1]. Sol-gel processing [3] specifies a type of solid materials synthesis method, performed in a liquid and at low temperature. The produced inorganic solids, mostly oxides or hydroxides, are formed by chemical transformation of chemical solutes termed precursors [3]. The solid is formed as the result of a polymerization process, which involves the establishment of M–OH–M or M–O–M bridges between the metallic atoms, M, of the precursor molecules [6].

The drying process, after the gel formation, is carried out at a relatively low temperature to produce a xerogel [6,13] (see Figure 7.1). During this thermal drying, or room-temperature evaporation, capillary forces provoke stresses on the gel. This effect raises the coordination numbers of the particles and produces collapse of the

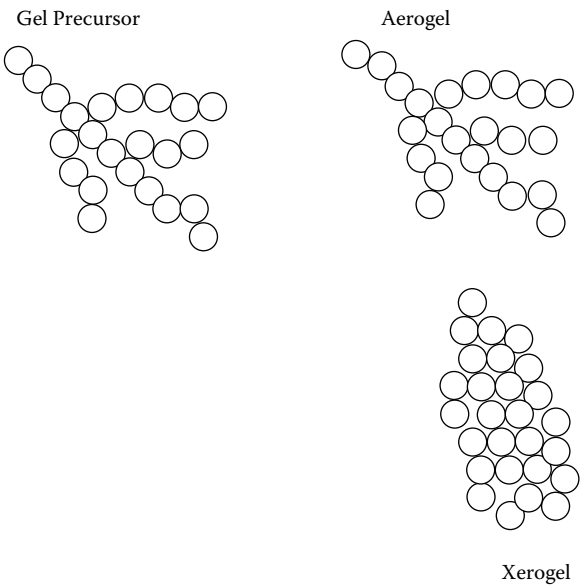

FIGURE 7.1 Formation of the aerogel and xerogel during the drying process.

network (i.e., particle agglomeration) [13]. In contrast, aerogels (Figure 7.1), namely, dried gels with a very high relative pore volume, are materials that are synthesized by traditional sol-gel chemistry, but which are dried, basically, by supercritical drying. As a result, the dry samples keep the porous texture, which they had in the wet stage [6]. The supercritical extraction of solvent from a gel does not induce capillary stresses, due to the lack of solvent-vapor interfaces [13]. Therefore, the compressive forces exerted on the gel network are significantly diminished relative to those created during formation of a xerogel [13]. Aerogels, consequently, retain a much stronger resemblance to their original gel network structure than do xerogels. Then aerogels are materials with lower apparent densities and larger specific surface areas than xerogels [13]. Porous xerogels and aerogels are used as catalysts, catalyst supports, chromatographic stationary phases, and adsorbents [6,9]. In the case of xerogels, there is no doubt that the amorphous framework is made up of very small globular units 10–20 Å in size. Commonly these particles are densely packed within secondary aggregates [6]. In the case of aerogels the structure is more open, and the primary particles are not densely packed [6].

Pyrogenic silica are nonporous materials, obtained by vaporizing SiO_2 in an arc or a plasma jet, or by the oxidation of silicon compounds [7]. This form of silica is composed of silica particles with a very narrow particle size distribution. Pyrogenic silica could be considered, from the standpoint of adsorption and electron microscopy, as consisting of discrete spheroidal particles with diameters 100–1000 Å. These particles are composed of even smaller particles with diameters of around 10 Å. The coordination between these small particles is so high that there is not a detectable micropore structure within the secondary globules [7].

Other forms of silica are mineral and artificial opals [8,10,17,18]. These are materials characterized by the presence of SiO_2 microspheres obtained by self-assembly methods [17–19]. The resulting material is periodically arranged, forming close-packed structures [10,17–19]. Artificial opals are colloidal "crystals," which have been the subject of numerous investigations. The enormous interest in artificial opals is mainly due to the interesting behavior imposed by the high order of the silica microspheres. In fact, these materials are dielectrics with periodic structures in which the refractive index varies in three dimensions (3D) [10].

Synthetic silica microspheres (Figure 7.2a), for synthetic opal preparation, can easily be obtained by using the Stobe-Fink-Bohn (SFB) method [2], which consists of two steps: the hydrolysis of tetraethyl orthosilicate (TEOS) in ethanol, methanol, n-propanol or n-butanol in presence of ammonia as catalyst, and the subsequent polymerization where the siloxane (Si–O–Si) bonds are formed. In this process, small nuclei with diameters of ca. 100–150 are formed, and subsequent growth of the silica particles takes place [2].

If the SFB process is modified [14–16], and the hydrolysis and condensation of tetraethyl orthosilicate (TEOS) is catalyzed, for example, by triethylamine (TEA), the amine will have a template effect and will cause the dispersion of silica particles through aggregation of inorganic–organic composite species. Consequently, the microsphere configuration will be lost (see Figure 7.2b), and the surface of the obtained silica will be increased [16].

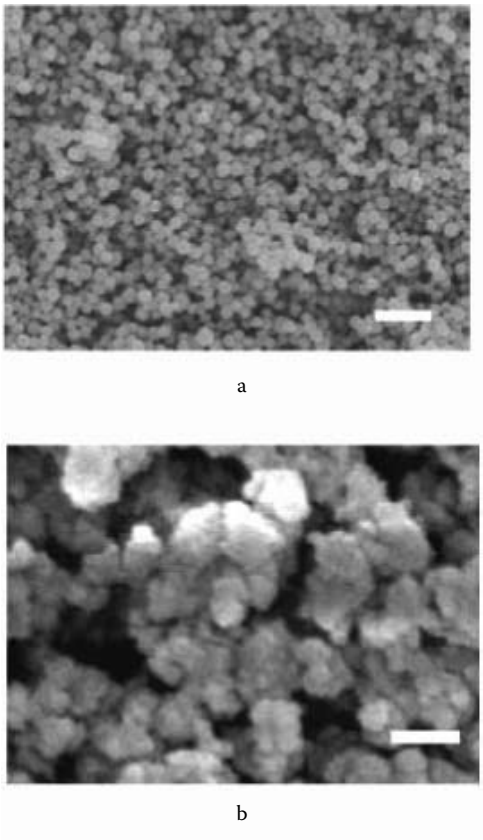

FIGURE 7.2 SEM micrographs of samples (a) 68C (Bar = 10,000) and (b) 70bs2 (Bar = 5000) [16].

The common points linking the different forms of silica are the tetrahedral silicon–oxygen blocks [11]. One of the Pauling ionic radius ratio rules affirms that, because

$$\frac{R(Si^{4+})}{R(O^{2-})}$$

is between 0.225 and 0.414, then silicon is tetrahedrically joined to oxygen in silica [20]. If the tetrahedral units are regularly arranged, periodic structures are developed, materializing the different crystalline polymorphs [20]. If the tetrahedra are randomly packed, with a nonperiodic structure, the various forms of amorphous silica are produced [1,11]. This random association of tetrahedra shapes the complexity of the nanoscale and mesoscale morphology of amorphous silica pore systems [21].

Any porous medium could be described as a tridimensional arrangement of matter and empty space, where matter and empty space are divided by an interface. In the case of amorphous silica, the complexity of that interface is virtually unlimited [21]. The morphological complexity of the interface is classified into three categories [21]:

1. At atomic and molecular level it is common to imagine a surface roughness.
2. At larger scales the notion of pore size and pore shape is very convenient.
3. At even larger scales the concept of pore network topology is valuable.

However, it is the author's opinion that, instead of a theoretical discussion of the possible morphologies, it is a better approach to experimentally study the morphology of the silica surface with the help of physical adsorption, and then, with the data obtained, calculate some very well-defined parameters, such as surface area, pore volume, and pore size distribution, as was previously explained (see Chapters 3 and 4). This line of attack should be complemented with a study of the morphology of these materials by scanning electron microscopy (SEM), transmission electron microscopy (TEM), scanning probe microscopy (SPM), or atomic force microscopy (AFM), and the characterization of their molecular and supra-molecular structure by Fourier transform infrared (FTIR) spectrometry, nuclear magnetic resonance spectrometry [NMR], thermal methods, and other methods.

The molecular properties of silica are strongly affected by the nature of their surface sites [22–28]. In sol-gel-synthesized porous silica surfaces the unsaturated surface valencies are satisfied by surface hydroxyl functionalities, which, depending on the calcination temperature, exist as: (a) vicinal (hydrogen-bonded silanols), (b) geminal (two hydroxyl groups attached to the same silicon atom), or (c) isolated (no hydrogen bonds possible) silanol sites (see Figure 7.3) [23,25,26].

The hydrogen-bond interaction of OH groups at the surface is determined by the Si–O–Si ring size and its opening degree, the number of hydroxyls per silicon site, and the surface curvature [3]. The concentration of OH groups at the surface is approximately $4–5 \times 10^{18}$ OH/m^2, and it is found to be almost independent of the synthesis conditions of porous silica [3]. These silanols are preferential adsorption sites for different molecules. As a result, surface hydroxyls are, indeed, particularly reactive with H_2O and other polar molecules such as NH_3, which are likely to be physically adsorbed to form a multiply hydrogen-bonded layer [3].

7.3 PRECIPITATED AMORPHOUS SILICA SYNTHESIS

Porous silica is one of the different forms of amorphous silica; it can be prepared by acidification of basic aqueous silicate solutions, and when reaction conditions are correctly adjusted, porous silica gels are obtained [1]. Silica gel can be synthesized by acidification of basic aqueous silicate solutions, as in the next reaction [1]:

$$Na_2SiO_3 + 2\ H^+ \overset{H_2O}{\Rightarrow} SiO_2 + H_2O + 2\ Na^+$$

As soon as the reaction requirements are correctly regulated, porous silica gels are obtained [1,9]. The reaction mechanism has two steps: silicate neutralization

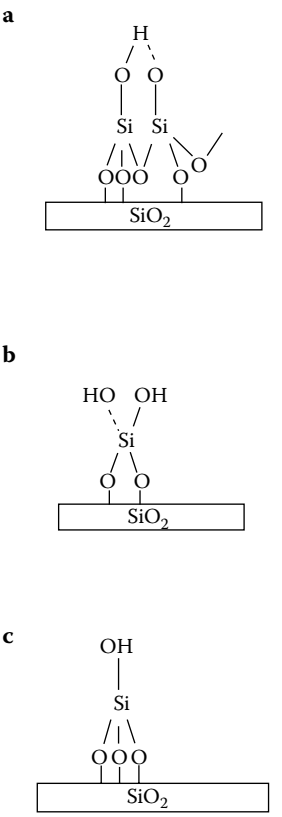

FIGURE 7.3 Schematic presentation of three types of silanol groups occurring on silica surfaces: (a) vicinal silanols, (b) geminal silanols, and (c) isolated silanols.

reaction producing silicic acids, followed by condensation polymerization of the silicic acids. If water is evaporated from the pores of silica hydrogels prepared in this fashion, porous xerogels are obtained [1,6]. Using this methodology, high-surface-area catalysts and catalyst supports, chromatographic stationary phases, and adsorbents are commercially prepared [1,6].

Sol-gel processing, as was formerly acknowledged, is a method of solid materials synthesis, performed in a liquid at low temperature (typically $T < 100°C$). The synthesized inorganic solids are formed by chemical transformation of chemical solutes termed precursors [6]. More specifically for silica synthesis, sol-gel processing refers to the hydrolysis and condensation of alkoxide-based precursors, such as tetraethyl orthosilicate (TEOS), $Si(OC_2H_5)_4$. The earliest examples of such reactions date to the nineteenth century [13]. However, sol-gel methods did not get broad attention until a methodology was created for preparing oxide films from sol-gel precursors in the late 1930s, which proved useful in the manufacturing of stained glass [13]

Other forms of silica, such as pyrogenic silica and mineral opals, are nonporous [8]. Pyrogenic silica is composed of silica particles with a very narrow particle size

TABLE 7.1
Batch Composition for the Synthesis of the Silica Microspheres by Means of the Hydrolysis of Tetraethyl Orthosilicate

Sample	TEOS [ml]	DDW [ml]	Meoh [ml]	Isoprop [ml]	NH_4OH [ml]
68F	0.75	0	30	0	3.0
80	1.5	0	30	0	6.0
81C	1.5	8.4	30	0	6.0
68C	1.5	4.5	30	0	6.0
69B	1.5	0.6	0	30	6.0
10	1.5	0.6	0	30	6.0
68E	2.4	0	30	0	6.0

spreading. This material is obtained by vaporizing SiO_2 in an arc or a plasma jet, or by the oxidation of silicon compounds [7]. Opals are materials characterized by the presence of SiO_2 microspheres. They are obtained by self-assembly methods (i.e., are arranged to form close-packed structures) [10].

Synthetic silica microspheres (Figure 7.2a) for synthetic opal preparation can easily be obtained by using the Stobe-Fink-Bohn (SFB) method [2]. The SFB method, as was previously stated, consists of the hydrolysis of $(Si(OC_2H_5)_4)$ in ethanol, methanol, n-propanol, or n-butanol, in the presence of ammonia as a catalyst. The batch composition for the synthesis of silica microspheres, by means of TEOS in an alcohol (methanol or isopropanol) in the presence of ammonia as a catalyst, and without double distilled water (DDW) in the synthesis media, is presented in Table 7.1.

In this case, the source materials for the synthesis were: tetraethyl orthosilicate (TEOS), DDW, methanol (MeOH), isopropanol, and ammonium hydroxide (40 wt. % NH_4OH in water). The batch preparation to carry out the synthesis following the recipes shown in Table 7.1 was as follows [2,14–16,29]:

1. Alcohol + catalysts (base) + DDW (if needed) (mixed with strong agitation).
2. TEOS is added to the reaction mixture.
3. The mixture is stirred at room temperature for 1.5 hours.
4. After the synthetic procedure the product is heated at 70°C during 20 hours.

Table 7.2 reports the microsphere diameter determined by SEM (D_{SEM}) of the materials synthesized following the above explained procedure, and Table 7.3 reports the BET-specific surface area, the DFT-pore volume, and the DFT-pore width mode, corresponding to the synthesized samples and the MCM-41 mesoporous material [14,15].

In addition, recently some modifications to SFB method were introduced to synthesize silica-based materials of remarkably high specific surface area [16,29]. To be precise, in some instances isopropanol was used as solvent and synthesis media. In some cases, DDW (double distilled water) was eliminated [14,15]. Also, amines dissolved in water or in a strong base were used as catalysts, instead of

TABLE 7.2
Microsphere Diameter Determined by Scanning Electron Microscopy (D_{SEM})

Sample	D_{SEM} [Å]
68F	500
80	2000
81C	2250
68C	2750
10	3750
68E	4500

TABLE 7.3
BET-Specific Surface Area (S), DFT-Pore Volume (W), and DFT-Pore Width Mode (d) Corresponding to the Synthesized Samples and the MCM-41 Mesoporous Material

Sample	S [m^2/g]	W [cm^3/g]	d [Å]
68F	625	1.18	81
80	440	0.49	39
81C	438	0.58	35
68C	320	0.46	21
69B	300	0.52	35
68E	18	0.04	61
MCM-41	820	1.69	35

Note: Relative error in reported data, 20%.

NH_4OH, in order to get materials of particularly high specific surface area [16,29]. The recipes used to synthesize these materials, also following the above explained procedure, are reported in Table 7.4 [16,29].

In Chapters 3 and 4 were reported, the micropore volume (W_{Mic}) (Table 3.6), the BET-specific surface area (S) (Table 3.7), the DFT-pore volume (W) (Table 4.3), and DFT-pore width mode (d) (Table 4.3) corresponding to the high-specific-surface silica samples synthesized using the recipes reported in Table 7.4 [16,29].

7.4 SILICA MODIFICATION

Silica samples contain a large concentration of silanols, which can be functionalized via simple elimination reactions [1,28,30–33]. This post-synthesis technique can be used to alter the pore size or affect the hydrophobicity of the pore wall [24]. As was

TABLE 7.4
Batch Composition for the Synthesis of the Silica by Means of the Hydrolysis of Tetraethyl Orthosilicate (TEOS) in an Alcohol (Methanol or Ethanol) in the Presence of an Amine as a Catalyst with and without DDW in the Synthesis Media

Sample	TEOS [ml]	DDW [ml]	NH_4OH [ml]	Amine [ml]	MeOH [ml]	EtOH [ml]	T [K]
70bs2	0.25	0	0	2	0	10	300
68bs1E	0.25	0	0	1	10	0	300
75bs1	0.35	0	0	2.5	10	0	300
79BS2	0.45	0	0	2.5	0	10	300
74bs5	0.35	2	0	2.5	9	1	300
68C	0.50	1.5	2	0	10	0	300

previously stated, the surfaces of silica are constituted by silanol groups that can be chemically modified. It is well known that the incorporation of hydrophobic terminal groups improves substantially the interaction with nonpolar molecules.

Binding of an organic functional group to a silica surface via a covalent bond is the most reliable method of alteration of the silica surface [28]. The covalent bond used for the binding is mostly the Si–O–Si bond, where one of the silicon atoms is on the silica surface, and the other comes from organosilicon compounds, and the Si–O–Si bond is formed by the reaction of an Si–OH group on the silica surface with the organosilicon compounds containing a leaving group of high reactivity on the silicon atom [28].

The organosilicon compounds most commonly used are those containing an alkoxy leaving group [28,31,33]. Halides and amino groups on the silicon atom have been also used for the Si–O–Si bond formation [30]. Unfortunately, these functional groups are so reactive toward hydrolysis that the silicon compounds cannot be handled under hydrolytic conditions or cannot be purified by silica gel chromatography [30].

One possible functionalization mechanism is shown in Figure 7.4. The organic additives should have a reactive alkoxysilane group that will serve to attach the molecule to silanol groups (–Si–OH) present on the silica surface [30].

On the other hand, many practical catalysts consist of one or several active components, deposited on a high-surface-area support [34]. Highly dispersed transition metal clusters supported on oxides, such as silica, have broad applications in many areas. Various of these areas are: heterogeneous catalysis, ceramics, and microelectronic devices [35,36]. Metals are widely used as catalysts. These catalysts are used for reforming, abatement of automobile emissions, oxidation, hydrogenation and other reactions [35–44]. Because the catalytic metal is often expensive, it is usually applied in finely dispersed form as particles on a high-surface-area support. In these circumstances a large fraction of the metals atoms are exposed to the reactant molecules [35,42]. The usual method for the metal preparation is the impregnation of a preformed support with metal precursors and subsequent calcinations and

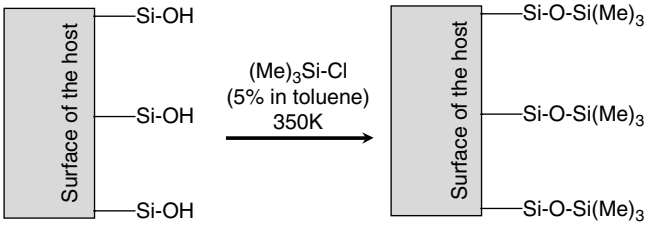

FIGURE 7.4 Functionalization mechanism where the organic additives have a reactive alkoxysilane group that serves to attach the molecule to silanol groups present on the silica surface.

reduction [34]. Heterogeneous catalysis by well-dispersed transition metal catalysts has widespread industrial applications.

7.5 FUNDAMENTAL CHARACTERISTICS OF ACTIVE CARBON

Activated carbons [45–57] are amorphous solid adsorbents that can be produced from almost all carbon-rich materials, including wood, fruit stones, peat, lignite, anthracite, shells, and other raw materials. The properties of the obtained active carbon will depend not only on the preparation method, but also on the starting raw material used for its production. Notwithstanding the great variety of accessible carbonaceous materials, lignocellulosic materials account for 47% of the total raw materials used for active carbon production [48].

The organic material is normally converted into activated carbon by carbonization (i.e., pyrolysis under inert atmosphere). This is followed by activation, specifically, heat treatment with an oxidizing agent, or by simultaneous carbonization and activation with a dehydrating compound [48]. These processes create a very large adsorption capacity, in some cases up to 3000 m^2/g, through the formation of an amorphous microporous structure, and so can yield high separation factors for some adsorbate mixtures [53]. Its unique adsorption properties result from its high-surface area, adequate pore size distribution, broad range of surface functional groups, and relatively high mechanical strength [45,49]. Consequently, porous carbonaceous materials are used routinely in many industrial processes for the removal of impurities from gases and liquids, including: gas separation and purification, vehicle exhaust emission control, solvent recovery, environmental technology, or for high-grade products [45,49]. They can also be used as a catalyst support [48].

In addition to their developed pore structure, small pore sizes, and large surface area, surface hydrophobicity is a very useful property of active carbon, [50–55]. The hydrophobicity, especially useful for sorption of organic species [56], is the result of the high density of carbon atoms in graphitelike sheets. Those sheets are spatially organized in such a way that small slit-shape pores are present in the bulk material. All of these factors significantly enhance the sorption capacity of carbons and their ability to remove contaminants and pollutants interacting with the surface of carbons in a dispersive way [57]. On the other hand, active carbon, as well as carbon, contains heteroatoms such as oxygen, and to a smaller degree, nitrogen and sulfur. These

atoms are bound to the activated carbon surface in the form of functional groups which are acidic or basic, providing the activated carbon surface an acidic or basic character [47,48]. The chemical heterogeneity of the carbon surface is mainly the result of the presence of heteroatoms [47].

7.6 ACTIVE CARBON MORPHOLOGY, SURFACE CHEMISTRY, AND SURFACE MODIFICATION

The structure of activated carbon consists of carbon atoms that are ordered in parallel stacks of hexagonal layers similar to graphite (see Figure 7.5) [58,59]. To be precise, graphite is formed of layer planes of sp^2 carbon atoms forming regular hexagons. That is, each carbon is bonded to the other three carbons by a σ bond, and the p_z orbitals containing one electron from a delocalized π bond [58–61]. The different layers are linked by van der Waals forces [58].

As was previously stated, numerous heteroatoms, including oxygen, hydrogen, nitrogen, phosphorous, and sulfur, can be found in the carbon matrix, in the form of single atoms and/or functional groups [60]. These atoms are chemically connected to the carbon atoms with unsaturated valences that are located at the edges of graphite basal planes [58,60].

Oxygen is the main heteroatom in the carbon matrix, and the occurrence of functional groups such as carboxyl, carbonyl, phenols, enols, lactones, and quinones has been suggested (see Figure 7.6 [48,56,61]). When specific interactions are taken into consideration, the chemical heterogeneity of the carbon surface caused by the heteroatoms [47] becomes an important factor. Those groups can be acidic, basic, or neutral, and their polarity depends on the nature of the main heteroatom and its position in the carbon matrix [47].

The most important and common groups influencing the surface and adsorption properties of activated carbon are functional groups containing oxygen, and their presence enhances the adsorption of polar species [57]. These surface groups can be produced during the activation procedure and can also be introduced subsequent to preparation by an oxidation treatment [48].

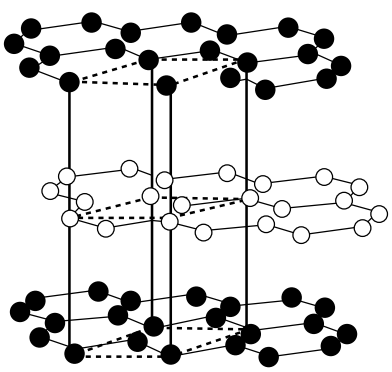

FIGURE 7.5 Structure of hexagonal graphite.

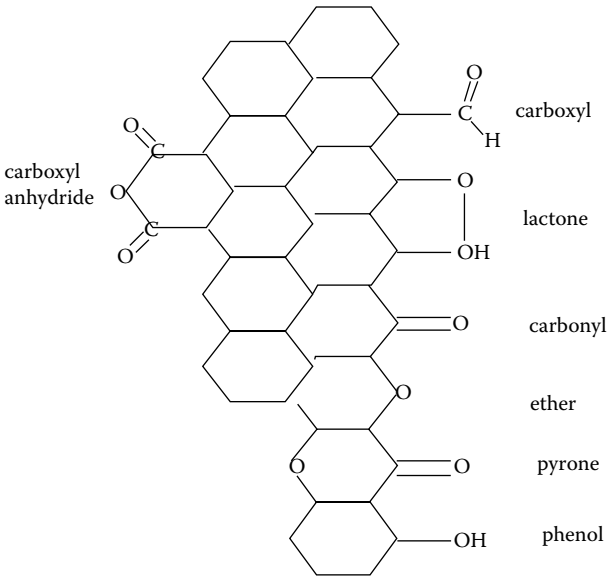

FIGURE 7.6 Most important classes of oxygen surface groups on a carbon surface.

The different types of oxygen functional groups determine the acidic and basic character of the carbon surfaces [47]. The acidic character is usually linked with surface complexes like carboxyl, lactone, and phenol, while the basic nature is usually assigned to surface groups such as pyrone, ether, and carbonyl [50].

Surface groups can be computed using a selective titration technique [55]. In classical titration, a solution of accurately known concentration, called a standard solution, is added gradually to another solution of unknown concentration, until the chemical reaction between both solutions is complete. In the surface titration method, a known quantity of the tested carbon is shaken in closed bottles containing 0.05–0.1 *N* solutions of a series of basic compounds possessing different strengths, such as: sodium bicarbonate ($NaHCO_3$), sodium carbonate (Na_2CO_3), sodium hydroxide (NaOH), and sodium ethoxide ($NaOC_2H_5$) [48]. This technique will allow a selective titration of the diverse surface oxygen groups, because a base with a specified pK_a will only neutralize the oxygen complexes with the same or lower pK_a [55]. Thus, by taking into consideration the pK_a of these bases and those of typical oxygen surface complexes, it can be expected that $NaHCO_3$, the weakest base in the selected group, will titrate exclusively carboxyl groups [56]. In addition, phenolic groups with a pK_a between 8 and 11, in addition to carboxylic groups, will react with the stronger base NaOH [48]. The groups with intermediate acid strength, including those of carboxylic and phenolic groups, can be measured by means of Na_2CO_3, because this base can neutralize lactone groups, together with carboxylic groups. Finally, $NaOC_2H_5$, the strongest base, is used to get information about all acidic groups, including those with very low acidity [48].

Our current knowledge indicates that adsorption of organic compounds by activated carbon is controlled by two major interactions [46]: physical interactions, which include size exclusion and microporosity effects, and chemical interactions, which include the chemical nature of the surface, the adsorbate, and the solvent. More specifically, for example, in liquid-phase adsorption, it has been established that the adsorption capacity of an activated carbon depends on the adsorbent pore structure, ash content, and functional groups [62–64], the nature of the adsorbate, its pK_a, functional groups present, polarity, molecular weight, and size [65–67], and finally, the solution conditions such as pH, ionic strength, and the adsorbate concentration [68,69].

Since surface functional groups affect adsorption properties and the reactivity of activated carbons, numerous methods, including heat treatment, oxidation, amination, and impregnation with various inorganic compounds, are available to modify activated carbons [46]. These alterations may change surface reactivity as well as structural and chemical properties of the carbon, which can be characterized using various methods, as described in detail elsewhere [56].

7.7 ACTIVE CARBON PRODUCTION METHODS

Generally, the starting materials used in commercial production of activated carbons are those with high carbon contents, such as wood, lignite, peat, and coal of different ranks [48]. However, in recent years, growing interest has shifted to the use of other low-cost, and profusely accessible agricultural by-products such as coconut shell, rockrose, eucalyptus kraft, lignin, apricot stone, cherry stone, and olive stone to be converted into activated carbons [70].

In general, there are two main methods for the preparation of activated carbons, specifically, physical and chemical activation methods. Physical activation consists of a two-step procedure, performed at high temperature (800–1000°C): carbonization under inert gas, normally nitrogen, and activation under oxidizing agents (as a rule, carbon dioxide, or water vapor) [48]. Chemical activation involves the treatment of the initial material with a dehydrating agent, such as sulfuric acid, phosphoric acid, zinc chloride, potassium hydroxide, or other substances, at temperatures varying from 400 to 1000°C, followed by the elimination of the dehydrating agent by meticulous washing [48].

An example of a concrete physical activation process is as follows [70]: the dried raw material is crushed and sieved to the desired size fraction. During carbonization, purified nitrogen at a convenient flow rate is used as the purge gas. The furnace temperature is increased from room temperature to 600°C and held at this temperature for about 3 h. The resulting chars are then activated at 500–900°C for 10–60 min under purified CO_2 flush at an appropriate flow rate. In both cases, a heating rate of 10°C/min could be applied. Figure 7.7 shows a flowchart for the diagrammatic explanation of the physical activation method [48].

A standard chemical activation process is as follows [48]: the dried raw material is crushed and sieved to the desired size fraction. Then the obtained powdered

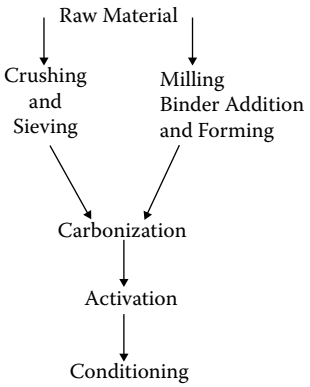

FIGURE 7.7 Flowchart for the schematic description of the physical activation method.

material is mixed with a concentrated solution of a dehydrating compound, for example, sulfuric acid. The mixture of powdered raw material and dehydrating agent is subsequently dried and heated under inert atmosphere, normally purified nitrogen, in a furnace whose temperature is increased from room temperature to 400–700°C, and held at this temperature for several hours. The resulting material is thoroughly washed in order to remove the activating agent. After that, the activated carbon is separated from the slurry, dried, and conditioned. Figure 7.8 shows a flowchart for the visual account of the chemical activation method [48].

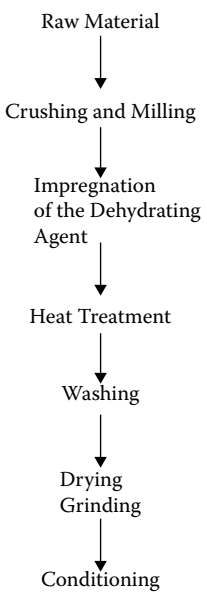

FIGURE 7.8 Flowchart for the schematic description of the chemical activation method.

7.8 SOME APPLICATIONS OF PRECIPITATED SILICA IN GAS PHASE ADSORPTION PROCESSES

Sorption operations used for separation processes imply molecular transfer from a gas or a liquid to the adsorbent pore network [71–84].

7.8.1 Adsorption of NH_3, H_2O, CO, N_2O, CO_2, and SH_2 in Precipitated Silica

In this section we will discuss some applications of silica in gas phase adsorption processes. As was formerly acknowledged, the silica gel surface is generally terminated with OH groups bonded with a silicon atom, SiOH units (i.e., silanols; see Figure 7.3) [23,25,26]. The concentration of OH groups at the surface is approximately 4–5 $\times$ 10^{18} OH/m^2, and it is found to be almost independent of the synthesis conditions of porous silica [3]. These silanol groups are particularly reactive with H_2O and other polar molecules, such as SH_2, CO, N_2O, CH_3Cl, CH_3F, HCl, and NH_3 among others [85–88]. These molecules are likely to be physically adsorbed to form a multiply hydrogen-bonded layer [3,85–88], because when a molecule contacts a solid surface, it becomes subjected to diverse energy fields characterized by different potentials. These include (see Chapter 2) [22,77,89]:

1. dispersion (ϕ_D), repulsion (ϕ_R)
2. polarization (ϕ_P), field dipole energy ($\phi_{E\mu}$), field gradient quadrupole energy (ϕ_{EQ})
3. sorbate–sorbate interaction energy (ϕ_{AA})
4. acid-base interactions (ϕ_{AB}) if the surface contains hydroxyl sites

Dispersion and repulsion are the fundamental forces present during the adsorption of nonpolar molecules in silica, because the dipole moment of this molecule is null, the quadrupole moment is very low, and interactions with the hydroxyl groups do not exist. In the case of polar molecules, dispersion and repulsion interactions are present. However, specific interactions between the silica surface and polar molecules, such as the dipole interaction and interactions with hydroxyl groups [85–88], are responsible for a more intense interaction of the silica surface with polar molecules in comparison to nonpolar molecules [22].

For NH_3 adsorption, the experimental evidence has shown that the main interaction mechanism is hydrogen bonding of SiOH to the N atom in NH_3 [85]. That is, the surface complex shows the features of the hydrogen bonding between the isolated hydroxyl groups and the N atom of the ammonia molecule [86]. The ammonia molecule readily adsorbs, almost entirely and reversibly, on dehydrated silica samples [86]. In addition, the molar heats of adsorption of NH_3 on highly dehydrated amorphous silica samples have been measured by means of calorimetric experiments as averaging around –40 kJ/mol [87]. This is a considerable molar adsorption heat, which indicates a strong interaction between the NH_3 molecule and the silica surface.

Ammonia gas is one of the most widely used chemicals in the industry, and it has to be removed to less than one ppm, for example, from the gaseous effluents of ammonia, fertilizers, urea plants, and other sources [90]. It is evident that silica is a good adsorbent of NH_3 [85–87]. Adsorption of ammonia on silica gel has also received considerable interest recently because of its potential use in solar energy cooling cycles [91].

In the case of H_2O, CO, and N_2O, the experimental evidence has shown that the main interaction mechanism is also hydrogen bonding of SiOH to the C end of CO, to the O end of N_20, and to the 0 atom in H_20 [85]. Due to these properties, silica gels could serve as good adsorbents for water vapor and pollution gases. Specifically, zeolites and silica gels are the most common drying adsorbents today, exhibiting adsorption capacities of water vapor around 0.3 to 0.4 kg of water/kg of adsorbent [92].

Another possible application of silica is hydrogen sulfide and carbon dioxide adsorption. The removing process of acidic gases such as carbon dioxide and hydrogen sulfide from natural gas is, as a rule, called "sweetening" and is a significant step in natural gas processing. The "sweetening" of crude natural gas (i.e., the removal of acidic gases such as carbon dioxide, and hydrogen sulfide) is an important process in the natural gas industry [93,94]. Usually, this sweetening is carried out by gas–liquid absorption–stripping procedures by means of aqueous solutions of alkanolamines. However, this gas absorption method is extremely energy intensive for regeneration of the solvents and is also overwhelmed by corrosion problems [94]. Chemical adsorption of SH_2 on ferrous oxide is also applied; however, the adsorbents used for chemical adsorption cannot be regenerated, a fact that causes environmental problems [93].

Sweetening by physical adsorption allows regeneration of the adsorbent [93,95]. But sweeping of the adsorbent bed with a hot stream is required, which increases the cost of energy and investment on heating facility [93]. As the need for natural gas has increased in recent years, the requirement has arisen for the development of an efficient technique for acid gas elimination with lower economic costs [94]. The development of solid adsorbents which could be regenerated and which possess high selectivity for acidic gases and high adsorption capacity is a possible option for natural gas purification. Such materials are more environmentally benevolent and easier to deal with. In addition, they can be regenerated under mild conditions and are thus more energy efficient [94]. Hypothetically, many solid materials are potential sorbents for carbon dioxide and hydrogen sulfide; for example, activated carbon and zeolites have been the most widely used solid sorption materials. However, the industrial application of these materials as acidic gas adsorbents is limited, because of the low selectivity toward acidic gases for activated carbon and a strong water inhibition effect for zeolite and silica materials [94].

However, by attaching functional groups onto the pore walls of silica it is possible to modify the surface and then develop a selective adsorbent for acidic gas (CO_2 and H_2S) removal from natural gas mixtures [94]. It was recently reported that the adsorption of CO_2 and H_2S on amine-surface-modified silica xerogels show that this modified silica is an excellent adsorbent for selective removal of CO_2 and H_2S from natural gas [94].

The idea of attaching functional groups onto the pore walls of silica is a known strategy for the design of promising new adsorbents and catalysts [27,28]. Recently

the adsorption of CO_2 and H_2S on amine-surface-modified silica xerogels was reported, and the results show that this modified silica is an excellent adsorbent for selective removal of CO_2 and H_2S from natural gas [95].

7.8.2 Application of Precipitated Silica in Hydrogen Storage

It is the author's view that another possible application of NH_3 adsorption in silica is hydrogen storage. In the general case, this process is the confinement of hydrogen for delivery and use, which involves tanks for both gases and liquids at ambient and high pressure and includes reversible and irreversible systems [96–98]. In the past two decades, interest has been growing in the development of transportable reversible systems for high-capacity hydrogen storage, which is critical to the large-scale application of hydrogen fuel cells, in particular for mobile applications [96,98]. New techniques for storing hydrogen more effectively could accelerate the pace of the transition to the hydrogen economy dramatically [98]. Consequently, new methods of hydrogen storage must be considered [96–98]. A very promising method of storage is by physical adsorption of molecular hydrogen on different materials (i.e., carbon, silica, alumina, or zeolites) [97].

To date, the focus in hydrogen storage has mostly been on liquid hydrogen, and also on metal hydride systems [96,98]. Liquid hydrogen is the basic fuel choice for various hydrogen-fueled cars. However, this is very dangerous, energy intensive, and requires a big tank volume [96]. The interstitial hydride method suffers from high cost and weight [96]. The noninterstitial hydride methods have different problems such as instability, in some cases [96], and reversibility control to regenerate the material used in other cases [96]. In addition, both the liquid hydrogen and hydride methods have low energy efficiency [97]. Higher energy efficiency is achievable with systems in which hydrogen is concentrated by physical adsorption, above 70 K, using a suitable adsorbent [97]. Pursuing this objective, activated carbons have been studied with promising results [48]. Much excitement has arisen on recent reports on the use of carbon nanotubes [99], but because of further research, the obtained results have become questionable [97]. Zeolites, silica, and alumina have been also studied; however, the adsorption results are nowhere near the target figure of 6.5 wt. % [97].

The criteria for the ideal solid hydrogen storage systems for practical applications are [96]:

1. high storage capacity, i.e., a minimum of 6.5 wt. %
2. reversibility of uptake and release
3. low cost
4. low toxicity
5. nonexplosive
6. inertness

As an interesting alternative, one could envision hydrogen storage by physical adsorption of ammonia in optimized extremely high-specific-surface silica materials recently developed [16,29]. The first criterion for the ideal solid hydrogen system indicates that only light elements such as Li, Be, B, C, N, O, F, Na, Mg, Al, Si, and

P can be included in the solid storage system [96]. Consequently, silica (SiO_2) could be considered for these purposes. Moreover, silica is nontoxic, nonexplosive, inert, and inexpensive, and ammonia adsorption on silica is highly reversible [90]. Therefore, as an interesting alternative, one could envisage hydrogen storage by physical adsorption of NH_3 in micro/mesoporous silica particle packing materials [16,29], where the accumulated NH_3 could be decomposed into H_2 and N_2 using, for instance, Ir catalysts [98].

Recently obtained silica particle-packing materials show extremely high specific surface area, i.e., up to 2,200 m^2/g [29]. Now, the hydroxyl concentration in the surface of silica adsorbents is $4.5 \pm 0.5 \times 10^{18}$ OH/m^2 [3]; therefore, 9.9×10^{22} OH/g will be present in the surface of such extremely high-surface-area silica materials, if an adsorption proportion of one NH_3 per OH is predicted. Thus, 0.44 gram of H adsorbed per gram of silica will be obtained in the surface of the silica materials, or 31 wt. %. This is a huge quantity, far larger than the goal of 6.5 wt. %. However, in practice this will not be the case. Taking into consideration real data reported for NH_3 adsorption in silica materials [90], it is feasible to anticipate that at least 0.09 gram, or 8.3 wt. % of H per gram of silica will be stored in the extremely high-specific-surface area materials. This is also a considerable amount, above the present estimates of H storage for transportation purposes which, as was previously stated, is 6.5 wt. %.

Now, it is necessary to state (and previously commented), that extremely high surface area silica are generally unstable. Then these materials in the course of time reduce their surface area because the particles forming the xerogel coalesce. However, even in this case, the adsorption of NH_3 will be very high according to our preliminary data [100].

7.8.3 Adsorption of Volatile Organic Compounds (VOCs) in Precipitated Silica

Volatile organic compounds (VOCs) are among the most widespread air pollutants released by chemical, petrochemical, and related industries [48,101,102]. Volatile organic compounds (VOCs) can be defined as those possessing a vapor pressure greater than 133.3 Pa (1 mm Hg) at room temperature [102]. Benzene, toluene, xylenes, hexane, cyclohexane, thiophene, diethylamine, acetone, and acetaldehyde are examples of VOCs [48]. VOCs are crucial reactants involved in photochemical reactions happening in the atmosphere, which lead to severe environmental hazards [101]. A considerable quantity of VOCs can be emitted in processes such as drying, gluing, and coating using solvents, perfume, and fabrics. The VOCs of oxygenated hydrocarbons are emitted significantly in the printing, painting, and solvent industries [102]. Adsorption processes give a method for removing VOCs from the air. Activated carbon, silica gel, and zeolite are common adsorbents used to attain VOC reduction in industry [48,102–105]. Among VOCs, benzene derivatives are particularly dangerous to the environment and human health; therefore strict control of VOC emissions is one of the chief purposes of government regulations introduced under, for example, the 1990 USA Clean Air Act Amendment [103].

Some VOC pollution sources are [46,48,102]:

1. automobile exhaust emissions due to incomplete hydrocarbon combustion (aromatics, olefins, and paraffins)
2. vapor releases associated to the paint, dye, lacquer, and varnish industries (alkanes and cycloalkanes)
3. gas fumes given off from storage tanks
4. solvent vapors emanating from paints as well as from liquids utilized in cleaning or degreasing operations (hexane, cyclohexane, and aromatic compounds derived from toluene and xylene)
5. adhesives (methyl ethyl ketones, naphtha type derivatives, trichororoethane)
6. aerosols
7. discharges originated by plastic industries (chlorinated compounds)

It is also relevant to state that adsorption processes represent an important alternative to eliminate VOCs from process gas streams [106]. In industrial applications numerous microporous solids are frequently used as selective adsorbents, owing to the physicochemical specificity benefits these materials offer. In contrast to normal mesoporous adsorbents, adsorbents of these selective properties include activated carbons, zeolites, and microporous silica [8,103].

Owing to their environmental connotation, the elimination of VOCs from a bulk gas stream by an adsorption process is an ordinary engineering procedure that has been getting growing consideration during the last years [103,107,108]. Among adsorbents potentially helpful for effective VOC removal, microporous inorganic materials represent one of the best alternatives to carry out this job [103]. At present, the most extensively used adsorbent for environmental cleaning is high-surface-area activated carbon [48]. In general, activated carbon has a high affinity for volatile organic compounds, owing to the nonpolar character of its surface, in contrast to other solid sorbents [48,102,103]. However, this material presents certain drawbacks, including the fact that the adsorbed molecules are very often not destroyed, or decomposed, but instead are merely weakly held at the surface [109]. Owing to the polar surface of silica gel, it adsorbs molecules from the gas phase and keeps them on the surface. Subsequently, a systematic evaluation of the adsorption capacities of organic vapors on silica gel was started in the late 1980s [102]. For this reason, it is worth trying to investigate the performance of silica microporous adsorbents, which can have stronger interactions toward the adsorbed molecules [103].

7.9 SOME APPLICATIONS OF ACTIVATED CARBONS AND OTHER CARBONACEOUS MATERIALS IN GAS-PHASE ADSORPTION PROCESSES

7.9.1 Adsorption of H_2O and CO_2 and Removal of SH_2 and SO_2 with Active Carbon

Activated carbons are the most extensively applied adsorbent for the elimination of contaminants from gaseous, aqueous, and nonaqueous streams. The adsorptive

properties of activated carbons are determined by their porous structure and their surface chemical properties. The largely nonpolar character of the carbon surface causes activated carbon to selectively adsorb nonpolar rather than polar molecules [48]. In order to properly apply these adsorbents, like any other ones, equilibrium adsorption isotherms are used to calculate the optimum size of the adsorbent bed and its operating conditions [110,111].

For gas-phase applications, carbon adsorbents are usually used in the shape of hard granules, hard pellets, fiber, cloths, and monoliths, since these prevent an extreme pressure drop [48].

A subject that has come under growing study in recent years is the interaction between water vapor and activated carbon [112]. The adsorption of water molecules on carbon surfaces is a phenomenon that is relevant to a wide variety of commercial processes [113]. In active carbon uses (for example, VOC elimination from humid air streams, and steam regeneration of activated carbon), adsorption of water vapor has been found [112]. Formerly, this fact was disregarded, or looked upon as an inconvenience. However experimental observations have revealed that the condensation and subsequent adsorption of water have a significant effect on the operation of adsorbers and cannot be ignored [112]. Carbon-supported platinum catalysts used in fuel cells are affected by the presence of water vapor [114]. Adsorption of water on carbon is reported to augment platinum use, thus permitting increased fuel cell efficiency [115]. In adsorption applications, the existence of water is supposed to increase the storage of methane in activated carbon [116]. Nevertheless, unfavorable effects, such as by reduced breakthrough times and lower production rates, have been found in commercial air separation processes that utilize carbon molecular sieves [117,118].

Regardless of the significance to these commercial applications, the basic understanding of water adsorption in carbon is still elementary [22]. Existing theories connect surface chemistry and structure of carbon to water adsorption affinity [22]. Carbon adsorbents are composed of misaligned aromatic platelets that form a nanoporous network in which oxygenated functional groups are contained [48,119]; then the oxygenated functional groups form primary sites for the adsorption of water [120]. At very low relative pressures, the polar character of the water molecule permits it to bond with individual oxygenated functional groups. Henry's law is followed at very low pressures, and the quantity of water adsorbed is established by the total amount of primary adsorption sites [114]. At greater relative pressures, hydrogen bonding among free and adsorbed water molecules takes place, and the development of clusters begins. At even greater relative pressures, water clusters enlarge, and hydrogen bonding between clusters happens [114]. The characteristics of the resultant equilibrium isotherm is dependent, not merely on the total amount of primary adsorption sites, but also on their surface density [121,122]. As a conclusion, it is possible to affirm that the presence of water in activated carbons has a large effect on the performance of industrial adsorbers, often reducing their useful lifetime by as much as 50% [123].

Carbon dioxide adsorption in activated carbon could be used for characterization purposes [49]. As previously discussed (see Chapters 3 and 4), N_2 at 77 K is the generally used gas for the characterization of porous solids and, typically, has

the special status of recommended adsorptive. Nevertheless, the most important inconvenience of N_2 adsorption at 77 K is that, when it is used for the characterization of microporous solids, diffusional problems of the molecules inside the narrow porosity range (size < 0.7 nm) take place [124]. In addition, there is a supplementary experimental problem in the adsorption of subcritical nitrogen, as very low relative pressures are necessary to extend the range of porosity studied to narrow microporosity [49]. To surmount these problems, the use of new adsorptives has been proposed. In adsorption studies it has been shown that a good option to complement N_2 adsorption could be the use of CO_2 adsorption at 273 K [125]. While the critical dimension of the CO_2 molecule is comparable to that of N_2 the higher temperature of adsorption used for CO_2 results in a larger kinetic energy, enabling the molecules to enter into the narrow porosity [49]. However, the high vapor pressure of carbon dioxide at 273 K requires the use of high-pressure adsorption apparatus in order to cover the same range of relative pressure as in the case of N_2 at 77 K [49].

On the other hand, commercial CO_2 capture technology that exists today is very expensive and energy intensive [126]. Pressure swing adsorption (PSA) is one of the possible methods that could be pertinent for elimination of CO_2 from gas streams [126]. PSA procedures are founded on favored adsorption of the desired gas (e.g., CO_2) on a porous adsorbent at high pressure and recuperation of the gas at low pressure [127–129]. Consequently, the porous sorbent can be reused for subsequent adsorption [127,128]. Development of restorable adsorbents that have elevated selectivity, high adsorption capacity, and high desorption rate for CO_2 adsorption/desorption is significant for the success of the PSA process [126]. Activated carbon showed preferential adsorption of CO_2 at 25°C and pressures up to 300 psi, and the adsorption of CO_2 was found to be reversible [126]. Excellent separation of CO_2 was obtained from gas mixtures containing both CO_2/N_2 and CO_2/H_2 utilizing activated carbon during competitive gas adsorption studies performed with a microreactor [126].

In the majority of applications of activated carbons as adsorbents of vapors and gases, contaminants are removed due to an enhanced adsorption potential in small pores of carbons [50,120]. In those pores the adsorbed molecules are stored, gradually decreasing the capacity of adsorbents and the efficiency of their performance [130]. In the case of hydrogen sulfide removal from air using activated carbons, H_2S is not only adsorbed, but it is also oxidized due to the catalytic effect of the carbon surface [131–133]. Elemental sulfur and sulfuric acid are the main products of surface reactions [133]. The spent carbons have to be replaced by the fresh materials. A regeneration process, if feasible, has to be done *in situ* [130]. Applying excess water or steam to the carbon bed is the regeneration method of the spent carbon adsorbent [130].

The removal of SO_2 with active carbon is similar to SH_2 elimination with carbon, since the reaction of SO_2 with carbon in the presence of O_2 and H_2O at relatively low temperatures (20–150°C) involves a series of reactions that leads to the formation of sulfuric acid as the final product [134].

The overall reaction is [134]:

$$SO_2 + ½O_2 + H_2O + C \rightarrow C{-}H_2SO_4.$$

7.9.2 Hydrogen Storage with Active Carbon and other Carbonaceous Materials

As was previously commented, a secure, effective, and inexpensive storage system is vital for the upcoming utilization of hydrogen as energy carrier. The established techniques (for example, liquid hydrogen, compressed gas, and the storage in a solid-state matrix as a metal hydride [96]) have the advantage of being safe, but fail because of the total weight of the tank system [135]. Consequently carbon, with its low atomic weight, could help to surmount these drawbacks [97,135–140].

In contract to the chemisorption in metal hydrides, microporous carbon adsorbs the undissociated hydrogen molecules by van der Waals forces at its pore network and surface. However, as these binding forces are weak, thermal motion interferes with the physisorption process at room temperature. Consequently, to store large amounts of hydrogen the carbon samples have to be cooled [135]. But, a cryogenic hydrogen storage method is, in the majority of cases, economically unsuccessful [137].

In recent years, the storage of hydrogen in carbon has involved consideration due to the accessibility of novel carbon nanomaterials, such as, fullerenes, nanotubes, and nanofibers [97,135]. The cylindrical structure of carbon nanotubes could increase the adsorption potential in the tube core, leading to capillary forces and to enhanced storage capability [99,135]. However, notwithstanding the optimism raised with the reports on the use of carbon nanotubes [99] and carbon nanofibers [138], the obtained results have become questionable, owing to further research [97]. Thus, with the study of hydrogen storage in carbonaceous materials, with the current type of carbonaceous adsorbents and sorption conditions, a maximum uptake of 2.1 wt. %, has been observed, significantly below the DOE figure target of 6.5 wt. % for mobile applications [97].

A new type of carbonaceous porous materials, called mesocarbon microbeads (MCMBs), are microcarbon spheres produced by mesophase pitches. These materials have been principally used as filler in paints, elastomers, and plastics to change the mechanical and electrical properties of the materials [53]. Activated MCMBs (a-MCMBs) with high specific surface area greater than 3000 m^2/g can be prepared. This type of MCBs is called super-high-surface-area carbons, or super surface carbons [53]. Many investigations show that a-MCMBs are expected to be more ordered in structure than the activated carbon fibers (ACF), and the calculations show that the adsorption amount of hydrogen at 10 MPa can reach 3.2 wt. %, and 15 wt. % at 298 K, and 77 K, respectively, which are also higher scores, compared with the other carbon materials [53].

7.9.3 Methane Storage in Activated Carbon and Other Carbonaceous Materials

During recent years the interest in natural gas as a vehicular fuel has increased significantly, since natural gas has important benefits over standard fuels, both from an environmental point of view and for its natural abundance [48]. However, it is recognized that its great inconvenience is its lower heat of combustion per unit of volume, when compared with usual fuels [141]. Another motive for this growing

interest is for the reason that natural gas is much cheaper than usual petroleum-based gasoline, and diesel fuel [142]. Consequently, the attention of different countries in diminishing their dependence on imported oil has been directed to the creation of new technologies to facilitate the employ of other fuels, such as natural gas, to meet their transportation energy needs [142,143].

Regrettably, methane cannot be stored at a density as high as other fuels. As a result, methane (as compressed natural gas [CNG] at 24.8 MPa) has an energy density about one-third that of gasoline [48,143]. In addition, the use of CNG has some disadvantages, for example the high cost of the used cylinders [144].

Among other options, the employ of adsorbents (adsorbed natural gas, or ANG) has been thought to be a way for obtaining methane densities comparable to CNG, but at much lower pressure (3.5–4 MPa) [48,142,144–147]. This lower storage pressure reduces the cost of the storage vessel, allows the use of single-stage compressors, and represents a lesser safety hazard than the higher pressures used for CNG [48,143,144]. The U.S. Department of Energy storage goal for ANG has been set at 150 V/V (150 STP liters of gas stored per liter vessel volume, where STP conditions are: pressure, P = 101.325 kPa, and temperature, T = 298 K) [142]. Among the available adsorbents, activated carbons exhibit the largest adsorptive capacity for methane storage [48, 145,148]. The recent growth of high-capacity carbonaceous adsorbents has generated a great amount of literature, showing the fast increase and significance of the area under discussion [48,142–153], indicating that activated carbons are very good adsorbents, presenting the highest ANG energy densities [142–144,146].

Methane storage in activated carbon fibers (ACFs) [142, 146] and chemically activated carbons prepared from an anthracite [142] have shown that these adsorbents can meet the above-mentioned DOE target presenting quite high storage capacities. In addition, the amount of methane adsorbed in mesocarbon microbeads (MCMBs), at 298 K, and 4 MPa, could reache 36 wt. %, a huge figure [53,154].

7.9.4 Adsorption of Volatile Organic Compounds (VOCs) in Activated Carbon

As was before stated, volatile organic compounds (VOCs) are among the most widespread air contaminants released by chemical, petrochemical, and other industries. Benzene, toluene, xylenes, hexane, cyclohexane, thiophene, diethylamine, acetone, and acetaldehyde are examples of VOCs [48]. Control of air emissions of organic vapors is one of the primary objectives of the stringent regulations introduced under the Clean Air Act amendments [48,155,156]. One of the most formidable challenges posed by the increasingly stringent regulations on air pollution in many countries is the search for efficient and economical control strategies for volatile organic compounds (VOCs) [157]. There are several methods, such as condensation, absorption, adsorption, contact oxidation, and incineration, for removal and/or recovery of organic vapors [48,155,156]. However, the most presently relevant technology for VOC control is adsorption on activated carbon [48,156,158–167]. It is a well-known technology, broadly used in industrial processes for the elimination and recovery of hydrocarbon vapors from gaseous streams [48,155,156]. In addition, it

offers several benefits over the others, i.e., the opportunity of pure product retrieval for reuse, high removal efficiency at low inlet concentrations, and low fuel/energy costs [155].

One of the major uses of activated carbon is in the recovery of solvents from industrial process effluents. Dry cleaning, paints, adhesives and polymers manufacturing, and printing are some examples, since, as a result of the highly volatile character of many solvents, they cannot be emitted directly to the atmosphere [156]. Typical solvents recovered by active carbon are acetone, benzene, ethanol, ethyl ether, pentane, methylene chloride, tetrahydrofuran, toluene, xylene, chlorinated hydrocarbons, and other aromatic compounds [48]. Automotive emissions make a large contribution to urban, and global air pollution [156]. Some VOCs and other air contaminants are emitted by automobiles through the exhaust system, and also by the fuel system [48]. Activated carbons are used to control these emissions [48,156].

7.9.5 Air-Conditioning with Activated Carbon

Growing public alertness and general alarm over air quality have produced a need for enhanced treatment of the air that is supplied to public spaces like airports, hospitals, theaters, and office blocks [156]. Therefore, granular activated carbon filters have been developed in combination with air-conditioning systems for the elimination of harmful traces contaminants from air [156]. On the other hand, the construction of adsorption refrigerating machines constitutes another application of these materials which is currently undergoing rapid development [168]. Both the operational principle and the first commercial applications of the adsorption refrigerating cycle were developed several years ago [169]. However, this technique of cold production was abandoned for the advantage of the gas compression cycle [168]. Nevertheless, the study of adsorption refrigerating cycles has been encouraged by new regulations on the use of chlorofluorocarbons (CFCs); these can be found in the Montreal Protocol edited in 1987, and in the new amendments made during the London Conference in 1990 [168].

There are many possibilities for utilization of an adsorption cycle covering a great range of temperatures, for instance, refrigeration and ice making from solar energy [170]. From the fundamental discontinuous cycle, numerous procedures were projected to permit, on the one hand, for pseudocontinuous cold production and, on the other hand, enhancement in the efficiency of the adsorption systems [168].

REFERENCES

1. Iler, R.K., *The Chemistry of Silica,* J. Wiley & Sons, New York, 1979.
2. Stobe, W., Fink, A., and Bohn, E., *J. Colloids Interface Sci.*, 26, 62, 1968.
3. Brinker, C.J. and Scherer, G.W., *Sol-Gel Science,* Academic Press, New York, 1990.
4. Unger, K. and Kumar, D., in *Adsorption on Silica Surfaces,* Papirer, E., Ed., Marcel Dekker Inc., New York, 2000, p. 1.
5. Burda, C., Chen, X., Narayanan, R., and El-Sayed, M.A., *Chem. Rev.*, 105, 1025, 2005.
6. Pierre, A.C. and Pajonk, G.M., *Chem. Rev.*, 102, 4243, 2002.

7. El Shaffey, G.M.S., in *Adsorption on Silica Surfaces,* Papirer, E., Ed., Marcel Dekker Inc., New York, 2000, p. 35.
8. Hernandez, M.A., Velazquez, J.A., Asomoza, M., Solis, S., Rojas, F., Lara, V.H., Portillo, R., and Salgado, M.A., *Energy Fuels,* 17, 262, 2003.
9. Barton, T.J., Bull, L.M., Klemperer, G., Loy, D.A., McEnaney, B., Misono, M., Monson, P.A., Pez, G., Scherer, G.W., Vartulli, J.C., and Yaghi, O.M., *Chem. Mater.*, 11, 2633, 1999.
10. Yang, S.M., Miguez, H. and Ozin, G.F., *Adv. Funct. Mater.*, 11, 425, 2002.
11. Persello, J., in *Adsorption on Silica Surfaces,* Papirer, E., Ed., Marcel Dekker Inc., New York, 2000, p. 297.
12. Soler-Illia, G.J.A.A., Sanchez, C., Lebeau, B., and Patarin, J., *Chem. Rev.*, 102, 4093, 2002.
13. Cushing, B.L., Kolesnichenko, V.L., and O'Connor, C.J., *Chem. Rev.*,104, 3893, 2004.
14. Roque-Malherbe, R. and Marquez-Linares, F., *Mat. Sci. Semicond. Proc.*, 7, 467, 2004.
15. Roque-Malherbe, R. and Marquez-Linares, F., *Surf. Interf. Anal.*, 37, 393, 2005.
16. Marquez-Linares, F. and Roque-Malherbe, R., *J. Nanosc. Nanotech.*, 6, 1114, 2006.
17. Miguez, H., Messeguer, F., Lopez, C., Mifsud, A., Moya, J.S., and Vazquez, L., *Langmuir,* 13, 6009, 1997.
18. Messeguer, F., Miguez, H., Blanco, A., and Lopez, C., *Recent. Res. Devel. App. Phys.*, 2, 327, 1999.
19. Garcia-Santamaria, F., Miguez, H., Ibiste, M., Meseguer, F., and Lopez, C., *Langmuir,* 18, 1942, 2002.
20. Porterfield, W.W., *Inorganic Chemistry: A Unified Approach,* Academic Press, New York, 1993.
21. van Damme, H., in *Adsorption on Silica Surfaces,* Papirer, E., Ed., Marcel Dekker Inc., New York, 2000, p. 119.
22. Rouquerol, J., Rouquerol, F., and Sing, K., *Adsorption by Powder and Porous Solids,* Academic Press, New York, 1999.
23. Morrow, B.A. and Gay, I.D., in *Adsorption on Silica Surfaces,* Papirer, E., Ed., Marcel Dekker: New York, 2000, p 9.
24. Goworek, J., in *Adsorption on Silica Surfaces,* Papirer, E., Ed., Marcel Dekker: New York, 2000, p 167.
25. Duchateau, R., *Chem. Rev,* 102, 3525, 2002.
26. Vansant, E.F., van der Voort, P., and Vranken, K.C., *Stud. Surf. Sci. Catal.*, 93, 59, 1995.
27. Dijkstra, T.W., Duchateau, R., van Santen, R.A., Meetsma, A., and Yap, G.P.A., *J. Am. Chem. Soc.*, 124, 9856, 2002.
28. Shimada, T., Aoki, K., Shinoda, Y., Nakamura, T., Tokunaga, N., Inagaki, S., and Hayashi, T., *J. Amer. Chem. Soc.*, 125, 4689, 2003.
29. Roque-Malherbe, R. and Marquez-Linares, F., U.S. Provisional Patent Application No. 10/982,798, filed November 8, 2004.
30. Zhao, X.S. and Lu, G.Q., *J. Phys. Chem. B.*, 102, 1556, 1998.
31. Plueddemann, E.P., *Silane Coupling Agents,* 2nd ed., Plenum Press, New York, 1991.
32. Voronkov, M.G., Kirpichenko, S.V., Abrosimova, A.T., Albanov, A.I., Keiko, V.V., and Lavrentyev, V.I., *J. Organomet. Chem.*, 326, 159, 1987.
33. Tertych, V.A. and Belyckova, L.A., *Stud. Surf. Sci. Catal.,* 99, 147, 1996.
34. Gates, B.C., in *Handbook of Heterogeneous Catalysis,* Ertl, G., Knozinger, H., and Weitkamp, J., Eds., VCH, Weinheim, 1997, p. 793.

35. Thomas, J.M. and Thomas, W.J., *Principles and Practice of Heterogeneous Catalysis,* VCH, Weinheim, 1996.
36. Ma, Q., Klier, K., Cheng, H., Mitchell, J.W., and Hayes, K.S., *J. Phys. Chem. B,* 105, 9230, 2001.
37. Dunn, B.C., Covington, D.J., Cole, P., Pugmire, R.J., Meuzelaar, H.L.C., Ernst, R.D., Heider, E.C., and Eyring, E.M., *Energy Fuels,* 18, 1519, 2004.
38. Ma, Q., Klier, K., Cheng, H., Mitchell, J.W., and Hayes, K.S., *J. Phys. Chem. B,* 104, 10618, 2000.
39. Ermakova, M.A., Ermakov, D.Yu., Cherepanova, S.V., and Plyasova, L.M., *J. Phys. Chem. B,* 106, 11922, 2002.
40. Kim, S.-W., Son, S.U., Lee, S.I., Hyeon, T., and Chung, Y.K., *J. Am. Chem. Soc.*, 122, 1550, 2000.
41. Zhu, J. and Somorjai, G.A., *Nano Lett.*, 1, 8, 2001.
42. Chandler, B.D., Schabel, A.B., and Pignolet, L.H., *J. Phys. Chem. B,* 105, 149, 2001.
43. Che, M. and Bennett, C., *Adv. Catal.*, 36, 55, 1989.
44. Savargaonkar, N., Uner, D., Pruski, M., and King, T.S., *Langmuir,* 18, 4005, 2002.
45. Mattson, J.S. and Marck, H.B., *Activated Carbon,* Marcel Dekker, New York, 1971.
46. Karanfil, T. and Kilduff, J.E., *Environ. Sci. Technol.*, 33, 3217, 1999.
47. Salame, I.I. and Bandosz, T.J., *Langmuir,* 16, 5435, 2000.
48. Rodriguez-Reinoso, F. and Sepulveda-Escribano, A., in *Handbook of Surfaces and Interfaces of Materials,* Vol. 5, Nalwa, H.S., Ed., Academic Press, New York, 2001, p. 309.
49. Lozano-Castello, D., Cazorla-Amoros, D., Linares-Solano, A., and Quinn, D.F., *J. Phys. Chem. B,* 106, 9372, 2002.
50. Bansal, R.C., Donnet, J.B., Stoeckli, F., *Active Carbon,* Marcel Dekker, New York, 1988.
51. Bandocz, T.J., *Activated Carbon Surfaces in Environmental Remediation,* Elsevier, Amsterdam, 2006.
52. Puri, B.R., in *Chemistry and Physics of Carbon,* Vol. 6, Walker, P.J., Ed., Marcel Dekker, New York, 1970, p. 191.
53. Shao, X., Wang, W., Xue, R., and Shen, Z., *J. Phys. Chem. B,* 108, 2970, 2004.
54. Dubinin, M.M., *Carbon,* 18, 355, 1980.
55. Boehm, H.P., *Adv. Catal.*, 16, 179, 1966; and *Carbon,* 32, 759, 1994.
56. Leon-Leon, C.A. and Radovic, L.R., in *Chemistry and Physics of Carbon,* Vol. 24, Thrower, P.A., Ed., Marcel Dekker, New York, 1992, p. 213.
57. Avgul, N.N. and Kiselev, A.V., in *Chemistry and Physics of Carbon,* Vol. 6, Walker, P.J., Jr., Ed., Marcel Dekker, New York, 1970, p.1.
58. Housecroft, C.E. and Sharpe, A.G., *Inorganic Chemistry,* 2nd ed., Pearson-Prentice-Hall, Essex, England, 2005.
59. Callister, W.D., *Materials Science and Enginering: An Introduction,* 5th ed., J. Wiley & Sons, New York, 2000.
60. Turov, V.V. and Leboda, R., in *Chemistry and Physics of Carbon,* Vol. 27, Radovic, L.R., Ed., Marcel Dekker, New York, 2001, p. 67.
61. Ege, S., *Organic Chemistry,* 4th ed., Houghton-Mifflin Co., Boston, 1999.
62. Hsieh, C. and Teng, H., *J. Colloid Interface Sci.*, 230, 171, 2000.
63. Leng, C.C. and Pinto, N.G., *Carbon,* 35, 1375, 1997.
64. Laszlo, K. and Nagy, L.G., *Carbon,* 35, 593, 1997.
65. Tamon, H. and Okazaki, M., *Carbon,* 34, 741, 1996.
66. Arafat, H.A., Franz, M., and Pinto, N.G., *Langmuir,* 15, 5997, 1999.
67. Franz, M., Arafat, H.A., and Pinto, N.G., *Carbon,* 38, 1807, 2000.

68. Radovic, L.R., Silva, I.F., Ume, J.I., Menendez, J.A., Leon, Y., Leon, C.A., and Scaroni, A.W., *Carbon,* 35, 1339, 1997.
69. Haghseresht, F., Nouri, S., Finnerty, J.J., and Lu, G.Q., *J. Phys. Chem. B,* 106, 10935, 2002.
70. Lua, A.C. and Guo, J., *Langmuir,* 17, 7112, 2001.
71. Seader, J.D. and Henley, E.J., *Separation Process Principles,* J. Wiley & Sons, New York, 1998.
72. Chatzopoulos, D. and Varma, A., *Chem. Eng. Sci.*, 50, 127, 1995.
73. Slaney, A.J. and Bhamidimarri, R., *Water Sci. Technol.*, 38, 227, 1998.
74. Wolborska, A., *Chem. Eng. J.*, 37, 85, 1999.
75. Droste, R., *Theory and Practice of Water and Wastewater Treatment,* J. Wiley & Sons, 1997.
76. Scott-Fogler, H., *Elements of Chemical Reaction Engineering,* Prentice-Hall, Upper Saddle River, New Jersey, 1999.
77. Ruthven, D.W., *Principles of Adsorption and Adsorption Processes,* Wiley, New York, 1984.
78. Helfferich, F.G. and Klein, G., *Multicomponent Chromatography: Theory of Interference,* Marcel Dekker, New York, 1970.
79. Chern, J.-M. and Chien, Y.-W., *Ind. Eng. Chem. Res.*, 40, 3775, 2001.
80. Sherwood, T.K., Pigford, R.L., and Wilke, C.R., *Mass Transfer,* McGraw-Hill, New York, 1975.
81. Michaels, A.C., *Ind. Eng. Chem.*, 44, 1922, 1952.
82. De Vault, D., *J. Amer. Chem. Soc.*, 65, 532, 1943.
83. Rice, R.G. and Do, D.D., *Applied Mathematics and Modeling for Chemical Engineers,* John Wiley & Sons, New York, 1995.
84. Tien, C., *Adsorption Calculation and Modeling,* Butterworth-Heineman, Boston, 1994.
85. Garrone, E. and Ugliengo, P., *Langmuir,* 7, 1409, 1991.
86. Civalleri, B., Garrone, E., and Ugliengo, P., *Langmuir,* 9, 2712, 1993.
87. Fubini, B., Bolis, V., Cavenago, A., Garrone, E., and Ugliengo, P., *Langmuir,* 15, 5829, 1999.
88. Zhang, J. and Grischkowsky, D., *J. Phys. Chem. B,* 108, 18590, 2004.
89. Sauer, J., Upliengo, P., Garrone, E., and Saunders, V.R., *Chem. Rev.*, 94, 2095, 1994.
90. Helmenin, J., Helenius, J., and Paatero, E., *J. Chem. Eng. Data,* 46, 391, 2001.
91. Kuo, S.-L., Pedram, E.O., and Hilnes, A.L., *J. Chem. Eng. Data,* 30, 330, 1985.
92. Knez, Z. and Novak, Z., *J. Chem. Eng. Data,* 46, 858, 2001.
93. Zhou, L., Zhong, L., Yu, M., and Zhou, Y., *Ind. Eng. Chem. Res.*, 43, 1765, 2004.
94. Huang, H.Y., Yang, R.T., Chinn, D., and Munson, C.L., *Ind. Eng. Chem. Res.*, 42, 2427, 2003.
95. Chou, T., Lin, T.Y., Hwang, B.J., and Wang, C.C., *Biotechnol. Prog.*, 2, 203, 1986.
96. Grochala, W. and Edwards, P.E., *Chem. Rev.*, 104, 1283, 2004.
97. Nijkamp, M.G., Raymakers, J.E.M.J., van Dillen, A.J., and de Jong, K.P., *Appl. Phys. A,* 72, 619, 2001.
98. Crabtree, G.W., Dresselhaus, M.S., and Buchanan, M.V. *Phys. Today,* 57(12), 39, 2004.
99. Dillon, A.C., Jones, K.M., Bekkedahl, T.A., Kiang, C.H., Bethune, D.S., and Heben, M.J., *Nature,* 387, 377, 1997.
100. Rogue-Malherbe, R., Morquez, F., dil Volle, W. and Thommes, M., paper in progress.
101. Choung, J.H., Lee, Y.W., and Choi, D.K., *J. Chem. Eng. Data,* 46, 954, 2001.
102. Wang, C.-M., Chung, T.-W., Huang, C.-M., and Wu, H., *J. Chem. Eng. Data,* 50, 811, 2005.

103. Hernandez, M.A., Velasco, J.A., Asomoza, M., Sols, S., Rojas, F., and Lara, V.H., *Ind. Eng. Chem. Res.*, 43, 1779, 2004.
104. Won, D., Corsi, R.L., and Rynes, M., *Environ. Sci. Technol.*, 34, 4193, 2000.
105. Lordgooei, M., Rood, M.J., and Abadi, M.R., *Environ. Sci. Technol.*, 35, 613, 2001.
106. D. Bathen, H.S. Traub, and M. Simon, *Ind. Eng. Chem. Res.*, 36, 3993, 1997.
107. Benkhedda, J., Jaubert, J.N., and Barth, D.J., *J. Chem. Eng. Data,* 45, 650, 2000.
108. Yun, J.H., Hwang, K.Y., and Choi, D.K., *J. Chem. Eng. Data,* 43, 843, 1998.
109. Khaleel, A. and Dellinger, B., *Environ. Sci. Technol.*, 36, 1620, 2000.
110. Kim, M.-B., Ryu, Y.-K., and Lee, C.-H., *J. Chem. Eng. Data,* 50, 951, 2005.
111. Yang, R.T., *Gas Separation by Adsorption Process,* Butterworth, Boston, MA, 1987.
112. Huggahalli, M. and Fair, J.R., *Ind. Eng. Chem. Res.*, 35, 2071, 1996.
113. Yang, R.T., *Adsorbents: Fundamentals and Applications,* J. Wiley & Sons, New York, 2003.
114. Rutherford, S.W. and Coons, J.E., *Langmuir,* 20, 8681, 2004.
115. Maruyama, J. and Abe, I., *J. Electroanal. Chem.*, 545, 109, 2003.
116. Zhou, L., Sun, Y., and Zhou, Y.P., *AIChE J.*, 48, 2412, 2002.
117. Harding, A.W., Foley, N.J., Norman, R.P., Francis, D.C., and Thomas, K.M., *Langmuir,* 14, 3858, 1998.
118. O'Koye, I.P., Benham, M., and Thomas, K.M., *Langmuir,* 13, 4054, 1997.
119. Marsh, H., Ed., *Introduction to Carbon Science,* Butterworths, London, 1989.
120. Gregg, S.J. and Sing, K.S.W., *Adsorption, Surface Area and Porosity,* Academic Press, New York, 1982.
121. McCallum, C.L., Bandosz, T.J., McGrother, S.C., Muller, E.A., and Gubbins, K.E., *Langmuir,* 15, 533, 1999.
122. Brennan, J.K., Thomsom, K.T., and Gubbins, K.E., *Langmuir,* 18, 5438, 2002.
123. Brennan, J.K., Bandosz, T.J., Thomson, K.T., and Gubbins, K.E., *Colloids Surf. A: Physicochem. Eng. Aspects,* 187–188, 539, 2001.
124. Rodrguez-Reinoso, F. and Linares-Solano, A., *Chem. Phys. Carbon,* 21, 1, 1988.
125. Cazorla-Amoros, D., Alcaniz-Monge, J., and Linares-Solano, A., *Langmuir,* 12, 2820, 1996.
126. Siriwardane, R.V., Shen, M.S., Fisher, E.P., and Poston, J.A., *Energy Fuels,* 15, 279, 2001.
127. Sircar, S., *Ind. Eng. Chem. Res.*, 41, 1389, 2002.
128. Sircar, S., in *The Engineering Handbook,* Dorf, R.C., Ed., CRC Press, Boca Raton, FL, 1996, chap. 59.
129. Dong, F., Lou, H., Goto, M., and Hirose, T., *Sep. Purif. Technol.*, 15, 31, 1990.
130. Bagreev, A., Rahman, H., and Bandosz, T.J., *Ind. Eng. Chem. Res.*, 39, 3849, 2000.
131. Meeyoo, V., Trimm, D.L., and Cant, N.W., *J. Chem. Technol. Biotechnol.*, 68, 411, 1997.
132. Meeyoo, V., Lee, J.H., Trimm, D.L., and Cant, N.W., *Catal. Today,* 44, 67, 1998.
133. Adib, F., Bagreev, A., and Bandosz, T.J., *Environ. Sci. Technol.*, 34, 686, 2000.
134. Lizzio, A.A. and DeBarr, J.A., *Energy Fuels,* 11, 284, 1997.
135. Rzepka, M., Lamp, P., and de la Casa-Lillo, M.A., *J. Phys. Chem. B,* 102, 10894, 1998.
136. Zhou, L. and Zhou, Y., *Ind. Eng. Chem. Res.*, 35, 4166, 1996.
137. Hynek, S., Fuller, W., and Bentley, J., *Int. J. Hydrogen Energy,* 22, 601, 1997.
138. Chambers, A., Park, C., Baker, T.K., and Rodriguez, N.M., *J. Phys. Chem. B,* 102, 4253, 1998.
139. Amankwah, K.A.G. and Schwarz, J.A., *Int. J. Hydrogen Energy,* 14, 437, 1989.
140. Jagiello, J., Bandosz, T.J., Putyera, K., and Schwarz, J.A., *J. Chem. Soc., Faraday Trans.*, 91, 2929, 1995.

141. Eberhardt, J.J., Gaseous Fuels in Transportations Prospects and Promise, presented at the Gas Storage Workshop, Kingston, Ontario, Canada, July 10–12, 2001; Royal Military College of Canada and the American Carbon Society.
142. Lozano-Castello, D., Cazorla-Amoros, D., and Linares-Solano, A., *Energy Fuels,* 16, 1321, 2002.
143. Cook, T.L., Komodromos, C., Quinn, D.F., and D.F., Ragan, D.F., in *Carbon Materials for Advanced Technologies,* Burchell, T.D., Ed., Pergamon, Amsterdam, 1999.
144. Parkyns, N.D. and Quinn, D.F., in *Porosity in Carbons: Characterization and Applications,* Patrick, J.W., Ed., Edward Arnold, London, 1995, p. 302.
145. Muto, A., Bhaskar, T., Tsuneishi, S., and Sakata, Y., *Energy Fuels,* 19, 251, 2005.
146. Alcañiz-Monge, J., De la Casa-Lillo, M.A., Cazorla-Amoros, D., and Linares-Solano, A., *Carbon,* 35, 291, 1997.
147. Bekyarova, E., Murata, K., Yudasaka, M., Kasuya, D., Iijima, S., Tanaka, H., Kahoh, H., and Kaneko, K., *J. Phys. Chem. B,* 107, 4682, 2003.
148. Cracknell, R.F., Gordon, P., and Gubbins, K.E., *J. Phys. Chem.*, 97, 494, 1993.
149. Agarwal, R.K. and Schwarz, J.A., *J. Colloid Interface Sci.*, 130, 137, 1989.
150. Matranga, R.K., Myers, A.L., and Glandt, E.D., *Chem. Eng. Sci.*, 47, 1569, 1992.
151. Lozano-Castello, D., Alcaniz-Monge, J., De La Casa-Lillo, M.A., Cazorla-Amoros, D., and Linares-Solano, A., *Fuel,* 81, 1777, 2002.
152. Alicaniz-Monge, J., De La Casa-Lillo, M.A., Cazorla-Amoros, D., and Linares-Solano, A., *Carbon,* 35, 291, 1997.
153. MacDonald, J.A.F. and Quinn, D.F., *Fuel,* 77, 61, 1998.
154. Ishii, C. and Kaneko, K., *Prog. Org. Coatings,* 31, 147, 1997.
155. Benkhedda, J., Jaubert, J.N., Barth, D., and Perrin, L., *J. Chem. Eng. Data,* 45, 650, 2000.
156. Derbyshire, F., Jagtoyen, M., Andrews, R., Rao, A., Martin-Guillon, I., and Grulke, E.A., in *Chemistry and Physics of Carbon,* Vol. 27, Radovic, L.R., Ed., Marcel Dekker, New York, 2001, p. 1.
157. Zhao, X.S., Ma, Q., and Lu, G.Q., *Energy Fuels,* 12, 1051, 1998.
158. Rubby, E.N. and Carroll, L.A., *Chem. Eng. Prog.*, 28, 1993.
159. Stenzel, M.H., *Chem. Eng. Prog.*, 36, 1993.
160. Valenzuela, D.P. and Myers, A.L., *Adsorption Equilibrium Data Handbook,* Prentice Hall, Englewood Cliffs, NJ, 1989.
161. Myers, A.L., Minka, C., and Ou, D.Y., *AIChE J.*, 28, 97, 1982.
162. Hall, P.G. and Williams, R.T., *J. Colloid Interface Sci.*, 113, 301, 1986.
163. Nabarawy, T., Petro, N.S., and Abdel-Aziz, S., *Adsorpt. Sci. Technol.,* 15, 47, 1997.
164. Yun, J.H. and Choi, D.K., *J. Chem. Eng. Data,* 42, 894, 1997.
165. Gadkaree, K.P., *Carbon,* 36, 981, 1998.
166. Benkhedda, J., Jaubert, J.N., Barth, D., Perrin, J., and Bailly, M., *J. Chem. Thermodyn.*, 32, 401, 2000.
167. Shojibara, H., Sato, Y., Takishima, S., and Masuoka, H., *J. Chem. Eng. Jpn.*, 28, 245, 1995.
168. S., Follin, V., Goetz, and A., Guillot, *Ind. Eng. Chem. Res.*, 35, 2632, 1996.
169. Miller, E.B., *Am. Soc. Refrig. Eng.*, 17, 103. 1929.
170. Critoph, R.E., *Carbon,* 27, 63, 1989.

8 Crystalline and Ordered Nanoporous Materials

8.1 INTRODUCTION

The development of new materials is an essential objective of materials science research. This attention is demanded by the progress in all fields of industry and technology [1–10]. For instance, the evolution of the electronic industry started the development of smaller and smaller elements. The dimension of these components is approaching nanometer dimensions, and as this dominion is entered, scientists have found that properties of materials with nanometer dimensions (i.e., on the length scale of about 1–100 nm) can differ from those of the bulk material [1–5].

As was formerly commented, according to the definition of IUPAC, microporous materials are those with pore diameters between 3 and 20 Å, mesoporous materials are those that have pore diameters between 20 and 500 Å, and macroporous materials are those with pores bigger than 500 Å [11]. Porous materials have drawn the interest of chemists and materials scientists owing to commercial interest in their applications, as well as scientific curiosity in the challenges posed by their synthesis, processing and characterization. The distribution of sizes, shapes, and volumes of the void spaces in porous materials relates to their capacity to execute diverse functions in specific applications [10–31].

The application of fundamental scientific principles to the significant technological topics associated with porous materials has been difficult. Nevertheless, chemical processes at relatively low temperatures and pressures, from molecular or colloidal precursors, obviously offer an original approach to obtain customized nanostructured materials [10,12–30]. For example, the mild conditions of sol-gel chemistry offer reacting systems generally under kinetic control [5,10,27,29]. Consequently, small modifications of the experimental parameters, specifically, pH, concentrations, temperatures, nature of the solvent, counterions, and structure-directing agents, can lead to considerable alteration of the resulting supramolecular assemblies [10].

Zeolites and related materials and mesoporous molecular sieves could be included in a group of materials which we call here crystalline and ordered nanoporous materials, respectively. Synthetic zeolites are crystalline materials containing pores and cavities of molecular dimensions from 3 to 15 Å, creating a microscale framework which can be filled with water or other guest molecules. On the other hand, mesoporous ordered silicas and aluminosilicates containing pores of mesoporous dimensions from 20 to 100 Å and exhibiting different ordered, noncrystalline structures build up a mesoscale framework which could also be occupied with water or other molecules.

8.2 FUNDAMENTAL CHARACTERISTICS OF ZEOLITES AND MESOPOROUS MOLECULAR SIEVES

In relation to synthetic zeolites, the resulting molecular sieving ability has enabled the creation of new types of selective separation processes. Zeolites in their acid form are probably the most important heterogeneous acid catalysts used in industry [16,30]. The majority of the world's gasoline is produced by the fluidized catalytic cracking (FCC) of petroleum using zeolite catalysts; their key properties are size and shape selectivity, together with the potential for strong acidity [30].

In addition, some minerals are distinguished by a negatively charged framework bearing cavities, cages, or tunnels where water molecules or inorganic cations (as charge-compensating ions) are occluded. For example, natural zeolites define a family of crystalline microporous aluminosilicates, presenting pore sizes of $d < 1$ nm. These materials have many applications in wastewater cleaning, agriculture, fertilizers, aquaculture, animal health, animal nourishment, gas separation, solar refrigeration, gas cleaning, deodorization, solid electrolytes, construction materials, and cleaning of radioactive wastes [31].

In reply to the developing needs in both industry and fundamental research, there has been a growing interest in increasing the pore sizes of materials from the micropore region to the mesopore subdivision of porosity. In 1988 the first description of a crystalline microporous material with regular pores larger than 10 Å appeared. To be exact, the aluminophosphate VPI-5 was synthesized, opening the area of extra-large-pore crystalline materials [18,19]. Later more extra-large-pore crystalline materials were developed (e.g., ALPO4-8, Cloverite, JDF-20, ULM-5, UTD-1, ULM-16, CIT-5, ND-1, FDU-4, NTHU-1) [18].

In parallel to the work on extra-large-pore crystalline materials, scientist working at Mobil Corporation, developing the concepts used in zeolite synthesis [12–20], have taken advantage of this methodology to generate novel inorganic materials [21,22]. This resulted in the discovery of the M41S family of mesoporous ordered silicas, with hexagonal and cubic symmetry and pore sizes ranging from 20 to 100 Å, through the use of surfactants as organizing agents [21,22]. The mesoporous structure can be regulated by a complex choice of templates (i.e., surfactants, adding auxiliary organic chemicals such as mesitylene, and changing reaction parameters such as temperature and compositions) [10,21–24,32–34].

For the synthesis of mesoporous molecular sieves (MMS), surfactant liquid crystals with long n-alkyl chains are used as structure-directing agents. By applying the developed methodology, a thorough control of the pore size was attained, with pore diameters tunable from, in general, 2 to 100 nm, narrow pore size distributions, and high surface area and pore volumes [21,22,28,32–34]. A family of a hexagonal phase known as MCM-41, a cubic phase known as MCM-48, and a lamellar phase known as MCM-50 were developed [22]. The understanding of the formation mechanism of these mesostructured materials laid the foundations for the synthesis of silicas with a defined pore size distribution, such as silica thin films [32,33], fibers [34], and spheres [34].

8.3 STRUCTURE

8.3.1 Crystalline Microporous Materials

The first zeolite, stilbite, was discovered in 1756 by the Swedish scientist Freiherr Axel Fredrick Cronsted during the collection of minerals in a cooper mine in Lappmark, Sweden. Cronsted baptized the new mineral with the name zeolite, because of the characteristic intumescence of the mineral observed by him during the blowpipe test of the found crystals [12,31]. The term zeolite is derived from two Greek roots; "zeo," to boil, and "lithos," a stone [12,31]. The term molecular sieve was derived from McBain in 1932, when he found that chabazite, a mineral, had a property of selective adsorption of molecules smaller than 5 Å in diameter [35]. Zeolites belong to the group of molecular sieves, and about 150 structure types are known today [36,37].

Aluminosilicate zeolites are three-dimensional microporous crystalline solids (see Figure 8.1, 8.2, and 8.3). These materials are built from $(AlO_2)^-$ and (SiO_2) tetrahedra. The (TO_2) tetrahedra are linked in the corners, sharing all oxygen atoms [12,14,16,36–38]. Each of the framework tetrahedra really contains two oxygen atoms, since each oxygen atom is shared between two tetrahedra. This is the reason that (TO_2) was used to indicate the tetrahedra, and not (TO_4). The presence of tetracoordinated Al(III) generates negative charge. This negative charge must be balanced by extraframework cations (one per Al(III)). The chemical composition of aluminosilicate zeolites can be expressed as:

$$M_{\frac{x}{n}}\left\{\left(AlO_2\right)_x\left(SiO_2\right)\right\}zH_2O$$

in which M represents the balancing cations (charge, +n) compensating the charge from the Al(III), and z is the water contained in the voids of the zeolite [12,14,31,36].

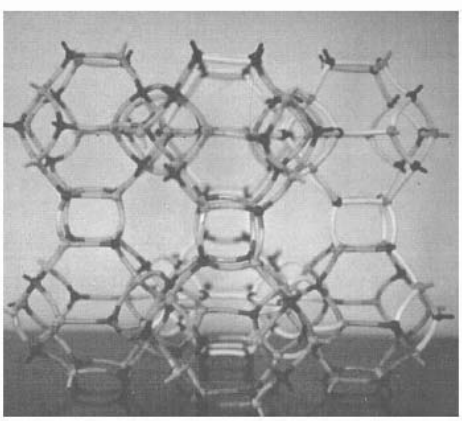

FIGURE 8.1 Framework type LTA.

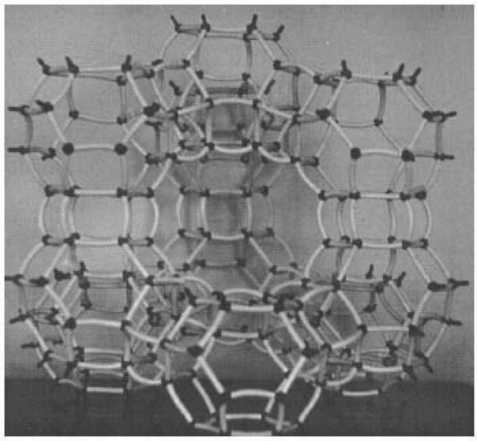

FIGURE 8.2 Framework type FAU.

The balancing cation can be a metal or another species, for example ammonium. If this cation is located within the zeolite channel or cavity it can be exchanged, giving the zeolite its ion-exchange property [10,12,31].

Si and Al are the T atoms in aluminosilicate zeolites. However, other elements, such as P, Ge, Ga, Fe, B, Be, Cr, V, Zn, Zr, Co, Mn, and other metals could also be T atoms [10,14–16]. These elements are tetrahedrically combined to form a zeolite, with or without charge compensating cations, in such a way that the electroneutrality principle is fulfilled [12,15,16,36–38]. Most of the existing zeolites are synthetic. There are more than 1000 different materials, and this number is constantly increasing [37]. In addition, about 40 natural zeolites have been found in the Earth's crust [31].

In zeolite, cages, channels, and pores of different sizes and shapes, depending on the zeolitic structure, are found [31,36,37]. Their dimensions depend on the arrangement of the $(AlO_2)^-$ and (SiO_2) or, in general, the (TO_2) tetrahedra to form substructures. Two of these substructures are the sodalite and pentasil units, and along with other substructurres, they are the building blocks of an amazing variety of zeolites and related materials [36–38].

The structure of zeolites and related materials is well explained in different textbooks, handbooks, and articles [12–14,37,38]. Consequently, it is unnecessary to describe it here. Nevertheless, three of the most important framework types are shown here. The first is the LTA framework type (Figure 8.1), corresponding to the following synthetic zeolites and related materials: A, LZ-215, SAPO-42, ZK-4, ZK-21, ZK-22, and alpha [37].

The framework type FAU (Figure 8.2) is related to the natural zeolite faujasite [38] and the synthetics zeolites and related materials, X, Y, EMC-2, EMT, ZSM-3, and ZSM-20 [37]. Finally, the HEU framework type (Figure 8.3) is compatible with the natural zeolites heulandite and clinoptilolite [31] and the synthetic zeolite LZ-219 [37].

The LTA framework structure is composed of sodalite cages placed in the corners of a cube with axis, a ≈ 11.9 Å, linked by 4-4 secondary building units (see Figure 8.1)

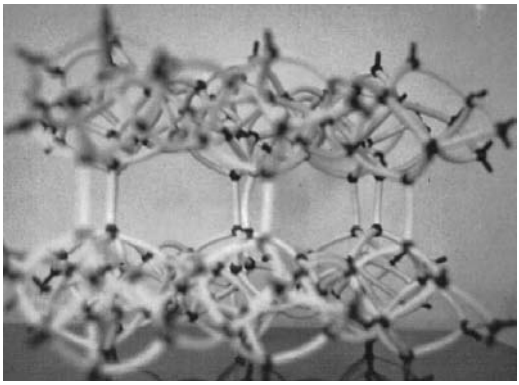

FIGURE 8.3 Framework type HEU.

[37]. The shaped framework contains 8-member-ring (MR) windows which lead to an α-type supercage [12,38].

The FAU framework structure is composed of sodalite cages, linked by 6-6 secondary building units, and located in a face-centered cubic lattice (FCC), where half of the tetrahedral sites of the FCC lattice are also occupied, as is the case in the structure of diamond. The formed cube has an axis, a ≈ 24.3 Å (see Figure 8.2) [37]. The produced framework contains 12-member-ring (MR) windows which lead to a β-type supercage [12,38].

The structure of clinoptilolite (HEU framework type [37]) shows three channels: one 8-MR channel along [100], with an access of 2.6 Å × 4.7 Å, and two parallel channels along [001], one 8-MR with a window of access with 3.3 Å × 4.6 Å, and a 10-MR with an access of 3.0 Å × 7.6 Å (See Figure 8.3) [37,38].

One of the most important groups of molecular sieves is microporous solids with high Si/T ratio, where T represents trivalent Al, Fe, B, Ga, or tetravalent Ti or Ge [10–20]. As a function of the Si/T ratio, the following categories have been established: zeolites, Si/T < 10; and high-silica zeolites,

$$10 < \frac{\mathrm{Si}}{\mathrm{T}} < 500;$$

and all-silica zeolites, Si/T > 500 [10,39–58]. The last mentioned compounds are essentially Si-based molecular sieves. However, contrary to clathrasils, the porosity of these materials is accessible.

The majority of the members of the ZSM family of molecular sieves and some of the members of the SSZ family are high-silica zeolites [37]. These ZSM-5, with MFI framework type, and ZSM-11 with MEL [37] types include some of the most important materials in zeolite science and technology. All these materials are synthetic.

The Si/Al ratios of aluminosilicate zeolites are increased by dealumination [59]. This process can be made by hydrothermal treatments such as steaming [59], acid leaching [60], or treatments in flowing $SiCl_4$ at 200–300°C, or hexafluorosilicates

[59]. Dealuminated materials have different uses in catalysis and adsorption, specifically USY zeolite (ultrastable zeolite Y) is widely used in catalytic cracking [30]. DAY zeolite is a FAU-type zeolite. However, unlike Na-Y, DAY ideally has no Al in the framework and, hence, no Na^+ ions to balance charge [61,62].

All-silica zeolites are three-dimensional microporous crystalline solids, which are built from (SiO_2) tetrahedra linked in the corners, sharing all oxygen atoms [16,37]. In 1978 a new polymorph of silica was found [39]. This material, called silicalite, has an MFI framework, that is to say, the silicalite structure consist of a three-dimensional system of intersecting 10-MR channels [16,37]. Two main components constitute the MFI framework type: ZSM-5 zeolite, the high-silica constituent, where the Si/Al ratio varies between 10 and 500, and the all-silica member, silicalite (Si/Al > 500) [16,37].

To date, the following framework types: MFI [39], MEL[40], MTW[41], AFI [42] BEA [43], IFR [44], ITE[45], AST[46], CFI [47], CHA [48], MWW [49], STF [50], STT [51], ISV [52], CON [53], MTT [54], RUT [55], ITW [56], and LTA [57] have been synthesized in pure silica form, mostly in fluoride media [58].

8.3.2 Ordered Mesoporous Materials

Despite of the vast quantity of work devoted to zeolites and related materials, the dimensions and ease of access of pores in these materials are restrained to the microporous scale. This fact limits the use of zeolites and related materials to small molecules. Consequently, during the last few years a significant effort has been focused on obtaining materials showing larger pore size [10,16]. As a significant result of this endeavor, in 1992 researchers at Mobil Corporation discovered the M41S family of mesoporous molecular sieves [21,22]. These materials possess exceptionally large uniform pore structures.

This new family of mesoporous silica and aluminosilicate compounds were obtained by the introduction of supramolecular assemblies. Micellar aggregates, rather than molecular species, were used as structure-directing agents. Then the growth of inorganic or hybrid networks templated by structured surfactant assemblies permitted the construction of a novel type of nanostructured materials in the mesoscopic scale, in general, from 2 to 100 nm [10,21–24,32–34,63–68].

This supramolecular directing concept has led to a family of materials whose structure, composition, and pore size can be tailored during synthesis by variation of the reactant stoichiometry, nature of the surfactant molecule, or by postsynthesis functionalization techniques [21–24]. The obtained solid phases are characterized by an ordered, not crystalline, pore wall structure, presenting sharp pore size dispersions. The obtained mesoporous materials are ordered, but noncrystalline, because of the lack of precise atomic positioning in the pores wall structure, as was shown by MAS-NMR and Raman spectroscopy [18]. This gave rise to inorganic solids with enormous differences in morphology and structure [10,23,24].

The assembly mechanism of this mesoporous type of molecular sieves is determined by two attributes. The first is the dynamics of surfactant molecules to develop molecular structures which lead to micelle and, ultimately, liquid crystal formation [24]. The second is the capacity of the inorganic oxide to experience condensation

reactions to structure extended thermally stable configurations [24]. The initial discovery involved the formation of silicates using alkyltrimethylammonium cationic surfactants in a basic medium [24]. Subsequent efforts have shown these structures can also be formed in acid media [69,70] and by using neutral normal amines, [71] nonionic surfactants [72], and dialkyldimethylammonium cationic surfactants [73]. In addition, several mechanistic studies have expanded the initial pathway studies to a more generalized view of an organic/inorganic charge balance driving force for the formation of these structures [18,24,69–71,74–77].

The original members of the M41S family consisted of MCM-41 (hexagonal phase) (see Figure 8.4), MCM-48 (cubic Ia3d phase), and MCM-50 (a stabilized lamellar phase) (see Figure 8.5) [21–24].

MCM-41 shows an X-ray diffraction pattern including three or more low-angle (below 10° in 2θ) peaks that can be indexed to an hexagonal lattice [23,24]. The

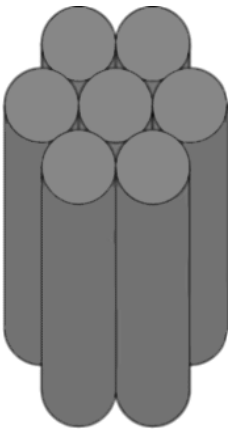

FIGURE 8.4 Hexagonal pore configuration of MCM-41.

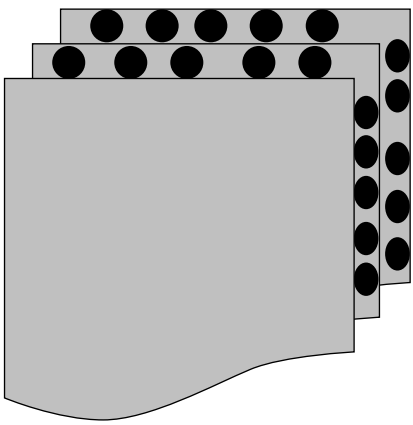

FIGURE 8.5 Lamellar configuration of MCM-50.

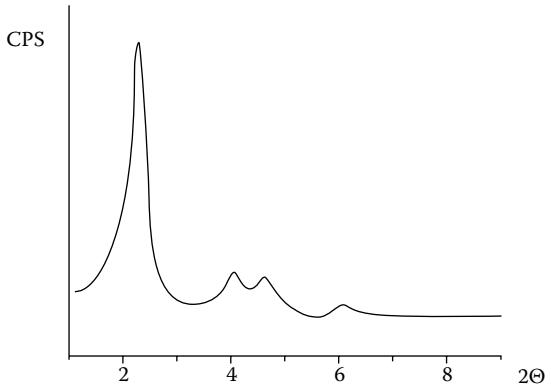

FIGURE 8.6 X-ray diffraction pattern corresponding to MCM-41.

structure is proposed to have a hexagonal stacking of uniform-diameter porous tubes whose size can be varied from about 15 to more than 100 Å [24]. An example of the characteristic X-ray diffraction pattern is shown in Figure 8.6 [78,79].

MCM-48, the cubic material, exhibits an X-ray diffraction pattern consisting of several peaks that can be assigned to the Ia3d space group [24]. The structure of MCM-48 has been proposed to be bicontinuous, with a simplified representation of two infinite three-dimensional, mutually intertwined, unconnected networks of rods [2,4,69,80].

MCM-50, the stabilized lamellar structure, exhibits an X-ray diffraction pattern consisting of several low-angle peaks that can be indexed to (h00) reflections [24]. This material could be a pillared layered material, with inorganic oxide pillars separating a two-dimensional sheet similar to that of layered silicates such as magadiite or kenyaite [24]. Alternatively, the lamellar phase could be represented by a variation in the stacking of surfactant rods such that the pores of the inorganic oxide product would be arranged in a layered form [24].

Other M41S type mesoporous materials are SBA-1 (cubic Pm3n phase) [24] and SBA-2 (cubic $p6_3/mmc$ phase) [81]. Additional materials have been synthesized that are not as readily classified. These materials generally exhibit limited X-ray diffraction information (one peak) and may contain a random array of pores as shown in transmission electron micrographs. All of these mesoporous materials are characterized by having narrow pore size distributions comparable to microporous materials and extraordinary hydrocarbon sorption capacities (up to, and equal to their weight). The initial forms of the M41S family were synthesized as silicates and aluminosilicates.

Subsequent synthesis efforts have produced new materials such as SBA-15. These mesoporous silicas present a well-defined hexagonal structure, large surface area, and high hydrothermal stability, which give them high potential for a variety of technological applications [82–84]. Among the wide variety of silica mesophases, MCM-41 [21,22] and SBA-15 [81] have been the most extensively investigated. Though both of them exhibit two-dimensional hexagonal structures (p6mm), they have some notable differences:

1. SBA-15 is endowed with larger pores, and thicker pore walls than MCM-41 [81].
2. MCM-41 is purely mesoporous in nature, whereas typical SBA-15 silica contains a significant amount of micropores within the pore walls [85–87].
3. While the channels of MCM-41 are not connected to each other, those of SBA-15 are interconnected via micropores [86], or secondary mesopores [67,88].

In addition to the nature of the pore system (i.e., pore size, shape, and connectivity), depending on the targeted application, the morphology of the mesophase may be particularly important [89]. Simple morphologies with short, unhindered path lengths such as small spheres, and crystal-like particles as well as short, straight rods are beneficial for applications limited by intraparticle diffusion processes such as catalysis, separation, guest molecule encapsulation, and internal surface modification [89]. Thus, not surprising, extensive work was devoted to the morphological control of mesoporous silicas [89–92]. Most approaches were based on changes in synthesis conditions, including the silica source, the nature of the surfactants, cosurfactants, cosolvents, and additives and the overall composition of the synthesis mixture [89]. The understanding of the formation mechanism of these mesostructured materials laid the foundations for the synthesis of silica mesophase with a defined pore size distribution, such as thin films [32,33], fibers [34], spheres [34,82], and short rodlike particles [82]. More exotic particles having doughnut, discoidlike, and other shapes have been also obtained [90] using organic additives and inorganic salts [90].

8.4 SYNTHESIS AND MODIFICATION

8.4.1 Zeolite Synthesis

Aluminosilicate zeolites are normally synthesized in hydrothermal conditions, from solutions including sodium hydroxide, sodium silicate, or sodium aluminate [12,13]. The specific zeolite synthesized is obviously determined by the reactants, and mainly by the synthesis specifications used, such as temperature, pH, and time [10–14,93]. Aluminosilicate zeolites are synthesized in three steps: induction, nucleation, and crystallization. Nucleation is a step where germ nuclei are obtained from very small aggregates of precursors becoming larger with time. Crystallization begins, involving the germ nuclei from the nucleation step and other components of the reaction mixture. This process is affected by several factors that can be modified during the synthesis procedure. These factors include: presence of cations in the reaction mixture, OH^- concentration, SiO_2/Al_2O_3 ratio, H_2O content, temperature, pH, time, aging, stirring of the reaction mixture, order of mixing, and other factors [12,13,44].

The first hypothesis, proposed by Breck and Flanigen [12,16] to explain the crystallization of aluminosilicate zeolites, states that it proceeds through the formation of the aluminosilicate gel, or reaction mixture, and the nucleation and growth of zeolite crystals from the reaction mixture. This pioneering model has been practically abandoned and displaced by the hypothesis of Barrer and others [13,16]. In

this hypothesis, it is supposed that the formation of zeolite crystals takes place in solution. Accordingly, in this model the nucleation and growth of crystalline nuclei are a result of condensation reactions between soluble species, where the gel performs a limited role as a reservoir of matter.

The synthesis methods in the cases of high-silica, all-silica, and other nonaluminosilicate zeolites are analogous to the methods used in aluminosilicate zeolites, but the initial gel composition is different [14–16,93–122]. The fundamental purpose of zeolite synthesis is the creation of new zeolitic structures by altering the diverse aspects involved in the process. In order to do that, the use of organic substances known as structure-directing agents (SDA) has substantially increased the number of new structures synthesized and accepted as new materials [10,14–16]. These organic cations can stabilize structures with cavities and shapes of similar dimensions to the ones of the organic cations [14,16,93]. Up to now, amines and related compounds (quaternary ammonium cations), linear or cyclic ethers, and coordination compounds (organometallic complexes) have been the most commonly used organic templates [10,14–16].

The first high-silica zeolites (i.e., eta, EU, NU, and the ZSM series) were patented in the late 1970s or early 1980s [14,16,94,95]. The first all-silica zeolite, silicalite, was obtained in 1978 [39]. Microporous aluminophosphate molecular sieves, AlPO, SAPO, and MeAPO, were developed by Union Carbide [15,96]. SAPO molecular sieves were obtained by incorporation of Si [96] in the AlPO framework. MeAPO molecular sieves were obtained by the inclusion of Me (Me = Co, Fe, Mg, Mn, Zn) in the AlPO framework. The family of crystalline microporous phosphates grew considerably, some examples include gallophosphates [97–99], zincophosphates [100,101], beryllophosphates [102], vanadophosphates, [103] and ferrophosphates. [104].

Pure silica zeolites have been synthesized primarilly in fluoride media [58] using different SDA. As was previously stated, the following framework types are represented as members of this series of molecular sieves: MFI [39], MEL[40], MTW[41], AFI [42] BEA [43], IFR [44], ITE[45], AST[46], CFI [47], CHA [48], MWW [49], STF [50], STT [51], ISV [52], CON [53], MTT [54], RUT [55], ITW [56], and LTA [57].

Nonaluminosilicate zeolites are generally obtained by hydrothermal crystallization of a heterogeneous gel, which consists of a liquid and a solid phase [10]. The reaction media contain the following: sources of the cation(s) that form the framework (T: Si, Al, P, …), sources of mineralizing agents (HO^-, F^-), mineral cations and/or organic species (cations or neutral molecules), and solvent (generally water).

In the case of aluminophosphate families and derived compounds (SAPO, MeAPO, etc.), the reaction pH is between 3 and 10 [15]. Anions such as hydroxide or fluoride collaborate in the dissolution of the reactive silica moieties in the gel and their transport to the developing crystals [10]. In addition, F^- anions can play the role of a costructuring agent, by stabilizing certain building blocks of the inorganic network. [105]. Nonaqueous routes [106, 107] or dry synthesis methods [109] have also been explored.

The SDAs are often occluded in the microporous cavities and channels of the synthesized material, contributing to the stability of the obtained zeolite. The

guest–framework stabilizing interactions can be of Coulombic, H-bonding, or van der Waals nature. Guest–guest interactions can also contribute to the total energy [10,14–16]. Different factors concerning SDA must also be considered, for instance [10,16,109] size. The size of the SDA is in direct relation with the cavity, or pore size of the zeolite, even though this effect clearly depends on the temperature.

Besides SDAs and temperature, other components and/or factors in the synthesis are relevant [10,16]. The hydroxide ion acts by controlling the degree of polymerization increasing the crystal growth. In addition, the OH^-/SiO_2 ratio has been correlated with the pore size (larger pores with higher ratios) [10,16].

On the other hand, many synthesis procedures are using fluoride anions instead of hydroxide ions, resulting in zeolites or related material with higher crystal sizes and lower structural defects with respect to conventional procedures using OH^- [110–118]. Temperature is also a very important factor. Usually temperatures are below 350°C, but high values of temperature yield more condensed-phase species. The pH of the synthesis mixture is of crucial importance. It is alkaline (normally pH > 10) and controls the particle size. The reaction time is another parameter to consider. It should be optimized, because with different reaction times different zeolites or phases can be obtained at the same reaction mixture. Stirring the reaction mixture affects the zeolitic structure and clearly the particle size.

All silica zeolite phases can be prepared hydrothermally using either hydroxide or fluoride as mineralizers. Both methods will be designated here, according to the mineralizer, as the OH^- and F^- methods [110]. Usually, tetraethylorthosilicate (TEOS) is hydrolyzed in an aqueous solution of the suitable structure-directing agent in its hydroxide form. The resultant mixture is left under stirring until complete evaporation of the ethanol produced (i.e., within the detection limit of ^1H MAS NMR, no ethanol could remain in the synthesis mixture after evaporation). This indicates that these water/alcohol/silica/SDA mixtures do not form azeotropic compositions, as opposed to the known behavior of water/ethanol mixtures. After ethanol evaporation, HF (48% aqueous solution) is added, and the mixture is homogenized by stirring. The resulting mixture is always a slurry with a viscosity that depends on the specific SDA used and the final water content [110].

For the synthesis of pure silica phases, it is possible to use different SDAs in fluoride media. The SDAs are chosen primarily according to criteria defined as significant in determining a high structure-directing ability (rigidity, size, shape, C/N^+ ratio) [110,119] and the availability of the cation or of the parent amine [110]. Consequently, SDAs with polycyclic moieties (giving rise to SDAs with relatively large and rigid portions) predominate [110].

After the synthesis procedure, the zeolite should be calcined to remove the organic compounds that are blocking the pores. Calcination entails heating the as-synthesized zeolite in an air flow, to a temperature normally ranging from 350 to 400°C.

In general, zeolite synthesis requires considering many factors, and unfortunately, the relation between these experimental conditions and the nature of the synthesized product is not trivial. To overcome this problem, different strategies have been proposed, and among them the combinatorial approach is a very promising methodology, consisting of the use of miniaturized multiautoclave systems to finally explore a very high number of possibilities.

8.4.2 Zeolite Modification

The majority of the methods developed for zeolite modification are related to aluminosilicate zeolites [59]. For example, one very common modification is the ion-exchanging of the zeolitic structures. Synthetic zeolites are normally obtained in the sodic form, and natural zeolites contain, in their mineral form, Na^+, K^+, Ca^{2+}, Mg^{2+}, and other cations [31]. Therefore, sometimes it is necessary to exchange these cations for other cations, or also to obtain the zeolites in their acid form by exchanging the sodium for ammonium, and heating in an air flow [12,59].

Aluminosilicate zeolites are also dealuminated. The dealumination process can be done by hydrothermal treatments (steaming), acid leaching, or treatments in flowing $SiCl_4$ or hexafluorsilicates at 200–300°C [59]. These treatments produce high-silica zeolites. The dealumination treatment also creates mesopores by extraction of Al from the zeolite lattice, thus causing partial collapse of the framework. These dealuminated materials have different uses, for example in catalysis. USY zeolite (i.e., Ultra Stable zeolite Y) is widely used in catalytic cracking [30]. In addition, hydrophobic zeolites such as DAY (DeAluminatedY) zeolite (i.e., a zeolite with a very low aluminum content) possess a high adsorption capacity of organic compounds dissolved in water [62,120–123].

The incorporation of molecules inside the zeolite cavities is a very interesting tool for zeolite modification. Neutral molecules can be adsorbed by stirring the compound with the zeolite in an appropriate solvent. This process is normally very efficient with small molecules. The incorporation of large molecules in the zeolite can be accomplished in solution, and it depends on the dimensions of the molecule and also on the diffusion properties across the zeolite channels [36,59]. For example, iridium carbonyl can be deposited on zeolites by adsorbing the complex $[Ir(CO)_2(acac)]$ from a solution in hexane [126]. Rhodium neutral clusters, $[Rh_6(CO)_{16}]$, could also be obtained when $[Rh(CO)_2Cl]_2$ is introduced in the cages of NaY, or even acidic HY zeolites, and treated at room temperature with 1 atm of CO in the presence of water; then $[Rh_6(CO)_{16}]$ is formed [127].

However, sometimes the molecules to incorporate have dimensions larger than the zeolite channels. For instance, faujasite has supercages of 13 Å diameter with windows giving access to these cages of ca. 7.4 Å [36]. Molecules larger than 7.4 Å could not be incorporated by conventional procedures. To overcome this difficulty, the large molecules can be synthesized within the zeolite supercages; this procedure is called ship-in-a-bottle synthesis [128]. Examples published so far are the incorporation of tetra-t-butyl substituted iron phtalocyanine [129], perfluorphthalocyanines of iron [130], cobalt cooper, [131,132] and manganese [133], and iron-tetranitrophthalocyanine. However, in the case of the nitro substituted phyalocyanine, the complex was formed in the outer surface of the zeolite [133]. In the case of porphyrin-type ligands, the encapsulation of iron and manganese tetramethylporphyrins in the supergage of zeolite Y was claimed [134].

It is possible also to incorporate transition metal complexes by synthesizing the molecular sieve structure around the preformed complexes [128,135,136]. To carry out this procedure, the complex must be stable under the conditions of zeolite synthesis (i.e., pH, temperature, and hydrothermal conditions) and should also show

solubility in the synthesis medium [128]. The syntheisis of mordenite has been reported from gels containing bipyridine, phenantonitrile, or phthalocyaninen complexes [135]. However, the encapsulation of the complexes was not clearly shown [128]. It was also claimed that homogeneous encapsulation of transition metal complexes in zeolites is possible in zeolite X [136,137].

8.4.3 Synthesis of Ordered Silica Mesoporous Materials

In the past two decades, a major effort has been made to obtain molecular sieves showing larger pore size [18]. The introduction of supramolecular assemblies (i.e., micellar aggregates), rather than molecular species, as SDAs allowed a new family of mesoporous silica and aluminosilicate compounds (M41S) to be obtained [21,22]. The novel group of mesoporous molecular sieves (MMS), M41S was discovered by expanding the concept of zeolite synthesis with small organic molecules as SDAs to longer-chain surfactant molecules [21,22]. Then, rather than individual molecular-directing agents participating in the ordering of the reagents to form the porous material, assemblies of molecules are responsible for the formation of these pore systems [24]. This supramolecular directing notion has led to a type of materials whose structure, composition, and pore size can be tailored during synthesis by variation of the reactant stoichiometry and nature of the surfactant molecule, or by postsynthesis functionalization techniques [24].

The typical methodology for the development of mesostructured materials is the use of the following standard synthesis conditions: low temperatures, coexistence of inorganic and organic moieties, and extensive choice of precursors [10]. The large collection of materials, extending from nanostructured materials to more complicated materials having hierarchical architectures, reported during recent years, is testimony to the scientific success of this scientific subject [10]. In the course of the synthesis of complicated materials having hierarchical architectures, the chemical, spatial, and structural properties of the texturing agent must be cautiously adjusted. Controlling the rates of chemical reactions, the nature of the interfaces, and the encapsulation of the growing inorganic phase is carried out by regulation of the synthesis conditions. Satisfactory tailoring of the organomineral interface is of utmost importance to obtain well-defined textured phases. The chemical, spatial, and temporal control of this "hybrid interface" is a major task in the challenge of developing cooperatively assembled inorganic–organic integrated systems [10].

The formation mechanism of this mesoporous group of molecular sieves is determined by two features [24]. The first is the dynamics of surfactant molecules to form molecular assemblies which lead to micelle and, ultimately, liquid crystal formation. The second is the ability of the inorganic oxide to undergo condensation reactions to form extended, thermally stable structures. Reaction gel chemistry is considered to perform a significant role in mesoporous molecular sieve (MMS) synthesis. The comprehension of the chemistry of surfactant/silicate solution is a prerequisite for understanding the synthesis and mechanisms responsible for the formation of MCM-41 and other MMS from its precursors [10,24]. In a simple binary system of water–surfactant, surfactant molecules show themselves as very active constituents with changeable structures that are related to concentrations [23].

At low concentrations, they energetically exist as monomolecules; with growing concentration, surfactant molecules merge together to form micelles in order to reduce the system entropy. The initial concentration limit at which monatomic molecules accumulate to form isotropic micelles is called cmc (critical micellization concentration) [23]. As the concentration process persists, hexagonal-close-packed arrays appear, producing the hexagonal phases. The next step in the process is the coalescence of the adjacent, mutually parallel cylinders to produce the lamellar phase. In some cases, the cubic phase also appears prior to the lamellar phase [23].

The precise phase present in a surfactant aqueous solution at a particular concentration depends not only on the concentrations, but also on the nature of the surfactant itself (the length of the hydrophobic carbon chain, hydrophilic head group, and counterion) and the following parameters: pH, temperature, the ionic strength, and other additives [138]. This is reflected by the effect of the abovementioned matters on cmc. Usually, the cmc decreases with the grow of the chain length of a surfactant, the valency of the counterions, and the ion strength in a solution [23]. In contrast, it increases with growing counterion radius, pH, and temperature.

For instance, in an aqueous solution at 25°C, the cmc is about 0.83 m*M* for surfactant, $C_{16}H_{33}(CH_3)_3N^+Br^-$; between the cmc and 11 wt. %, small spherical micelles are present; in the concentration range of 11–20.5 wt. %, elongated flexible rodlike micelles are formed [139]. Hexagonal liquid crystal phases appear in the concentration region between 26 and 65 wt. %, followed by the formation of cubic, lamellar, and reverse phases with increasing concentration [23]. At 90°C, the hexagonal phase is observed at a surfactant concentration of more than 65% [140]. The significance of this new "organized matter soft chemistry synthesis" is endlessly growing [141]. These materials are possible candidates for a variety of applications in the fields of catalysis [142], optics, photonics, sensors, separation, drug delivery [62], sorption, acoustic, or electrical insulation, and ultralight structural materials [143,144].

Silica-based materials are the most studied systems, for several reasons: a great variety of possible structures, a precise control of the hydrolysis–condensation reactions, enhanced thermal stability of the obtained amorphous networks, and strong grafting of organic functions [10].

The M41S family was originally obtained by hydrothermal synthesis, in basic media, from inorganic gels containing silicate (or aluminosilicate) in the presence of quaternary trimethylammonium cations [21–23]. Lately, a pseudomorphic synthesis founded on the dissolution–reprecipitation of silica microspheres in alkaline media in the presence of C_{16}TMABr allows production of morphologically controlled MCM-41 [145]. Hexagonal mesoporous silica (HMS) compounds are obtained at neutral pH, according to a new synthesis path using primary amines $C_nH_{2n+1}NH_2$ (n = 8–18) as amphiphilic molecules [146,147].

A great deal of work has been dedicated to pore size control. Beck et al. were able to tailor the pore size from 15 to 45 Å by varying the chain length of C_nTMA$^+$ cations between 8 and 18 carbon atoms [10, 22]. The addition of organic molecules such as 1,3,5-trimethylbenzene [22] or alkanes [148] permitted increased pore size up to 100 Å. These swelling agents are soluble in the hydrophobic part of the micelle, increasing the volume of the template [10]. This method, although simple in form, is difficult to put into practice, lacks reproducibility, and produces less organized

mesophases. As an option to the swelling agent, an efficient method relies on extended hydrothermal treatment in TMA^+ solutions; this process improves the pore organization, as well as growing the pore size [149]. Nevertheless, the pore size of MCM-41 and related materials is limited by the size of the micellar templates; a natural expansion to increase the pore size consists of making use of bigger molecules such as polymers or more complex texturing agents.

Amphiphilic block copolymers (ABC) could be utilized for ordered mesoporous materials synthesis. ABCs represent a new class of functional polymers, with a strong application potential, mainly due to the high energetic and structural control that can be exerted on the material interfaces [10,150]. The chemical structure of ABCs can be programmed to tailor interfaces between materials of totally different chemical natures, polarities, and cohesion energies. Polymer organized systems (POS) formed by ABC polymers are excellent templates for the structuring of inorganic networks [10,151]. They have been also used for growth control of discrete mineral particles [151]. diblock (AB) or triblock (ABA) block copolymers are generally used, in which A represents a hydrophilic block [polyethylene oxide (PEO) or polyacrylic acid (PAA)], and B represents a hydrophobic block [polystyrene (PS), polypropylene oxide (PPO), polyisoprene (PI), or polyvinylpyridine (PVP)] [10,150].

8.4.4 Modification of Ordered Silica Mesoporous Materials

The enlarged pore size of ordered mesoporous silicas, contrasted with microporous zeolites, offers us many opportunities to include diverse organic guest species within extremely porous structures in a very methodical and planned way [10,152–165]. Organic moieties are easily able to be functionalized. This process creates active sites in the solid state for catalysis, ion exchange, or adsorption, while taking advantage of the exclusive textural properties of the mesoporous materials [165]. Such porous composite materials are expected to bring new possibilities for the investigation of exceptional physical and chemical behaviors of molecules confined inside nanospace, which will be significant for the design of innovative materials for chromatography, sensing, electronic, and optoelectric devices, or recyclable stable heterogeneous catalysts [165].

So far, mesoporous organic-silica composite materials were, as a rule, prepared either by co-condensation reactions of organosilanes directly during the synthesis of the mesoporous material, or by grafting organosilanes onto pre-prepared mesoporous silica surfaces [165]. Significant advantages of both approaches are on the chemical and thermal stability of the organic moieties resulting from the strong covalent bonding between the organics and the silica walls. The great order of MCM-41 and related phases makes these materials particularly interesting as support materials, since the framework ensures an ordered structure and thermal and mechanical stability [10].

Postsynthesis methods, such as functionalization of pore walls, can affect the pore size and surface chemistry in mesoporous molecular sieve materials. For example, MCM-41 samples contain a large concentration of silanols which can be functionalized via simple elimination reactions, this postsynthesis technique can be used to alter the pore size or affect the hydrophobicity of the pore wall [24]. Otherwise, others

species can be used to anchor moieties having specific catalytic or adsorptive properties. That is, the organic species incorporated to the material allow fine control of the interfacial and bulk properties, such as hydrophobicity, porosity, accessibility, and optical, electrical, or magnetic properties [10].

Organic functions can be attached onto the oxide walls, leading to hybrid mesostructured materials with tunable surfaces; this is certainly a promising subject in the design of sophisticated materials, such as catalysts, membranes, sensors, and nanoreactors [10,153]. A considerable number of methods have been developed or modified to add organic functions to the walls of mesoporous silica [154], combining the properties of a mesoporous inorganic structure with the surface organic groups [10].

The inclusion of the organic functions can, in principle, be carried out in two modes: covalent binding on the inorganic walls of the material, and direct inclusion of the organic functions upon the synthesis process [10]. In the first method, organochlorosilanes or organoalkoxysilanes have been extensively utilized to connect particular organic groups by condensation reactions with silanol or Si–O–Si groups of the silica framework [155,156]. The mesoporous hosts must be carefully dried before adding the organosilane precursors, to elude their autocondensation in the presence of water [10]. The concentration and delivery control of the organic functions is limited by the surface silanols and their ease of access. The grafting ratio depends of the precursor reactivity being also restricted by diffusion and steric features [10]. A substitute line of attack for pore functionalization relies on a direct synthesis, based on the co-condensation of siloxane and organosiloxane precursors *in situ* to give up modified MCM-41 in one step [157]. While siloxane precursors guarantee the formation of the mineral network, organosiloxane moieties perform a twofold role. That is, they contribute as building blocks of the inorganic structure and provide organic groups [10]. This one-pot pathway presents several advantages, such as high modification ratios, homogeneous incorporation, and short preparation times [158].

On the other hand, the periodic nanostructures of MCM-41 mesoporous oxides and other mesoporous molecular sieve materials recommend that they could operate as model hosts for reasonable nanomanufacturing [159]. The purpose of numerous studies has been to develop a methodology of using ordered nanoporous oxide materials as generic nanoscale reactors for making and replicating technically important nanomaterials [150–153].

Two approaches have been elaborated to transport precursor molecules or ions for the construction of nanoparticles or nanorods inside the channels of MCM-41 and related mesoporous oxides. The first technique requires the direct impregnation of mesoporous materials with precursor molecules or ions [160–162]. The next method uses functional ligands to, at random, functionalize together the internal and the external surfaces of mesoporous oxides, followed by inserting the precursor compounds through affinity interaction between the functional ligands and metal ions [163].

The construction of silver nanorods inside SBA-15 through the direct impregnation and evaporation of silver ion sources has been reported [161]. A new gas-phase transport method to load MCM-41 with cluster compounds has been also developed [162]. The main problem associated with these methodologies is the complication in controlling the site of the growth of nanoparticles and preventing their uncontrolled aggregation on external surfaces of the MCM-41 [159]. An accurately regulated

technique of building nanoparticles within the mesopores of externally functionalized MCM-41 materials through the controlled transport of metal ions via ion-exchange reactions has been also developed [159]. This new methodology makes use of the single mesoscopic arrangement of as-synthesized MCM-41, whose external surfaces can be selectively passivated with inert organic groups to remove the external nucleation sites but still retain the ion-exchange ability of the internal pore surfaces [159].

Copper-tellurolate cluster [$(Cu_6(TePh)_6(PPh_2Et)_5$] has been loaded into the pores of MCM-41 by solid-state impregnation techniques [164].

Independently, numerous studies were reported on the encapsulation of organic polymers within the channels of mesoporous silica materials. [165–171]. For example, Moller and Bein reported the polymerization of polyaniline and other monomers inside the mesopore system of MCM-41 [166]. The polyaniline system with conjugated polymers with mobile charge carriers within nanometer-size galleries can be considered as a noteworthy advance in the direction of the design of nanoscale electronic devices [166]. Afterward, Moller et al. studied the polymerization of methyl methacrylate within microporous and mesoporous silicas, with the resultant polymer possessing different physical properties compared with the bulk polymer [166,167]. Tolbert and coworkers demonstrated that semiconducting polymers aligned within mesopores showed exclusive energy transfer and photophysical properties, promising for the preparation of electronic and optoelectric devices [169,170].

In all of these studies, the polymers filled the entire volume of the silica mesopores, resulting, for most of the cases, in nonporous materials. However, certain notable aspects of the nanoscale chemistry and physics of polymers confined within mesoporous channels were revealed. Recently, Shantz and coworkers reported the synthesis of dendrimers inside the mesoporous silica [171].

8.5 SOME APPLICATIONS OF CRYSTALLINE AND ORDERED NANOPOROUS MATERIALS IN GAS SEPARATION AND ADSORPTION PROCESSES

8.5.1 Gas Cleaning

8.5.1.1 Zeolites

Gas or vapor molecules, after the degasification process, can go through the pore structure of crystalline and ordered nanoporus materials through a series of channels and/or cavities. Each layer of these channels and cavities is separated by a dense, gas-impermeable division, and within this adsorption space the molecules are subjected to force fields. The interaction with this adsorption field within the adsorption space is the basis for the use of these materials in adsorption process.

Zeolites A, X, ZSM-5, chabazite, clinoptilolite, mordenite, and other nanoporous materials are used for removing H_2O, NH_3, NO, NO_2, SO_2, SH_2, CO_2, and other impurities from gas streams [31,122,171–178]. For example, in gas cleaning zeolites are normally used for the removal of H_2O, SH_2, and CO_2 from sour natural gas streams [31,122,172–177]. They could be also used for drying of the CO_2 used in

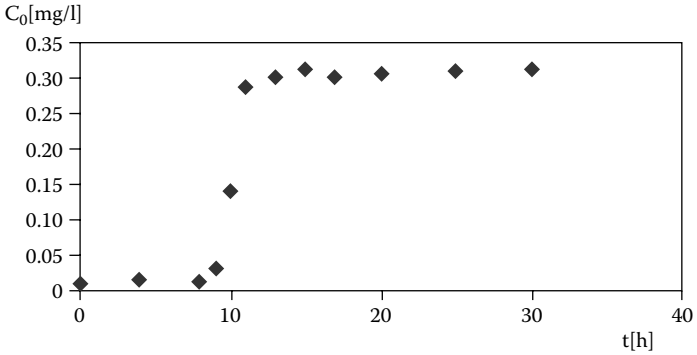

FIGURE 8.7 Breakthrough curve resulting from the dynamic adsorption of H_2O from a CO_2–H_2O mixture by a Mg-CMT natural zeolite [175,176].

cryosurgery; selective removal of NH_3 produced during the gasification of coal; removal of NH_3, SO_2, NO_x, and CO_2 from air; and for the selective adsorption of SH_2 from methane (CH_4) streams [31,122,172,173].

Among natural zeolites, clinoptilolite is the most profusely distributed in the Earth's crust and, consequently, is the most commonly applied in adsorption applications [31]. Clinoptilolite is a member of the heulandite family, with a molar ratio Si/Al > 4; about 22 water molecules compose the unit cell, where Na, K, Ca, and Mg are the most common charge-balancing cations [31].

Figure 8.7 shows the breakthrough curve following from the dynamic adsorption of H_2O from a CO_2–H_2O mixture by a Mg-CMT natural zeolite [175]. The water concentration in the mixture prior to breakthrough was C_0 = 0.32 mg/l, which was reduced, after the passage of the gas flow through the adsorption reactor, to 0.01–0.03 mg/l [175,176]. The reactor had a cross-sectional area, S = 10.2 cm^2, column length, D = 6.9 cm, adsorbent mass in the bed, M = 30 g. The volume of the bed was 70 cm^3, the volume free of adsorbent in the bed was about 35 cm^3, and the volumetric flow rate was F= 7.7 [cm^3/s] [175,176]. The Mg-CMT natural zeolite is an homoionic magnesium natural zeolite sample labeled CMT, which is a mixture of clinoptilolite (42 wt. %), and mordenite (39 wt, %), and other phases (15 wt. %), where the other phases are montmorinollite (2–10 wt. %), quartz (1–5 wt. %), calcite (1–6 wt. %), feldspars (0–1 wt. %), and volcanic glass [31,176]. The reactor had a cross-sectional area, S = 10.2 cm^2, column length, D = 6.9 cm, adsorbent mass in the bed, M = 30 g; the volume of the bed was 70 cm^3, the volume free of adsorbent in the bed was about 35 cm^3, and the volumetric flow rate was, F= 7 [cm^3/s] [175,176].

In Table 8.1 [176] are shown the breakthrough mass (B.M.) for air drying in an adsorption bed reactor filled with natural clinoptilolite (HC sample), and mordenite (MP sample), and ionic-exchanged clinoptilolite and mordenite, i.e., homoionic sodium clinoptilolite (Na-HC sample), and mordenite (Na-MP samle), and homoinic calcium clinoptilite (Ca-HC sample), and mordenite (Ca-MP sample). The B.M. was measured in mg of water/cm^3 of adsorption bed, where the volume of the bed was 70 cm^3, and the volume free of adsorbent in the bed was 35 cm^3 [176].

TABLE 8.1
Breakthrough Mass (B.M.) for Air Drying in the Adsorption Reactor Filled with Natural (HC Sample) and Homoionic Sodium Clinoptilolite (Na-HC) and Homoinic Calcium Clinoptilite (Ca-HC) [176]

Sample	B.M. [mg of H_2O/cm^3]	Sample	B.M. [mg of H_2O/cm^3]
HC	39	MP	32
Na-HC	44	Na-MP	42
Ca-HC	67	Ca-MP	49
Na-X	96	Alumina	28

The natural zeolite sample labeled HC is relatively pure clinoptilolite containing 85 wt. % of clinoptilolite and 15 wt. % of other phases, where the other phases are: montmorinollite (2–10 wt. %), quartz (1–5 wt. %), calcite (1–6 wt. %), feldspars (0–1 wt. %), and volcanic glass [31,176]. The natural zeolite sample labeled MP is a reasonably pure mordenite containing 80 wt. % of mordenite and 20 wt. % of other phases, where the other phases are montmorinollite (2–10 wt. %), clinoptilolite (1–5 wt. %), quartz (1–5 wt. %), calcite (1–6 wt. %), feldspars (0–1 wt. %), and volcanic glass [31,176]. The adsorbents used for comparison in the present experiment were a synthetic Na-X zeolite provided by Laporte and alumina (Al_2O_3) provided by Neobor [176]. The water concentration in the tested air prior to breakthrough was 1.2 mg/l, and it was reduced after the pass of the air flow through the adsorption reactor to 0.01–0.03 mg/l [176].

The HEU framework of clinoptilolite is a two-dimensional micropore channel system, where the 10-membered-rings (MR) channel A and the 8-MR channel B run parallel to each other and to the *c* axis of the unit cell, while channel C (8-MR) is placed along the *a* axis, intersecting both the A and B channels (see Figure 8.3) [37]. The elliptical shaped 8-MR and 10-MR that make up the channel system are nonplanar and, consequently, cannot be simply dimensioned. The structure of mordenite (MOR framework type [37]) is characterized by the presence of a two-dimensional micropore channel system. One of the channels, the principal of the system because the other channel is normally blocked, is a 12-MR channel running along the [001] axis with free access of 6.5 Å × 7 Å, the other channel is a 8-MR side pocket channel running along [010], with a window of access of 2.6 Å × 5.7 Å connecting the 12-MR channels [12,38].

The selectivity and uptake rate of gases by clinoptilolite and mordenite natural zeolites, and also by other zeolites, are influenced by the type, number, and location of the charge-balancing cations residing in the A–C channels [12,31,38,173–181]. Therefore, the positions adopted by exchangeable cations and the adsorbed molecules are interdependent; then variations in the cation composition cause changes in the amount of adsorbed molecules as is evident from Table 8.1 [176].

In the case of the synthetic zeolite Na-A, it is possible to cation exchange it with potassium and calcium, in order to get the 3A and 5A molecular sieves, respectively. Different studies [173,174,178,182,183] have shown that the pore-opening size of zeolite and other molecular sieves can be controlled to fit desired applications by post-synthesis modification techniques such as internal or external surface modification by chemical reactions, preadsorption of polar molecules [173], chemical vapor deposition [181] or similar coating processes, and thermal treatment [182].

It has also been reported that, by calcination of Na-A zeolites at 953–1033 K after water vapor adsorption, the adsorption predilection toward oxygen over nitrogen is improved, a fact which can be credited fundamentally to pore-size shrinkage [178]. It has also been shown [174] that the pore size and the affinity of a zeolite structure can be modified by chemical treatment of the zeolite structure; the silane, borane, or disilane molecules are chemisorbed on the zeolite surface by reacting with the silanol groups of the zeolite [178]. Polar molecules, as for example water and amines, presorbed in the zeolite can also be applied to modify the molecular sieve performance and the interaction toward adsorbate molecules of the zeolite [178].

8.5.1.2 Mesoporous Molecular Sieves

The attention paid to this new family of adsorbents is mainly due to the unique mesopore structure, which is not shared by any other families of adsorbent [184–186]. Consequently, mesoporous ordered silica has been proposed as a reference material for the study of adsorption processes in mesopores [187–190]. In addition, to the pore structure, one of the most striking features of these novel materials is the large BET surface area and pore volume [191,192]. The surface properties of MMS could be of major importance both for the preparation of active and stable catalysts [156] and for the modification of their sorption properties.

The interactions of the mesoporous molecular sieve surface and test molecules can provide useful information on the nature and local arrangement of the surface groups, which cause either hydrophobic or hydrophilic behavior, characterized by a heat of adsorption smaller or larger than the heat of liquefaction of water, respectively [184]. Accordingly, adsorption of water on M41 systems has been studied using microcalorimetry and IR spectroscopy. It was shown that, after thermal treatment at 423 K, the samples exhibit two types of surface patches, one hydrophobic, distinguished by isolated silanols not interacting with water, and the other highly hydrophilic [184]. However, it is generally recognized that the internal surface of these materials is hydrophobic, notwithstanding the presence of silanol groups [193–196]. Consequently, the hydrophobic surface nature reveals these materials as selective adsorbents for the removal of volatile organic compounds (VOCs) and other organic compounds presented in high-humidity gas streams or wastewater [193]. Consequently, MCM-41 is a possible adsorbent to substitute for activated carbon for controlling VOCs. [185,193,195]. However, the adsorption equilibrium of VOCs on MCM-41 regularly shows very low adsorption capacity in the low-concentration region because of its mesoporous structure. This fact considerably limits the application of MCM-41 as an adsorbent for low-concentration VOC abatement [193].

The pore sizes of MCM-41 materials can be modified during synthesis by selecting various surfactants with different carbon chain lengths; the minimum pore size that can be obtained seems to be about 2 nm [21–24]. Simultaneously, as the pore size is lessened, the pore volume is also diminished. The modification of the pore diameter of MCM-41 by post-modification is attractive and essential to attain a shape-selective adsorption property [185]. Consequently, the pore-opening size of MCM-41 could be reduced to be in the microporous region, using a chemical vapor deposition technique, for a selective modification, in order to improve the adsorption properties of the modified MCM-41, which significantly improves the adsorption performance of MCM-41 for low-concentration volatile organic compounds [193].

The adsorption characteristics of MCM-41 for polar molecules depend greatly on the concentrations of surface silanol groups (SiOH) [184,193–196]. It has been demonstrated that several types of SiOH groups exist over MCM-41 surfaces, which can be qualitatively and quantitatively determined by a number of techniques [184,193–196]. Those SiOH groups allow various modifications of MCM-41 for catalysis, adsorption, and novel composites [196]. For example, a sorption separation process using modified MCM- 41 for purification of water has been proposed [197].

The large pore volume, pore size flexibility, and structural variety of MCM-41 can be extensively used for the selective adsorption of a diversity of gases and liquids [185,186,193–196]. It has shown, for example, an extremely high sorption capacity for benzene [186,193,195]. Widespread work has been carried out on sorption properties of some adsorbates, such as nitrogen, argon, oxygen, water, benzene, cyclopentane, toluene, and carbon tetrachloride, as well as certain lower hydrocarbons and alcohols on MCM-41 [194].

It was also shown that the adsorptive capacity of the mesoporous materials is more than an order of magnitude superior to that of conventional porous adsorbent materials. MCM-41 is therefore promising as a selective adsorbent in separation techniques, for example, high-performance liquid chromatography and supercritical fluid chromatography [194].

In addition, the substitution of the surface hydroxyl groups in the pore wall with trimethylchlorosilane groups creates a more hydrophobic environment that substantially reduces the sorption capacity of polar molecules [196]. The surface chemistry of MCM-41 and other ordered mesoporous molecular sieves can be efficiently modified to be more hydrophobic by chemical addition of organic species, a process called silylation. The surface modification of ordered mesoporous molecular sieves can be conducted in various other ways, such as esterification and chemical depositions [196]. A few types of silanol groups exist on MCM-41 surfaces, among which both free and geminal ones (see Chapter 7, Section 7.2) are responsible for active silylation. Consequently, free and germinal silanol groups over MCM-41 surfaces are responsible for such active modification [196]. Siliceous MCM-41 samples were modified by silylation using trimethylchlorosilane (TMCS); the degree of silylation was found to linearly increase with increasing pre-outgassing temperature prior to silylation [196]. It was finally shown that surface modification of MCM-41 by silylation is an effective technique in the development of selective adsorbents for the removal of organic compounds from streams or wastewater [196].

In summary, the outstanding characteristics of the majority of ordered mesoporous materials are the following: well-defined pore shapes, fine distribution of pore sizes, insignificant pore networking or pore blocking effects, especially high degree of pore ordering over micrometer length scales, tailoring and modification of the pore dimensions, large pore volumes, excellent sorption capacity as a result of the large pore volume, very high surface area (700–1500 m^2/g), large amounts of internal hydroxyl (silanol) groups (40–60%), high surface reactivity, ease of modification of the surface properties, enhanced catalytic selectivity in certain rections, and excellent thermal, hydrothermal, and mechanical properties [194].

8.5.2 Pressure Swing Adsorption

In the present monograph we have not discussed the adsorption process in multicomponent gas systems. We are studying adsorption here primarily from the point of view of materials science; therefore we are interested in the methods for the use of single-component adsorption in the characterization of the adsorbent surface and pore volume, the study of the parameters characterizing single-component transport processes in porous systems, and to a lesser extent, the adsorption energy and dynamic adsorption in bed reactors. However, from the point of view of the application of adsorbent materials, it is necessary to discuss gas mixture separation, and this is the aim of the present section.

Pressure-swing adsorption (PSA) is a cyclic process used to selectively adsorb and separate components of a feed gas mixture, thereby producing partially purified gas products. Since the first patent of a PSA process [198], a great variety of complicated PSA processes have been developed and commercialized, largely taking advantage of PSA's low energy requirement and low capital investment [199]. It is a very multipurpose technology for separation and purification of gas mixtures, which offers an additional level of thermodynamic freedom for describing the adsorption process in comparison with other standard separation methods, as for example, distillation, extraction, or absorption [200].

Some of the main industrial applications include [200–212]:

1. gas drying
2. solvent vapor recovery
3. fractionation of air
4. production of hydrogen from steam methane reformer and petroleum refinery off-gases
5. separation of carbon dioxide and methane from landfill gas
6. carbon monoxide–hydrogen separation
7. normal isoparaffin separation
8. alcohol dehydration

The concept of PSA for gas separation is fairly simple. Some components of a gas mixture are selectively adsorbed on a microporous–mesoporous solid adsorbent at a comparatively high pressure, by contacting the gas with the solid in a packed column of the adsorbent, in order to yield a gas stream enriched in the less strongly

adsorbed components of the feed gas [200]. The adsorbed components are, after that, desorbed from the solid by reducing their superincumbent gas-phase partial pressures in the interior of the column, in order that the adsorbent can be reused [200]. Then, the desorbed gases are enriched in the more strongly adsorbed components of the feed gas [200–208]. During the process no external heat is generally used for desorption [200]. On the other hand, a vacuum swing adsorption (VSA) process undergoes the adsorption step at a near-ambient pressure level, and the desorption is achieved under vacuum [200].

In PSA processes presently available, as a rule, only one component is the chosen product, this is usually the most weakly adsorbed one; nevertheless, for a better economics, it is imperative to recover as many of the components from the feed as is possible [200].

Many microporous–mesoporous types of adsorbents, as synthesized or modified (such as activated carbons, zeolites, aluminas, silica gels, and polymeric sorbents exhibiting different adsorptive properties for separation of gas mixtures, i.e., equilibria, kinetics, and heats), are accessible for application in PSA or VSA processes [200–212].

For example, many different zeolites having diverse thermodynamic selectivities and capacities for adsorption are employed to develop PSA process for gas separation [200,212]. More concrete, zeolites A and X, chabazite, clinoptilolite, mordenite, and other zeolites can be used for PSA separation processes. For example, H_2–N_2, N_2–CH_4, and other couples can be separated with the assistance of zeolites [31]. The zeolite-related processes for N_2–O_2 separation are based, in general, in nitrogen-selective zeolite adsorbents [200,201] such as natural chabazite, clinoptilolite, and mordenite, which could be used for this purposes with a performance comparable to or better than those reported for synthetic mordenite or zeolites type A [198,199]. The PSA method with natural zeolite was also employed for methane purification [200].

The working principle of a PSA installation where vacuum is used for desorption, more exactly a VSA apparatus for N_2–O_2 separation with zeolites [209] (see Figure 8.8), is as follows. The pretreatment columns are filled with silica gel desiccant followed by a granulated zeolite; the main column is filled with a zeolite. The main (3a and 3b) and pretreatment columns (4a and 4b) are activated at 500°C. Filtered air is sent to the pretreatment column (4a for example), where H_2O, CO_2, and SO_2 are eliminated. The purified gas is sent to the main column (3a); nitrogen is mainly adsorbed in the columns, and O_2 with a small amount of Ar and N_2 in the gas tank (1). Before the column is exhausted, the air supply is sent to the pretreatment column (4b), and main column (4b) and the columns (3a and 4a) are connected automatically with the vacuum pump exhausting the N_2 [209].

8.5.3 Other Separation Applications

Gas separation with zeolites is also applied as an analytical tool, using zeolites as adsorbent columns for analysis in a gas chromatograph [213–215].

Additionally, we have previously discussed gas separation with the help of pressure swing methods, which imply cycles of favored adsorption of one component over the other and succeeding desorption [200]. The replacement of swing adsorption

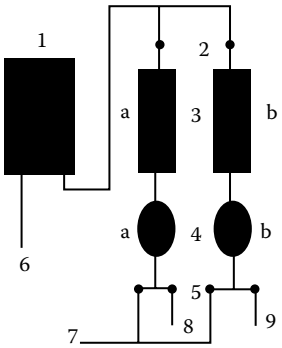

FIGURE 8.8 The vacuum swing adsorption (VSA) equipment for oxygen generation from air include the oxygen gas tank (1), automatic stopcocks (2 and 5), multiple zeolite adsorption beds (3a and 3b), pretreatment columns (4a and 4b), vacuum pump (7), and the air supply (8 and 9).

methods with a steady-state membrane process could be useful, because of the reduction of operating costs and energy consumption. In this sense, microporous inorganic membranes could be very useful in gas separation [216]. These membranes could be manufactured with zeolites and are potentially useful in gas separation for cleaning processes and catalytic reactors [217]. The zeolite in these membranes should be placed in the form of a thin film supported on a macroporous substrate [216,218].

In Chapter 5, we discussed the gas transport mechanism through microporous inorganic membranes, and it was shown that the transport of molecules through zeolite cavities and channels determines the molecular sieving nature of these materials. Then zeolite-based membranes will be molecular sieves, and consequently they can be used for gas separation processes. The pore size distribution of these materials can be controlled by synthesis procedures, so that their molecular sieving properties can be tailored to selectively separate gases and purify them [216].

8.5.4 Air-Conditioning

Solar energy storage [31,219] and solar cooling [31,220–222] applications of natural zeolites are closely connected with the adsorption properties of these minerals. In solar cooling installations (see Figure 8.9), solar heating is utilized to induce water desorption, and consequently the dehydration of a zeolite contained in a solar panel (1). The desorbed water is later condensed (2) and allowed to pass into a deposit (6). Water is allowed, through a heat exchanger (7), to advance to an evaporator system (8), where water is able to diffuse to the previously dehydrated zeolite (1). The cooling is provided by water evaporation to the dehydrated zeolite. The process is cyclic; this means that zeolite desorption is carried out during the day and water adsorption in the zeolite at night [53].

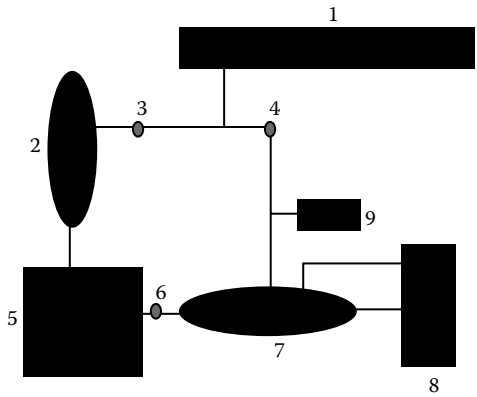

FIGURE 8.9 Solar cooling installation, zeolite-filled solar panel (1), water condenser (2), stopcocks (3, 4, and 6), water deposit (5), heat exchanger (7), evaporator (8), and buffer storage (9).

REFERENCES

1. Nalwa, H.S., Ed., *Encyclopedia of Nanoscience and Nanotechnology,* Vol. 1–10, American Scientific Publishers, Stevenson Ranch, California, 2004.
2. Borisenko, V.E. and Ossicini, S., *What Is What in the Nanoworld: A Handbook on Nanoscience and Nanotechnology,* J. Wiley & Sons, New York, 2004
3. Wolf, E.L., *Nanophysics and Nanotechnology: An Introduction to Modern Concepts in Nanoscience,* J. Wiley & Sons, New York, 2004.
4. Delerue, C. and Lannoo, M., *Nanostructures,* Springer-Verlag, New York, 2004.
5. Cushing, B.L., Kolesnichenko, V.L., and O'Connor, C.J., *Chem. Rev.*, 104, 3893, 2004.
6. Rouvray, D., *Chem. Br.*, 36, 46, 2000.
7. Lawton, G., *Chem. Ind.* (*London*), 174, 2001.
8. Havancsak, K., *Mater. Sci. Forum,* 414, 85, 2003.
9. Siegel, R.W., Hu, E., and Roco, M.C., Eds., *WTEC Panel Report on Nanostructure Science and Technology: R & D Status and Trends in Nanoparticles, Nanostructured Materials, and Nanodevices,* Kluwer, Dordrecht, The Netherlands, 1999.
10. Soler-Illia, G.J.A.A., Sanchez, C., Lebeau, B., and Patarin, J., *Chem. Rev.*, 102, 4093, 2002.
11. Sing, K.S.W., Everett, D.H., Haul, R.A.W., Moscou, L., Pirotti, R.A., Rouquerol, J., and Siemieniewska, T., *Pure App. Chem.*, 57, 603, 1985.
12. Breck, D.W., *Zeolite Molecular Sieves,* Wiley, New York, 1974.
13. Barrer, R.M., *Hydrothermal Chemistry of Zeolites,* Academic Press, London, 1982.
14. Szostak, R., *Handbook of Molecular Sieves,* Van Nostrand Reinhold, New York, 1992.
15. Flanigen, E.M., Patton, R.L., and Wilson, S.T., *Stud. Surf. Sci. Catal.*, 37, 13, 1988.
16. Cundy, C.S. and Cox, P.A., *Chem. Rev.*, 103, 663, 2003.
17. Kessler, H., in *Comprehensive Supramoleular Chemistry, Vol. 7, Solid-State Supramolecular Chemistry: Two- and Three-Dimensional Inorganic Networks,* Atwood, J.L., Davis, J.E., MacNicol, D.D., and Vogtle, F., eds., Pergamon, London, United Kingdom, 1996, p. 425.

18. Davies, M.E., *Nature,* 417, 813, 2002.
19. Garces, J.M., Kuperman, A., Millar, D.M., Olken, M., Pyzik, A., and Rafaniello, W., *Adv. Mat.*, 12, 1725, 2000.
20. Occelli, M.L. and Kessler, H., Eds., *Synthesis of Porous Materials,* Marcel Dekker, New York, 1997.
21. Kresge, C.T., Leonowicz, M.E., Roth, W.J., Vartuli, J.C., and Beck, J.S., *Nature,* 359, 710, 1992.
22. Beck, J.S., Vartuli, J.C., Roth, W.J., Leonowicz, M.E., Kresge, C.T., Schmitt, K.D., Chu, C.T.-W., Olson, D.H., Sheppard, E.W., McCullen, S.B., Higgins, J.B., and Schlenker, J.L., *J. Am. Chem. Soc.*, 114, 10834, 1992.
23. Zhao, X.S., Lu, G.Q., and Millar, G.J., *Ind. Eng. Chem. Res.*, 35, 2075, 1996.
24. Barton, T.J., Bull, L.M., Klemperer, G., Loy, D.A., McEnaney, B., Misono, M., Monson, P.A., Pez, G., Scherer, G.W., Vartulli, J.C., and Yaghi, O.M., *Chem. Mater.*, 11, 2633, 1999.
25. Iler, R.K., *The Chemistry of Silica,* Wiley, New York, 1979.
26. Stober, W., Fink, A., and Bohn, E., *J. Colloids Interface Sci.*, 26, 62, 1968.
27. Brinker, C.J. and Scherer, G.W., *Sol-Gel Science,* Academic Press, New York, 1990.
28. Unger, K., and Kumar, D., in *Adsorption on Silica Surfaces,* Papirer, E., Ed., Marcel Dekker Inc., New York, 2000, p. 1.
29. Burda, C., Chen, X., Narayanan, R., and El-Sayed, M.A., *Chem. Rev.*, 105, 1025, 2005.
30. Corma, A., *Chem. Rev.*, 95, 559, 1995.
31. Roque-Malherbe, R., in *Handbook of Surfaces and Interfaces of Materials,* Volume 5, Nalwa, H.S., Ed., Academic Press, New York, 2001, p. 495.
32. Martin, J.E., Anderson, M.T., Odinek, J., and Newcomer, P., *Langmuir,* 13, 4133, 1997.
33. Tolbert, S.H., Schaffer, T.E., Feng, J., Hansma, P.K., Stucky, G.D., *Chem. Mater.*, 9, 1962, 1997.
34. Bruinsma, P.J., Kim, A.Y., Liu, J., and Baskaran, S., *Chem. Mater.*, 9, 2507, 1997.
35. Kerr, G.T., *American Chemical Society, Symposium Series,* 368, xiii, 1988.
36. Marquez-Linares, F. and Roque-Malherbe, R., *Facets IUMRS J.*, 2, 14, 2003.
37. Baerlocher, C., Meier, W.M., and Olson, D.M., *Atlas of Zeolite Framework Types,* 5th ed., Elsevier, Amsterdam, 2001.
38. Smith, J., *Chem. Rev.*, 88, 149, 1988.
39. Flanigen, E.M., Bennett, J.M., Grose, R.W., Cohen, J.P., Patton, R.L., Kirchner, R.M., Smith, J.V., *Nature,* 271, 512, 1978.
40. Bibby, D.M., Milestone, N.B., and Aldridge, L.P., *Nature,* 280, 664, 1979.
41. Fyfe, C.A., Gies, H., Kokotailo, G.T., Marler, B., and Cox, D.E., *J. Phys. Chem.,* 94, 3718, 1990.
42. Bialek, R., Meier, W.M., Davis, M., and Annen, M.J., *Zeolites,* 11, 438, 1991.
43. Camblor, M.A., Corma, A., and Valencia, S., *J. Chem. Soc. Chem. Commun.*, 2365, 1996.
44. Barrett, P.A., Camblor, M.A., Corma, A., Jones, R.H., and Villaescusa, L.A., *Chem. Mater.*, 9, 1713, 1997.
45. Camblor, M.A., Corma, A., Lightfoot, P., Villaescusa, L.A., and Wright, P.A., *Angew. Chem., Int. Ed. Engl.*, 36, 2659, 1997.
46. Villaescusa, L.A., Barrett, P.A., and Camblor, M.A., *Chem. Mater.*, 10, 3966, 1998.
47. Barrett, P.A., Diaz-Cabanas, M.J., Camblor, M.A., and Jones, R.H., *J. Chem. Soc. Faraday Trans.*, 94, 2475, 1998.
48. Diaz-Cabanas, M.J., Barrett, P.A., and Camblor, M.A., *Chem. Commun. Cambridge,* 1881, 1998.

49. Camblor, M.A., Corma, A., Diaz-Cabanas, M.J., and Baerlocher, C., *J. Phys. Chem. B,* 102, 44, 1998.
50. Villaescusa, L.A., Barrett, P.A., and Camblor, M.A., *Chem. Commun. Cambridge,* 2329, 1998.
51. Camblor, M.A., Diaz-Cabanas, M.J., Perez-Pariente, J., Teat, S.J., Clegg, W., Shannon, I.J., Lightfoot, P., Wright, P.A., and Morris, R.E., *Angew. Chem., Int. Ed.*, 37, 2122, 1998.
52. Villaescusa, L.A., Barrett, P.A., and Camblor, M.A., *Angew. Chem. Int. Ed.*, 38, 1997, 1999.
53. Jones, C., Hwang, S., Okubo, T., and Davis, M., *Chem. Mater.*, 13, 1041, 2001.
54. Piccione, P.M., Woodfield, B.F., Boerio-Goates, J., Navrotsky, A., and Davis, M., *J. Phys. Chem. B,* 105, 6025, 2001.
55. Marler, B., Werthmann, U., and Gies, H., *Mic. Mes. Mat.*, 43, 329, 2001.
56. Barrett, P.A., Boix, T., Puche, M., Olson, D.H., Jordan, E., Koller, H., and Camblor, M.A., *Chem. Commun. Cambridge,* 2114, 2003.
57. Corma, A., Rey, F., Rius, Sabater, M.J., and Valencia, S., *Nature,* 431, 287, 2004.
58. Li, Z., Lew, C.M., Li, S., Medina, D.I., and Yan, Y., *J. Phys. Chem. B,* 109, 8652, 2005.
59. Kühl, G.H., in *Catalysis and Zeolites: Fundamentals and Applications,* Weitkamp, J. and Puppe, L., Eds., Springer-Verlag, Berlin, 1999, p. 81.
60. Roque-Malherbe, R., Díaz, C., Reguera, E., Fundora, J., López-Colado, L., and Hernández-Vélez, M., *Zeolites,* 10, 685, 1990.
61. Blawhoff, P.M.M., Gosselink, J.W., Kieffer, E.P., Sie, S.T., and Stork, W.H.J., in *Catalysis and Zeolites: Fundamentals and Applications,* Weitkamp, J. and Puppe, L., Eds., Springer-Verlag, Berlin, 1999, p. 437.
62. Blanco, C. and Auerbach, S.M., *J. Phys. Chem. B,* 107, 2490, 2003.
63. Samanta, S., Giri, S., Sastry, P.U., Mal, N.K., Manna, A., and Bhaumik, A., *Ind. Eng. Chem. Res.*, 42, 3012, 2001.
64. Cai, Q., Luo, Z.-S., Pang, W.-Q., Fan, Y.-W., Chen, X.-H., and Cui, F.-Z., *Chem. Mater.*, 13, 258, 2001.
65. Widenmeyer, M. and Anwander, R., *Chem. Mater.*, 14, 1827, 2002.
66. Han, S., Hou, W., Yan, X., Li, Z., Peng Zhang, and Li, D., *Langmuir,* 19, 4269, 2003.
67. Fan, J., Yu, C., Wang, L., Tu, B., Zhao, D., Sakamoto, Y., and Terasaki, O., *J. Am. Chem. Soc.,* 123, 12113, 2001.
68. Pantazis, C.C. and Pomonis, P.J., *Chem. Mater.*, 15, 2299, 2001.
69. Monnier, A., Schüth, F., Huo, Q., Kumar, D., Margolese, D., Maxwell, R.S., Stucky, G.D., Krishnamurthy, M., Petroff, P., Firouzi, A., Janicke, M., and Chmelka, B.F., *Science,* 261, 1299, 1993.
70. Huo, Q., Margolese, D., Ciesia, U., Feng, P., Gier, T.E., Sieger, P., Leon, R., Petroff, P.M., Schuth, F., and Stucky, G.D., *Nature,* 368, 317, 1994.
71. Tanev, P.T. and Pinnavaia, T.J., *Science,* 267, 865, 1995.
72. Bagshaw, S., Prouzet, E., and Pinnavaia, T.J., *Science,* 269, 1242, 1995.
73. Karra, V.R., Moudrakovski, I.L., and Sayari, A., *J. Porous Mater.*, 3, 77, 1996.
74. Huo, Q., Margolese, D.I., Ciesla, U., Demuth, D.K., Feng, P., Gier, T.E., Sieger, P., Firouzi, A., Shmelka, B.F., Schuth, F., and Stucky, G.D., *Chem. Mater.*, 6, 1176, 1994,
75. Beck, J.S., Vartuli, J.C., Kennedy, G.J., Kresge, C.T., Roth, W.J., and Schramm, S.E., *Chem. Mater.*, 6, 1816, 1994.
76. Stucky, G.D., Monnier, A., Schuth, F., Huo, Q., Margolese, D., Kumar, D., Krishnamurthy, M., Petroff, P.M., Firouzi, A., Janicke, M., and Chmelka, B.F., *Mol. Cryst. Liq. Cryst.*, 240, 187, 1994.

77. Firouzi, A., Kumar, D., Bull, L.M., Besler, T., Sieger, P., Huo, Q., Walker, S.A., Zasadzinski, J.A., Glinka, C., Nicol, J., Margolese, D., Stucky, G.D., and Chmelka, B.F., *Science,* 267, 1138, 1995.
78. Roque-Malherbe, R. and Marquez-Linares, F., *Mat. Sci. Semicond. Proc.*, 7, 467, 2004.
79. Roque-Malherbe, R. and Marquez-Linares, F., *Surf. Interf. Anal.*, 37, 393, 2005.
80. Husson, F., Mustacchi, H., and Luzzatti, V., *Acta Crystallogr.*, 13, 668, 1960.
81. Huo, Q., Leon, R., Petroff, P., and Stucky, G.D., *Science,* 268, 1324, 1995.
82. Zhao, D., Feng, J., Huo, Q., Melosh, N., Fredrickson, G.H., Chmelka, B.F., and Stucky, G.D., *Science,* 279, 548, 1998.
83. Nossov, A., Haddad, E., Guenneau, F., Galarneau, A., Di Renzo, F., Fajula, F., and Gedeon, A., *J. Phys. Chem. B,* 107, 12456, 2003.
84. Fan, J., Chengzhong, Y., Wang, Y.L., Tu, B., Zhao, D., Sakamoto, Y., and Terasaki, O., *J. Am. Chem. Soc.,* 123, 12113, 2001.
85. Lukens, W.W., Jr., Schmidt-Winkel, P., Zhao, D., Feng, J., and Stucky, G.D., *Langmuir,* 15, 5403, 2001.
86. Ryoo, R., Ko, C.H., Kruk, M., Antochshuk, V., and Jaroniec, M., *J. Phys. Chem. B,* 104, 11465, 2000.
87. Galarneau, A., Cambon, H., Di Renzo, F., and Fajula, F., *Langmuir,* 17, 8328, 2001.
88. Galarneau, A., Cambon, H., Di Renzo, F., Ryoo, R., Choi, M., and Fajula, F., *New J. Chem.,* 27, 73, 2001.
89. Sayari, A., Han, B.-H., and Yang, Y., *J. Am. Chem. Soc.,* 126, 14384, 2001.
90. Zhao, D., Sun, J., Li, Q., and Stucky, G.D., *Chem. Mater.*, 12, 275, 2000.
91. Zhao, D., Yang, P., Chmelka, B.F., and Stucky, G.D., *Chem. Mater.*, 11, 1174, 1999.
92. Huo, Q., Feng, J., Schuth, F., and Stucky, G.D., *Chem. Mater.*, 9, 14, 1997.
93. Robson, H., *Verified Synthesis of Zeolitic Materials,* 2nd ed., Elsevier, Amsterdam, 2001.
94. Wadlinger, R.L., Kerr, G.T., and Rosinski, E.J., U.S. Patent 3,308,069, 1967.
95. Argauer, R.J. and Landolt, G.R., U.S. Patent 3,702,886, 1972.
96. Lok, B.M., Messina, C.A., Patton, R.L., Gajek, R.T., Cannan, T.R., and Flanigen, E.M., *J. Am. Chem. Soc.*, 106, 6092, 1984.
97. Parise, J.B., *Chem. Commun.*, 606, 1985.
98. Merrouche, A., Patarin, J., Kessler, H., Soulard, M., Delmotte, L., Guth, J.L., and Joly, J.F., *Zeolites,* 12, 22, 1992.
99. Ferey, G., *J. Fluorine Chem.*, 72, 187, 1995.
100. Harrison, W.T.A., Martin, T.E., Gier, T.E., and Stucky, J.D., *J. Mater. Chem.*, 2, 2175, 1992.
101. Wallau, M., Patarin, J., Widmer, I., Caullet, P., Guth, J.L., and Huve, L., *Zeolites,* 14, 402, 1994.
102. Harvey, G. and Meier, W.M., *Stud. Surf. Sci. Catal.*, 49A 411, 1989.
103. Soghomoniam, V., Chen, Q., Haushalter, R.C., and Zubieta, J., *Angew. Chem. Int. Ed. Engl.*, 32, 610, 1993.
104. Debord, J.R.D., Reiff, W.M., Warren, C.J., Haushalter, R.C., and Zubieta, J., *Chem. Mater.*, 9, 1994, 1997.
105. Kessler, H., Patarin, J., and Schott-Darie, C., *Stud. Surf. Sci. Catal.*, 85, 75, 1994.
106. Bibby, D.M. and Dale, M.P., *Nature,* 317, 157, 1985.
107. Huo, Q., Xu, R., Li, S., Ma, Z., Thomas, J.M., Jones, R.H., and Chippindale, A.M., *Chem. Commun.*, 875, 1992.
108. Althoff, R., Unger, K., and Schüth, F., *Microporous Mater.*, 2, 557, 1994.

109. Lobo, R.F., Zones, S.I., and Davis, M.E., *J. Inclusion Phenom. Mol. Recogn. Chem.*, 21, 47, 1995.
110. Camblor, M.A., Villaescusa, L.A., and Diaz-Cabañas, M.J., *Top. Catal.*, 9, 59, 1999.
111. Flanigen, E.M. and Patton, R.L., U.S. Pat. 4,073,865, 1978.
112. Guth, J.L., Kessler, H., and Wey, R., in *New Developments in Zeolite Science and Technology,* Murakami, Y., Iijima, A., and Ward, J.W., Eds., Elsevier, Amsterdam, 1986, p. 121.
113. Gilson, J.P., in *Zeolite Microporous Solids: Synthesis, Structure and Reactivity,* Derouane, E.G., Lemos, F., Naccache, C., and Ribeiro, F.R., Eds., NATO ASI Series, No. C352, Kluwer, Dordrecht, 1992, p. 19.
114. Szostak, R., *Molecular Sieves. Principles of Synthesis, and Identification,* 2nd ed., Blackie, London, 1998.
115. Camblor, M.A., Barrett, P.A., Diaz-Cabañas, M.J., Villaescusa, L.A., Puche, M., Boix, T., Perez, E., and Koller, H., *Mic. Mes. Mat.*, 48, 11, 2001.
116. Barrett, P.A., Boix, E.T., Camblor, M.A., Corma, A., Diaz-Cabañas, M.J., Valencia, S., and Villaescusa, L.A., in *Proceedings of the 12th International Zeolite Conference, Baltimore, 1998,* Treacy, M.M.J., Marcus, B.K., Bisher, M.E., and Higgins, J.B., Materials Research Society, Warrendale, PA, 1999, p. 1495.
117. Villaescusa, L.A. and Camblor, M.A., *Recent. Res. Devel. Chem.*, 1, 93, 2001.
118. Zones, S.I., Darton, R.J., Morris, R., and Hwang, S.-J., *J. Phys. Chem. B,* 109, 652, 2005.
119. Kubota, Y., Helmkamp, M.M., Zones, S.I., and Davis, M.E., *Mic. Mater.*, 6, 213, 1996.
120. Auerbach, S.M., Bull, L.M., Henson, N.J., Metiu, H.I., and Cheetham, A.K., *J. Phys. Chem.*, 100, 5923, 1996.
121. Ryu, Y.-K., Chang, J.W., Jung, S.-Y., and Lee, C.-H., *J. Chem. Eng. Data,* 47, 363, 2002.
122. Roque-Malherbe, R., and Marquez-Linares, F., *Facets IUMRS J.*, 3, 8, 2004.
123. Kim, M.-B., Ryu, Y.-K., and Lee, C.-H., *J. Chem. Eng. Data,* 50, 951, 2005.
124. Kawi, S. and Gates, B.C., *J. Chem. Soc. Chem. Commun.*, 994, 1991.
125. Kawi, S. and Gates, B.C., *Catal. Lett.*, 10, 263, 1991.
126. Kawi, S., Chanf, J.-R., and Gates, B.C., *J. Amer. Chem. Soc.*, 115, 4830, 1993.
127. Cariati, E., Roberto, D., and Ugo, R., *Chem. Rev.*, 103, 3707, 2003.
128. Schulz-Ekloff, G. and Ernst, S., in *Preparation of Solid Catalysts,* Ertl, G., Knozinger, H., and Weitkamp, J., Ed., Wiley-VCH, New York, 1997, p. 405.
129. Ichikawa, M., Kimura, T., and Fukoaka, A., *Stud. Surf. Sci. Catal.*, 60, 335, 1991.
130. Gabrielov, A.G., Balkus, K.J., Jr., Bell, S.L., Bedioui, F., and Devynck, J., *Mic. Mat.*, 2, 119, 1994.
131. Bedioui, F., Roue, L., Gaillon, L., Devynck, J., Bell, S.L., and Balkus, K.J., Jr., *Preprints Division of Petroleum Chemistry, Amer. Chem. Soc.*, 38, 529, 1993.
132. Balkus, K.J., Jr., Gabrielov, A.G., Bell, S.L., Bedioui, F., Roue, L., and Devynck, J., *Inorg. Chem.*, 33, 67, 1993.
133. Parton, R.F., Bezoukhanova, C.P., Grobet, J., Grobet, P.J., and Jacobs, P.A., *Stud. Surf. Sci. Catal.*, 83, 371, 1994.
134. Chan, Y.-W. and Wilson, R.B., *Preprints Division of Petroleum Chemistry, Amer. Chem. Soc.* 33, 453, 1988.
135. Rankel, L.A. and Valyocsik, E.W., U.S. Patent 4,500,503, 1985.
136. Balkus, K.J., Jr., Kowalak, S., Ly, K.T., and Hargis, D.C., *Stud. Surf. Sci. Catal.*, 69, 93, 1991.
137. Balkus, K.J., Jr., Hargis, C.D., and Kowalak, S., in *Supramolecular Architecture,* Bein, T., Ed., *ACS Symposium Series,* 499, 347, 1992.

138. Myers, D., *Surfactant Science, and Technology,* 3rd ed., J. Wiley & Sons, New York, 2005.
139. Chen, C.Y., Li, H.Y., and Davis, M.E., *Mic. Mat.*, 2, 27, 1993.
140. Steel, A., Carr, S.W., and Anderson, M.W., *J. Chem. Soc. Chem. Commun.*, 1571, 1994.
141. Mann, S., Burkett, S.L., Davis, S.A., Fowler, C.E., Mendelson, N.H., Sims, S.D., Walsh, D. and Whilton, N.T., *Chem. Mater.*, 9, 2300, 1997.
142. Corma, A., *Chem. Rev.*, 97, 2372, 1997.
143. Imhof, A. and Pine, D.J., *Nature,* 389, 948, 1997.
144. Wijnhoven, J.E.G. and Vos, W.L., *Science,* 281, 802, 1998.
145. Martin, T., Galarneau, A., Di Renzo, F., Fajula, F., and Plee, D., *Angew. Chem. Int. Ed.*, 41, 2590, 2002.
146. Tanev, P.T., Chibwe, M., and Pinnavaia, T., *Nature,* 368, 321, 1994.
147. Tanev, P.T. and Pinnavaia, T., *Science,* 267, 865, 1995.
148. Ulagappan, N. and Rao, C.N.R., *Chem. Commun.*, 2759, 1996.
149. Khushalani, D., Kuperman, A., Ozin, G.A., Tanaka, K., Garces, J., Olken, M.M., and Coombs, N., *Adv. Mater.*, 7, 842, 1995.
150. Förster, S. and Plantenberg, T., *Angew. Chem. Int. Ed.*, 41, 688, 2002.
151. Förster, S. and Antonietti, M., *Adv. Mater.*, 10, 195, 1998.
152. Huber, C., Moller, K., and Bein, T.J., *Chem. Soc. Chem. Commun.*, 2619, 1994.
153. Clark, J.H. and MacQuarrie, D., *Chem. Commun.*, 853, 1998.
154. Stein, A., Melde, B.J., and Schroden, R.C., *Adv. Mater.*, 12, 1403, 2000.
155. Maschmeyer, T., Rey, F., Sankar, G., and Thomas, J.M., *Nature,* 378, 159, 1995.
156. Brunel, D., Cauvel, A., Fajula, F., and Di Renzo, F., *Stud. Surf. Sci. Catal.*, 97, 173, 1995.
157. Burkett, S., Sims, S.D., and Mann, S., *Chem. Commun.*, 1367, 1996.
158. Lim, M.H. and Stein, A., *Chem. Mater.*, 11, 3285, 1999.
159. Zhang, Z., Dai, S., Fan, X., Blom, D.A., Pennycook, S.J., and Wei, Y., *J. Phys. Chem. B,* 105, 6755, 2001.
160. Ying, J.Y., Mehnert, C.P., and Wong, M.S., *Angew. Chem. Int. Ed.*, 38, 56, 1999.
161. Han, Y.J., Kim, J.M., and Stucky, G.D., *Chem. Mater.*, 12, 2068, 2000.
162. Huang, M.H., Choudrey, A., and Yang, P.D., *Chem. Commun.*, 1063, 2000.
163. Zhang, W.H., Shi, J.L., Wang, L.Z., and Yan, D.S., *Chem. Mater.*, 12, 1408, 2000.
164. Kowalchuk, C.M., Schmid, G., Meyer-Zaika, W., Huang, Y., and Corrigan, J.F., *Inorg. Chem.*, 43, 173, 2004.
165. Choi, M., Kleitz, F., Liu, D., Lee, H.Y., Ahn, W.-S., and Ryoo, R., *J. Am. Chem. Soc.*, 127, 1924, 2005.
166. Moller, K. and Bein, T., *Chem. Mater.*, 10, 2950, 1998.
167. Wu, C.-G. and Bein, T., *Science,* 264, 175, 1994.
168. Moller, K., Bein, T., and Fischer, R.X., *Chem. Mater.*, 10, 1841, 1998.
169. Nguyen, T.Q., Wu, J.J., Doan, V., Schwartz, B.T., and Tolbert, S.H., *Science,* 288, 652, 2000.
170. Molenkamp, W.C., Watanabe, M., Miyata, H., and Tolbert, S.H., *J. Am. Chem. Soc.*, 126, 4476, 2004.
171. Acosta, E.J., Carr, C.S., Simanek, E.E., and Shantz, D.F., *Adv. Mater.*, 16, 985, 2004.
172. Barrer, R.M., *Zeolites and Clay Minerals as Sorbents and Molecular Sieves,* Academic Press, London, 1978.
173. Vansant, E.F., *Stud., Surf. Sci. Catal.*, 37, 143, 1988.
174. Vansant, E.F., *Pore Size Engineering in Zeolites,* J. Wiley & Sons, New York, 1990.

175. Roque-Malherbe, R., Lemes, L., Autie, M., and Herrera, O., in *Zeolite of the Nineties, Recent Research Reports,* 8th International Zeolite Conference, Amsterdam, July 1989, Hansen, J.C., Moscou, L., and Post, M.F.M., Eds., IZA, 1989, p. 137.
176. Roque-Malherbe, R., Lemes, L., López-Colado, L., and Montes, A., in *Zeolites '93 Full Papers Volume,* Ming, D. and Mumpton, F.A., Eds., International Committee on Natural Zeolites, Brockport, New York, 1995, p. 299.
177. Hernandez, M.A., Corona, L., Gonzalez, A.I., Rojas, F., Lara, V.H., and Silva, F., *Ind. Eng. Chem. Res.*, 44, 2908, 2005.
178. Chudasama, D., Sebastian, J., and Jasra, R.V., *Ind. Eng. Chem. Res.*, 44, 1780, 2005.
179. de las Pozas, C., López-Cordero, R., Díaz-Aguilas, C., Cora, M., and Roque-Malherbe, R., *J. Solid State Chem.*, 114, 108, 1995.
180. Niwa, M., Yamazaki, K., and Murakami, Y., *Ind. Eng. Chem. Res.*, 30, 38, 1991.
181. Kuznicki, S.M., Bell, V.A., Nair, S., Hillhouse, H.G., Jacubinas, R.M., Carola, M.B., Toby, B.H., *Nature,* 412, 720, 2001.
182. Giannetto, G., *Zeolitas,* Editorial Caracas, Caracas, Venezuela, 1990.
183. Mortier, W.J., *Compilation of Extraframework Sites in Zeolites,* Butterworth, London, 1982
184. Cauvel, A., Brunel, D., Di Renzo, F., Garrone, E., and Fubini, B., *Langmuir,* 13, 2773, 1997.
185. Nguyen, C., Sonwane, C.G., Bhatia, S.K., and Do, D.D., *Langmuir,* 14, 4950, 1998.
186. Zhao, X.S., Ma, Q., and Lu, G.Q., *Energy Fuels*, 12, 1051, 1998.
187. Neimark, A.V., Ravikovitch, P.I., and Vishnyakov, A., *J. Phys. Condens. Matter.*, 15, 347, 2003.
188. Neimark, A.V. and Ravikovitch, P.I., *Mic. Mes. Mat.*, 44, 697, 2001.
189. Ravikovitch, P.I. and Neimark, A.V., *Colloids Surf. A,* 187, 11, 2001.
190. Thommes, M., Kohn, R., and Froba, M., *J. Phys. Chem. B,* 104, 7932, 2000.
191. Maddox, M.W., Olivier, J.P., and Gubbins, K.E., *Langmuir,* 13, 1737, 1997.
192. Llewellyn, P.L., Sauerland, C., Martin, C., Grillet, Y., Coulomb, Y.J.P., Rouquerol, F., and Rouquerol, J., in *Characterization of Porous Solids IV,* McEnaney, B., Yans, T.J., Rouquerol, J., Rodriguez-Reinoso, F., Sing, K.S.W., Unger, K.K., Eds., The Royal Society of Chemistry, Cambridge, England, 1997.
193. Hu, X., Qiao, S., Zhao, X.S., and Lu, G.Q., *Ind. Eng. Chem. Res.*, 40, 862, 2001.
194. Selvam, P., Bhatia, S.K., and Sonwane, C.G., *Ind. Eng. Chem. Res.*, 40, 3237, 2001.
195. Zhao, X.S., Lu, G.Q., and Hu, X., *Colloids Surf. A Physicochem. Eng. Aspects,* 179, 261, 2001.
196. Zhao, X.S. and Lu, G.Q., *J. Phys. Chem. B,* 102, 1556, 1998.
197. Beck, J.S., Calabro, D.C., McCullen, S.B., Pelrine, B.P., Schmitt, K.D., and Vartuli, J.C., U.S. Patent 5,220,101, 1993.
198. Skarstrom, C.W., U.S. Patent, 2,944,627, 1960.
199. Dong, F., Lou, H., Kodama, A., Goto, M., and Hirose, T., *Ind. Eng. Chem. Res.*, 38, 233, 1999.
200. Sircar, S., *Ind. Eng. Chem. Res.*, 41, 1389, 2002.
201. Ruthven, D.M., *Principles of Adsorption and Adsorption,* Processes, John Wiley, New York, 1984.
202. Yang, R.T., *Gas Separation by Adsorption Processes,* Butterworth, London, 1987.
203. Suzuki, M., *Adsorption Engineering,* Kodansha, Tokyo, 1990.
204. Ruthven, D.M., Farooq, S., and Knaebel, K.S., *Pressure Swing Adsorption,* VCH, Publishers, New York, 1994.

205. Crittenden, B. and Thomas, W.J., *Adsorption Technology and Design,* Butterworth-Heinemann, Oxford, U.K., 1998.
206. Keller, G.E., Anderson, R.A., and Yon, C.M., in *Handbook of Separation Process Technology,* Rousseau, R.W., Ed., J. Wiley & Sons, New York, 1987, chap. 12.
207. Humphrey, J.L. and Keller, G.E., *Adsorption. Separation Process Technology,* McGraw-Hill, New York, 1997, chap. 4.
208. Sircar, S., in *The Engineering Handbook,* Dorf, R.C., Ed., CRC Press, Boca Raton, FL, 1996, chap. 59.
209. Minato, H. and Tamura, T., in *Natural Zeolites, Occurrence, Properties, Use,* Sand, L.B. and Mumpton, F.A., Eds., Pergamon Press, New York, 1978, p. 509.
210. Galabova, I.M., Haralampiev, G.A., and Alexiev, B., in *Natural Zeolites, Occurrence, Properties, Use,* Sand, L.B. and Mumpton, F.A., Eds., Pergamon Press, New York, 1978, p. 431; and in *Natural Zeolites: Occurence, Properties, Uses of Natural Zeolites,* Kallo, D. and Sherry, H.S., Eds., Akademiai Kiado, Budapest, 1988, p. 577.
211. Flanigen, E.M., in *Zeo-Agriculture: Use of Natural Zeolites in Agriculture and Aquaculture,* Pond, W.G. and Mumpton, F.A., Eds., Westview, Boulder, CO, 1984, p. 55.
212. Sircar, S. and Hanley, F., *Separation Sci. Tech.,* 28, 2553, 1993.
213. Tsisihsvili, G.V., Andronikashvili, T.G., Kirov, G.N., and Filizova, L.D., *Natural Zeolites,* Ellis Horwood, New York, 1992.
214. Kopecni, M.M., Todorovic, M., Comor, J.J., and Laub, R.J., *Cromatographia,* 26, 408, 1988.
215. Kopecni, M.M. and Todorovic, M., *Chromatographia,* 30, 287, 1990.
216. Sankar, N. and Tsapatsis, M., in *Handbook of Zeolite Science and Technology,* Auerbach, S., Carrado, K.A., and Dutta, P.K., Eds., Marcell Dekker, New York, 2003, p. 867.
217. Morooka, S. and Kusakabe, K., *MRS Bulletin,* March, 1999, p. 25.
218. Roque-Malherbe, R., del Valle, W., Marquez, F., Duconge, J., and Goosen, M.F.A., *Sep. Sci. Tech.*, 41, 73, 2006.
219. Aiello, A., Nastro, G., Giordano, G., and Colella, C., in *Natural Zeolites: Occurence, Properties, Uses of Natural Zeolites,* Kallo, D. and Sherry, H.S., Eds., Akademiai Kiado, Budapest, 1988, p. 763.
220. Tchernev, D.I., in *Natural Zeolites, Occurrence, Properties, Use,* Sand, L.B. and Mumpton, F.A., Eds., Pergamon Press, New York, 1978, p. 79.
221. Tchernev, D.I., in *Zeo-Agriculture: Use of Natural Zeolites in Agriculture Aquaculture,* Pond, W.G. and Mumpton, F.A., Eds., Westview, Boulder, CO, 1984, p. 273.
222. Tchernev, D.I., *Natural Zeolites 93 Conference Volume,* Ming, D.W. and Mumpton, F.A., Eds., International Committee on Natural Zeolites, Brockport, New York, 1995, p. 613.

9 Adsorption from Liquid Solution

9.1 INTRODUCTION

Multicomponent adsorption at air/water, oil/water, gas/solid, and liquid/solid interfaces is a significant practical problem in foams, emulsions, detergency, catalysis, pollution abatement, and separation methods [1–35]. In general, the adsorption equilibrium of the individual components is determined, and after that the adsorption of the mixtures is described [1,2,7–16].

For the correlation of the liquid-phase adsorption equilibrium of a single component, several isotherm equations for gas-phase adsorption can in principle be extended to liquid-phase adsorption by the simple replacement of adsorbate pressure by its concentration [29]. These equations are the Langmuir, Freundlich, Sips, Toth, and Dubinin-Radushkevich equations [27–29]. However, the Langmuir and Freudlich equations are the most widely used to correlate liquid-phase adsorption data [21,31–35].

Adsorption from liquid solution is practically another planet with respect to gas-phase adsorption, because the fundamental principles and methodology are different in almost all aspects [11,12]. In the simplest case, a binary solution, the composition of the adsorbed phase is usually unknown. Adsorption in the liquid phase is influenced by many factors such as pH, type of adsorbent, solubility of adsorbate in the solvent, and temperature, as well adsorptive concentration [10,11,13,14]. This is the reason that, despite the industrial importance of adsorption from liquid phase, it is less studied than adsorption from the gas phase. However, the design of liquid-phase adsorptive separation processes requires adsorption equilibrium data; these data have to be experimentally measured or calculated using various predictive multicomponent adsorption models or empirical correlations.

Liquid phase adsorption [10–23], primarily onto activated carbon [10,13,14,22], silica [20,21], zeolites [15,17,18] and resins [16], provides a feasible technique and is one of the most extensively used technologies for removal of organic pollutants from industrial wastewater [10,13–23]. In adsorption on activated carbon, the type of activated carbon plays an important role, since the carbon has a complex porous structure, with associated energetic as well as chemical heterogeneities [10] (see Chapter 7, Sections 7.5 and 7.6). The energetic and chemical heterogeneities are determined by the variety of surface functional groups, irregularities, and strongly bound impurities, as well as structural nonuniformity; this heterogeneity significantly influences the process of physical adsorption [10].

On the other hand, the adsorption literature gives an account of extensive pure gas adsorption equilibrium data on various porous adsorbents of practical interest,

such as activated carbons, silica and alumina gels, zeolites, and polymeric sorbents [24–26]. In comparison, the number of published reports on binary gas equilibrium adsorption are less, and the data for gas mixtures with three or more components are infrequent [25]. Mathematical models for design and optimization of adsorptive separation processes such as pressure swing and thermal swing adsorption, on the other hand, require accurate multicomponent adsorption equilibrium data, as was previously stated (see Chapter 8, Section 8.5.2) [26]. These data have to be experimentally measured in the complete range of pressure, temperature, and gas composition met by the adsorbent during the separation processes, or calculated from corresponding pure gas equilibrium data using various predictive multicomponent adsorption models or empirical correlations [26].

In the current book we will not discuss the adsorption process in multicomponent gas systems, since, as formerly acknowledged, we are studying adsorption, fundamentally, from the point of view of materials science (i.e., we are interested in the methods for the use of single-component adsorption in the characterization of the adsorbent surface and pore volume, the study of the parameters characterizing single-component transport processes in porous systems, and to a lesser extent, the adsorption energy and dynamic adsorption in bed reactors). However the adsorption process from the liquid phase notwithstanding, the fact that it is a multicomponent process will be discussed here, because of its fundamental and practical importance.

9.2 SURFACE EXCESS AMOUNT AND AMOUNT OF ADSORPTION FOR LIQUID–SOLID ADSORPTION SYSTEMS

The interfacial layer is the inhomogeneous space region intermediate between two bulk phases in contact, and where properties are significantly different from, but related to, the properties of the bulk phases. Examples of such properties are compositions, molecular density, orientation, or conformation, charge density, pressure tensor, electron density, etc. The interfacial properties vary in the direction normal to the surface. Complex profiles of interfacial properties occur in the case of multicomponent systems with coexisting bulk phases, where attractive/repulsive molecular interactions involve adsorption or depletion of one or several components.

The surface excess amount, or Gibbs adsorption (see Chapter 2, Section 2.2) of the component, *i,* that is, n_i^{σ}, is defined as the excess of the amount of this component actually present in the system over that present in a reference ideal system of the same volume as the real system, and in which the bulk concentrations in the two phases remain uniform up to the Gibbs dividing surface (GDS). That is, the surface excess amount, n_i^{σ}, for adsorption from liquid phase is

$$n_i^{\sigma} = n_i - V_o^l c_i^l \tag{9.1}$$

where n_i is the total amount of component i in the liquid, c_i^l is its concentration in the liquid phase after adsorption, and V_o^l is the volume of the liquid phase up to the GDS. This expression follows directly from the defining equation (see Figure 9.1)

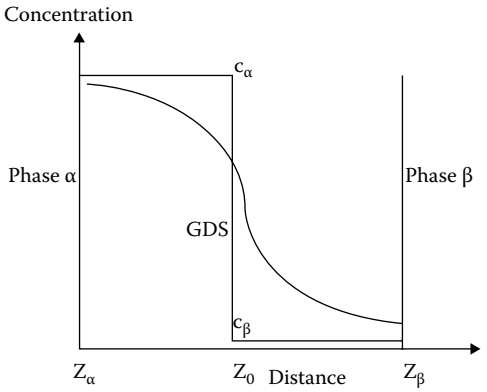

FIGURE 9.1 Gibbs dividing surface (GDS). In the reference system, the concentration remains constant up to the GDS. In the real system, the concentration, vary across the interface, of thickness: $\gamma = z_\beta - z_\alpha$ from that of phase α, concentration c_α to that of phase β, concentration c_β.

$$n_i^\sigma = n_i - V_o^\alpha c_\alpha^i + V_o^\beta c_\beta^i$$

However the value of n_i^σ is dependent on the position of the GDS through the value of V_o^l (see Chapter 2, Section 2.2) [11]. This fact causes some authors to prefer to adopt alternative approaches for the calculation of the surface excess amount.

One of the most meaningful presentations of the liquid-phase adsorption equilibrium is the reduced surface excess [4,18,27], a function invariant with respect to the position of the GDS (see Chapter 2, Section 2.2), which could be defined as a result of the following procedure [11]. First, from Equation 9.1, it is possible to write:

$$n_2^\sigma = n_2 - V_o^l c_2^l \tag{9.2a}$$

and

$$n^\sigma = n^0 - V_o^l c^l \tag{9.2b}$$

where $n^\sigma = n_1^\sigma + n_2^\sigma$, $n^0 = n_1 + n_2$, and $c^l = c_1^l + c_2^l$; n_i^σ, where $i = 1, 2$ is the surface excess amount of component *i;* total amount of component *i* in the liquid c_i^l is its concentration in the liquid phase after adsorption. Then the reduced excess amount, for the component, 1, is defined by the elimination of V_o^l from Equations 9.2a and 9.2b [4,11,18,27]:

$$n_1^e = n^0 \left(x_1^0 - x_1^e \right) \tag{9.3a}$$

or referred to an amount of adsorbent:

$$\Gamma_1^e = \frac{n^0}{m_a}\left(x_1^0 - x_1^e\right) \tag{9.3b}$$

where:

$$x_1^0 = \frac{n_1^0}{n_1^0 + n_2^0} = \frac{n_1^0}{n^0}$$

and

$$x_1^e = \frac{n_1^0 - n_1^s}{n_1^0 - n_1^s + n_2^0 - n_2^s}$$

where n^0, the total number of moles in contact with the adsorbent, describes the amount of substance of the liquid mixture, m_a is the adsorbent mass, and x_1^0 and x_1^e are the mole fractions of component 1 in the initial and equilibrium solution, respectively, and n_1^s and n_2^s are the moles adsorbed into the Gibbs phase (i.e., the amount that disappeared from the bulk phase solution) [4]. Consequently, for components, $i = 1, 2$, $\Delta x_i^l = x_i^0 - x_i^e$ is the change in the mole fraction of component i resulting from bringing a specified mass of adsorbent, m_a, into contact with a specified amount of solution n^0 [1,2].

The reduced surface excess amounts used is recommended by the IUPAC [2] as a convenient way of reporting the experimental results. For many years this description of the experimental adsorption data was intuitively selected as a method of plotting the experimental data without any reference to the Gibbs approach. The obtained isotherm is generally named a "composite isotherm" [11]. Consequently, adsorption isotherms are usually reported in the form of reduced surface excess amounts, Γ_1^e, versus x_1^l, the mole fraction of the solute component [1,2,4,9,11]. The five types of composite isotherms according to the classification of Schay and Nagy are represented in Figure 9.2 [9]. A negative value of Γ_1^e means that the solvent is preferentially adsorbed.

In practice, the amount of solute adsorbed from the liquid phase is also calculated by subtracting the remaining concentration after adsorption from the concentration at the beginning of the adsorption process [10]. First it is necessary to determine the particle size of the adsorbent, adsorption temperature, pH of the solution, and contact time necessary to achieve adsorption equilibrium [10,13,28]. Then different amounts of the solid adsorbent (generally a few milligrams, i.e., 1–10 mg) are contacted with equivalent volumes of solution (in general 25–50 mL of the solution) containing an established concentration of the substance to be adsorbed [10,15,28]. Thereafter, all solutions are equilibrated, normally for 0.5–5 hours, while being stirred. Once contact time has elapsed, the adsorbent is centrifuged and filtered. The resulting solutions are poured into vials, which are completely filled so the headspace is very low. Then, the lids are sealed with tape until the vials are analyzed by, for instance, with a spectrophotometer [28]. The amount of solute adsorbed from the liquid phase is calculated by subtracting the remaining analyzed concentration from

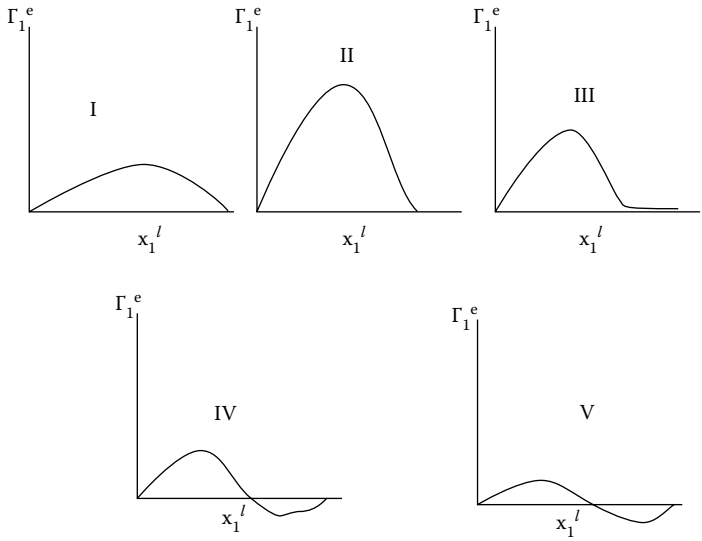

FIGURE 9.2 Composite isotherm according to the classification of Schay and Nagy.

the starting concentration [10,28]. Then, the amount adsorbed on the adsorbent is determined from the initial liquid-phase concentration and equilibrium concentration [28]:

$$q_1^e = \frac{V}{m_a}\left(C_1^0 - C_1^e\right) \tag{9.4}$$

that is, C_1^0 and C_1^e are the initial and equilibrium concentrations respectively, V is the volume of solution, and m_a is the mass of adsorbent.

9.3 EMPIRICAL ADSORPTION ISOTHERMS APPLIED FOR THE CORRELATION OF LIQUID–SOLID ADSORPTION EQUILIBRIA IN SYSTEMS CONTAINING ONE DISSOLVED COMPONENT

For the correlation of the liquid-phase adsorption equilibria of a single component, several isotherm equations for gas-phase adsorption can in principle be extended to liquid-phase adsorption by the simple replacement of adsorbate pressure by its concentration [29]. These equations are the Langmuir, Freundlich, Sips, Toth, and Dubinin-Radushkevich equations [27–29]. The Langmuir:

$$q_1^e = \frac{q_m b_0 C_1^e}{1 + b_0 C_1^e} \tag{9.5}$$

and the Freundlich:

$$q_1^e = k\left(C_1^e\right)^{1/n} \tag{9.6}$$

equations are the most widely used to correlate liquid-phase adsorption data. [21,31–35]. The experimental equilibrium data, expressed as q_1^e, is the amount of the solute component, 1, adsorbed per mass of adsorbent. This parameter is expressed in [mg/g] or [mmol/g]. C_1^e is the final solute concentration in solution, or the equilibrium concentration, in [mg/L], or [mmol/L]. In addition, q_m and b_0 are the Langmuir's parameters, and k and n are the Freundlich parameters [28].

The Sips equation is [28,36]:

$$q_1^e = \frac{q_0(dC_1^e)^{1/S}}{1+(dC_1^e)^{1/S}} \tag{9.7}$$

where q_0, d, and S are parameters of the Sips equation. The other three-parameter equation is the Toth equation [4,28]:

$$q_1^e = \frac{q_0 bC_1^e}{1+(bC_1^e)^{1/t}} \tag{9.8}$$

in which, q_0, b, and t are parameters of the Toth equation. The calculation of the parameters for the Langmuir equation is generally carried out by linearly regressing each set of experimental data using the following equation:

$$y = C_1^e = q_m\left(\frac{C_1^e}{q_e}\right)+\frac{1}{b_0} = mx+b \tag{9.9}$$

which is a linear form of the Langmuir equation.

A standard regression analysis could be performed on each set of data, to calculate the correlation coefficient for each regression, as well as the standard error of the estimate and the values of the standard errors for the parameters, applying a commercial regression software [37,38]. The calculation could be also carried out by nonlinearly regressing each set of experimental data using Equation 9.5 directly [37,38].

Calculations of the parameters for the Freundlich equation are obtained by linearly regressing each set of experimental data using the following equation [21]:

$$y = \log\left(q_e\right) = \log\left(k\right)+\left(\frac{1}{n}\right)\log\left(C_1^e\right) = mx+b \tag{9.10}$$

The linear regression analysis could also be carried out applying commercial regression software, which could also be used to nonlinearly regressing each set of experimental data using Equation 9.6 directly [37,38]. The non-linear regression process should be carried out with Equation 9.5 directly [37,38].

It has also been shown that the preferential adsorption of various compounds from aqueous solutions by activated carbons follows an equation of the Dubinin-Radushkevihs-Kaganer type [39,40]:

$$q_1^e = q_m^{DRK} \exp\left\{-\left[\frac{RT}{E_S}\ln\left(\frac{C_1^0}{C_1^e}\right)\right]^2\right\} \tag{9.11}$$

In this expression, the vapor–solid adsorption potential

$$RT\ln\left(\frac{P_0}{P}\right),$$

(see Chapter 3, Section 3.2) is replaced by a new thermodynamic potential,

$$RT\ln\left(\frac{C_1^0}{C_1^e}\right),$$

where C_1^0 is the saturation concentration of the adsorbed species, C_1^e is the concentration at equilibrium, which corresponds to the amount adsorbed, q_e, and E_S is similar to the characteristic energy [40]. A generalization of Equation 9.11 is [40–42]:

$$q_1^e = q_m^{DRK} \exp\left\{-\left[\frac{RT}{E_S}\ln\left(\frac{C_1^0}{C_1^e}\right)\right]^n\right\} \tag{9.12}$$

where n is a constant parameter. Equation 9.11 is similar to the previously explained Dubinin equation (see Chapter 3, Section 3.2), where E_S, which is related to the characteristic energy, must be temperature-invariant [40].

Currently, the majority of authors use Langmuir's equation, Equation 9.5, adapted to solution work, instead of Equation 9.12. The Freundlich equation, on the other hand, suffers from the shortcoming that the variation of the main parameters with temperature cannot be predicted in a simple fashion, as opposed to Dubinin's equation [40].

Finally, it is necessary to state that any one of the equations displayed in this section to correlate the relation between the amount adsorbed, q_1^e, and the equilibrium concentration in solution, C_1^e,corresponds to an specific model for adsorption from the solutions. That is, they should be considered as empirical isotherm equations.

9.4 MODEL DESCRIPTION OF ADSORPTION FROM THE LIQUID PHASE ON SOLIDS

Adsorption from a binary liquid mixture can be described as a phase-exchange reaction [3]:

$$N_2^l \text{ (solute in solution)} + N_1^s \text{ (adsorbed solvent)} \Leftrightarrow$$
$$N_2^s \text{ (adsorbed solute)} + N_1^l \text{ (solvent in solution)}$$

On a homogeneous surface, which is characterized by a unique adsorption energy for all the surface, the equilibrium constant is defined by the following equation [2,20,43]:

$$K_{12} = K_0 \exp\left(\frac{\varepsilon_1 - \varepsilon_2}{RT}\right) = \frac{x_1^s x_2^l \gamma_1 \gamma_2^l}{x_2^s x_1^l \gamma_2 \gamma_1^l} = \alpha\beta_{12} \tag{9.13}$$

where x_i^l and x_i^s are the mole fractions of the *i*th component in the bulk, *l,* and surface, *s,* phases; γ_i^l and γ_i^s are the activity coefficients in the bulk and surface phases, respectively; α is the separation factor; ε_i is the adsorption energy of the *i*th component; and K_0 is the preexponential factor.

In addition, the validity of the monolayer character of the adsorption process [43], the equality of the molecular sizes of solution components, and the constancy of the total number of molecules in the surface phase will be considered in the present model description. Since $x_1^s + x_2^s = 1$, then [3]:

$$x_1^s = \frac{K_{12} x_{12}^l \gamma_{12}(x_1^s, x_1^l)}{1 + K_{12} x_{12}^l \gamma_{12}(x_1^s, x_1^l)}$$

where

$$x_{12}^l = \frac{x_1^l}{x_2^l}, \quad \gamma_{12}^l = \frac{\gamma_1^l}{\gamma_2^l}, \text{ and } \gamma_{21}^s = \frac{\gamma_2^s}{\gamma_1^s}.$$

However most adsorbents have heterogeneous surfaces, that is, the heat evolved during adsorption is dependent on the adsorption amount. To be more precise, a heterogeneous surface is characterized by different surface sections, which have different adsorption energies. Consequently the surface is characterized by a distribution of adsorption energies, and each surface section is the place of an independent adsorbed phase [36,44].

Let us then suppose adsorption on a heterogeneous solid while supposing the random distribution of surface sites. Consequently, the overall integral equation for the calculation of the mole fraction of the first component over the whole surface phase has the following form [20,43]:

$$x_{1,t}^{s} = \int_{\Delta} \frac{K_{12} x_{12}^{l} \gamma_{12}(x_{1t}^{s}, x_{1}^{l})}{1 + K_{12} x_{12}^{j} \gamma_{12}(x_{1t}^{s}, x_{1}^{l})} F(\varepsilon_{12}) d\varepsilon_{12} \tag{9.14}$$

where

$$x_{12}^{l} = \frac{x_{1}^{l}}{x_{2}^{l}}, \quad \gamma_{12}^{l} = \frac{\gamma_{1}^{l}}{\gamma_{2}^{l}}, \quad \gamma_{21}^{s} = \frac{\gamma_{2}^{s}}{\gamma_{1}^{s}}, \quad F(\varepsilon_{12})$$

is the distribution function of differences of adsorption energies $\varepsilon_1 - \varepsilon_2$, and Δ is the integration region.

The integral Equation 9.14 generates various isotherm equations. One of them is a general expression introduced by Jaroniec and Marczewski [20,45]:

$$x_{1t}^{s} = \left(\frac{[\bar{K}_{12} x_{12}^{l} \gamma_{12}(x_{1}^{s}, x_{1}^{l})]^{n}}{[1 + \bar{K}_{12} x_{12}^{l} \gamma_{12}(x_{1}^{s}, x_{1}^{l})]^{n}} \right)^{m/n} \tag{9.15}$$

The parameters $\bar{K}_{12}$, m, and n characterize the distribution function, $F(\varepsilon_{12})$; $\bar{K}_{12}$, the characteristic equilibrium constant describes the position of $F(\varepsilon_{12})$ on the axis of energy differences; $\varepsilon_{12} = \varepsilon_1 - \varepsilon_2$, and $0 < m < 1$, and $0 < n < 1$ are the heterogeneity parameters characterizing the distribution function.

Equation 9.15 is called the general Langmuir equation [20]. For special values of the heterogeneity parameters, m and n, it is reduced to different well-known isotherm equations, such as the Langmuir-Freundlich equation for $0 < m = n < 1$, the generalized Freundlich isotherm equation, in the case where $n = 1$ and $0 < m < 1$, and the Toth isotherm equation for $m = 1$ and $0 < n < 1$ [20].

The previous discussion of a model description of adsorption from the liquid phase on solids, has justified the use of empirical equations formally similar to the Langmuir, Freundlich, Sips, and Toth isotherms [27–29]. The use of Dubinin-type equations was also phenomenologically justified previously [40]. The effects of surface heterogeneity, and nonideality of the bulk, and the surface phases on adsorption equilibrium were taken into account in the model described in the present section. However, the complexity of liquid adsorption systems makes it very difficult to separate the effects of solution nonideality and surface heterogeneity [43]. Rather, the global nonideality of experimental systems caused by both adsorbate and adsorbent imperfections is observed [20]. The effect of solid-surface heterogeneity and solution nonideality on adsorption equilibria can be discussed in terms of some theoretical models, and the values of surface activity coefficient may also be measured experimentally. Nevertheless, the surface activity coefficients, and heterogeneity can be regarded only for assumed models of adsorption process [20].

These difficulties require researchers to use the following approach: first, experimentally determine the adsorption isotherm, applying a methodology analogous to those explained in Section 9.2, and then correlate the data set with the Langmuir, Freundlich, or Dubinin isotherms [27–29,40]. In the next section we will see some examples of this line of attack.

9.5 SOME APPLICATIONS OF LIQUID–SOLID ADSORPTION

Waters polluted by organic compounds are often treated by adsorption processes in which activated carbons and other materials act as adsorbents [10,13–23]. Several studies have been made in order to comprehend thoroughly the adsorption mechanisms involved in these processes [10,13–23,25–35,39–43,46–64]. The information obtained in this mode leads to a superior design, as well as to a better effectiveness for the materials used as adsorbents.

9.5.1 Activated Carbons

Activated carbons are the most widely used industrial adsorbent for removing contaminants and pollutants from gaseous, aqueous, and nonaqueous streams, due in part to their uniquely powerful adsorption properties and the ability to readily modify their surface chemistry [48,65]. Carbon is the main adsorbent used in the case of liquid–solid adsorption systems. As already stated, the adsorption capacity of an activated carbon depends on the nature of the adsorbent, the nature of the adsorbate, and the solution conditions, i.e., pH, temperature, ionic strength [10,13]. Regarding the activated carbon surface, the main components are the carbon basal planes, edges, and crystal defects and ash impurities, that is, metal oxides and oxygen surface groups [10,13]. The last are principally located on the edges of the graphitic basal planes (see Chapter 7, Sections 7.5 and 7.6) [10,13]. Surface functional groups can be classified as acidic (i.e., carboxyl, carbonyl, phenolic, hydroxyl, lactone, anhydride) or basic (chromene- and pyrone-like structures) [63]. Despite being a small fraction of the overall carbon surface, the oxygen groups are, however, very active, exhibiting a significant influence on the adsorption capacity [64].

Phenol is one of the most important compounds adsorbed by carbon from liquid phase. Phenol is a fundamental structural part for a variety of synthetic organic compounds. Thus, wastewater originating from many chemical plants and pesticide and dye manufacturing industries contains phenols [46]. In addition, wastewater originating from other industries such as paper and pulp, resin manufacturing, gas, and coke manufacturing, tanning, textile, plastic, rubber, pharmaceutical, and petroleum also includes diverse types of phenols [22,46]. In addition to the phenols generated as a consequence of industrial activity, wastewaters also contain phenols produced as a product of decay of vegetation [46]. In view of the wide prevalence of phenols in different wastewaters and their toxicity to human and animal life even at low concentration, it is essential to remove them before discharge of wastewater into water bodies [22,46]. Several techniques, such as oxidation with ozone/hydrogen peroxide, biological methods, membrane filtration, ion exchange, electrochemical oxidation, reverse osmosis, photocatalytic degradation, and adsorption, have been used for the removal of phenols [46]. However, regardless of the accessibility of the aforementioned methods for the removal of phenols, the adsorption process even now remains the best, as it can in general remove all types of phenols, and the effluent treatment is convenient because of simple design and easy operations [46].

Adsorption of phenol and substituted phenols from aqueous solutions on activated carbons is one of the most studied of all liquid-phase applications of carbon adsorbents [22,40,47]. Today, it is known that the adsorption process on carbon materials basically depends on several variables such as the pH of the solution, the electron-donating or electron-withdrawing properties of the phenolic compound, and the surface area of the adsorbent and its surface chemistry, which is determined by the nature of its oxygen surface functionalities and its surface charge [10]. Phenol and substituted phenol compounds in aqueous solutions, in their uncharged form, are adsorbed on the carbon surface by dispersion forces between the π electrons of aromatic ring and the π electrons of the graphene layers; nevertheless, the pH of the solution can affect the charge of phenolic compounds and consequently affects the electrostatic interactions between the adsorbent and the adsorbate [13].

Due to the lack of data, in general, an experimental investigation of the adsorption equilibrium has to be carried out in order to establish the calculation basics for engineering [23]. To analyze the adsorption isotherms of phenolic compounds obtained at equilibrium, many authors use the Langmuir or Freundlich equations [21,28]. It is also possible to investigate the adsorption of phenol compounds from aqueous solutions [40], within the framework of Dubinin's theory [40–42]. With the obtained empirical correlations of equilibrium data, it is possible to get the calculation basis for the design of liquid phase adsorptive separation processes.

Active carbons are also applied in the removal of oil and other organic compounds from effluent water in petroleum refining, petrochemicals, metal extraction, detergent, margarine, and soft fat manufacture, mineral extraction, and other industries [10,28,49–53]. In the food and beverage industries, active carbon is used to remove color or odor from the produced products; in the chemical and pharmaceutical industry active carbons are applied for the elimination of impurities to improve product quality [10]. As was previously stated, the liquid-phase adsorption isotherm data of various organic compounds in carbon and in other systems are essential parts of the information needed in the analysis and design of adsorption separation processes; these data have been obtained and reported over the years [10,13–23,25–35, 39–43,47–62].

For example, benzene and toluene are significant materials in the chemical industry, since they are initial materials in the chemical production of a lot of products, and they are frequently used as solvent in a broad diversity of manufacturing processes [28,52,53]. Given that these compounds are classified as flammable and toxic materials, their occurrence in the environment, generally in wastewater at low concentration, is of primary concern. For this reason, the subtraction of these compounds from an aqueous waste stream is also necessary [28]. Adsorption onto activated carbon offers a viable method for the elimination of these organic pollutants from industrial wastewater [28].

9.5.2 Precipitated Silica

Another important adsorbent is silica (see Chapter 7, Sections 7.1–7.4) [66–87]. Adsorption phenomena in silica also play a major role in many industrial and

technological processes [72–76], as well as in liquid solid chromatography [77]. In the case of silica adsorption, the difficulties in the interpretation of the result arise from a variety of interactions between molecules of liquid components and the previously analyzed complex character of the solid surface, which is usually energetically heterogeneous [20,78–80]. The distribution at the surface of morphological irregularities and various silanol groups determines the surface heterogeneity of silica gel [78–80]. In addition, dimensions of the open space in capillaries of silica gels establish the adsorption of molecules, particularly in the form of clusters or mixed complexes that go through the pore systems of solids where, because of steric reasons, the adsorption process of clusters and complexes is restricted in very narrow pores. In this case, the complexes containing weakly bonded molecules may be destroyed, and the adsorption is difficult in comparison to adsorption in macropores [20]. Consequently, it is possible to observe the influence of geometrical structure on the adsorption selectivity as well as on the global characteristic of surface heterogeneity [72,73]

As one example of adsorption in silica, the competition of liquid components for silica gel surface in binary liquid mixtures of methanol-benzene and 2-propanol-*n*-heptane was reported by Goworek et al. [20]. The binary liquid mixture–silica gel adsorption isotherms were measured using the commercial silica gels Si-40 and Si-100 from Merck (see Table 9.1 [20]). On the basis of specific surface excess isotherms, the surface layer capacities were calculated. In the present case, $\Delta x_i^l = x_i^0 - x_i^e$ is also the change in the mole fraction of component i, resulting from bringing a specified mass of adsorbent m_a into contact with a specified amount of solution, n^0 [1,2], but it will be reported as the areal reduced excess amount, which is defined as [11]:

$$\Gamma_1^e = \frac{n^0}{A}\left(x_1^0 - x_1^e\right)$$

where A is the area exposed by the adsorbent. The areal reduced excess adsorption isotherms for methanol (component 1) + benzene (component 2), and 2-propanol (component 1) + *n*-heptane (component 2) systems on silica gel Si-40 and Si-100 are presented in the form shown in Figure 9.2, and the shape of experimental isotherms is of the type II according to Schay-Nagy classification [9].

TABLE 9.1
Textural Characterization of Silica Gels

Adsorbent	BET Area, S [m^2/g]	Pore Volume [cm^3/g]	Average Pore Diameter [nm]
Si-40	814	0.60	3
Si-100	348	1.15	10

9.5.3 Zeolites

Zeolites are crystalline materials containing pores and cavities of molecular dimensions (ca. 3–15 Å), creating a nanoscale framework which can be filled with water or other guest molecules (see Chapter 8, Sections 8.2, 8.3.1, 8.4.1, and 8.4.2) [17,88–93]. The resulting molecular sieving ability has enabled the creation of new types of selective separation processes. More specifically, hydrophobic zeolites, such as all silica zeolites or zeolites with a very low aluminum content, possess a high capacity for adsorbing organic compounds dissolved in water. Some recent studies showed that hydrophobic, dealuminated zeolites adsorbed organic compounds from water as effectively as activated carbon [15,18,94,95]. The hydrophobicity of zeolitesis is controlled, fundamentally, by changing the Si/Al ratio in the framework by synthesis conditions and post-synthesis modification treatments [93,94,96].

The most studied hydrophobic zeolite in adsorption of organic compounds from water solutions is silicalite-1 [18]. Silicalite-1 is a molecular sieve with MFI structure composed of pure silica. The MFI framework has a 10-MR channel system with elliptical pore with diameters of 5.2×5.7 Å [89]. In addition, other zeolites, such as all-silica Beta zeolite [97], which possesses a three-dimensional, 12-mebered ring and interconnected channel system with pore diameters of 7.1×7.3 Å [89], have been applied to the removal of methyl *tert*-butyl ether (MTBE) from water solutions [15]. These diameters are similar to those of dealuminated mordenite, a 12-membered ring zeolite with 6.5×7.0 Å pores [89]. A recent study [95] showed that hydrophobic, dealuminated mordenite adsorbed MTBE from water better than activated carbon. In this study 5 mg of zeolite powders was equilibrated with 25 mL of aqueous solutions containing 100 μg/L of MTBE for 15 min, and the dealuminated mordenite removed 96% of the MTBE [15,95].

Likewise, dealuminated Y zeolite (DAY), also a zeolite with a very low aluminum content, has a high capacity for adsorbing organic compounds dissolved in water. For example, meta-nitrophenol dissolved in water solution (200 mg/L) was efficiently removed by liquid phase adsorption in DAY zeolite as effectively as with activated carbon [94].

REFERENCES

1. Everett, D.H., Ed., IUPAC, *Manual on Definitions, Terminology and Symbols in Colloid and Surface Chemistry;* and *Pure Appl. Chem.*, 58, 967, 1986.
2. Berti, C., Ulbig, P., Burdorf, A., Seippel, J., and Schulz, S., *Langmuir,* 15, 6035, 1999.
3. Adamson, A.W., and Gast, A.P., *Physical Chemistry of Surfaces,* 6th ed., J. Wiley & Sons, New York, 1997.
4. Toth, J., in *Adsorption. Theory, Modeling and Analysis,* Toth, J., Ed., Marcel Dekker, New York, 2002, p. 1.
5. Myers, A.L. and Monson, P.A., *Langmuir,* 18, 10261, 2002.
6. Frances, E.I., Siddiqui, F.A., Ahn, D.J., Chang, C.-H., and Wang, N.-H.L., *Langmuir,* 11, 3177, 1995.
7. Myers, A.L. and Prausnitz, J.M., *AIChE J.*, 11, 121, 1965.
8. Myers, A.L. and Moser, F., *Chem. Eng. Sci.*, 32, 529, 1977.

9. Schay, G. and Nagy, L.G., *J. Chim. Phys.,* 58, 149, 1961.
10. Rodriguez-Reinoso, F. and Sepulveda-Escribano, A., in *Handbook of Surfaces and Interfaces of Materials,* Vol. 5, Nalwa, H.S., Ed., Academic Press, New York, 2001, p. 309.
11. Rouquerol, F., Rouquerol, J., and Sing, K., *Adsorption by Powders and Porous Solids,* Academic Press, New York, 1999.
12. Gregg, S.J. and Sing, K.S.W., *Adsorption Surface Area and Porosity,* Academic Press, London, 1982.
13. Nevskaia, D., Castillejos-Lopez, E., Muñoz, V.N., and Guerrero-Yuiz, A., *Environ. Sci. Technol.*, 38, 5786, 2004.
14. Radovic, L.R., Moreno-Castilla, C., and Rivera-Utrilla, J., in *Chemistry and Physics of Carbon,* Vol. 27, Radovic, L.R., Ed., Marcell Dekker, New York, 2001, p. 227.
15. Li, S., Tuan, V.A., Noble, R., and Falcone, J., *Environ. Sci. Technol.*, 37, 4007, 2003.
16. Wagner, K. and Schul, S., *J. Chem. Eng. Data,* 46, 322, 2001.
17. Ruthven, D.W., *Principles of Adsorption and Adsorption Processes,* Wiley, New York, 1984.
18. Chempath, S., Denayer, J.F.M., De Meyer, K.M.A., Baron, G.V., and Snurr, R.Q., *Langmuir,* 20, 150, 2004.
19. Olafadehan, O.A. and Susu, A.A., *Ind. Eng. Chem. Res.*, 43, 8107, 2004.
20. Goworek, J., Derylo-Marczewska, A., and Borowka, A., *Langmuir,* 15, 6103, 1999.
21. Andrieux, D., Jestin, J., Kervarec, N., Pichon, R., Privat, M., and Olier, R., *Langmuir,* 20, 10591, 2004.
22. Colella, L.S., Armenante, P.M., Kafkewitz, D., Allen, S.J., and Balasundaram, V., *J. Chem. Eng. Data,* 43, 573, 1998.
23. Seippel, J., Ulbig, P., and Schulz, S., *J. Chem. Eng. Data,* 45, 780, 2000.
24. Sircar, S., Novosad, J., and Myers, A.L., *Ind. Eng. Chem. Fundam.*, 11, 249, 1972.
25. Valenzuela, D.P. and Myers, A.L., *Adsorption Equilibrium Data Book,* Prentice Hall: Englewood Cliffs, New Jersey, 1989.
26. Rao, M.B. and Sircar, S., *Langmuir, 15,* 7258, 1999.
27. Oscik, J., *Adsorption,* Ellis Horwood, Chichester, U.K, 1982.
28. Hindarso, H., Ismadji, S., Wicaksana, F., Mudjijati, and Indraswati, N., *J. Chem. Eng. Data,* 46, 788, 2001.
29. Tien, C., *Adsorption Calculations and Modeling,* Butterworth, Boston, 1994.
30. Do, D.D., *Adsorption Analysis: Equilibria and Kinetics,* Imperial College Press, London, 1998.
31. Abe, I., Hayashi, K., and Hirashima, T., *J. Colloid Interface Sci.*, 94, 577, 1983.
32. Avom, J., Mbadcam, J.K., Noubactep, C., and Germain, P., *Carbon,* 35, 365, 1997.
33. Khan, M.A. and Khattak, Y.I., *Carbon,* 30, 957, 1992.
34. Teng, H. and Hsieh, C.T., *Ind. Eng. Chem. Res.*, 37, 3618, 1998.
35. Juang, R.-S., Wu, F.-C., and Tseng, R.-L., *J. Chem. Eng. Data,* 41, 487, 1996.
36. Rudzinski, W. and Everett, D.H., *Adsorption of Gases in Heterogeneous Surfaces,* Academic Press, London, 1992.
37. Peak Fit, Peak separation and analysis software, Sea Solve Software Inc., 235 Walnut Street, Framingham, MA 01702.
38. Draper, N.R. and Smith, H., *Applied Regression Analysis (third edition),* J. Wiley & Sons, New York, 1998.
39. Jaroniec, M. and Derylo, A., *J. Colloid Interface Sci.*, 84, 191, 1981.
40. Stoeckli, F., Lopez-Ramon, M.V., and Moreno-Castilla, C., *Langmuir,* 17, 3301, 2001.
41. Dubinin, M.M., *Carbon,* 27, 457, 1989.
42. Stoeckli, F., in *Porosity in Carbons,* Patrick, J., Ed., Arnold, London, 1995.

43. Jaroniec, M. and Madey, R., *Physical Adsorption on Heterogeneous Surfaces,* Academic Press, London, 1988.
44. Ross, S. and Olivier, J.P., *On Physical Adsorption,* J. Wiley & Sons, New York, 1964.
45. Jaroniec, M. and Marczewski, A.W., *Monatsh. Chem.*, 15, 997, 1984.
46. Jain, A., Gupta, V.K., Jain, S., and Suhas, *Environ. Sci. Technol.*, 38, 1195, 2004.
47. Radovic, L.R., Moreno-Castilla, C., and Rivera-Utrilla, J., *J. Chem. Phys. Carbon,* 27, 227, 2000.
48. Singh, B., Madhusudhanan, S., Dubey, V., Nath, R., and Rao, N.B.S.N., *Carbon,* 34, 327, 1996.
49. Lin, S.H. and Hsu, F.M., *Ind. Eng. Chem. Res.,* 34, 2110, 1995.
50. Avom, J., Mbadcam, J.K., Noubactep, C., and Germain, P., *Carbon,* 35, 365, 1997.
51. McKay, G. and Duri, B.A., *Chem. Eng. Process.*, 24, 1, 1988.
52. Chatzopoulos, D., Varma, A., Irvine, R.L., *AIChE J.*, 39, 392027, 1993.
53. Choma, J., Burakiewitz-Mortka, W., Jaroniec, M., and Gilpin, R.K., *Langmuir,* 9, 2555, 1993.
54. Abe, I., Hayashi, K., and Hirashima, T., *J. Colloid Interface Sci.*, 94, 577, 1983.
55. Cookson, J.T., Cheremishinoff, P.N., and Eclerbusch, F., Eds., *Carbon Adsorption Handbook,* Ann Arbor Science, Ann Arbor, MI, 1978.
56. Suffet, I.H. and McGuire, M.J., Eds., *Activated Carbon Adsorption of Organics from the Aqueous Phase,* Vols. 1 and 2, Ann Arbor Science, Ann Arbor, MI, 1980.
57. Slejko, F.L., *Adsorption Technology. A Step-by-Step Approach to Process Valuation, and Application,* Marcel Dekker, New York, 1985.
58. Faust, S.D. and Aly, O.M., *Adsorption Processes for Water Treatment,* Butterworth Publishers, London, 1987.
59. Perrich, J.R., *Carbon Adsorption for Wastewater Treatment,* CRC Press, Boca Raton, FL, 1981.
60. Cheremishinoff, N.P., *Carbon Adsorption for Pollution Control,* Prentice Hall, Upper Saddle River, NJ, 1993.
61. Nevskaia, D.M., Santianes, A., Munoz, V., and Guerrero-Ruiz, A., *Carbon,* 37, 1065, 1999.
62. Nevskaia, D.M. and Guerrero-Ruiz, A., *J. Colloid Interface Sci.*, 234, 316, 2001.
63. Boehm, H.P., *Carbon,* 32, 759, 1994.
64. Leon-Leon, C. and Radovic, L., in *Chemistry and Physics of Carbon,* Vol. 24, Thrower, P., Ed., Marcel Dekker, New York, 1994.
65. Brennan, J.K., Bandosz, T.J., Thomson, K.T., and Gubbins, K.E., *Colloids and Surfaces A,* 187–188, 539, 2001.
66. Persello, J., in *Adsorption on Silica Surfaces,* Papirer, E., Ed., Marcel Dekker Inc., New York, 2000, p. 297.
67. Hernandez, M.A., Velazquez, J.A., Asomoza, M., Solis, S., Rojas, F., Lara, V.H., Portillo, R., and Salgado, M.A., *Energy Fuels,* 17, 262, 2003.
68. El Shaffey, G.M.S., in *Adsorption on Silica Surfaces,* Papirer, E., Ed., Marcel Dekker Inc., New York, 2000, p. 35.
69. Yang, S.M., Miguez, H., and Ozin, G.F., *Adv. Funct. Mater.*, 11, 425, 2002.
70. Porterfield, W.W., *Inorganic Chemistry. A Unified Approach,* Academic Press, New York, 1993.
71. van Damme, H., in *Adsorption on Silica Surfaces,* Papirer, E., Ed., Marcel Dekker Inc., New York, 2000, p. 119.
72. Borowko, M. and Rzuysko, W., *Ber. Bunsen Ges. Phys. Chem.*, 101, 1050, 1997.
73. Goworek, J., Nieradka, A., and Dabrowski, A., *Fluid Phase Equilibr.*, 136, 333, 1997.
74. Hamraoui, A. and Privat, M., *J. Chem. Phys.*, 107, 6936, 1997.

75. Sellami, H., Hamraoui, A., Privat, M., and Olier, R., *Langmuir,* 14, 2402, 1998.
76. Hamraoui, A. and Privat, M., *J. Colloid Interface Sci.*, 207, 46, 1998.
77. Unger, K., Kumar, D., Ehwald, V., and Grossmann, F., in *Adsorption on Silica*, Papirer, E., Ed., Marcel Dekker Inc., New York, 2000, p. 565.
78. Morrow, B.A. and Gay, I.D., in *Adsorption on Silica Surfaces,* Papirer, E., Ed., Marcel Dekker Inc., New York, 2000, p. 9.
79. Duchateau, R., *Chem. Rev.*, 102, 3525, 2002.
80. Vansant, E.F., van der Voort, P., and Vranken, K.C., *Stud. Surf. Sci. Catal.*, 93, 59, 1995.
81 Dijkstra, T.W., Duchateau, R., van Santen, R.A., Meetsma, A., and Yap, G.P.A., *J. Am. Chem. Soc.*, 124, 9856, 2002.
82. Shimada, T., Aoki, K., Shinoda, Y., Nakamura, T., Tokunaga, N., Inagaki, S., and Hayashi, T., *J. Amer. Chem. Soc.*, 125, 4688, 2003.
83. Anedda, A., Carbonaro, C.M., Clemente, F., Corpino, R., and Ricci, P.C., *J. Phys. Chem. B*, 107, 13661, 2003.
84. Brinker, C.J. and Scherer, G.W., *Sol-Gel Science,* Academic Press, New York, 1990.
85. Roque-Malherbe, R. and Marquez, F., *Mat. Sci. Semicond. Proc.*, 7, 467, 2004.
86. Roque-Malherbe, R. and Marquez, F., *Surf. Interf. Anal.*, 37, 393, 2005.
87. Marquez-Linares, F. and Roque-Malherbe, R., *J. Nanosci. Nanotech.*, 6, 1114, 2006, in press.
88. Cundy, C.S. and Cox, P.A., *Chem. Rev.*, 103, 663, 2003.
89. Baerlocher, C., Meier, W.M., and Olson, D.H., *Atlas of Zeolite Framework Types,* Elsevier, Amsterdam, 2001.
90. Davies, M.E., *Nature,* 417, 813, 2002.
91. Corma, A., *Chem. Rev.*, 95, 559, 1995.
92. Marquez-Linares, F. and Roque-Malherbe, R., *Facets IUMRS J.*, 2, 14, 2003.
93. Roque-Malherbe, R., in *Handbook of Surfaces and Interfaces of Materials,* Vol. 5, Nalwa, H.S., Ed., Academic Press, New York, 2001, p. 495.
94. Roque-Malherbe, R. and Marquez-Linares, F., *Facets IUMRS J.*, 3, 8, 2004.
95. Anderson, M.A., *Environ. Sci. Technol.*, 34, 725, 2000.
96. Occelli, M.L. and Kessler, K., Eds., *Synthesis of Porous Materials,* Marcel Dekker, New York, 1997.
97. Camblor, M.A., Corma, A., and Valencia, S., *J. Chem. Soc. Chem. Commun.*, 2365, 1996.

Index

A

B

C

D

E

F

G

H

I

J

K

L

M

N

O

P

Q

R

S

T

U

V

W

X

Y

Z

CHEMISTRY

As nanomaterials get smaller, their properties increasingly diverge from their bulk material counterparts. Written from a materials science perspective, ***Adsorption and Diffusion in Nanoporous Materials*** describes the methodology for using single-component gas adsorption and diffusion measurements to characterize nanoporous solids.

Concise, yet comprehensive, the book covers both equilibrium adsorption and adsorption kinetics in dynamic systems in a single source. It presents the theoretical and mathematical tools for analyzing microporosity, kinetics, thermodynamics, and transport processes of the adsorbent surface. Then it examines how these measurements elucidate structural and morphological characteristics of the materials. Detailed descriptions of the phenomena include diagrams, essential equations, and fully derived, concrete examples based on the author's own research experiences and insight. The book contains chapters on statistical physics, dynamic adsorption in plug flow bed reactors, and the synthesis and modification of important nanoporous materials. The final chapter covers the principles and applications of adsorption for multicomponent systems in the liquid phase.

Features:

- Dedicates an entire chapter to statistical physics, particularly useful for scientists with little or no training in this area
- Provides a detailed treatment of density functional theory in the study of fluid adsorption in enclosed porous systems
- Focuses on the analysis of microporous crystalline, mesoporous ordered, and micro-and mesoporous amorphous materials
- Presents the necessary equations for calculating adsorption in porous systems rates, pore volume, pore size distribution, and more
- Includes two chapters on the synthesis and modification of silica, active carbons, zeolites and related materials, and mesoporous molecular sieves

Connecting recent advances in adsorption characterization with developments in the transport and diffusion of nanoporous materials, this book is ideal for scientists involved in the research, development, and applications of new nanoporous materials.

46756

ISBN 1-4200-4675-6

90000

9 781420 046755

CRC Press
Taylor & Francis Group
an informa business
www.taylorandfrancisgroup.com

6000 Broken Sound Parkway, NW
Suite 300, Boca Raton, FL 33487
270 Madison Avenue
New York, NY 10016
2 Park Square, Milton Park
Abingdon, Oxon OX14 4RN, UK

www.crcpress.com